LARGE EDDY SIMULATION OF UNDER-VENTILATED FIRES

Sergio Adrián Ferraris
Kingston University

A thesis submitted for the degree of Doctor of Philosophy at Kingston University

Acknowledgements

I would like to dedicate this thesis firstly to my parents and brother who were always close to me at every moment.
To my supervisor Jennifer for offering me the chance to realise one of my dreams. And to all who were involved directly or indirectly in helping me with this arduous and long work. I am especially grateful to Jason and Barbara whose help improved my English.

El valer de un hombre reside en el corazón y en la voluntad; en ellos yace el verdadero honor. La valentía es la firmeza, no de las piernas ni de los brazos, sino la del vigor y la del alma. No consiste en el valor de nuestro caballo ni en la solidez de nuestra armadura, sino en el temple de nuestro pecho. El que cae lleno de ánimo en el combate, si cae en tierra combate de rodillas; el que desafiando todos los peligros ve la muerte cercana y por ello no disminuye un punto en su fortaleza; quien al exhalar el ultimo suspiro mira todavía a su enemigo con altivez y desdén, son derrotados no por nosotros, sino por la mala fortuna; muertos pueden ser, mas no vencidos.

Montaige
Para mi padre.

Abstract

The present thesis constitutes an important contribution to the understanding of a partially premixed combustion system associated with the hazardous backdraft phenomena. Backdraft may occur when fresh air is suddenly introduced into a vitiated environment where fire has already died out due to lack of oxygen but there are still unburnt fuel and products of incomplete combustion left.

In the context of backdraft or deflagration, a complex flame structure is expected. Both, non-premixed and diffusion combustion might, in principle, be present. The present study focuses on the development of sub-grid scale (SGS) models to facilitate the study of such complex flame structure using the large eddy simulation (LES) technique. Before applying the model to the backdraft simulation, the individual SGS models were firstly validated using simple configurations where detailed experimental data is available.

A flamelet-like model for premixed combustion was introduced and thereafter coupled with the non-premixed combustion model through a "flame index" parameter. This concept makes use of the gradient signs of oxygen and fuel mass concentrations to distinguish between premixed and diffusion combustion regimes. In the present implementation in LES, an improved version of the flame index concept developed by Domingo et al. [67] was adopted. The model takes into account the fluctuations of both gradients at sub-grid level, which subsequently, might affect the filtered flame index value.

In order to track the premixed flame front we used an approach which filters the progress variable balance equation using a filter larger than the actual LES grid. This approach has the advantage that it represents a physical meaningful variable and is stable from the numerical point of view because of the smooth gradients of the progress variable at the flame front and the species concentrations related to it.

The flame front tracking technique was tested with an unstrained planar hydrogen flame front. Reasonably good results in burning speed and density ratio were obtained.

The non-premixed or diffusion combustion regime was modelled using a flamelet-like model which considers the flame to be located at the stoichiometric value of the mixture fraction and it is related to the strain rate imposed by the counter flow of oxygen and fuel mass concentration feeding streams. This approach has the advantage that it has been tested for different scenarios and it is relatively fast as the variables can be pre-stored in a table.

The flame index approach was tested using a laminar triple flame configuration. It was observed that the model could capture the different combustion regimes and predicted the lift-off height with reasonable accuracy. The location of the triple point was well predicted and the three branches further downstream could also be easily discerned from the predictions.

Subsequently, a partially premixed turbulent lifted flame was simulated. In this case, it was necessary to introduce the augment of burning velocity induced by the wrinkling of the flame front at sub-grid level. The SGS flame front wrinkling factor is defined as the sub-grid scale flame surface divided by its projection in the resolved propagating direction. This can be regarded as the ratio of the sub-grid turbulent flame speed at grid scale ($S_{T\Delta}$) and the laminar flame speed (s_l^0). Reasonably good agreement was found on the lift-off prediction, the flame structure, and the mixture fraction profiles. A stabilization mechanism was discussed based on concepts previously exposed where the flame base faces a high velocity flow and a flammable mixture. Thereafter, the flame attempts to find its way upstream through low-speed flammable sections of the flow. It was found that in this process the stabilization point, herein identified as the maximum premixed heat release, plays an important role driving the flame base upstream the flow.

Finally, two real scenarios of backdraft in a full scale fire test were simulated. These include the full scale backdraft experiment of Gojkovic [94] and the reduced scale experiment of Weng and Fan [254] . Unfortunately, there exist neither extensive nor accurate measurements for the former one and hence, the comparison against the numerical simulation was largely carried out on qualitative grounds. Five different stages were identified: 1) initial phase, 2) spherical propagation, 3) planar propagation, 4) flame front stretching and 5) fire ball. Qualitatively, the simulation agreed well with the experiment. The ignition delay time (the time from the opening of the hatch until the time when the ignition occurs) was well predicted by the simulation. It was also observed that the flame structure in the backdraft was predominantly premixed.

More detailed measurements were available in the tests of Weng and Fan [254]. These included the upper layer temperatures, mass concentrations and pressures at the openings. Different opening geometries were used and the total mass flow rates in and out of the container were also measured. Overall, the predictions were in good agreement with the measurements and the model predicted the correct trend for pressure and mass flow rates in the tests with different openings. Furthermore, the predicted occurrence and non-occurrence of backdraft in different geometrical configurations was in line with the experimental observations in which backdraft did not always happen.

During the earlier stages of the study, some effort was devoted to improving the SGS turbulence models and to implement a CMC type SGS combustion model into the code. Unfortunately both models were later found to be unsuitable for the backdraft simulation. The first one suffered numerical instabilities caused by the under prediction of the Smagorinsky constant when applied to the backdraft case. The second one was deemed inappropriate due to its requirement of an homogeneous plane of conditional values. Nevertheless, some reasonably good results have been obtained with both models during the validation using simple geometrical configurations, namely a buoyant plume, a backward facing step and the Sandia-D

non-premixed turbulent flame. The effort in this direction is therefore still included in the thesis as summarised below.

A Lagrangian SGS turbulence model was implemented. Good results were found for classical benchmarking flow configurations such as the buoyant turbulent plume and the backward facing step. It was, however, found that the SGS turbulence viscosity became negative in a larger percentage than originally stated by Maneveour. Because of this, the model is prone to numerical instability. When applied to the backdraft simulation, the dynamically calculated Smagorinsky constant using this model was found to be consistently lower than the conventional range (0.1-0.23). This caused stability problem and made it very difficult to achieve converged solutions.

The conditional source estimation (CSE) approach, which is a variation of the Conditional Moment Closure (CMC) approach, was also implemented. This model produced good results for the classical turbulent diffusion flame (SANDIA flame D). Even though the present implementation is not capable of predicting extinction/re-ignition events it was showed that it is very economic from computational point of view. However, as explained above, this model was also considered as unsuitable for the backdraft simulation.

CONTENTS

List of figures

Nomenclature

a	thermal diffusivity
[a]	coefficients vector B_k: frequency factor
C	progress variable
C_p	specific heat capacity
C_s	Smagorinsky constant
D	molecular diffusion
Da	Damokler number
Da_q	Damokler number at extinction
Da_i	Damokler number at ignition
D_Z	scalar diffusivity
Dt	turbulent diffusivity
E	efficiency function in the thickened flame approach
E_k	activation energy
EQ	equilibrium chemistry condition
Fr:	Froud number
G	G-equation iso-surface
g	gravity vector
h	specific enthalpy
I	identity matrix
K	inversion kernel matrix
Ka	Karlovitz number
L_t	turbulent integral velocity
L_e	Lewis number
l_k	Karlovitz length scale
l_d	mixing characteristic length
l_r	reaction zone thickness
P	probability density function distribution
Qp	premixed heat release rate

Qd diffusion heat release rate

Qt total heat release rate for partially premixed combustion

R universal ideal gas constant

Re Reynolds number

S stress tensor

S_c reactant consumption

s_l^0 laminar burning velocity

S_T turbulent burning speed

$\widetilde{S}_L$ filtered laminar flame speed

Sc Schmidt number

T temperature

t time

u, v, w velocities in x, y and z directions

u_k Karlovitz velocity

W specie molar weight

$\dot{w}$ reaction rate

w_G propagation speed

w_U unburnt gas propagation speed

Y specie mass concentration

Z mixture fraction.

Greek symbols

ρ density

υ kinematic viscosity or molar coefficients

τ_t turbulent time scale

τ_c chemical time scale

τ_k Karlovitz time scale

τ_{ij} viscous stress tensor

δ_l^0 laminar flame thickness

δ_l^1 resolved flame thickness

ϕ	equivalence ratio
χ	dissipation rate.
ε	kinetic turbulence
k	dissipation turbulence
$\dot{\Omega}$	reaction rate per unit area of flamelets
Σ	flame surface density
Ξ	wrinkling factor
μ	viscosity
θ	flamelet functions
Δ	grid size.
Δ_C	C balance equation filter size
ξ	flame index
λ	regularization parameter

Upper scripts

u	unburnt
b	burnt
‘	fluctuation
r:	resolved
s	sub-grid

Sub scripts

f	fuel
o	oxygen
f,o	fuel feeding stream
0,o	oxidizer feeding stream
l	laminar
t	turbulent
st	at stoichiometric mixture
∞	reference value

Operators

$\perp$	derivatives in the stoichiometric plane operator
$\bar{x}$	Reynolds-averaged quantity
$\tilde{x}$	Favre-averaged quantity
Tr	matrix trace
$Q\|Z=Z^*$	conditioned value of Q on Z at Z^*
n	normal vector
∇	gradient operator

Chapter 1

Introduction

Fire development in buildings is an extremely important topic in fire protection engineering. Fire spreading rates, combustion gases temperatures and concentration, evolution of toxic gases and the available time to evacuate the occupants safely are all topics of concern in the fire research community.

The fast development in construction technology has resulted in an extraordinary enlargement of the size of buildings. Public places such as shopping, stadiums, skyscrapers, etc. can accommodate hundreds if not thousands of people, highlighting fire safety issues.

Several scientific disciplines such as chemistry, physics, flow dynamics and heat transfer are involved and play their part in fires. Technical information about fuels, burning rates, fire spread, flashover and backdraft phenomenon is also relevant. Experimental studies, fire modelling and fire investigation are also strongly related to the fire dynamic discipline.

Simple empirical relationships have been developed to provide estimates of fire growth in general. The advance in computational facilities in the 1980s has led to an improvement in fire prediction and allowed the development of more accurate tools aiming at solving the basic physics involved in fires. The improvement of fire modelling is assisted by experimental studies which help to understand the actual behaviour of fires in real-life and in laboratory situations. Some of these studies focused on hazardous flashover and backdraft phenomenon, and more importantly how these events can be delayed or suppressed. On another front, the understanding of the fire dynamic can also assist in the investigation of destructions after the fire is extinguished.

Chemical reactions are governed by the laws of chemistry and physics, and in specific situations one can be more relevant than the other or can control the burning process. Combustion is an exothermic reaction (heat released) where fuel and oxidizer (usually air) are involved and converted into other components (products of combustion) thus, as a consequence, energy in the form of heat is released.

In general, there are two types of fire scenarios: 1) open or well ventilated fires, where the air supply never runs out and the combustion is evenly sustained and 2) indoor or enclosure fires, where oxygen is fed through the openings of the enclosure and hence the flame behaviour depends on both the geometry and location of the openings. Herein, we are concerned mainly with the latter.

1.1 Enclosure Fires

This section provides an overview and a qualitative description about fire development in enclosures.

1.1.1 Terminology

Backdraft: Under certain circumstances, the lack of oxygen supply during an enclosure fire can lead to fire extinction and the production of a large amount of hot, unburnt gases. If a window or a door is opened, cold fresh air might establish a gravity current flowing into the room and mixing between the unburnt fuel and oxygen occurs. Any ignition source can trigger the burning of this flammable mixture resulting in a rapid deflagration towards the opening. The expansion of gases will create an over pressure inside the room and the products will be expelled leading to a fire ball outside the enclosure.

Flashover: The transition from the fire growth period to the fully developed stage in an enclosure fire. In flashover, fire is spread throughout almost all the combustible items within the room. This term serves to differentiate between two stages of a room fire, i.e. pre-flashover and post-flashover.

Fuel-controlled fire: During the initial phase of a fire oxygen is available. Therefore the heat released is fully determined by the burning rate of the specific fuel.

Fully developed fire: It is the period from the flashover through the decay stage to the extinction. In this phase the fire is mostly ventilation controlled.

Pre-flashover: It is the stage when the fire grows and spreads through the room. Usually, the fire is localized but the high risk of spreading makes it potentially dangerous for people and it can potentially lead to flashover.

Ventilation-controlled fire. If the fire becomes large enough to deplete the available oxygen in the room and the opening areas are not sufficient to provide the oxygen for combustion, the fire will develop into ventilation controlled condition. In such

situation, the heat release rate will be determined by the air supply through the openings.

1.1.2 Description of enclosure fire behaviour

The interaction between the physical and chemical processes in a fire is extremely complex. There is a strong coupling and interaction between the flame, the fuel (which might be unevenly distributed into the room) and the surroundings.

A single room fire is considered for the following characterization of fire phases. A fire inside a room can evolve in many different ways depending on factors such as furniture disposition, enclosure geometry, ventilation, and type of fuels available.

Commonly, four stages of an enclosure fire are accepted:

- Ignition
- Growth
- Flashover
- Fully developed fire-decay/backdraft

Ignition: It is the process through. which a fire is set off. It can be produced by both punctual sources such as sparks, cigarettes, etc. or excess of accumulated heat into a combustible element. The ignition mechanism will persist along the fire, setting alight other fuel packages such as curtains, carpets, etc. by mean of heat fluxes or fire spread.

Growth: Following ignition the fire may spread within the room. The advance can occur in many different ways depending on the interaction of the fire with the surroundings. Initially, the localized fire will produce a plume of hot gases rising upward to the ceiling. The flowing of products will result in a current of air entraining at the base of the fire with a subsequent increase in mass flow rate in the plume.

Eventually, if this process continues, the products will accumulate at the top of the room forming an upper layer of high temperature whose layer interface will descend toward the floor. The smoke-filling process is of extreme importance from the fire safety point of view because it imposes the time available for a safe evacuation of the building and determines location and technical specifications for smoke detectors.

During the growing phase, the fire is fuel-controlled because the oxygen is sufficient for combustion. During the fire progress, the fuel packages and gases inside the room are heated either by direct contact with the flame, flame spread, convection or radiation and, if the temperature reached is high enough, secondary items might ignite.

Flashover: flashover is the transition from the growth period to fully developed stage. There is not a fixed definition for the flashover event. Nevertheless, while some conventions consider temperature as criteria, others take into account the heat fluxes inside the room. From a qualitative point of view, it can be said that flashover happens when the fire, originally localized in the growing stage, suddenly spreads to others fuel packages.

Fully developed fire and decay/backdraft: after flashover occurs, a fully developed fire scenario is reached. At this point, the fire is at its maximum burning rate and is often limited by the air supply. Hence, this sort of fire is called ventilation-controlled and the oxygen is fed through the openings. Under these circumstances, un-burnt fuel is accumulated at the ceiling level and, as these gases leave through the openings, they might burn. This situation can last for hours depending on the amount of fuel and oxygen available in the room.

In the event where there are no openings or ventilation is severely restricted, hot products and un-burnt fuel will descent towards the floor and, eventually the fire will be covered. The atmosphere becomes oxygen starved and the fire will gradually die down. Even though they are no flames inside the room, the accumulation of un-burnt gases into the enclosure might continue.

Under these circumstances the fire might mainly evolve in two different ways:

Decay: As the fuel is completely consumed, the burning rate is greatly reduced and the room is gradually cooled down through the walls and/or openings.

Backdraft: In the case where a vent is opened either by a fire fighter or window fallout, a current of fresh air can mix with the hot un-burnt products or fuel. Any ignition source can ignite the flammable mixture and a fast deflagration travelling in the direction to the opening air might happen.

1.1.3 Important aspects affecting an enclosure fire.

Considering the stages of a fire evolution inside an enclosure, it is important to reach an understanding of the factors whose variations and combinations may influence the fire behaviour and, as a consequence, might be used to avoid its hazards.

From the above, it can be inferred that there are many circumstances which can either change or affect the fire evolution, briefly:

1) Room size and geometry.
2) Openings sizes and locations.
3) Thermal boundaries of the room.
4) Type and distribution of the fuel within the room.
5) Ignition source

Similar burning load in a room with a higher ceiling will produce lower upper layer temperature and hence lower radiation heat back to the fuel package and, consequently, a slower growth of the flame. Similarly, different arrangement of openings can cause a fire to be under-ventilated under some circumstances and well-ventilated under others. The layout and material properties of the fuel are important part of the fire spreading mechanism. A compact outline and highly flammable fuel might dramatically accelerate the fire growing. If the air re-entrainment is large the

fire plume might reach the ceiling and the fire will spread horizontally towards the wall with big risk of flashover.

The position of the ignition source plays an important role. A candle located at the bottom of a curtain will trigger a rapid spread of the fire upwards, contrarily, if the fire is originated on the top of a cupboard the flame may spread downward at a much slower rate. Similarly, the heat losses through the wall can play an important role. The more the heat lost to the neighbour room the more the flashback is likely to be delayed or avoided.

It is patent that the interconnections among theses factors are numerous and very complex. Correspondently, several studies have been dedicated to different stages of the under ventilated fire. Both, experimental and theoretical studies are aimed at reproducing simplified scenarios in order to come up with simple rules (correlations) which are able to extrapolate different set ups and to weight the influence of each factor. Equally, the use of Computation Fluid Dynamics (CFD) codes has helped to advance further the fire research.

1.2 Computer Fire Modelling

The use of computer models for simulating fires has increased dramatically in the last decade. This might be attributed to several factors such as the emergence of fire regulations, new building designs, better understanding of the fire underlying physics and the advancement of computational capabilities.

The assessment of fire hazards can be carried out using several techniques characterized by different degrees of complexity and accuracy. All the techniques rely on models that should ideally be able to take into account all the variables involved in the problem, to describe the physical phenomena accurately and to deal with different situations without special tuning of constants. The numerical methods used to implement the model should be accurate allowing a precise description of the geometry and not time expensive. But some of the requirements are in contradiction with one another, therefore a range of modelling approaches is available, each one

with its strengths and weaknesses. They can be broadly classified as: empirical models, zone model technique and Computational Fluid Dynamics (CFD) based models.

Empirical models contain correlations obtained from analysis of experimental data and contain little or no physics.

Zone models are simplified physical models, which seek to represent only the essential physics. The greatest simplification made is with respect to the modelled geometry, usually two zones are considered inside the enclosure with homogeneous temperature varying in time. The accuracy of the result depends on the agreement between the simplified and actual conditions. The run times for zone models are short, of the order of a few seconds. This type of model is well suited to running through large numbers of different scenarios and can be used to pick out particular situations which can then be investigated using a CFD code to obtain further details.

Finally, CFD models involve numerical evaluation of the partial differential equations governing the fire process and yield a great deal of information about the flow field. This approach is also called field model. In theory, CFD solves the physic underlying the process but restrictions of time and computational resource result in the development of shortcomings in the shape of sub models such as combustion, soot, radiation, etc. with each carrying its own degree of assumptions and range of applicability.

1.3 Summary

In Fire Research, many scientific disciplines come together in order to solve the very difficult problem posed by fire. In most combustion contexts the maximum and minimum scale either in time or in space are separated by several orders of magnitude. For instance, considering that the thickness of a premixed laminar flame is in the order of 1 mm or less and that a ordinary room has few meters in size and, on the other hand, a typical chemical reaction time is less than 1 msec. and usually a fire

may last at least many minutes or hours, it is easy to observe the challenge and the difficulty of combustion modelling.

As a result, two approaches to the fire puzzle have been broadly delineated:

1) Simplified and controlled experiments where computational simulations are carried out using detailed physics and chemistry.

2) Realistic scenarios, commonly larger domains, where predictions and measurements should broadly outline the overall behaviour of fire, smoke and heat transport.

Normally, the first group is called basic research and important advances have been observed. The experimental and computational modelling are advancing parallel. Multiple laser techniques are used for predicting species concentrations while particle image velocimeter (PIV) provides accurate measurements of velocity field on planes. In the mean time, better and cheaper computational facilities facilitate the advancement of increasingly more advanced numerical sub-models such as radiation, turbulence, soot transport, combustion, etc. which are coupled with flow dynamic solver (DNS, RANS or LES) to provide a more detailed 3-D representation of fire processes.

In the second group, where reallife scenarios are studied, the use of sophisticated models is constrained by the running time. Similarly, and because of the dimensional scale, the measurements are less detailed and therefore they provide less specific data to compare. In industrial design, it is almost always necessary to run many simulations in order to obtain a trend of the parameter under study or to achieve the design requirement. Under these circumstances, the accuracy of the results (within certain range) is relegated to a lower priority by the running time.

1.4 Aim of the PhD thesis

Considering the complexity and the extent of the fire field it is necessary to carefully delineate the scope of the present thesis.

Among the stages of a fire development inside a room, probably the most studied cases are the circumstances leading to flashover (pre-flashover) and its consequences (post- flashover). The reasons are clear from a fire safety point of view; flashover is particularly threatening for human life and structures alike.

On the other hand, relatively few works have been dedicated to analyse the backdraft phenomena, a possible outcome of an enclosure fire in the decay phase. This event, probably not the most common in fire scenarios, is particularly dangerous for fire-fighters when they arrive at the scene when the fire is almost extinguished. Un-burnt fuel might have been accumulating in the upper section of the tightly sealed building and some smouldering combustion might still been taking place. Hence, if a ventilation is opened, mixing of fresh air and unburnt fuel can trigger a fast deflagration.

The main goal of this thesis is to investigate the backdraft phenomenon using LES based numerical techniques.

The structure of this thesis is such that it deals with the development and implementation of combustion models, which can handle the backdraft phenomenon.

1.5 Thesis layout

The thesis is organized so that the development, implementation and validation of each individual model are described separate chapters. The validated model is then finally applied to simulate the backdraft phenomena.

The thesis is divided into eight chapters.

Chapter 2 introduces experimental, analytical and computational studies in enclosure fires in general.

Chapter 3 reviews the basic structures of non-premixed and premixed flames and presents the background of laminar and turbulent combustion models. An emphasis is given to the LES approach.

Chapter 4 presents the governing equations in FDS, which is used as the basic LES code. It then introduces several sub grid turbulence models and describes a Lagrangian approach, which is applied to simple isothermal flow configurations for benchmarking.

Chapter 5 lays down the fundamentals of diffusion combustion and describes the implementation of the Conditional Source Estimation (CSE) model with its validation using the turbulent diffusion Sandia flame D.

Chapter 6 presents numerical modelling related to premixed and partially premixed combustion; implementation of a geometric approach to track the flame front and laminar/turbulent burning velocity. It also describes the implementation of the flame index approach for LES.

Chapter 7 presents large eddy simulations of different premixed and partially premixed systems such as planar laminar flame propagation, laminar triple flame and turbulent lifted flame.

Chapter 8 presents previous work related to backdraft and applies the combined turbulent combustion model to simulate full-scale backdraft tests.

Chapter 9 summarizes the main findings of the thesis and their implications and presents suggestions for future work.

Chapter 2

Fire in enclosures background

The basic processes involved in enclosure fires are briefly commented in this chapter. Fundamental references are given to important numerical and experimental studies on relevant subjects such as fire growth, radiation, soot, combustion, dispersion, ventilation, etc. within the frame of under-ventilated fire. This is followed by a brief review about numerical fire simulations using the LES approach in general and using the code Fire Dynamic Simulator (FDS) in particular.

2.1 Numerical and experimental studies on enclosure fires

The emergence of performance-based fire codes has shifted the emphasis on experimental research towards fulfilling the requirements of new design techniques. While in the past, most fire safety design systems and specifications were based on empirical relationships, there has been an increase in the use of CFD in recent years.

However, before such numerical models can be applied to realistic scenarios, their predictions need to be validated against experiments. Experimental investigation is still our main source of information in both designing standard for fire safety and benchmarking CFD models. Therefore, there exists a need to provide full-scale experimental data. In the following, experimental works and numerical studies are briefly reviewed.

2.1.1 Flashover

Predominantly, most experimental and numerical works on enclosure fires are concerned with pre-flashover scenarios or the conditions leading to flashover. The occurrence of flashover within a room is of considerable interest since it is perhaps the ultimate signal of untenable conditions and the immediate increase of risk to the occupants. Ideally, the use of any tool available for predicting this phenomenon should evaluate objectively the appropriate criterion.

Peacock et al. [182] reviewed experimental studies of real-scale fires that quantified the onset of flashover in terms of measurable physical properties. Albeit with considerable scatter, they found definitions, which were consistent with a broad range of experimental data. Among them, the upper layer temperature of 600 °C and heat flux at floor level of 20 KW/m^2 [7]. Babrauskas et al. [7] defined the flashover from two points of view: 1) as the occurrence of criticality in a thermal sense and 2) defined as a fluid-mechanical filling process.

Graham et al. [97] investigated the impact of the thermal inertia of the wall upon flashover development. Using a two zones model, they carried out a dimensionless group analysis and inferred that thermal inertia of the walls makes it harder to achieve

flashover.

In the late 90's Luo and Beck [145] carried out a study on flashover in a full-scale multi-room building. In their work, a multi storey building configuration, temperature, heat flux, gas concentration and mass release rate were measured. The experiment was designed to obtain flashover in one of the rooms and a numerical simulation was carried out using a relatively coarse mesh (24000 cells) utilizing a RANS method (CESARE) with simple flame spread model. They concluded that the predicted reasonably well the fire even when using a very simple fire-growth model. Luo et al. [146], using the same experimental data but for a single level building, applied a similar numeric methodology and arrived at similar conclusion. More recently, Yeoh et al. [268] performed another numerical simulation of the Beck's full scale experiment using a more refined mesh (135000) and more sophisticated combustion, soot and spread models. In particular, they applied the laminar flamelets concept (see chapter 3) to model the combustion process and a soot model that incorporates physical processes of soot such as nucleation, coagulation, surface growth, etc. They found a good agreement with the experiment and concluded that soot concentration is of primary importance in large fires.

2.1.2 Fire growth

In the process leading to flash-over one of the paramount mechanisms is the fire spread or fire growth. An early attempt to model fire growth on walls or floor from the basic equations was made by Yan and Holmstedt [265]. They discarded the semi-empirical flame spread model developed to analyse one-dimensional lateral flame spread and introduced a more realistic physical sub-model in which three-dimensional transient turbulent gas, combustion, heat transfer, pyrolysis and charring solid fuel were considered. They obtained good results but failed in some quantities, possibly due to uncertainties in material properties.

Lattimer et al.[131] applied a two zone model for predicting a corner fire. They tested three different linen materials and obtained an under-prediction of 25% for the heat

release and 30% of error in the flame length estimation. Lennon and Moore [140] conducted a series of full-scale tests at Cardington where the influence of the compartment linings and fire load types were tested to validate the natural fire safety concept. Another full-scale test was carried out by Newman and Xin [178], it included two liquid and gaseous pool fires located at the centre of a large enclosure (18x12x6) m heavily instrumented. Their goal was to test scaling techniques, derived from similarity relationships of steady ceiling flow, for temperatures and concentrations in growing fires. The found that non-dimensional temperatures and species concentrations derived from scaling techniques correlates well with the experiment.

2.1.3 Fire behaviour vs. ventilation factors

Some studies have also been carried out concerning the influence of ventilation configurations such as opening areas, vent dispositions and delaying times on fire behaviour.

Klopovic and Turan [126] provided a set of experiments aiming at studying flame venting during full-scale flashover fires. They studied the venting plume for two ventilation configurations in a multi-room building. They arrived at the conclusion that the existing empirical prediction are conservative and that there can be secondary fire in the floor above through direct flame contact. On this basis, they suggested that flashover produces conditions favourable for external flaming, such as windows cracking or failure. Whilst windows act as barriers during the initial stages of the fire and may delay the onset of the flashover, their sudden fall out could supply the fire with air.

Along the same line, Delichatsios et al. [63] examined three different geometries, a rectangular ventilation controlled (small opening), a rectangular fuel controlled (large opening) and a corridor. They performed measurements using methanol, PMMA, wood and ethanol as fuels and established steady volumetric conservation equations for each geometry. They concluded that small openings increase the excess of

pyrolysate and the flame spread through the openings and that increasing the vent the fire is reduced until it becomes well-ventilated and free burning fire.

Sinai [225] studied the role of leakages in an under-ventilated compartment fire. In his study, Sinai utilized a RANS approach for a 600 m^3 room with a 10MW fire and concluded that the locations and proportions of leakages can influence the collapse of temperature stratification in the numerical simulation inside the building.

2.1.4 Radiation and Soot

It is widely recognized that thermal radiation is an important mechanism of heat transfer in large-scale fires since 20-40% of energy released is externally radiated. Radiation has an important impact on the chemistry and on the flame structure. It is generally accepted that for small flames, lower than 0.2 m, radiation has a negligible effect. However, its influence for larger fire is important and needs to be considered.

Soot produced during high-temperature pyrolysis or combustion of hydrocarbons in significant amounts can augment the local and global radiation in enclosures. The treatment of radiative heat transfer can be compromised in the absence of a satisfactory description of the spatially varying absorption coefficient of which soot is a major contributor.

In enclosure fires, as the combustion becomes more incomplete due to the lack of oxygen, the products of incomplete combustion tend to cover the flames. In this process, soot plays a fundamental role as it enhances the heat fluxes due to radiation to the surroundings. This mechanism is especially critical when there are several fuel pockets inside the room, which might ignite. To this purpose, several works have been dedicated to analyse and to improve both soot and radiative flux predictions in enclosure fires.

Wen et al. [252] studied the effect of microscopic and global radiative heat exchange on compartment fires. They simulated a single room fire of 135 m^3 with

approximately 110000 cells using the commercial package CFX. In this study, they utilized a flamelet combustion model considering radiation losses inside the flamelets and found that both microscopic and global radiative heat exchange have significant effect on the overall fire development and affect the prediction of soot and OH but not CO_2, CO and H_2O. Interestingly, they experienced an over prediction of 50% in the soot concentration when the heat losses by radiation were not taken into account.

Yeoh et al. [267] applied a RANS model to three full scale fire tests: 1) Steckler et al's. [230] single fire compartment which consisted of a square enclosure of (2.8 x 2.1) m with a circular methane gas burner flushed to the door located at the centre of the room, 2) Nielsen and Fleischmann's [179] test which included a burning room and an adjacent compartment and 3) Mingchum and Beck's [145] multi-room and multi-storey fire. They employed a detailed model for soot, which accounts for soot nucleation, coagulation, surface growth and oxidation. They introduced two extra transport equations for soot particle number density and soot volume fraction and coupled it with the Discrete Ordinates Method (DOM) for radiation heat transfer. The eddy break-up mode (EBU) and flamelets were used as combustion models and detailed fire growth mechanism was included in the calculation. The simulations were carried out using up to 135200 grid nodes. They found that the combustion model plays an important role resolving the two layer structure and that radiation and soot affect the prediction of the flame tip length. They also commented that Large Eddy Simulation (LES) might provide better time-resolved information essential for fire chemistry and soot formation.

2.1.5 Combustion

Particularly important in the computational simulation of fires is the combustion sub-model. It has been previously noted that the principal goal of pyrolysis models is to predict the heat release rate. The combustion of fuel is strongly coupled with the flow field (turbulence), temperature (radiation fluxes) and concentration distribution (chemistry). Therefore, it is essential to determine the correct amount of energy released inside the enclosure if a good field prediction is sought. Generally, the same

type of combustion models used for well ventilated or open fires, namely eddy break up, pdf, etc (see chapter 3) have been used for poor ventilated cases even though their capability to handle such scenarios has not been tested.

Xue et al. [261] stressed the need for adequate turbulent combustion models in enclosure and set about to compare three different combustion models, the volumetric heat source (VHS), the eddy break-up (EBU) and the presumed probability density function (pre pdf) for three fire scenarios: a tunnel, a single room and a shopping mall. They found that, in general, the performance of the pdf model is more consistent, although there is not a distinct performance that stands out as most suitable for such application. Similarly, Yeoh et al. [267] tested two different turbulent combustion models (EBU and flamelets) in a multi-compartment building using a RANS approach. Their conclusions were similar to Xue et al. [261].

As the present thesis focuses mainly on turbulent combustion models, a more detailed account of different combustion models will be given in chapter 3.

2.2 The application of Large Eddy Simulation (LES) to enclosure fires

The LES technique was developed in the early 1960's by Smagorinsky and Deardorff [227]. It assumes that turbulent motion can be separated into large and small eddies. The large eddies (grid scale) motion is directly calculated, and the behaviour of the small eddies (sub-grid scale) is modelled. Since LES solves time dependent flow, it can provide detailed information on instantaneous field quantities. This technique is inherently three-dimensional and requires a reasonable time step to capture most of the important turbulent motion. Because of this, LES is computationally more expensive than RANS. One example of LES code for fire and smoke simulation is the Fire Dynamic Simulator (FDS) developed by the National Institute of Standards and Technology (NIST). FDS is by far the most used LES code in the fire research community.

This section is aimed at introducing several fire-related studies using LES (mainly

FDS) while the theoretical background of FDS can be found in [162].

A LES approach is especially attractive when accurate time-resolved variables are needed. There are many works addressing smoke development in both tunnel and plume fires [87, 103, 138, 160, 217]. McGrattan et al. [160] performed a numerical simulation of smoke plumes from large open oil fires and obtained good results even when some of the assumptions made, such as Boussineq approximation and 2-D time-dependent, brake down close to the fire.

FDS has also been applied to predict smoke behaviour in tunnel fires with relative success on predicting temperature, flame shape and the smoke movement patterns. Gao et al. [87] found that thermal stratification and smoke backflow can be successfully predicted by LES. Tunnel geometries have been tested using FDS for different aspect ratios, where temperature distribution under the ceiling showed a relatively good agreement with experimental results within 10 ^{0}C and the velocities were about 3% higher than the measurements [138]. Hwang and Edwards [103] conducted a series of simulations in order to evaluate the grid sensitivity of FDS on velocity predictions in small and large tunnel fires. They used a grid size ranging from 0.0094 m to 0.23 m for two fires of 10 KW and 16 MW, respectively. This study stressed the importance of a good grid resolution inherited in LES. In all of the previous cases the heat release rate was specified as an input to the simulation.

The combustion model in FDS was originally developed for well-ventilated fires but it has been also applied to under-ventilated enclosure fires. Ryder et al. [218] utilized FDS to predict two fire experiments and fuel dispersion in both a small room fire and a large (15 m diameter) pool fire. The results were favourably compared with experimental data.

An interesting numerical simulation of a post-flashover compartment fire was carried out by Pope and Bailey [201]. They compared two parametric fire modelling techniques (Eurocode 1 and the BFD curve method) and FDS. The experiment comprised a multi-compartment building with eight fuel wooden packages. The heat

release was calculated from the mass lost measured during the experiment and input into the model. Two meshes with grid size of 0.58 m and 0.73 m were used. They concluded that the BFD curve predictions are most closely representative of reality and that the fine mesh with FDS has comparable results with the BFD method. A direct comparison of the maximum gas temperature showed that FDS under predicted the maximum temperature by 50%.
It is worth noting that in this study the grid size might have not been sufficiently fine to resolve the flow dynamic and, probably more relevant, the experimental uncertainty of the heat release may have been of importance, leading to erroneous temperature predictions.

Chow and Zou [48] attempted to draw correlations of air flow rates through openings induced by fire in enclosures. They utilized an 86400 cells mesh in a multi-room compartment of 36 m^3 and obtained reasonable correlations for ventilation in enclosure fires. Zhang et al. [271] used LES to predict turbulence statistics in an iso-room where instead of fire a heated plate was used as a flow-driven force. In their work, the turbulence structure and the temperature field were predicted using different mesh sizes (0.046/0.02m) and Smagorinsky constants (0.14/0.18). It was found that the predictions were in good agreement except near the ceiling and when the coarser mesh was used the results were slightly poorer. The use of two Smagorinsky constants showed little effect when the buoyancy force was weak but its influence was greater when the flow became more turbulent.

A simulation of a pool fire of a 7.1 cm in diameter using a mixture-fraction-based combustion model was carried out by Xin et al.[260]. They captured the qualitative and quantitative fire behaviour very well. Ma and Quintiere [147] undertook a simulation of a (0.3x0.3) m burner fire with heat release between 7.37 and 737 KW and performed a very detailed mesh sensitivity analysis using FDS 2.0 and compared their results with empirical correlations. They arrived at the conclusion that the flame height prediction fitted well with correlations and that temperature and mixture fraction values near the flame tip were very close to empirical findings. Nevertheless, the temperature near the burner was over-predicted, while the centreline temperature

and velocity in non-combustion region was well predicted.

FDS has been also used in predicting fire spread through combustible wall. Wang et al. [250] performed a LES of buoyancy-driven fire propagation behind a pyrolysis zone along a vertical wall. A relatively good agreement was obtained in the time-averaged flame height, velocity and temperature profiles and the predicted entrainment rate closely followed an empirical correlation. The behaviour of the large-scale and highly transient structure of the wall were reasonably well reproduced.

2.3 Summary

For the last ten years the use of LES by the fire community has been constantly increasing, mainly because of an easier access to cheaper computational facilities. The fire research community has found in LES, and especially in the FDS code, a tool that can cope with more realistic fire behaviour and this tendency is consistently expanding to the industry as a designing tool. Moreover, the FDS code developed by NIST has been used by fire researchers as well as designers. The release of a parallel version of FDS (version 4) has further contributed to this expansion enormously.

Nevertheless, caution must be drawn when the LES approach is used. As it was seen, LES is far more sensible than RANS to external parameters such as grid size, sub-grid turbulence, boundary conditions, etc. Hence, mesh and boundary condition sensitivity studies should be carried out when LES is used.

The author believes that LES can deliver with relative confidence accurate results in iso-thermal flows such as gravity current, turbulent jet, etc, even though care should be taken regarding the use of SGS turbulence models and boundary conditions. On the other hand, combustion models for LES are still subjected to continuous improvement. Research in this field is retracing the steps previously covered in the RANS context. Some combustion models developed initially for RANS have been used into the LES approach. However, theses models have many limitations and have not been properly validated in many fire scenarios. For example, the built-in

combustion in FDS can not handle the flame structure expected in a turbulent deflagration. In the present study, we set about to asses the available models in the literature and implement the appropriate turbulence and combustion models to facilitate such simulation.

Chapter 3

Flames and combustion modelling

In this chapter, the very basics of flame structures are firstly introduced. This is followed by a brief introduction to turbulent combustion models for premixed and non-premixed for RANS. The chapter finishes with a detailed review of combustion models used in LES and several cutting edge numerical simulations of practical devices. Special emphasis is given to models, which are either most commonly used or are used in the following chapters of this thesis.

3.1 Properties of premixed, non-premixed and partially premixed flames

3.1.1 Laminar premixed flames

Premixed combustion requires that fuel and oxidizer be completely mixed for combustion to be allowed. The premixing is only possible at low temperatures. Under these conditions the reaction is unable to begin. Once fuel and oxidizer have been homogeneously mixed and a heat source is supplied it becomes possible for a flame front to propagate through the mixture. Flammable limits range typically from $\phi = 0.5$ to $\phi = 1.5$, where ϕ is the fuel-air ratio.

The structure of the premixed flame is illustrated in Fig 3.1. Fresh gases, fuel and oxidiser are previously "pre-mixed" and burnt gases (combustion products) are separated by a thin reaction zone (typical thermal flame thickness, δ_l^0, is about 0.1 to 1 mm). A sharp temperature gradient is observed (typical ratios between burnt and fresh gases temperatures are about 5 to 7). Another characteristic of the premixed flame is its ability to propagate towards the fresh gases. Because of the thermal gradient, fresh gases are preheated and then start to burn. The local imbalance between diffusion of heat and chemical consumption leads to the propagation of the front. The propagation speed s_l^0 of a laminar flame depends on various parameters (fuel and oxidizer compositions, fresh gases temperatures, pressure, etc...) and is about 0.1 to 1 m/sec

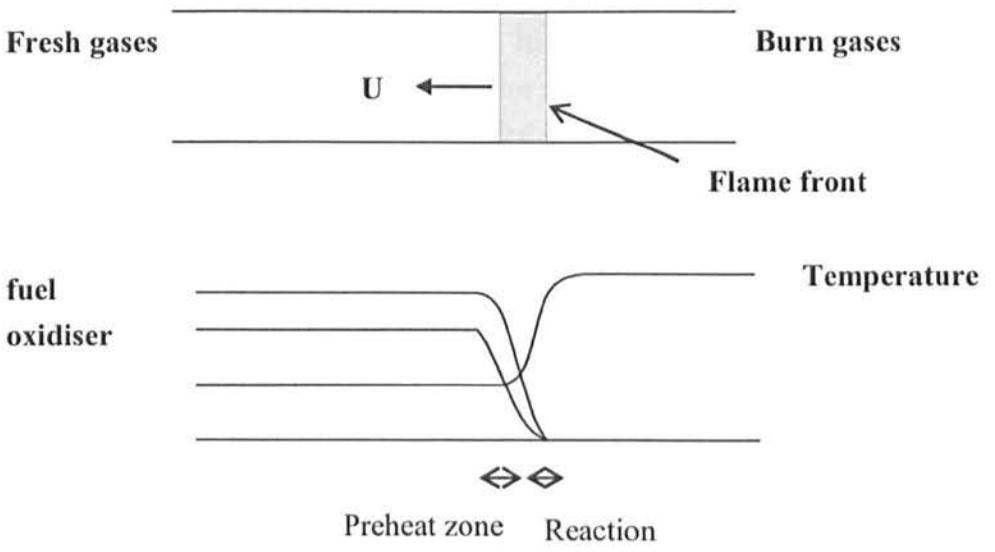

Figure 3.1. Structure of a laminar premixed flame.

The flame can be described using a progress variable c, such as c = 0 in the fresh gases and c = 1 in the fully burnt gases. The progress variable may be defined as a reduced temperature or a reduced mass fraction:

$$c = \frac{T - T_u}{T_b - T_u} \text{ or } c = \frac{Y_F - Y_F^u}{Y_F^b - Y_F^u} \tag{3.1}$$

where T, T_u and T_b are the local, unburnt gases and burnt gases temperatures, respectively. Y_F, Y_F^u and Y_F^b are the local, unburnt and burnt gases fuel mass fraction, respectively. Y_F^b is non-zero for rich combustion.

For unity Lewis number and without heat losses and compressibility affects, the two definitions of Eq. 3.1 are similar and the balance equation for c can be written as,

$$\frac{\partial(\rho C)}{\partial t} + \frac{\partial(\rho u_j C)}{\partial x_j} = \frac{\partial}{\partial x_j}(\rho D \frac{\partial C}{\partial x_j}) + \dot{w}_c \tag{3.2}$$

Eq. 3.2 can be written in different ways. Its propagative form uses the displacement of the iso-c surface. Hence, using the vector normal to the iso surface ($n = -\nabla c/|\nabla c|$), the total displacement speed can be divided into three terms, 1) the normal molecular diffusion speed, 2) tangential diffusion (due to the curvature of the flame front) and 3) due to the reaction rate $\dot{w}_c$. In a first approximation, 1) and 3) can be modelled using the laminar flame speed, s_l^0, while the effects of the curvature, 2), can be modelled by a wrinkling surface model. This later is analysed in more detail in the next paragraph and in chapter 6.

It is clear that the propagation velocity through the mixture is a very important quantity that needs to be known. Combustion models that are unable to predict this quantity clearly are incomplete and of little interest for practical purposes. Hence, the major concern of the premixed turbulent combustion models is to predict accurately this quantity throughout the mixture.

3.1.2 Premixed combustion regimes

The present physical analysis is based on the comparison of different time and length scales of the interacting turbulent flow and chemical reactions. In this examination, time and length scales are inspected to analyze premixed turbulent combustion regimes. This evaluation leads to combustion diagrams, which could be used to select and develop the relevant combustion model for a given situation [21, 23, 28, 184, 186, 258].

The turbulent flow is characterized by a Reynolds number comparing turbulent transport to viscous effects,

$$\mathrm{Re}_t = u' L_t / \upsilon \tag{3.3}$$

where u' is the velocity rms, L_t is the turbulent integral length scale and υ is the kinematic viscosity of the flow.

The Damkohler number compares the turbulent (τ_t) and the chemical (τ_c) time

scales:

$$Da = \frac{\tau_t}{\tau_c} \tag{3.4}$$

For turbulent premixed flames, the chemical time scale, τ_c may be estimated as the ratio of the laminar flame thickness, δ_l^0 and the laminar flame propagation speed, s_l^0. Following this, the Da number becomes,

$$Da = \frac{\tau_t}{\tau_c} = \frac{L_t s_l^0}{\delta_l^0 u'} \tag{3.5}$$

In the limit of high Da numbers (Da >>1), the chemical time is short compared to the turbulent one, corresponding to a thin reaction zone distorted and convected by the flow. The internal structure is not strongly affected by turbulence and may be described as a laminar flame element called "flamelet". The turbulent structures wrinkle and strain the flame surface. On the contrary, a low Da number (Da << 1) corresponds to a slow chemical reaction. Reactants and products are mixed by turbulent structures before reaction.

In order to identify the transition, another dimensionless number must be introduced. The Karlovitz number (Ka),

$$Ka = \frac{\tau_c}{\tau_k} = \frac{\delta_l^0 u_k}{l_k s_l^0} \tag{3.6}$$

where l_k and u_k are given in [234]. The Karlovitz number is used to define the Klimov-Williams criterion, corresponding to Ka = 1, between two combustion regimes. In general terms, for Ka > 1 the inner structure of the flame may be affected by the turbulent motion of the flow [186]. The next relation is found

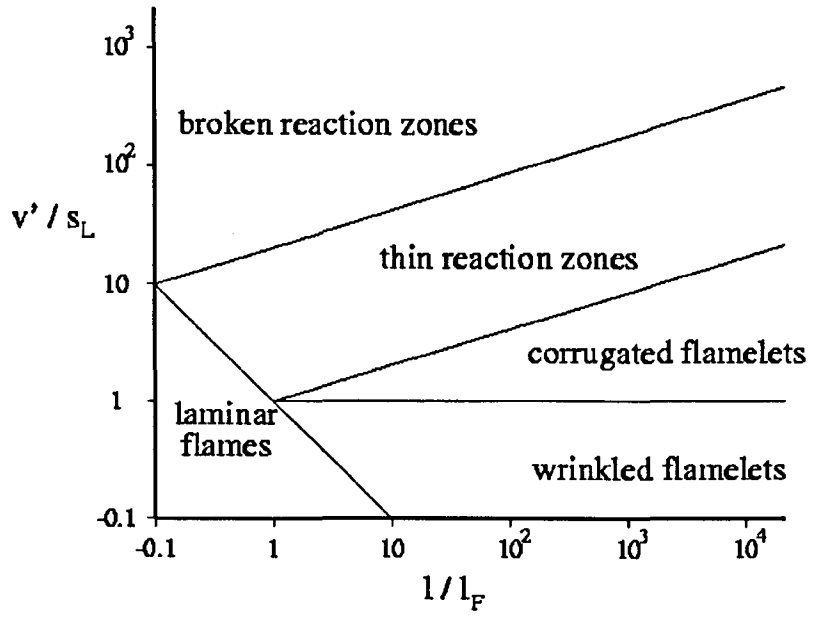

Figure 3.2. Turbulent premixed combustion diagram

between Re, Da and Ka numbers,

$$\mathrm{Re} = Da^2 Ka^2 \tag{3.7}$$

Following this analysis, three different premixed combustion regimes are classified:

1) Flamelet regime (thin wrinkled flame) for Ka < 1 and Da >>1.
2) Thickened wrinkled flame regime for 1 < Ka < 100.
3) Thickened flame regime for Ka > 100.

Fig. 3.2 shows a diagram indicating different combustion regimes for premixed flames. Following this classification, most practical applications correspond to the flamelet regime, which has significant repercussion on the development of premixed combustion models. Nevertheless, this analysis is only representative since the scale of the dimensionless quantities may differ up to one or two orders of magnitude. In the following chapters, the combustion systems are considered to be in the flamelet regime for premixed flames.

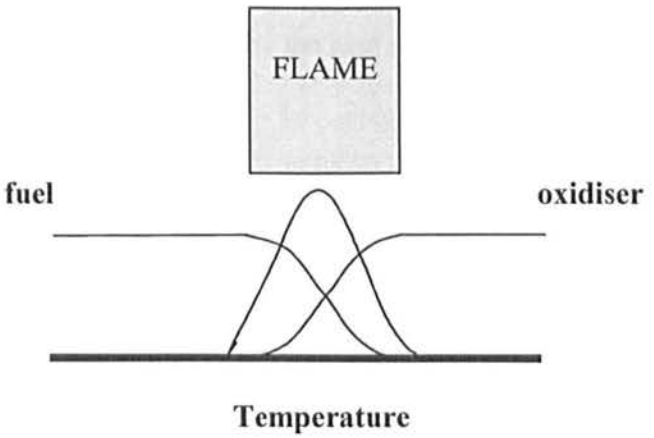

Figure 3.3. Structure of a laminar diffusion flame.

Some practical examples of premixed combustion are:

- In the spark-ignition engine, fuel and oxidizer are mixed by turbulence for a sufficiently long period of time before the electrical spark ignites the mixture.
- Stationary lean-burn gas turbines, the fuel is pre-vaporized and premixed with air before entering into the combustion chamber.
- Bunsen burners.

3.1.3 Non-premixed diffusion flames

Non-premixed combustion is sometimes called "diffusive combustion" or "combustion in diffusion flames" since diffusion is the rate-controlling process. The time needed for convection and diffusion is responsible for the mixing between fuel and oxidizer.

In laminar diffusion flames, fuel and oxidizer are on both sides of a reaction zone where the heat is released. The burning rate is controlled by the molecular diffusion of the reactants towards the reaction zone (Fig. 3.3).

In a counter-flowing configuration, the amount of heat transported away from the reaction zone is exactly balanced by the heat released by combustion (Fig. 3.4).

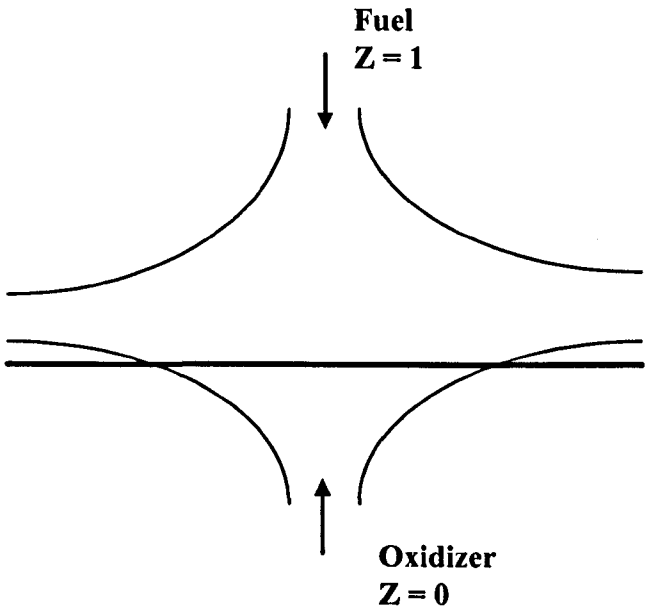

Figure 3.4. Counter-flowing fuel and oxidizer diffusion flame.

A steady planar diffusion flame with determined thickness is observed in the vicinity of the stagnation point. Increasing jet velocity will cause the heat fluxes leaving the reaction zone to be greater than the chemical heat production, leading to quenching. The structure of a steady diffusion flame, therefore, depends on ratios between characteristic time representative of molecular diffusion and chemistry [143]. The thicknesses of the mixing zone and of the reaction zone vary with these times. Diffusion flame does not have self-propagation mechanism and the thickness of the diffusion flame is not constant, but depends on local flow properties.

The internal structure of diffusion flames is usually discussed using the extent of mixing between fuel and oxidizer. It is firstly assumed that fuel and oxidizer molecular diffusivities are equal. Combining the transport equation for fuel and oxygen a conserved scalar, the mixture fraction Z is usually defined as,

$$Z = \frac{\phi \frac{Y_F}{Y_{F,0}} - \frac{Y_O}{Y_{O,0}} + 1}{\phi + 1} \tag{3.8}$$

where $Y_{F,0}$ is the fuel mass fraction in the fuel feeding stream. Similarly, $Y_{O,0}$ is the oxidizer mass fraction in the oxidizer stream and ϕ is the equivalence ratio defined as,

$$\phi = \frac{sY_{F,0}}{Y_{O,0}} \tag{3.9}$$

where $s = \nu_O W_O / \nu_F W_F$. Then, υ_i and W_i are the stoichiometric molar coefficients and species molar weight for the species i, respectively.

The mixture fraction follows the balance equation:

$$\frac{\partial(\rho Z)}{\partial t} + \frac{\partial(\rho u_j Z)}{\partial x_j} = \frac{\partial}{\partial x_j}(\rho D \frac{\partial Z}{\partial x_j}) \tag{3.10}$$

Following William and Bray [32, 257], the mass fractions and temperature balance equations may be reorganized into a new frame where Z is one of the coordinates (see). A local orthogonal coordinate system attached to the surface of stoichiometric mixture is introduced and the derivatives in the stoichiometric plane are denoted by $\perp$. For unity Lewis number and using Eq. 3.10,

$$\frac{\partial(\rho Y_i)}{\partial t} + \frac{\partial(\rho u_\perp Z)}{\partial x_\perp} = \rho\chi \frac{\partial^2 Y_i}{\partial Z^2} + \frac{\partial}{\partial x_\perp}(\rho D \frac{\partial Z}{\partial x_\perp}) - \rho D \frac{\partial}{\partial x_\perp}(\ln|\nabla Z|) \frac{\partial Y_i}{\partial x_\perp} + \dot{w}_i \tag{3.11}$$

where χ is the scalar dissipation rate of the mixture fraction Z:

$$\chi = D\left(\frac{\partial Z}{\partial x_j}\frac{\partial Z}{\partial x_j}\right) = D|\nabla Z|^2 \tag{3.12}$$

As χ^{-1} decreases, mass and heat transfers through the stoichiometric surface are enhanced.

When iso-Z surface curvatures are not too strong, the gradient measured along the stoichiometric surface is smaller than the gradient in the direction of Z, perpendicular to the stoichiometric surface, the balance equation for the mass fraction is reduced to:

$$\rho\frac{\partial Y_i}{\partial t} = \rho\chi\frac{\partial^2 Y_i}{\partial Z^2} + \dot{w}_i \tag{3.13}$$

Neglecting unsteady effects, the time derivative vanishes and for unity Lewis number, the flame structure is fully described by:

$$\rho\chi\frac{\partial^2 Y_i}{\partial Z^2} + \dot{w}_i = 0 \text{ and } \rho\chi\frac{\partial^2 T}{\partial Z^2} + \dot{w}_T = 0 \tag{3.14}$$

showing that the chemical reaction rate is directly related to the function $T(Z,\chi)$. Under these assumptions the diffusion flame is completely determined as a function of the mixture fraction, Z, and the scalar dissipation rate, χ.

Diffusion combustion is limited by two regimes corresponding to pure mixing (no combustion) of the reactants and infinitely fast chemistry (the combustion depends only on Z, but not on χ).

The infinitely fast chemistry hypothesis can not be invoked everywhere. This is the case in problems of ignition or close to stabilization zones, or more generally, when large velocity gradients are expected. This later approach is the flame structure used in the mixture fraction combustion model originally implemented in FDS.

The characterization of diffusion flames from the infinitely fast chemistry to the quenching of the flame is of vital importance to realistic combustion regimes. Making use of the counter-flow configuration and steadily increasing the velocity of the

feeding system and hence, increasing χ, makes the burning rate greater, until chemistry can not keep up with the large fluxes, then it extinguishes. The value of Da at extinction is nominated by Da_q. The response of the burning rate to variations of Da leads to the so-called "S" curve [257]. As shown in Fig. 3.5.

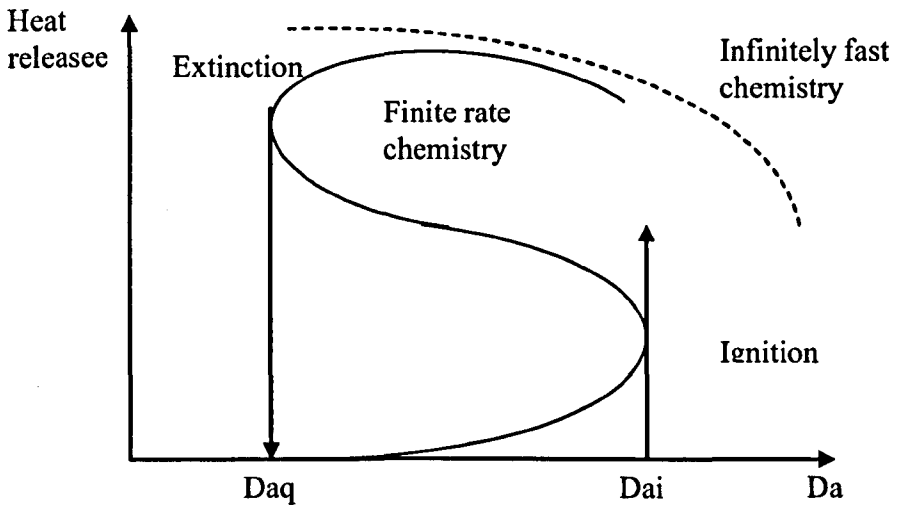

Figure 3.5. Generic response of the heat released by one-dimensional strained diffusion flame versus Da number. The dash line denoted infinitely fast chemistry.

3.1.4 Non-premixed combustion regimes

Two numbers have been used to identify premixed combustion regimes. In non-premixed turbulent combustion there is not characteristic speed because the flame does not propagate. Additionally, the thickness of the flame depends on the level of mixing developed between fuel and oxidizer and no reference length scale can easily be found for diffusion flames. This is supported by the various studies dedicated to this aim [15, 22, 32, 53, 57, 139].

The three major classifications of non-premixed flame are the following:

1. The turbulent flow regime is characterized by the Reynolds number and the chemical reaction by the Damkohler number [141].
2. The mixture fraction fluctuation $\widetilde{Z}''^2$ describes the turbulent mixing and the Da number characterizes the flame [32].
3. The ratio between turbulence intensity and flame speed is used alongside with the relation between the turbulent integral scale and flame thickness [22].

A laminar diffusion flame is determined with $Da = (\tau_c \chi_{st})^{-1}$, where $\chi_{st} = D|\nabla Z|^2_{st}$ and a characteristic mixing length of the order of $l_d = (D/\chi_{st})^{0.5}$. According to asymptotic developments the reaction zone thickness is about $l_r \approx l_d (Da)^{1/(\alpha+1)}$, where α is the order of the global one-step reaction.

When the velocity field fluctuates, the diffusion flame develops in two different ways. Firstly, the mixture fraction, Z, does not respond immediately to the fluctuations and a distribution of χ_{st} for different rates of strain appears. Secondly, for finite chemistry the burning rate does not follow the variations of χ_{st} leading to unsteadiness and modifying the burning rate.

Overall, the analysis given in [57] shows that, when Da number is larger than a minimum value, the flame front may be viewed as a steady laminar flame element and its inner structure is not affected by vortices. In the intermediate Da number range, strong unsteadiness effects are observed. Further in this study (chapter 5), the consequences of assuming steady flamelets are explained more in detail.

Fig. 3.6 shows these findings schematically. In practical combustion devices, the combustion regime may evolve from one regime to another according to flow conditions, velocity and scalar energetic spectrum. In a given burner, it could be expected to have three regimes: flamelets, strong unsteadiness and quenching.

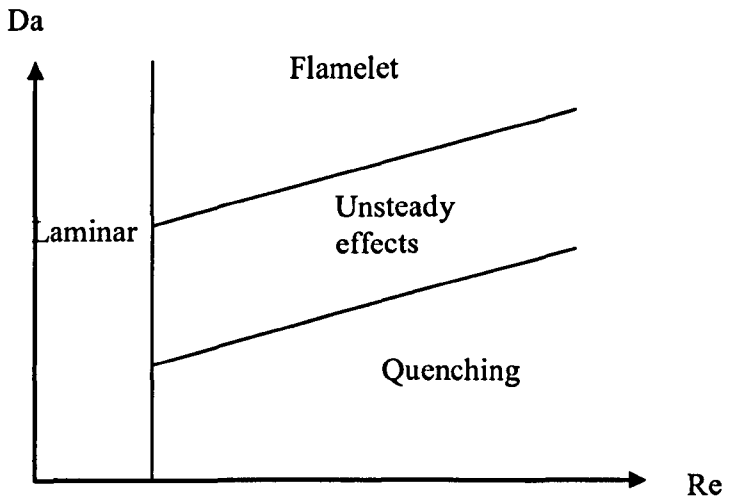

Figure 3.6. Schematic of non-premixed turbulent combustion regimes as a function of Da and Re numbers.

Some practical examples of non-premixed combustion are:

- Combustion in furnaces is mainly non-premixed for safety reasons. Fuel is supplied by jets or gaseous fuel, which entrains enough air from the surroundings, so that all the fuel can be burned.
- In diesel engines, the air is compressed by the piston before a liquid fuel spray is injected into the combustion chamber. The hot compressed air is entrained into the spray, leading to the liquid fuel break up, evaporation and auto-ignition.
- In aircraft gas turbine engines, non-premixed combustion occurs in the swirl-stabilized combustion zone downstream of the spray injector.
- Fire is another example of non-premixed combustion. If the fuel is a solid or a liquid, it can be first gasified by radiative flux from the fire, before mixing with the surrounding air. The mixing process is often dominated by buoyancy

rather than by forced convection as in jets and sprays.

3.1.5 Partially premixed flames

In terms of mixing, there are two extremes: premixed combustion, where fuel and oxidizer are completely mixed, and non-premixed combustion, where fuel and oxidizer are separated and burn when the come into contact.

In non-premixed combustion, some partial premixing of the reactants may exist before the reaction zone develops. Then, the pure diffusive layer, observed in diffusion flames, may not be present. Even more, some flames are stabilized by the recirculation of burnt gases, leading to stabilization mechanism controlled by the mixing between fuel, oxidizer and burnt gases. Sometimes, the mixing of the reactants are not pure fuel and oxidizer, but a mixing of these and the combustion products.

There are scenarios where partially premixed combustion is especially important.

- In combustion chambers, where the mixing is not homogeneous and the concentrations of fuel and oxidizer are randomly distributed in the domain, and ignition occurs.
- Occasionally, mixing between reactants can occur at low temperature and ignition does not start immediately, but further downstream [150].
- After quenching of the reaction zone, the reactants may mix leading to re-ignition and combustion in a partially premixed regime [78].

An example of the first group is aircraft gas turbines. Liquid kerosene is fed by an air-blast injector into the gas turbine combustion chamber and when the main injector is started, an inhomogeneous ignitable mixture is formed in its inlet. Another example is the partially premixed flame propagation in direct injection gasoline engines.

Another important manifestation of partially premixed combustion is the lifted

turbulent jet diffusion flame. In large industrial boilers, the lifted flame has the advantage of avoiding thermal contact with the burner to prevent erosion of the burner material. The disadvantage of this flame stabilization technique is that lifted flames blow off more easily than attached flames. Further discussion on this will be presented in chapter 6.

The typical and probably most studied partially premixed combustion configuration is the triple flame. In a laminar shear layer where the mixing between cold fuel and oxidizer develops, a diffusion flame may be stabilized at the splitter plate. In this case, combustion starts in a region where fuel and oxidizer have been mixed in stoichiometric proportion. The resulting premixed kernel tends to propagate towards fresh gases and contributes to the stabilization of the trailing diffusion flame. In a mixing layer configuration, the stoichiometric mixture evolves to a rich partially premixed flame in the direction of the fuel stream, while a lean partially premixed flame develops on the air side. See Fig. 3.7.

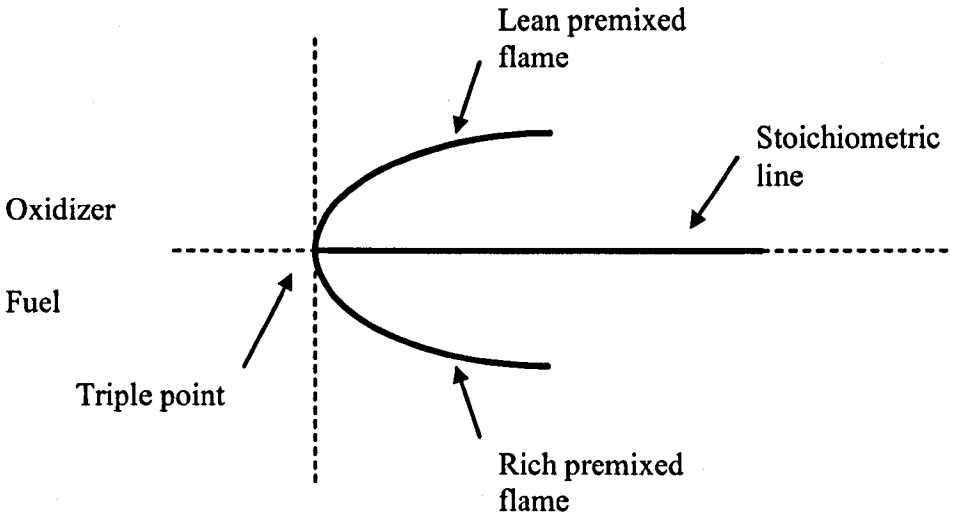

Figure 3.7. Schematic of a freely propagating triple flame

The two premixed flames are curved because their respective propagation speed decreases when moving away from the stoichiometric condition. The overall structure, composed by two premixed flames and a diffusion flame, is called "triple flame". Further discussion on the triple flame structure and the present LES prediction will be given in chapter 7.

3.2 Combustion Modelling

Turbulence is undoubtedly one of the most difficult problems of non-linear physics. In turbulent combustion, the difficulties are further compounded by the complexities of chemical kinetics and the strong non-linear coupling between turbulence and chemistry.

Some fundamental difficulties arise in dealing with the turbulence-chemistry interactions. Turbulence mixing is slower than chemical reaction and it involves large

spatial and time gradients. As a result, the system becomes very stiff due to the large differences between these two time scales. Chemical reactions cannot be evaluated from spatial or temporal mean values and are strongly coupled to molecular diffusion at the smallest scales of the turbulence.

If M chemical reactions are to be considered, then the chemical source term for species i becomes,

$$\dot{w}_i = W_i \sum_{K=1}^{M} (\eta''_{IK} - \eta'_{IK}) B_K T^{\kappa} e^{-\frac{E_K}{RT}} \prod_{J=1}^{N} \left(\frac{\rho Y_J}{W_J} \right)^{\eta'_{JK}} \tag{3.15}$$

where W_i is the molecular mass of species i, T is temperature, R is the universal ideal gas constant, E_K is the activation energy, and B_K is the frequency factor.

Furthermore, the heat release associated with combustion affects the turbulent flow, both from variation in the mean density and from the effects of local dilatation.

The mean heat release rate is one of the main quantities of practical interest that should be approximated by turbulent combustion models. The simplest and most direct approach is to develop the chemical rate in Taylor series, of Eq. 3.15, as a function of species mass fractions and temperature. This analysis is limited by its low accuracy and by the rapidly growing complexity of the chemistry. So, it is clear that new tools are necessary to approximate the source terms in the energy and species transport equation.

We classify the combustion turbulent models depending on the different approaches used, following Veynante and Vervisch [247]:

- The burning rate may be quantified in terms of turbulent mixing. When the Da number is large (general assumption in combustion models) the reaction rate is limited by turbulent mixing in terms of the scalar dissipation rate [29]. Therefore, χ plays a key role in the process

- The geometrical approach. The flame is observed as a thin geometrical surface. In this case the flame is treated as a geometrical division between fresh and burnt gases (premixed combustion) or fuel and oxidizer (non-premixed combustion) and using C or Z as scalar of reference, respectively. In this assumption, the flamelet modelling is generally accepted.

- In the statistical approach, mean values of scalars are extracted via the probability density function (pdf). This approach leads to the pdf modelling. Conditional Statistics are also linked to the geometrical analysis and to flame surfaces when the conditioning value is c* or Z_{st}.

Originally, combustion models were developed to work in a RANS context, where the time-averaged flow variables are solved. In this chapter, the basic concepts for combustion models and their implications will be discussed first. This will be followed by a discussion on combustion models within a LES frame.

3.2.1 Models for turbulent premixed combustion

Turbulent flame speed

The most important quantity in premixed combustion is the velocity at which the flame front propagates, normal to itself and relative to the flow into the un-burnt mixture.

Turbulent premixed flames may be described in terms of a global turbulent flame speed, S_T. From experimental data, the following expression has been proposed [1, 2]:

$$\frac{S_T}{s_l^0} = 1 + \theta(\frac{u'}{s_l^0})^n \tag{3.16}$$

where θ and n are two model constants, u' is the RMS velocity and s_l^0 is the laminar

burning velocity.

Unfortunately, S_T is not a fully well defined quantity [96]. Experiment exhibits a large scatter because they depend on various parameters such as chemistry characteristics, turbulence scales, flow geometry, etc. This model may suit particularly well to the LES approach [105, 228].

Eddy-Break-Up model

One of the earliest attempts to close the chemical source is due to Spalding [229]. This model is based on a phenomenological analysis of turbulent combustion assuming high Re >> 1 and Da >>1. The reaction zone is considered as a collection of fresh and burnt gases pockets, assuming an infinitely thin flame front. Accordingly, the mean reaction rate is mainly controlled by the turbulent mixing time and fast chemistry is also assumed. For practical simulations the following relation is used:

$$\overline{\dot{w}} = -C_{EBU}\overline{\rho}\frac{\varepsilon}{k}\frac{\overline{Y}_F}{Y_F^0}\left(1-\frac{\overline{Y}_F}{Y_F^0}\right) \tag{3.17}$$

where Y_F^0 is the initial fuel mass fraction in the reactant, C_{EBU} is a model constant in the order of unity, which needs to be "tuned" for specific applications, ε and k are the kinetic and dissipation turbulence, respectively.

The EBU model was found attractive because the reaction rate is simply written as a function of known variables without any other transport equation and is available in most CFD codes. The modelled reaction rate does not depend on chemical characteristics and assumes a homogeneous and isotropic turbulence. However, EBU tends to over predict the reaction rate, especially in highly strained regions. This model was primarily formulated for premixed combustion.

Bray-Moss-Libby model

This model is known as the BML model and it was primarily developed by Moss and Bray [173]. It has been the subject of a large amount of work leading to many improvements. Combining a statistical approach using probability density function and a physical analysis, this model evidenced some special features of turbulent premixed combustion (counter-gradient turbulent transport, flame turbulent generation, etc.).

The basic idea of the BML model is to presume the probability density function of the progress variable c at a given location as a sum of fresh, fully burnt and burning gases contributions.

$$\overline{P}(c^*,x,t) = \alpha(x,t)\delta(c^*) + \beta(x,t)\delta(1-c^*) + \gamma(x,t)f(c^*,x,t) \qquad (3.18)$$

where α, β and γ denote the probability to have at a location (x,t), fresh gases, burnt gases and burning gases, respectively, δ is the Dirac delta and c^* is the progress variable.

Considering normalization of the probability density function such as $\int_0^1 \overline{P}(c^*,x,t)dc^* = 1$ leads to the following relation:

$$\alpha + \beta + \gamma = 1 \qquad (3.19)$$

$$\int_0^1 f(c^*,x,t)dc^* = 1 \qquad (3.20)$$

with $f(0) = f(1) = 0$.

The balance equation for the progress variable, c, may be written as:

$$\frac{\partial(\rho c)}{\partial t} + \frac{\partial(\rho u_j c)}{\partial x_j} = \frac{\partial}{\partial x_j}(\rho D \frac{\partial c}{\partial x_j}) + \dot{w}_c \qquad (3.21)$$

This equation is averaged and the mean reaction rate is:

$$\overline{\dot{w}}_c(x,t) = \gamma(x,t)\int_0^1 \dot{w}_c(c) f(c,x,t) dc \tag{3.22}$$

Using Da and Re numbers two cases arise:

- Re >> 1 and Da >>1. The combustion is controlled by turbulent transport and the reaction layer is assumed infinitely thin. Accordingly, $\gamma << 1$, this simplification leads to the well know BML source term formulation.
- Re >> Da or Re > Da >>1. Firstly, the thickness of the flame cannot be neglected. Secondly, the chemical source term is not fast in comparison with the turbulent time scale.

Herein, we consider the first case. The objective is to find an expression for α and β for a given location through which the flame front passes. Under this assumption, α and β are determined as a function of the Favre average progress variable $\tilde{c}$:

$$\overline{\rho c} = \overline{\rho}\tilde{c} = \int_0^1 \rho c \overline{P}(c) dc = \rho_b \beta \tag{3.23}$$

where ρ_u is the burnt gases density.

After some development,

$$\alpha = \frac{1-\tilde{c}}{1+\tau\tilde{c}}; \beta = \frac{(1+\tau)\tilde{c}}{1+\tau\tilde{c}} \tag{3.24}$$

where $\tilde{c}$ is the Favre averaged progress variable and τ is the reaction heat release factor, defined as $\tau = \rho_u/\rho_b - 1$, where ρ_u is the fresh gases density.

The probability density function $\overline{P}(c)$ is determined and depends only on the mean progress variable $\tilde{c}$ and τ.

Starting from the conservative and non-conservative forms of the progress variable balance equations and subtracting the balance equation for c^2, leads to the balance equation for c(1-c). Accordingly, c(1-c) = 0 resulting,

$$2\rho D\nabla c.\nabla c = 2c\dot{w}_c - \dot{w}_c \tag{3.25}$$

And averaging,

$$\overline{\rho D\nabla c \cdot \nabla c} = (2C_m - 1)\overline{\dot{w}_c} \tag{3.26}$$

And, it yields to the following expression for $\overline{\dot{w}}$:

$$\overline{\dot{w}_c} = 2\frac{\overline{\rho\chi}}{2c_m - 1} \tag{3.27}$$

where,

$$c_m = \frac{\int_0^1 c\dot{w}f(c)dc}{\int_0^1 \dot{w}f(c)dc} \tag{3.28}$$

where f is the pdf of the burning gases. c_m is introduced and characterizes the chemical reaction. Following from Eq. 3.27

$$\overline{\rho\chi} = \overline{\rho\chi} = \overline{\rho D\nabla c \cdot \nabla c} \tag{3.29}$$

The mean reaction rate is related to the dissipation rate, χ, describing the turbulent mixing.

A transport equation may be proposed for the scalar dissipation rate, χ, or a linear relaxation of the fluctuations generated by micromixing.

Models based on Geometrical description

The flame front is described here as a geometrical surface. The analysis is linked to the assumption of thin flames, the surface acts as an interface between fresh and burnt gases. There are two main approaches:

1) G-field equation
2) Coherent flamelet and flame surface density.

G-field equation

In this approach, the so-called G-field equation is developed. A fixed value of $G=G_0$ determines the position of the flame which propagates through the mixing [258]. The G-equation may be written as:

$$\frac{\partial G}{\partial t}+\vec{u}\cdot\nabla G = w_G|\nabla G| \tag{3.30}$$

where w_G is the propagation speed of the G-field.

This description of premixed combustion has some attractive aspects. Firstly, there is no need to resolve the internal flame structure: only the G-field, which is generally thicker than the flame front, needs to be solved on the computational grid. Secondly, this method is attractive for its low computational cost, which can be handled by DNS calculations.

The effect of thermal expansion must be explicitly incorporated into the displacement velocity, following this correction,

$$w_G = \frac{\rho_u}{\rho} w_u \tag{3.31}$$

Another important feature is the coupling needed between the burning velocity and the source terms of the balance equations for species and temperature. The reactants consumption (S_c) and the heat release rate ($\dot{w}$) are related through:

$$\rho_u S_c = \int_{-\infty}^{\infty} \dot{w} dn \tag{3.32}$$

where dn is the flame front normal coordinate. There is a relation between S_c and w_G, but it is not a definitive one. These two can be different especially when the premixed flame is curved.

The main disadvantage of this approach is the closure the G propagation velocity, w_G, which is related with the laminar or turbulent burning velocity. In other words, the coupling between the consumption speed and the displacement speed is a very key point in G-field modelling.

Probably, the most used technique is the one used by Piana et al. [190]. In their approach, the heat release rate is estimated from the G-field. Eq. 3.33 is the balance equation for turbulent flame brush:

$$\frac{\partial \tilde{G}}{\partial t} + \tilde{u} \cdot \nabla \tilde{G} = \frac{\rho_u}{\bar{\rho}} S_T \left| \nabla \tilde{G} \right| \tag{3.33}$$

where the turbulent flame speed, S_T, must be modelled.

The overall turbulent flame is only viewed as a propagating surface without any detail about the inner structure of the flame. Nevertheless, a model is needed for S_T, some examples can be found in [32, 186].

Coherent flamelet and flame surface density.

The coherent flamelet model is based on the concept that the mean chemical reaction rate per unit volume $\overline{\dot{w}}$ is the product of two quantities: the reaction rate per unit area of the flamelets $\dot{\Omega}_i$ and the average flamelet area per unit volume Σ.

$$\overline{\dot{w}} = \dot{\Omega}_i \Sigma \tag{3.34}$$

where $\dot{\Omega}_i$ is the mean local burning rate per unit of flame area integrated along the normal direction to the flame surface and Σ is the surface density function.

$\dot{\Omega}_i$ is related to the properties of the local flame front and is estimated from a prototype laminar flame, incorporating more or less complexity. For instance, one may consider a planar laminar flame, steady or not steady flame, curvature effects, etc.

The main advantage of this formulation is that it decouples the chemical description ($\dot{\Omega}_i$) from the flame/turbulence interaction (Σ). The flame surface is convected, diffused, curved by the velocity filed. In general, these models assume that the chemical reactions occur in very thin layers (Da >> 1) and therefore the flamelet theory is invoked.

The flame surface density may be obtained from algebraic relations or from a balance equation. This last approach was proposed by Marble and Broadwell [153] for non-premixed turbulent flames. More derivations were obtained from geometrical consideration [38, 237] and from an statistical point of view [110, 204, 245].

An algebraic expression for Σ has been developed by Bray [30], which depends on the progress variable, the chemical reaction and the flame wrinkling. The later needs a closure model [8, 9, 130].

The local reaction rate per unit flame area $\dot{\Omega}_C$ from laminar flame speed s_l^0 is generally assumed as $\dot{\Omega}_C = \rho_u s_l^0$, where ρ_u is the fresh gases density.

In premixed combustion, the flame surface density Σ of the iso-c* surface can be estimated from the conditional gradient of c:

$$\Sigma(c^*) = \overline{|\nabla c| \delta(c - c^*)} = \overline{(|\nabla c| \| c = c^*)} \overline{P}(c^*) \qquad (3.35)$$

where $\delta(c-c^*)$ is a local measure of the probability and $\overline{(|\nabla c| \| c=c^*)}$ is the conditional average of $|\nabla c|$ for $c=c^*$ and $\overline{P}(c^*)$ is the probability to find $c=c^*$ at a given location. From this definition and the balance equation for c, an exact equation for the flame surface density may be derived. This derivation is similar to the derivation of the balance equation for the probability density function (pdf) [245].

This surface balance equation Σ is unclosed and needs models. There are several models available in the literature; some of these are the following:

- The CPB model [39]
- The coherent flame model (CFM) [153]
- The MB model [152]
- The CD model [46]
- The CH model [47]

The details are not discussed here, but, all the closures for these models have strong similarities. A comparison between them can be found in [71].

3.2.2 Models for Non-Premixed Turbulent Combustion

The modelling of turbulent diffusion flames relies on assumptions made on the chemistry and the turbulent field. The most common simplifications are:

- Infinitely fast chemistry. In this case mixed is burnt or, in other words, the reaction rate does not depend on the strain caused by the turbulent flow. The species concentration depends only on the mixture fraction
- Finite rate chemistry assumes a local diffusive-reactive balance. The scalar dissipation rate, χ, takes part in the chemistry. Typical example is the flamelet assumption.
- Finite rate chemistry with independent calculation of the conditioned statistic variables. The reaction rate is closed separately. For instance, pdf and Conditional Moment Closure (CMC).

Eddy dissipation model

The Eddy Dissipation Model (EDC) is a direct extension to non-premixed flame of eddy break up (EBU) closure [148]. The burning rate is calculated according to:

$$\overline{\rho \dot{w}_F} = \alpha \bar{\rho} \min(\widetilde{Y}_F, \frac{\widetilde{Y}_O}{s}, \beta \frac{\widetilde{Y}_P}{1+s}) \tag{3.36}$$

where α and β are adjustable parameters and s is the stoichiometric ratio The reaction rate is limited by the minimum concentration species. $\widetilde{Y}_P$ is introduced to account for the contribution of the products to ignite the mixture.

This model does not respect the response of diffusion combustion in mixture fraction space and its use is only justified from a practical point of view.

Presumed pdf: Infinitely Fast Chemistry Model.

In this approach, a piecewise description is used,

$$Y_F = Y_F^{IFCM}(z), Yo = Y_O^{IFCM}(z), T = T^{IFCM}(z) \tag{3.37}$$

relating the fuel and the oxidiser mass fractions, and the temperature to the mixture fraction, mean quantities can be directly obtained with β-pdf assumed distribution. The expression for $\widetilde{Y}_F$ reads,

$$\overline{Y}_F^{IFCM} = \int_0^1 Y_F^{IFCM}(Z^*) P(Z^*; x, t) dZ^* \tag{3.38}$$

and similar for Y_F and T.

Infinitely Fast Chemistry Model (IFCM) is a two-equation model for non-premixed combustion. It is very popular and is usually coupled with low Match number solution. IFCM is an interesting tool to predict a first approximation. The piecewise relations only work properly when Da >> 1. However, this model is not capable of

predicting ignition or quenching events.

Flamelet modelling

Experiments in jet flames and direct numerical simulations (DNS) suggest that situations exist where the chemistry is fast, but not infinitely fast [11]. In these measurements and calculations, the response of the flame in mixture fraction space lies in the vicinity of the curves given by Y_F^{IFCM}.

For a given state of mixing in the turbulent flow, thus given Z and χ, flamelet models are derived assuming that local balance between diffusion and reaction is similar to the one found in a laminar flame with the same values of Z and χ.

The two parameters, which control the flamelet models, are the mixture fraction Z and the scalar dissipation rate χ.

Following the same concept used by pdf models, the mean quantities are calculated by:

$$\widetilde{Y}_i = \int\int Y_i^{SLFM}(Z^*, \chi^*) P(Z^*, \chi^*; x, t) d\chi^* dZ^* \tag{3.39}$$

where $Y_i^{SLFM}(Z^*, \chi^*)$ is the local flame structure in Z space and $P(Z^*, \chi^*; x, t)$ is the statistic of the mixture fraction. As non-time dependence is considered, this model is called Steady Laminar Flamelet Model (SLFM).

The methodology used in SLFM is similar to the one used in IFCM, but with the inclusion of χ . This extra dimension supplies the ability to deal with non-infinitely fast combustion and thereby to predict extinction and ignition phenomena. The inputs of SLFM are Z, Z'^2 and χ.

Assuming within the turbulent flow thin quasi-one-dimensional structures convected and stretched by fluid motions, and neglecting higher order terms, the equation for the species and temperature become:

$$\frac{\partial Y_i}{\partial t} = \dot{w}_i + (\frac{\chi}{Le_i})(\frac{\partial^2 Y_i}{\partial Z^2}) \tag{3.40}$$

$$\frac{\partial T}{\partial t} = -\sum_{n=1}^{N} \frac{h_n \dot{w}_n}{Cp} + \chi(\frac{\partial^2 T}{\partial Z^2}) \tag{3.41}$$

where Le_i is the Lewis number for species i, h_n is the specific enthalpy and Cp is the specific heat capacity. Considering steady solutions (SLFM) and selecting a given value of χ; yields,

$$\dot{w}_i = -\frac{\chi}{Le_i}\frac{\partial^2 Y_i}{\partial Z^2} \tag{3.42}$$

The solution of Eqs. 3.40 and 3.41 for given concentration and temperature boundary conditions, and various χ provides a Flamelet Library. A variety of techniques are available to construct these libraries [215].

In SLFM, the characteristic time required to balance diffusion and reaction terms in equations 3.40 and 3.41 is considered much smaller than any other time scale in the flow. Hence, many aspects can be drawn:

- Eq. 3.42 has been obtained by neglecting diffusion in the direction tangential to the iso-Z_{st} surface, considering that the gradient in the perpendicular direction are much larger that those within the iso-Z-surface.
- There are issues related to the multi-dimensional character of diffusion flames. Straining cannot be uniformly distributed along the flame sheet, leading to flamelet interactions when the distribution of χ is non-uniform in iso-Z_{st} [244].
- Boundary species may be different from pure air or fuel and, in order to tabulate, the flamelet may have to account for partial premixing [79].
- Unsteadiness is also an important aspect. Time dependent flamelets have been used to include unsteady effects [101, 272]. Unsteady flamelets were used

[157] to simulate extinction and re-ignition in a turbulent jet flame; history effects were included using a Lagrangian time measured along the stoichiometric line. DNS databases to study the reactive/diffusive layer in terms of flamelets can be found in [41, 57, 62, 149, 165]. These studies demonstrate to which extent the unsteadiness can affect the flamelets.

The flamelet approach has been taken up widely by modellers because it provides a simple and easy-to-implement physical picture of the turbulent flame structure. However, strong arguments have been put forward against flamelet models. These include the effects of variations in scalar dissipation through flamelets, and the influence of the neglected advection terms. It is clear that SLFM cannot remain valid close to extinction or re-ignition, where unsteady effects are important. Even more, the whole question about the range of applicability is an issue not yet resolved.

As pointed above, a relevant point in flamelet theory is the response of the turbulent flame when quenching zones develop. DNS studies have shown that extinction may occur at larger or smaller Da number than Da_q (extinction value predicted by flamelet theory). The DNS results of Favier and Vervisch [78] have shown that the scalar dissipation rate controlling the growth of the flame hole is lower than the one that should be applied to first quench the flame. Another of their DNS calculation [76] shows that a hole develops at the predicted χ, but once the hole is established, χ is smaller than χ_q. This was attributed to some partially premixed combustion at the edge of the hole. In order to overcome these difficulties, the SLFM has been modified to incorporate unsteady effects on the flamelets, which play an essential role in extinction and re-ignition [101, 183]. The modified SLFM has included a Lagrangian point of view [157, 187] , associating the strong fluctuation of the scalar dissipation rate, and to accommodate the effects of the advection terms parallel to the surface mixture fraction.

MIL model

MIL ('Modele Intermittent Lagrangien' or Lagrangian Intermittent Model) was proposed by Borghi [22].

As in SLFM, MIL incorporates the flame structure in Z space. Arguing that mixing occurs without reaction for large values of χ, the flame structure is constructed from two possibilities of diffusion combustion: Mixing without reaction (before ignition) and infinitely fast chemistry (after ignition). The transition between regimes is controlled by a time delay, τ_{ig}. τ_{ig} is associated with the scalar dissipation rate χ_{ig} ($\tau_{ig} \approx \chi_{ig}^{-1}$). The main objective of MIL is to account for unsteadiness in the coupling between small-scale diffusion and chemistry by means of the spectral distributions of micromixing times. For a given mixing time, τ, smaller than τ_{ig}, ignition does not take place and contributes to pure mixing. On the other hand, for $\chi < \chi_{ig}$ mixing is slower than chemistry and combustion develops. More details and model's applications are given in [210].

Conditional Moment Closure (CMC)

IFCM, SLFM and MIL suggest that non-premixed turbulent flames may be conveniently studied using conditional averaging in the mixture fraction space, Z. Conditional Moment Closure (CMC) approach proposes to solve the balance equations for obtaining Q_i [16, 123, 125]. CMC is a joint approach of two techniques, a probabilistic description of the turbulent flow, as it is the pdf, and mixture fraction-based models (fast chemistry and flamelets).

The balance equation reads,

$$\overline{(\rho \mid Z = Z^*)}\frac{\partial Q_i}{\partial t} = -\overline{(\rho u_i \mid Z = Z^*)}\frac{\partial Q_i}{\partial x_i} + \overline{(\rho\chi \mid Z = Z^*)}\frac{\partial^2 Q_i}{\partial Z^{*2}} + \overline{(\dot{w}_i \mid Z = Z^*)} \quad (3.43)$$

where Q_i can be either temperature or species mass fraction, $\overline{(\rho \mid Z = Z^*)}$ is the conditional term representing the value of ρ when $Z = Z^*$. In Eq. 3.43, three terms of the RHS need closure.

In the simplest version of CMC, the fluctuation of chemical source are neglected leading to a first order approximation of the source term,

$$\overline{(\dot{w}_i \mid Z = Z^*)} = \dot{w}_i(\overline{(Y_1 \mid Z = Z^*)},....,\overline{(Y_N \mid Z = Z^*)},\overline{(T \mid Z = Z^*)}) \qquad (3.44)$$

The second term of RHS, the conditional scalar dissipation rate, (Eq. 3.43) also needs closure. This conditional mean is an important ingredient of the pdf transport equation and micromixing models are available. Similarly, when the pdf is known via its presumed β-shape, the conditional value χ may be approximated by $\widetilde{P}(Z^*)$ to obtain $\overline{(\rho\chi \mid Z = Z^*)}$ [92].

The first RHS term can be easily modelled by a first order approximation and it is not very important in the general balance.

CMC has same attractive points:

- The approximation of the source term by Eq 3.44 approximates much better the heat release rate than unconditional averages. Similarly, it can be improved to take into account the concentration and temperature fluctuations in the burning rate by using a second order CMC.
- It has been measured in jet pilot flames that the conditional quantities do not depend strongly on the radio. Thus, two dimensions can be avoided in the conditional dimension space and computation is much less complicated.
- Theoretically, it can deal with events such as extinction, ignition and soot formation.

The CMC methodology is as follow:

The CMC equations are solved in parallel with a computational fluid dynamic (CFD) solver for the averaged velocity and mean, Z and $Z^{'2}$. The CFD code delivers to the CMC solver the velocity field and Z, then $\rho u_i \mid Z = Z$ and $\overline{(\rho\chi \mid Z = Z^*)}$ are evaluated by the CMC solver and the conditional variables are calculated. Then, CMC returns the conditional average density to the CFD code where it is used to calculate the unconditional average density, $\overline{\rho}$:

$$\overline{\rho} = \int_0^1 (\overline{\rho \mid Z = Z^*}) P(Z^*) dZ^* \tag{3.45}$$

Accordingly, for the species mass concentrations,

$$\widetilde{Y}_i = \int_0^1 (\overline{Y_i \mid Z = Z^*}) P(Z^*) dZ^* \tag{3.46}$$

On the other hand, the disadvantage of the CMC approach lays in its computational cost. The solution of the set of conditional equations present a stiff system and the coupling with the CFD solver can considerably increase the running time. This problem is accentuated if other dimensions such as time and 3D are added to the conditional system. Even more, the conditional dissipation rate $(\overline{\rho\chi \mid Z = Z^*})$ might not be easy to close.

In flames with significant local extinction and re-ignition it was found that the first-order closure is not sufficiently accurate. Therefore, second-order closure is necessary to incorporate the effects of conditional variances and co-variances in the conditional reaction rates. This may be computationally expensive, since a set of new equations are required.

An alternative to the second order closure is to use double conditioning on both mixture fraction and sensible enthalpy.

CMC is showing some success in predicting lifted diffusion flames [65, 118], the classical model problem of partially premixed combustion.

Pdf modelling

In premixed turbulent combustion modelling, BML assumes closures a bimodal probability density function of the progress variable. In non-premixed flames, using infinitely fast chemistry, steady laminar flamelet or conditional moment closure, the pdf of the mixture fraction is assigned a beta-distribution shape. The goal of the pdf modelling is to relax the pdf distribution regarding its shape.

The pdf transport equation predicts the probability to find certain values of reactive scalars such as temperature and the mass fractions between a limited ranges. In this approach, the probability vector is considered and a transport equation is derived for the probability density [144, 206].

We do not aim to study extensively the pdf transport equation, but it can be said that there are terms, which contain gradients of quantities conditioned on the values of velocity and composition, that need to be closed.

The predictive capability of pdf methods for turbulent combustion depends on the quality of the models that can be constructed for the unclosed terms. Good results have been obtained for slow chemistry [102].

In pdf methods, the turbulent combustion closure is modelled considering all the values taken by species and temperature in mixture fraction space. The chemical source term can be treated exactly for arbitrarily complex chemical kinetics and this is, probably, the best feature of the pdf approach.

From a numerical point of view, the most apparent property of the pdf transport equation is its high dimensionality. This makes this method intractable for ordinary finite differences or finite volumes. Consequently, almost all the numerical implementations of pdf for reacting flows are based on the Monte-Carlo techniques.[202, 203].

One of the major issues in the pdf approach is capturing correctly the micro-mixing and viscous effects. In this regard, many models are available such as IEM, LMSE, GIEM, etc. For more detail see [70, 82, 238].

pdf methods have also been applied to the challenging bluff-body stabilised jet flames [59] and to the swirling bluff-body flames [155].

pdf methods have reached the level of maturity that they are available in commercial CFD codes for use both in research and in industry.

3.2.3 Large Eddy Simulation and combustion models

Reynolds Averaged Navier-Stokes (RANS) equations employ turbulent transport approximations with an effective turbulent viscosity that is much larger than the molecular viscosity. This tends to suppress instabilities and makes the time-averaged flow very 'smooth'. These instabilities can be important and affect the flow behaviour at larger scales, particularly in reacting flows.

Large eddy simulation (LES) does not intend to resolve all turbulent length scales, but a fraction of the larger energy scales within the inertial range. Modelling is then applied to represent the smaller unresolved scales, which contain only a small fraction of the turbulent kinetic energy. The model for the smaller scales is called sub-grid model. In deriving the basic equations, the Navier Stokes equations are spatially filtered with a filter of size Δ, which is of the size of the grid (or a multiple) in order to remove the effect of the small-scale fluctuations. As a result, unresolved turbulent fluxes appear at the sub-grid scale, which need to be closed by models. A summary of sub-grid turbulence models is presented in chapter 4.

The main challenge faced in modelling combustion with LES, as similar to RANS, is that chemical reaction rates are usually highly non-linear functions of temperature, density and species mass fractions. In this regard, LES meets the same difficulties as RANS because the coupled process of chemistry-turbulence occurs at the smallest-unresolved scale and must be modelled. Probably, the challenge on the models is reduced, as the amplitudes of the sub-grid fluctuation are less than those presented by RANS.

Nevertheless, the intrinsically unsteady nature of LES seems to be particularly beneficial for the bluff-body and swirling flames, in which such large-scale unsteady motions are evident.

Substituting the LES-filtered temperature, density, and mass fraction into the original Arrhenius equation , yields:

$$\overline{\dot{w}}_F = A\overline{\rho}^2 \widetilde{Y}_F \widetilde{Y}_O \exp\left(-\frac{E}{R\widetilde{T}}\right) \tag{3.47}$$

where $\widetilde{X}$ is the Favre-filtered quantity.

Such simplified expression assumes a perfect mixing at sub-grid scale level and implicitly suppose that turbulent time scales are shorter than the chemical time scales. This assumption is not valid for most combustion applications and generally provides a very poor estimate for filtered reaction rates.

Another idea, not widely used, is to extent the RANS model, EBU, originally intended for premixed combustion, to LES for non-premixed combustion. The sub-grid scale Eddy-Break-Up model is written as [85, 86]:

$$\overline{\dot{w}}_F = C_{EBU}\overline{\rho}^2 \frac{1}{\tau_t^{SGS}} \frac{\widetilde{Y}_F}{\widetilde{Y}_F^0}\left(1-\frac{\widetilde{Y}_F}{\widetilde{Y}_F^0}\right) \tag{3.48}$$

where τ_t^{SGS} is a sub-grid turbulent time scale.

Nevertheless, this model suffers from the same drawbacks as its RANS version. Firstly, the reaction rate is independent of chemical reaction and overestimates the reaction rate and secondly, the determination of C_{EBU} is not straightforward.

Because of the substantial computational requirements of LES, there has been a tendency to use quiet simple turbulent-combustion sub-models, but we are beginning to see combinations of LES with more complex models such as EDM [90], pdf [224] and CMC [34]. These models were originally developed for RANS but their application to LES seems to be encouraging.

Non-premixed combustion in LES

Linear eddy Model

The Linear eddy Model (LEM) was firstly developed by Kerstein [114-116]. It is based on one dimensional stochastic description of turbulent stirring processes. In a LES framework, this analysis is used to describe the sub-grid process.

This sub-grid phenomenon is modelled by a 1-D scalar field and it may be interpreted as the effect of a single turbulent structure of size l located at x_0. A turbulent mixing is then simulated using a vortex of size l (smaller than the LES grid size) and at a frequency specified for a given spectra.

This approach provides a direct estimation of filtered mass fraction and temperature without solving the balance equations. Nevertheless, the mass fraction and the temperature transport through the cells' faces must be calculated. The LEM can be very time consuming because one-dimensional DNS calculations are required in each computational cell.

This approach appears to be well suited for non-premixed combustion, especially when the combustion is mixing controlled [37, 156, 164, 167].

Sankaran and Menon [221] recently applied a LEM combustion model within a LES framework to simulate a 3-D premixed flame in the thin-reaction-zone regime. A finite-rate, one-step methane-air chemistry with non-unity Lewis number was used. They also captured the thin reaction zone even when the preheated zone is broadened by small eddies.

Probability density function

Pope [205] introduced the concept of "filtered density function" (FDF) which is essentially the pdf of SGS scalar variables. Colucci et al. [51] developed a systematic approach for the FDF balance equation and compared results with DNS calculations.

This approach takes advantage of the closure proposed for RANS. Cook and Riley [52, 54] proposed a presumed shape beta function pdf formulation, avoiding both the pdf and FDF balance equations, and called it Large Eddy Probability Density Function (LEPDF). It uses the filtered mean and the sub-grid variance of the mixture fraction to achieve closure for non-premixed combustion in the following form:

$$\widetilde{Y}_i = \int_0^1 Y_f(Z)\widetilde{P}(Z)dZ \tag{3.49}$$

where $\widetilde{P}(Z)$ is the sub-grid probability density function.

It was found that a β function, based on the filtered mixture fraction, $\widetilde{Z}$ and the its sub-grid fluctuations $\widetilde{Z}''^2$, predicts very accurately $\widetilde{P}(Z)$.

A model to describe the variance $\widetilde{Z}''^2$ without adding a balance equation is proposed as:

$$\widetilde{Z}''^2 = C_Z(\overline{\widetilde{Z}^2} - \overline{\widetilde{Z}}^2) \tag{3.50}$$

where $\overline{Q}$ is a similarity filter and C_Z is a model constant.

Alternatively, there are available dynamic procedures for estimating C_Z [212-214]. It is generally accepted that a good prediction of the mixture fraction variance is obtained using this approach and avoiding an extra balance equation.

Optionally, a transport equation for the sub-grid scale pdf may be derived, but this was not extensively tested.

In an early version of LEPDF, $Y_f(Z)$ in Eq. 3.48, followed the equilibrium model. In later stages, the conditional values of the reactive scalars were taken from steady state flamelet theory, including the effect of turbulent in the combustion through the scalar dissipation rate, χ .This model rendered reasonable results [54].

De Bruyn Kops et al. [60] performed a full LES calculation using the balance equations of the filtered and variance of the mixture fraction. Presumed beta-shape pdf distribution was used for the sub-grid scale mixture fraction fluctuations. The model correctly reproduces the filtered species concentrations obtained from DNS data.

More recently, Raman and Pitsch [208] performed a LES-FDF of a bluff-body-stabilized non-premixed flame. They developed a methodology called recursive filter-refinement in order to find out the optimal LES mesh size. They found a good correlation with experimental evidence. A new hybrid large-eddy simulation and Lagrangian FDF approach was developed by Raman and Pitsch [209] using finite-rate-chemistry-based modelling. They showed that FDF scalars at select location are well approximated by the presumed beta function used in typical combustion LES.

A turbulent opposed-jet flame simulation was carried out by Geyer et al. [89] using a pre-calculated table or a look up table based on flamelets. They arrived at the conclusion that LES predicts a good overall agreement, although some discrepancy was found on the scalar dissipation rate.

Similarly, a pdf Eulerian Monte Carlo field method was successfully applied to simulate the turbulent piloted methane/air diffusion flame (Sandia D) [175].

Pitsch and Steiner [199] introduced a model called Lagrangian Flamelet Model in which the solution of the flamelets equation was coupled with LES. They resolved the filtered balance equations of energy and mixture fraction and obtained the burning rate from the flamelet equations. They used the probability density function concept, Eq. 3.49, to change from mixture fraction to physical space.

Similarly, Pitsch et al. [198] developed a stochastic, interacting flamelet model, which extends to unsteady flamelet model to account for re-ignition effects due to interactions of different flamelets.

Pierce and Moin [192] proposed a model based on the steady flamelet approach and applied LES to a turbulent combustion in a confined combustor. Their flamelet/progress variable approach (FPVA) introduces a new flamelet parameter, which is based on a reactive scalar and identifies uniquely each single state along the S-shape curve including the unstable branch. This allows, in principle, the prediction of extinction and re-ignition. Along the same line, Ihme et al. [104] showed that the steady flamelet assumption in the FPVA context leads to good predictions even for high levels of local extinction.

It can be noted that the different combustion modelling concepts tend to converge rather than diverge. Many hybrids and developments have been recently appearing of existing models using tools and concepts from other models. Especially in LES, the probability density function approach has been successfully used and modified in different combustion models. The author of this thesis believes that, to a large extent, this is due to the time accuracy capability of LES, which enables to obtain a correct description of the turbulence.

Following this, the LEPDF model is used for the non-premixed regime for the triple flame, turbulent lifted flame and backdraft simulations in chapter 8 and 9.

Conditional Moment Closure

Bushe and Steiner [34] introduced the CMC concept into the LES frame. CMC solves the conditional equations and feeds back to the LES flow-solver with the unconditional density. Bushe and Steiner applied this approach to simulation of nonpremixed turbulent reaction flow and obtained very encouraging results. This is somehow not surprising, since CMC is a good tool to approach the burning rate trough conditional quantities and LES resolves the turbulence-field with good

accuracy.

However, the CMC approach is computationally expensive to be used in the LES context. Hence, shortcomings have been developed to avoid solving the set of conditional equations needed in CMC. Bushe and Steiner [34] proposed to find out the conditional quantities through an inversion of an expression similar to Eq. 3.48. This method is called the Conditional Source Estimation (CSE) and will be further developed in chapter 5.

Other non-premixed turbulent combustion models used in LES, such as the Scale Similarity Filtered Reactive Rate Model (SSFRRM) or the Conserved Scalar Equilibrium Model (CSEM) can be found in [64].

Premixed combustion in LES

LES appears to be especially promising for the simulation of premixed combustion as it solves the large scale flow motions known to be significant when the reactants are mixed. Even more, premixed flame are sensitive to the burner geometry and to large scale, unsteady phenomenon such as the anchoring point, the passage of vortices, flame-wall interactions and the merging of adjacent flame brush regions. These factors are important because they control the large-scale wrinkling of the reaction surface.

LES faces the same difficulties as RANS in premixed turbulent combustion. The flame thickness is in the order of 0.1 to 1 mm and is much thinner than the LES grid size. Generally, the progress variable is a very stiff variable and the flame front can not be resolved in the computational domain.

To overcome this problem, three main concepts have been used:

1) An artificially thickened flame front model,
2) G-field equation or level set approach

3) Filtering the progress variable equation.

This classification is not unique and some authors have used different categorization.

Artificially thickened flames

This approach was first developed by Butler and O'Rourke [36] for the computation of laminar flames in complex geometries. Thibaut and Candel [235] have used TFM to a flashback simulation using $\alpha = 32$.

The principle behind the artificially thickened flame (TFM) is to consider a flame thicker than the actual one, but having the same laminar flame speed s_l^0 [36]. The flame speed s_l^0 and the flame thickness δ_l^0 may be expressed as:

$$s_l^0 \propto \sqrt{a\dot{\overline{w}}}; \delta_l^0 \propto \frac{a}{s_l^0} \tag{3.51}$$

where a is the thermal diffusivity and $\dot{\overline{w}}$ the mean reaction rate.

Then, an increase of the flame thickness δ_l^0 by a factor α with a constant speed is easily achieved by replacing the thermal diffusivity a by αa and the reaction rate $\dot{\overline{w}}$ by $\dot{\overline{w}}/\alpha$. If α is sufficiently large (typically from 5 to 20), the thickened flame front may then be resolved on the LES mesh without sub-grid modelling. The reaction rate is expressed using an Arrhenius law, as in DNS.

This approach posses some attractive features:

- There is no need of sub-grid turbulence modelling.
- The reaction rate is predicted using an Arrhenius law, hence events such as re-ignition, flam stabilization and flame/wall interaction can be taken into account without sub-models.
- In principle, this approach may be extended to complex chemistry.

As the thickness of the flame is enlarged, the interaction between turbulence and chemistry is modified. The Da number is divided by α. This has been investigated using DNS [5] and an efficiency function E was drawn depending on both velocity, u'/s_l^0 and the length scale, $\Delta/\alpha\delta_l^0$ to counteract this effect. Accordingly, the scaling of diffusivity and reaction rate for turbulent premixed combustion stands as follow:

$$a \rightarrow E\alpha a \; ; \; \overline{\dot{w}} \rightarrow E\overline{\dot{w}}/\alpha \tag{3.52}$$

This approach has not been extensively studied in LES, but seems to be promising [235, 246]. Selle et al. [223] carried out a LES of an industrial gas turbine burner using TFM with two-step mechanism for methane-air and about 2 million nodes. Partial-premixing is expected in this burner. Reasonably accurate predictions were obtained for the mean quantities such as temperature, velocity, etc.

G-field equation

This approach is similar to the one used in RANS framework. The key idea is to track the flame position at a given value of $G = G^*$. At G^*, a geometrical surface is posed which divided the fresh and burnt gases. This approach is in many ways similar to the flame surface density formulation. Furthermore, in both cases, the reaction zone is considered to have negligible thickness and the chemical closure is replaced by the need to specify the propagation speed of this reacting surface.

The balance equation for G is as follow:

$$\frac{\partial G}{\partial t} + \overline{u} \cdot \nabla G = w_G |\nabla G| \tag{3.53}$$

where w_G is the local displacement speed of the iso-surface.

The G field does not follow the stiff progress variable, but it can be smoother and resolved on the LES mesh.

The application of a LES filter to Eq. 3.53 leads to:

$$\frac{\partial \overline{G}}{\partial t} + \overline{u} \cdot \nabla \overline{G} = -(\overline{u.\nabla G} - \overline{u}.\nabla \overline{G}) + \overline{w_G |\nabla G|} \tag{3.54}$$

where there are two unclosed terms, the unresolved turbulent transport (first term of the RHS) and the flame front displacement (second term of the RHS). Usually, these two terms are merged into one introducing the turbulent flame speed, S_T:

$$\frac{\partial \overline{G}}{\partial t} + \overline{u} \cdot \nabla \overline{G} = \overline{S}_T |\overline{\nabla G}| \tag{3.55}$$

where $\overline{S}_T$ needs to be modelled. This closure is based on:

$$\frac{\overline{S}_T}{s_l^0} = 1 + \alpha \left(\frac{\overline{u'}}{s_l^0} \right)^n \tag{3.56}$$

where α and n have to be closed.

In this analysis, the turbulent flame speed is not a very well defined quantity and caution should be exerted when using it, as it is not a universal constant. Furthermore, there are some numerical problems associated with the appearance of cusps as the front propagates. Cups are natural consequence of constant-speed propagating fronts. They are related with the discontinuity in the derivative of the solution and render the numerical treatment very difficult. To overcome this, various types of diffusive terms have been proposed. Im et al. [105] investigated the influence of different diffusion terms on the burning velocity and found that the propagation speed decreases sharply with the diffusiveness of the equation. They also proposed a dynamic model for the turbulent flame speed for LES which depends on $\overline{u'}/s_l^0$ and the LES filter.

More recently, Pitsch [196] developed a consistent formulation of the G-equation. He stated that the unfiltered equation is valid only at instantaneous flame locations. Hence, if a proper LES filtered balance equation is required, the G-equation should be

filtered by a kernel located instantaneously along the surface. This formulation leads to an equation with two unclosed terms involving a flame front conditional flow velocity and a filtered propagation term.

Despite these setbacks, the G-equation approach has been used with reasonably success [26]. A similar approach was used by Molkov et al. [172] to simulate an actual deflagration in a vented enclosure-atmosphere system.

Filtering the progress variable equation

As in the G-equation approach, the flame front is too thin to be resolved by the computational grid. To overcome this, Boger et al. [20] proposed to filter the progress variable equation, c, using a LES filter bigger than the actual LES grid.

As described previously, the progress variable equation for c can be written as:

$$\frac{\partial(\rho c)}{\partial t}+\frac{\partial(\rho u_j c)}{\partial x_j}=\frac{\partial}{\partial x_j}(\rho D\frac{\partial c}{\partial x_j})+\dot{w}_c=\rho w_G|\nabla c| \tag{3.57}$$

Applying the LES filter, the previous equation becomes:

$$\frac{\partial(\overline{\rho c})}{\partial t}+\frac{\partial(\overline{\rho u}_j\widetilde{c})}{\partial x_j}+\frac{\partial}{\partial x_j}(\overline{\rho}(\overline{uc}-\widetilde{u}\widetilde{c})=\frac{\overline{\partial(\rho D\partial c/\partial x_i)}}{\partial x_j}+\overline{\dot{w}}_c \tag{3.58}$$

$$=\overline{\rho w_G|\nabla c|} \tag{3.59}$$

where the three LHS terms of Eq. 3.58 correspond respectively to unsteady effects, resolved convective fluxes and unresolved transport. The two RHS terms of Eq. 3.58 denote respectively filtered molecular diffusion and filtered reaction rate. The RHS term in Eq. 3.59 correspond to the flame front displacement.

When the balance equation for c is filtered using a LES filter size (Δ_c) larger than the mesh grid size Δ, the flame front is resolved with about 2 Δ_c/Δ grid points. The c

equation is similar to G-equation but the progress variable has the advantage that it is related to quantities such as $\Sigma, \Sigma^*, \langle \rho w_G \rangle_s$ which are physically defined and may be extracted from DNS or experimental measurements.

Boger et al. [20] closed the RHS term of Eq. 3.58 as follows:

$$\overline{\rho w_G |\nabla c|} = \langle \rho w_G \rangle_s \Sigma = \langle \rho w_G \rangle_s \Xi |\nabla \bar{c}| \tag{3.60}$$

where Ξ is the flame front wrinkling factor. It compares the sub-grid scale flame surface to its projection in the propagation direction. $\langle \rho w_G \rangle_s$ is the surface-averaged mass-weighted displacement speed and Σ is the sub-grid surface density (i.e. the sub-grid surface per unit volume).

These quantities, Ξ or Σ and $\langle \rho w_G \rangle_s$ need to be closured. The surface-averaged mass-weighted displacement speed may be estimated from laminar flame speed s_l^0 and the fresh gas density ρ_u as:

$$\langle \rho w_G \rangle_s \approx \rho_u s_l^o \tag{3.61}$$

In the same way as in RANS, the flame surface density Σ and the wrinkling factor Ξ may be expressed in an algebraic form or through a balance equation [100].

Several algebraic models are available for predicting the flame wrinkling factor. This depends on local quantities and can be dynamically calculated. In general, it follows a functional form which depends on [50] :

$$\frac{\bar{S}_T}{s_l^0} = \Xi\left(\frac{\Delta}{\delta_l^0}, \frac{u'}{s_l^0}, \mathrm{Re}_t\right) \tag{3.62}$$

where Δ is in the order of the flame front and u' is the velocity fluctuation at the same scale, and Re_t is the Reynolds number at grid level.

Alternatively, a balance equation for Σ can be obtained. In fact, the balance equation is formally identical to the balance equation for flame surface density widely used in RANS context. Similarly, this equation is necessary to close some terms [245].

Fureby [84] recently used the flame surface density balance equation together with a newly proposed fractal model for the wrinkling factor. He performed a LES of a premixed flame in an isotropic homogeneous turbulence and achieved good agreement with experiments.

A novel sub-grid scale closure for LES premixed combustion was developed by Domingo et al. [68] using DNS. They combined the flame surface density approach with a presumed probability density function of the progress variable that is used in FPI chemistry tabulation. The flame surface density is used to introduce in the pdf the influence of the filtered thin reaction zone within the sub-grid. The predictions were in good agreement with the experiment of a premixed turbulent V flame and a ducted flame.

The G-field equation and the filtered progress variable approaches are similar in their simplest form, but the later can take advantages of the tools developed for RANS. Furthermore, it has a clear physical interpretation and it does not suffer from the numerical instabilities inherent to the G-equation. This is probably because in the later the flame front is resolved using more points and the derivate is not very sharp.

3.3 Summary and conclusions

LES is recognised as a suitable tool for modelling the combustion processes. The increase of computational power and the development of more sophisticated sub-models are enabling LES to reveal an insight of the underlying physic, which was difficult to obtain with RANS. In this process, DNS is playing a major role by either providing direct simulation of small scale combustion processes or through assisting the development of SGS models for LES. However, the main constraint of DNS is its limitation of the Reynolds number. This means that SGS model can not be validated,

through this method, for high velocities in turbulent flows.

Even though the combustion models were originally developed under a RANS framework, their extension to the LES paradigm has been quite satisfactory. This is supported by good predictions obtained using LES in the early stages. More advanced SGS turbulent and combustion models for LES are being continuously developed. The filtered G-equation and the filtered density function for premixed combustion is an example. In these approaches, a consistent formulation of the SGS models for the LES context (Pitsch, [196]) was formulated later than the practical applications of those models. This is not the case of the Thickened Flame approach, which its extension into a LES context seems straightforward. Conversely, the approach of filtering the progress variable was especially developed for the LES framework. However, in this approach the size of the filter for the C balance equation is different from the one used in the other equations (momentum, energy, etc). This could lead to errors that need to be quantified. Little or nothing at all has been carried out yet in this direction.

Presently, there are several outstanding LES of practical devices such as swirl gas combustor [98], gas turbine combustor [154], etc. Similarly, new hybrid models which combine second order moment RANS (RANS-SOM) and Unsteady RANS (URANS) with LES [219] have recently been introduced. Alternatively, a combination of LES and RANS was implemented into the commercial package CFX 9.0 where large eddies are solved in the interior of the domain while RANS is used close to the walls where LES would require much more mesh refinement. All this indicates that the modelling development is far from over and plenty of research is still going on in the field.

Chapter 4

Sub-grid scale (SGS) turbulent model

In this chapter, the original set of Navier Stokes equations are presented and filtered using a LES filter. In this procedure, an unclosed term appears in the momentum equation, the so-called sub-grid scale (SGS) turbulent flux. This term accounts for the turbulent transport at sub-grid level. At this scale, LES is not able to calculate and, therefore, it is necessary to make an approximation.

A brief recount of the development of different turbulent closure models is given. Their application and limitations are discussed. This is followed by the description of the lagrangian dynamic approach proposed by Meneveau [166] and its implementation into the FDS v3 code.

Finally, the lagrangian model is tested on two isothermal turbulent flow configurations in order to test its performance. Case 1 is a backward facing step of Re = 5540 based on the step height and upstream centerline velocity and expansion ratio of 1.5. Case 2 a turbulent plume of Fr = 7.8. These configurations have very different stress tensor conditions, which make them particularly suitable for the evaluation of the model.

4.1 The governing equations in FDS

The Fire Dynamics Simulator (FDS), an LES code developed by the National Institute of Standards and Technology in the USA (NIST) [159] is used as the basic numerical tool. FDS solves the Navier-Stokes equations for low Mach number flows. Such approximation involves the filtering out of acoustic waves while allowing for large variations in temperature and density. It gives the equations an elliptic character, consistent with low speed, thermal convective processes. All the spatial derivatives are approximated by second order central differences and the flow variables are updated in time using an explicit second order predictor-corrector scheme. With these assumptions, the pressure-related terms in the ideal gas law and the energy equation are only functions of time. Although, in the momentum equation, the perturbation pressure is solved using a Poisson equation.

Basic equation for the flow field

The original filtered Navier Stokes equations as resolved by FDS are presented here. The filtered equations can be written as:

$$\frac{\partial \bar{\rho}}{\partial t} + \frac{\partial \overline{\rho u_j}}{\partial x_j} = 0 \tag{4.1}$$

$$\bar{\rho}\left(\frac{\partial \tilde{u}_i}{\partial t} + \frac{\partial \tilde{u}_i \tilde{u}_j}{\partial x_j}\right) = -\frac{\partial \bar{p}}{\partial x_i} + \bar{\rho} g + \frac{\partial \tau_{ij}}{\partial x_j} \tag{4.2}$$

$$\frac{\partial (\bar{\rho} \tilde{Y}_l)}{\partial t} + \frac{\partial (\overline{\rho u_j} \tilde{Y}_l)}{\partial x_j} = -\frac{\partial}{\partial x_j}\left(\overline{\rho u_j Y_l} - \overline{\rho u_j} \tilde{Y}_l\right) + \frac{\partial}{\partial x_j}\left(\overline{\rho D_l \frac{\partial Y_l}{\partial x_j}}\right) + \overline{\dot{w}}_l \tag{4.3}$$

$$\frac{\partial (\bar{\rho} \tilde{h})}{\partial t} + \frac{\partial (\overline{\rho u_j} \tilde{h})}{\partial x_j} = \frac{D\bar{p}}{Dt} - \frac{\partial q_j^r}{\partial x_j} + \frac{\partial}{\partial x_j}\left(k \frac{\partial \tilde{T}}{\partial x_j}\right) + \sum_l \frac{\partial}{\partial x_j}\left(\bar{\rho} D_l \tilde{h}_l \frac{\partial \tilde{Y}_l}{\partial x_j}\right) \tag{4.4}$$

where $\bar{\rho}$ is the filtered density, k is the thermal conductivity, C_p is the specific heat, D_l is the material diffusivity, $\tilde{u}_i$, $\tilde{Y}_l$ and $\tilde{h}$ are the Favre filtered velocity, mass species concentration and total enthalpy, q_r is the radiative heat flux, $D\bar{p}/Dt$ is the material derivative and $\tilde{w}_l$ is the Favre filtered species source term. A Favre-filtered quantity denoted by a tilde is defined by $\tilde{\phi} = \overline{\rho\phi}/\bar{\rho}$.

The first term of the RHS of Eq. 4.3 is generally closed assuming a gradient-transport concept:

$$(\overline{\rho u_j Y_l} - \bar{\rho}\tilde{u}_j\tilde{Y}_l) = -\bar{\rho}\frac{\upsilon_t}{Sc_t}\frac{\partial \tilde{Y}_l}{\partial x_i} \tag{4.5}$$

where υ_t is the Smagorinsky turbulent eddy-diffusivity and Sc_t is the turbulent Schmidt number.

In FDS, the viscous stress tensor $\tau_{ij} = -(\mu_t + \mu_l)\bar{S}_{ij}$ is the sub-grid-scale stress and it needs to be closed. By default, FDS follows Smagorinsky [227] to close the viscosity term as

$$\mu_t = \bar{\rho}(C_S\Delta)^2|\bar{S}|. \tag{4.6}$$

where Δ is the filter width (which is proportional to the grid size), C_S is a model constant the so-called Smagorinsky constant which needs to be chosen and $|\bar{S}| = (\bar{S}_{ij}\bar{S}_{ij})^{1/2}$ is the magnitude of the large-scale strain-rate tensor, $\bar{S}_{ij}$ reads,

$$\tilde{S}_{ij} = \frac{1}{2}\left(\frac{\partial \tilde{u}_i}{\partial x_j} + \frac{\partial \tilde{u}_j}{\partial x_i}\right) \tag{4.7}$$

and $\tilde{u}$ is the large-scale or filtered velocity.

The Smagorinsky approach is known to have setbacks regarding the value of its constant, C_S. It has been found, in several studies, that C_S depends on many factors

such as turbulence intensity, grid size, geometrical configuration, etc. and it does not remain constant throughout the turbulent field. Accordingly, the general trend of the development of sub-grid turbulent models in LES is towards constant independent models, where C_S is dynamically calculated depending on local flow conditions.

4.2 SGS background

Most sub-grid scale stress models (SGS) are based on an eddy viscosity assumption, originally developed by Smagorinsky [227]. In this model, the turbulent eddy viscosity (μ_t), is obtained by assuming that the small scales eddies are in equilibrium, therefore, the energy production and dissipation are in balance.

Smagorinsky [227] used C_s = 0.020 for a numerical atmospheric circulation experiment using the primitive equation of motion. Von Neumann and Richtmyer [177] reported that the equivalent of C_s = 0.25 yielded good results for one-dimensional shocks. On the other hand, Charney and Phillips found that the coefficient C_s = 0.016 gave reasonable results in quasi-geostrophic integrations.

Lilly [142] used a Smagorinsky constant of $C_s \cong 0.17$ in a homogeneous isotropic turbulence with cut-off in the inertial sub-range. Deardorff [61] found that the presence of a large shear would require a smaller value for C_s and that Lilly's value might cause excessive damping of large-scale fluctuations. Deardorff used $C_s \cong 0.094$ for his calculation. McMillan et al. [158], also found that C_s should be lowered in the presence of strain as in the case of a flow near a wall.

As a conclusion, the SGS stress tends to decrease towards the wall and is zero at the wall. Very close to the wall a laminar flow regime is expected. Therefore, the length scale needs to be modified accordingly.

Following this concept Moin at al. [171] modified the length scale proportionally to the distance from the wall. On the other hand, Moin and Kim [169] used damping

functions of the Van Driest type. In both cases, the results agreed well with the experimental data and the SGS stress profile close to the wall is well predicted.

Yakhot et al. [262] used a sub-grid scale model based on the Renormalization Group theory (RNG) of Yakhot and Orszag [263] in the LES of a channel flow. The SGS stress predicted by this model tends to zero at the wall without any extra wall function. However, the model has problems solving very high Reynolds number, and as a consequence, a very fine mesh is necessary to obtain the correct solution.

The dynamic model introduced by Germano et al. [88] evaluates the sub-grid scales viscosity directly from the information contained in the filtered large scale eddies. This model uses neither intermittency nor wall functions and it exhibits a proper behaviour near solid boundaries and in the transition regime. In principle, this model is also capable of predicting backscatter. Germano's model shows very good agreement with experimental data for a transitional and turbulent channel flow. Nevertheless, to avoid numeric destabilisation, due to negative viscosity values, a turbulent homogenous plane must be chosen in order to average the model coefficients.

Meneveau [166]developed a SGS model which dynamically predicts the sub-grid scale stresses as in the Germano's model but without the restriction of the turbulent homogenous plane. Both models are based on the same principle but instead of averaging in a plane, Meneveau's model averages over particle trajectories. In this way, the model does not need a homogeneous turbulent plane for averaging. Consequently, the model is to use in flows such as plumes where there are no surfaces of homogeneous turbulence. For this reason, it was decided to implement the model into the FDS code.

4.3 The Lagrangian sub-grid scale turbulence model

Meneveau suggested an alternative method of averaging along flow particle trajectories to overcome the restriction of averaging in planes of homogeneous turbulence.

The Lagrangian model is derived by minimising the error incurred by inserting the Smagorinsky model in the Germano identity along a fluid-particle trajectory.

The error to be minimised is:

$$e_{ij}(z,t') = L_{ij}(z,t') - C_S^2(x,t)M_{ij}(z,t') \tag{4.8}$$

where,

$$M_{ij} = 2\Delta^2[\overline{|\bar{S}|\bar{S}_{ij}} - 4|\bar{\bar{S}}|\bar{\bar{S}}_{ij}] \tag{4.9}$$

$$L_{ij} = (\overline{\bar{u}_i\bar{u}_j} - \bar{\bar{u}}_i\bar{\bar{u}}_j) - (\overline{\overline{u_i u_j}} - \overline{\bar{u}_i\bar{u}}_j) \tag{4.10}$$

$\bar{S}_{ij}$ and $\bar{\bar{S}}_{ij}$ are the filtered strain tensor at scale Δ and 2Δ, respectively.
This leads to,

$$C_s^2(x,t) = \frac{f_{LM}}{f_{MM}} \tag{4.11}$$

where C_S is the Smagorinsky constant, f_{LM} and f_{MM} are the values of L_{ij} and M_{ij} integrated over the particle trajectory.

Choosing an appropriate weighting function, the following transport equations are obtained,

$$\frac{Df_{LM}}{Dt} \equiv \frac{\partial f_{LM}}{\partial t} + \bar{u}.\nabla f_{LM} = \frac{1}{T}(L_{ij}M_{ij} - f_{LM}), \tag{4.12}$$

$$\frac{Df_{MM}}{Dt} \equiv \frac{\partial f_{MM}}{\partial t} + \bar{u}.\nabla f_{MM} = \frac{1}{T}(M_{ij}M_{ij} - f_{MM}), \qquad (4.13)$$

The time scale T controls the 'memory' of the average. Meneveau proposed $T = \theta\Delta[f_{LM} f_{MM}]^{-1/8}$. A constant of proportionality is needed. The model was applied to a case of homogeneous turbulence and θ = 1.5 was obtained. Meneveau stated that it is not necessary to solve these equations very accurately. Hence, a simple and fast numeric scheme can be used.

4.4. Numerical scheme of the Lagrangian model

The transport equations of the sub-grid-scale viscosity are solved using the following numeric scheme:

$$f_{LM}^{n+1}(x) = H\{\varepsilon[L_{ij}M_{ij}]^{n+1}(x) + (1-\varepsilon) f_{LM}^{n}(x - \bar{u}^{n}\Delta t)\} \qquad (4.14)$$

$$f_{MM}^{n+1}(x) = \varepsilon[M_{ij}M_{ij}]^{n+1}(x) + (1-\varepsilon) f_{MM}^{n}(x - \bar{u}^{n}\Delta t) \qquad (4.15)$$

where

$$\varepsilon \equiv \frac{\Delta t/T^{n}}{1+\Delta t/T^{n}} \text{ and } T^{n} = \theta\Delta(f_{LM}^{n} f_{MM}^{n})^{-1/8},\ \theta = 1.5 \qquad (4.16)$$

where the $H\{x\}$ is the ramp function ($H\{x\} = x$ if x≥0, and zero otherwise), Δt is the time step and θ is a model constant . The ramp function is introduced to clip the solution to zero in case of negative values of f_{LM}. This is done in order to ensure the stability of the numerical scheme.

It is clear in Eqs. 4.14 and 4.15 that only two time steps are needed for the backwards time integration along the path lines. The tensors M_{ij} and L_{ij} are computed by solving Eqs.4.9 and 4.10. The filtered stress and velocity at mesh grid level (Δ) are obtained from the LES calculation. The double filtered quantities at 2Δ are averaged on six

cells around the central one. The velocities are interpolated from the face to the centre of the cell.

Two additional arrays are created in order to store f_{LM} and f_{MM}. These are calculated on each iteration. Using Eqs.4.14 and 4.15, it is possible to obtain C_s from Eq.4.11. Due to the explicit numerical scheme used, the time step is short enough to avoid that a particle goes further than a cell distance. Therefore, the triple lineal interpolation used in calculating f_{LM} and f_{MM} at the previous time step is not further than a neighbour cell.

4.5 Test case characteristics

In this section, we describe the two cases on which the Lagrangian dynamic model is tested. These involve two types of flows, which have very different flow structures.

The turbulent plume case poses a difficult problem for the Germano's model. In this case, there is no plane of homogeneous turbulence in order to avoid negative values of turbulent viscosity.

The backward facing step presents high stress tensor near the walls and, consequently, requires a proper estimation of the Smagorinsky constant close to the walls. It is known that the Germano's model has been successfully applied to this case. The homogenous plane can be established equidistant to the walls. In spite of this, we consider the backward facing step a useful configuration to evaluate Meneveau's model and especially how it handles the high stresses close to the wall. Even more, the turbulence developed further downstream from the step creates a detached flow, which poses a new challenge to the Lagrangian model.

4.5.1 Buoyant Turbulent Plume

The structure of round buoyant turbulent plumes in still and unstratified environments is an important problem that has attracted significant attention since Rouse et al

[216]. However, a recent study has highlighted the need for more information about buoyant turbulent plumes in order to address the effects of turbulence and to help benchmark models in turbulent flows.

The source Froude number (Fr) is a measure of dominance of buoyancy at the source, e.g., $Fr_0 = 0$ for purely buoyant and $Fr_0 = \infty$ for purely non-buoyant (jets) sources, respectively. There is abundant information for pure jet plumes [241, 270]. Vortex dynamics is expected to be of major importance not only in the development and instabilities of the plume but also in the transition from laminar to turbulent regimes. It is important to highlight that the vortex stretching is vital in maintaining high levels of fluctuating vorticity [234].

Several authors have previously studied such turbulent plumes [44, 181]. These studies emphasised the relationships among the flow properties in the developed (self-preserving) flow. Nevertheless, there were discrepancies in the centreline values among these authors. They attributed these discrepancies mainly to the problem of fully reaching the self-preserving conditions. Dai et al. [58] explained the relations of non-dimensional values. There exist different opinions regarding the conditions that a plume should fulfil to be considered in a self-preserving regime.

Zhou [273] calculated a buoyant turbulent plume with $Fr = 1.54$ and presented the mean velocity radial distributions on planes much nearer to the nozzle than the present study ($x / D \approx 10$).

The self-preserving region of a buoyant plume of $Fr = 7.8$ at the source is studied in the present case using LES along with the Lagrangian approach for the sub-grid-scale turbulence model. The results are compared with the experiments of Dai et al. [58].

4.5.2 Backward facing step

Flow separation and reattachment are of great importance in many practical applications of aeronautical, mechanical and civil engineering. Hence, any

computational fluid dynamics code should be tested against a problem of separation and reattachment. It is of particular interest to test the accuracy of the turbulence models in these situations. Among all the flows with separations and reattachment, the flow over a backward facing step is one of very simple geometry, yet it offers highly desirable flow characteristics such as separation, reversal and recovery in the presence of a strong adverse pressure gradient, mixing, reattachment, and redeveloping velocity. Among the flow geometries used for the studies of separated flows, the most frequently selected is the backward-facing step.

The effects of the expansion ratio on the reattachment length were studied by Kuehn, Durst and Ra, among others [73, 129, 180, 207]. They concluded that the reattachment length increased with the expansion ratio. Effects of the Reynolds number on the reattachment length were numerically studied by Armaly et al. [6] and experimentally tested by Durst and Sinha [73, 226]. There exist other investigations addressing the influence of parameters such as upstream boundary layer profile [3], inlet turbulent intensity [106] and downstream duct angle on the reattachment length [234], etc.

Several numerical simulations of the backward-facing step flow were also conducted either in two dimensions [6, 72, 109] or in three dimensions [83] using LES. Simulations for isothermal turbulent flow for this geometry can be found in [4, 176].

In the present study, the Lagrangian sub-grid-scale turbulence model developed by Meneveau is used to simulate a backward facing step with Reynolds number of 5540 based on the upstream centre line and the step height. The results are compared with the experiments of Kasagi and Matsunaga [112].

4.6 SGS boundary and initial conditions

Additional boundary and initial conditions are needed for f_{LM} and f_{MM}.

As the flow at the inlet of the plume is laminar, the f_{LM} boundary condition is f_{LM}=0. In the open boundaries, the same condition is used, as large fluctuations are not expected there.

For the backward facing step case, the development length considered is long enough to allow the velocity profile to develop from the inlet to the step shoulder. Therefore, it is expected that f_{LM} and f_{MM} will develop accordingly through the channel. Considering this, f_{LM}=0 was set up at the inlet. At the wall f_{LM}=0 is considered too, since the flow is laminar there.

The main focus of this study is the quasi-steady state,. Hence, the flow is initialised as Meneveau recommended: f_{MM} (x, t = 0) = M_{ij} M_{ij}(x, t = 0) and f_{LM} (x, t = 0)=C_s^2(t = 0) M_{ij} M_{ij}(x, t = 0) [166].

Consequently, at the beginning of the simulation the standard value of the Smagorinsky constant is applied throughout the domain, but this situation soon evolves as the stress tensor builds up.

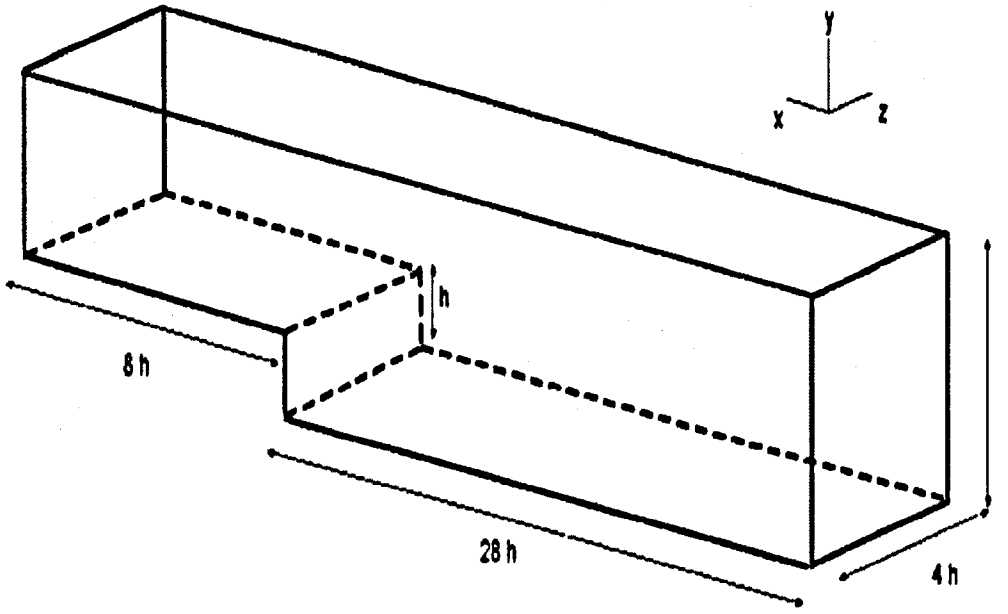

Figure 4.1. Backward-facing step geometry.

4.7 Simulation details and results for the backward facing step

4.7.1 Simulation details

The geometry of the backward facing step is shown in Fig. 4.1. The fluid under consideration is air. The step height (h) is 0.041 m and the upstream section has a height of 0.082 m (2h), resulting in an expansion ratio of 1.5. The total length of the geometry is 1.5 m and the development length before the step is 0.35 m. The Reynolds number based on the step height and upstream centreline velocity (U_c) is 5540. The reference values are: $U_c = 2.063$ m/s, $L = h = 0.041$ m, $\rho = 1.194$ kg m^{-3}, $\nu = 15.27 \times 10^{-6}$ m^{2}s^{-1}. The conditions are the same as those used by Kasagi and Matsunaga [112].

Non-slip boundary conditions are used at the top and bottom walls. Periodicity is assumed in the span wise direction. The Navier Stokes characteristic boundary conditions are employed at the inflow and outflow boundaries. At the inflow as

standard random perturbation of 7% is used. At the outflow, it is assumed that the total pressure is constant along the path lines.

The grid resolution used for the simulation is (100 x 72 x 48) in the streamwise, wall-normal and spanwise, respectively. The grid is shrunk on both streamwise and wall-normal directions at the step region using a parabolic function for the grid distribution. The selected grid resolution is chosen following careful study of the resulting flow field pattern in the experiments.

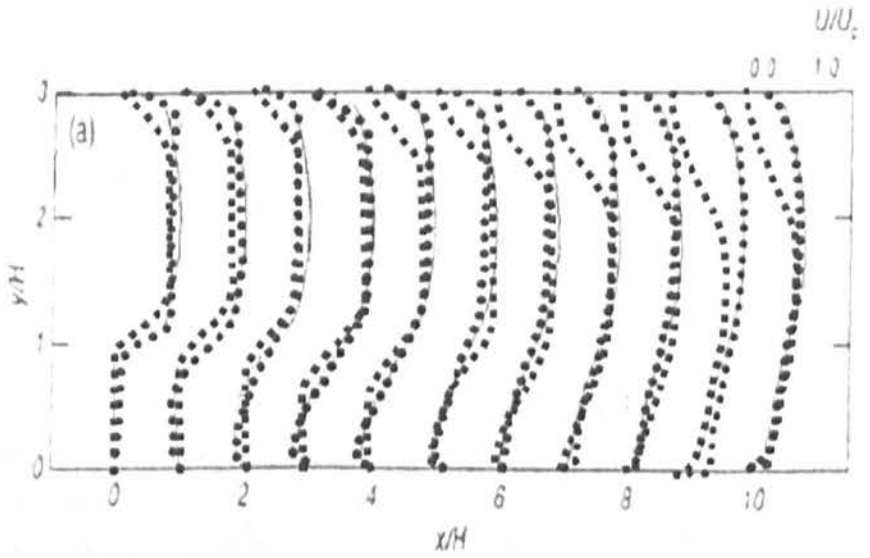

Figure 4.2a. Mean stream wise velocities at different locations downstream the step. — (line) measurements, • (circle) Lagrangian model, ■ (square) Smagorinsky model.

4.7.2 Results of the backward facing step

Reattachment length

There are many definitions of the mean reattachment length (X_r) in the literature: (a) by the location at which the mean velocity U = 0 at the first grid point away from the wall; (b) by the location of the zero wall-shear stress ($\tau_w = 0$); (c) by the location of the mean dividing stream line ($\psi = 0$); and (d) by a p.d.f. method in which the mean reattachment point is indicated by the location of 50% forward flow fraction. Le et al. [133] observed that the actual difference among the first three are only of 0.1% and the last one about 2%. In the present work the first definition is adopted.

The predicted mean reattachment length is 5.75h. This value is 11% smaller than the value obtained by Kasagi and Matsunaga of 6.51h [112].

Ravikanth et al. [211] solved the same configuration using the Garimaji's model [93] for homogeneous turbulence plane and obtained a reattachment length of 6.0h.

Le et al. [133] carried out a Direct Numerical Simulation (DNS) calculation of the backward facing step and obtained 6.28h for a Reynolds number of 5100 and expansion ration of 1.2. In a previous calculation they predicted a reattachment length of 6.0h -[132].

It is interesting to highlight that in the Le et al.'s DNS simulation, the inlet conditions, upstream of the step, do not totally match the condition for a fully turbulent channel used by Kasagi and Matsunaga [112]. Nevertheless, they obtained a good reattachment length prediction. Considering that in the present simulation, as it is shown in the good prediction of Le et al. [133], the channel is not fully turbulent at the step shoulder, the inlet condition should not be considered as the cause of the under prediction in the reattachment length.

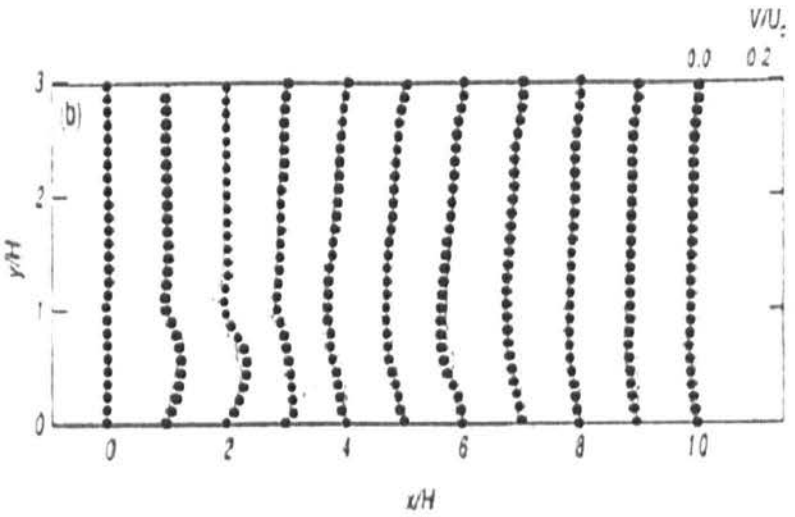

Figure 4.2b. Mean wall normal velocities at different locations downstream the step.
— (line) measurements, • (circle) Lagrangian model.

Mean velocity distributions

The mean velocity profiles in the wall normal (y) direction at various downstream sections are shown in Figs. 4.2a and 4.2b. In general, there is good agreement between experimental and simulated values in both directions.

In Fig 4.2a from the x / h = 2 to 5, the streamwise velocity has a negative component indicating the recirculating region. Fig. 4.2a also shows that the simulated velocity is flatter than the measurement in the bulk of the channel at x / h = 0. Consequently, the profile at the upper wall is steeper than the experiment. This could be attributed to the fact that in the present simulation not all the channel cross section is turbulent at the step shoulder as it will be shown later.

As the recirculating region is reached, the velocity on the upper wall agrees well with the experiment. On the other hand, the inverse situation is encountered on the lower wall, where at x / h = 9 a much steeper profile is predicted.

The velocity prediction using the Smagorinsky SGS turbulence model, C_S=0.2, (square symbols) is shown in Fig. 4.2a. It can be noted that the prediction fails to capture the correct velocity profile near the wall. This is most notorious on the upper wall where the model predicts a recirculating region at x / h = 7, which is not present in the measurements. Evidently, the Smagorinsky SGS turbulence can not predict the right behaviour near the wall without the help of wall-function or an *ad-doc* modification.

Fig. 4.2b shows the y direction velocities. They prove to be in very good agreement with the measurements. It shows positive and negative values, especially at x / h = 1 and at x / h = 4, respectively. This evidences the presence of the principal eddy. Toward the reattachment point and starting at x / h = 4, the velocity becomes negative and it remains negative in the recovering region further downstream up to x / h = 10.

The mean streamlines are shown in Fig. 4.3. They are the contour lines of a stream function ψ calculated by integrating the mean velocity components. It is seen that the centre of the principal recirculating region is located at x / h = 2.29 and y / h = 0.58. Kasagi and Matsunaga [112] measured this point at x / h = 3.0 and y / h = 0.6. The under prediction of the stream wise centre location of the principal eddy centre (about 23%) was somehow expected due to the under prediction of the reattachment length.

Nevertheless, the LES calculations carried out by Ravikanth et al. [211] predicted this position at x / h $\approx$ 2.3 for the main eddy centre and x / h = 6.1 for the reattachment length. These were closer to the values obtained in this study.

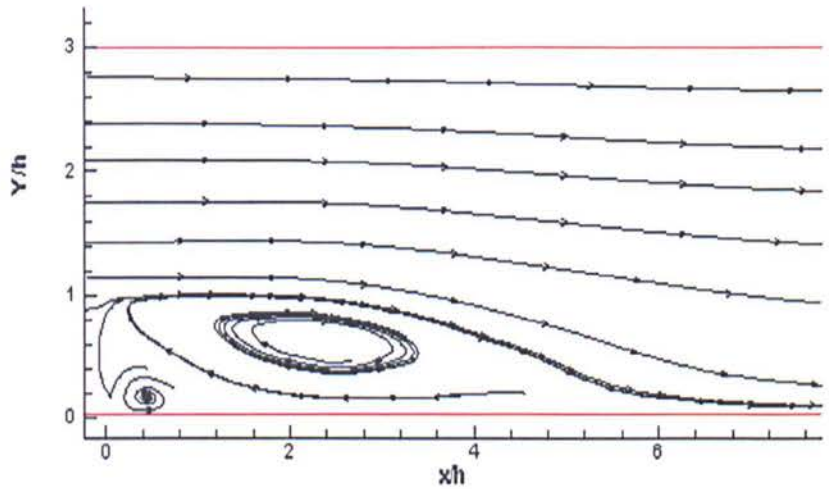

Figure 4.3. Mean streamlines.

Fig. 4.3. The secondary eddy prediction at x / h = 0.47., while Kasagi and Matsunaga [112] located it at x / h = 1.7.

Velocity fluctuations and turbulent kinetic energy

The root mean square (rms) velocity fluctuation predictions and measurements are shown in Fig. 4.4a. The fluctuation of the stream wise velocity shows, in general, a reasonable agreement with the measurements.

The U_{rms} profile at the separation point has a peak of 0.15 U_c at x / h = 0, y / h = 1. This peak increases slightly downstream and has a maximum of 0.2 U_c at x / h = 1. Thereafter, it exhibits a considerable diminishing along the step side together with a shift toward the wall. Simultaneously, as the peak moves downstream, a diffusive effect can be noticed after x / h ≈ 1 and further into the principal eddy region where the peak is softened forming a much softer profile at x / h ≈ 4.

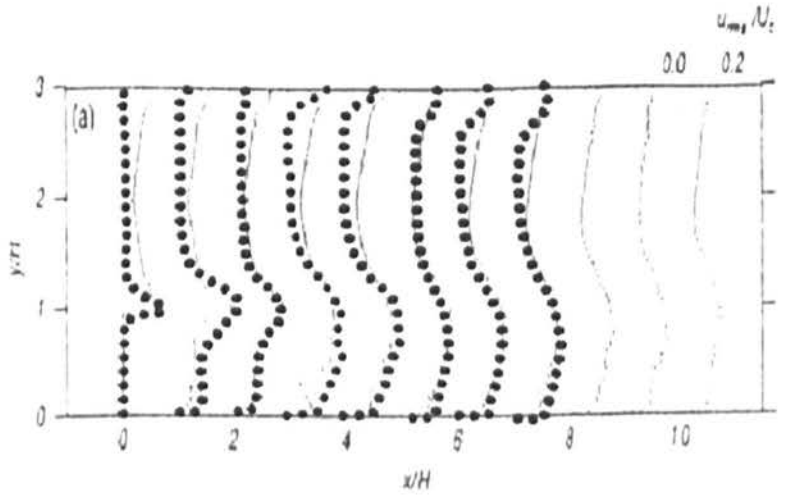

Figure 4.4a. Root-mean-square turbulent velocity fluctuations. Stream wise component. — (line) measurements, • (circle) Lagrangian model.

The main differences between predictions and experiments is at x / h = 1 and along the upper wall. At x / h = 1, a weaker fluctuations profile is predicted and on the upper wall the measurements are more turbulent than in the simulation. This can be attribute to the effect of the flow conditions upstream of the step. As it was mentioned earlier, in this study not all the channel cross section is turbulent (note the low turbulence prediction in the bulk of the channel). As shown in Fig. 4.4a.

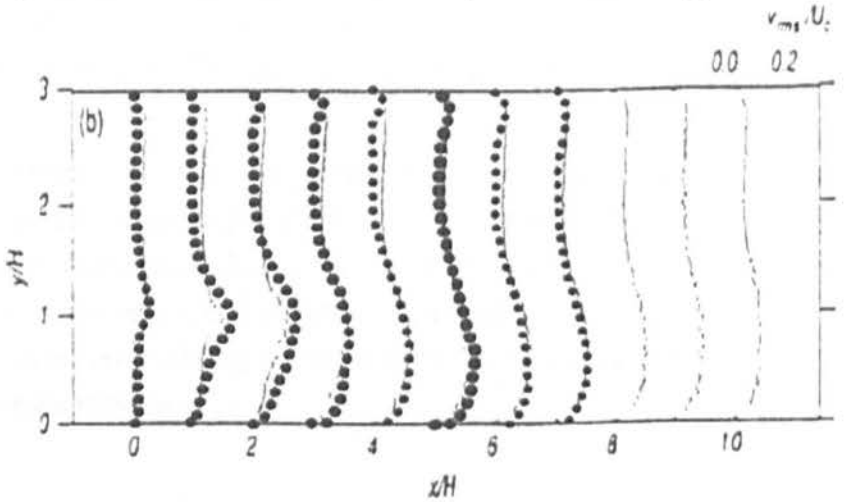

Figure 4.4b. Root-mean-square turbulent velocity fluctuations. Stream wall normal component. — (line) measurements, • (circle) Lagrangian model.

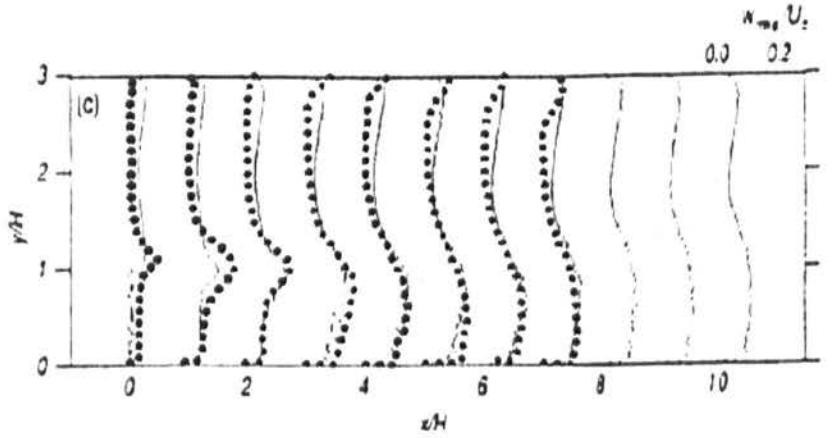

Figure 4.4c. Root-mean-square turbulent velocity fluctuations. Span wise component. — (line) measurements, • (circle) Lagrangian model.

In Fig. 4.4b, the wall-normal component v' shows a distribution qualitatively similar to u'. Its maximum is located downstream of the separation wall, but, its magnitude is smaller than u' as expected. The predictions show a similar behaviour for u'. A weaker profile and an under prediction of the magnitude at $x / h = 1$. Again, there is an under prediction in the bulk region of the channel, although less pronounced than in the stream-wise case. The agreement is very good for $x / h > 3$.

Fig. 4.4c shows the span-wise component of the fluctuation w'. The qualitative behaviour is the same as the other two components. The predicted magnitude is greater than v' but smaller than u'. As the recirculating region is reached w' becomes the biggest component near the wall as identified by See Itoh and Kasagi [107]. The prediction in the recirculating region and close to the lower wall is in good agreement with the measurements.

Fig. 4.5 shows the mean turbulent kinetic energy (k). It presents a behaviour qualitatively similar to the measurements. There are two maximums in the measurements; one at x / h = 2 and another at x / h = 4.5. In the simulation, these two maximums are located at x / h = 1.48 and x / h = 3.2. Nevertheless, in the simulation there is an extra maximum in the separation point. The main difference between the simulation and the measurements, regarding the kinetic energy, is that in the measurements the biggest maximum is at x / h = 4.5 while in the simulation it is around x / h = 1.

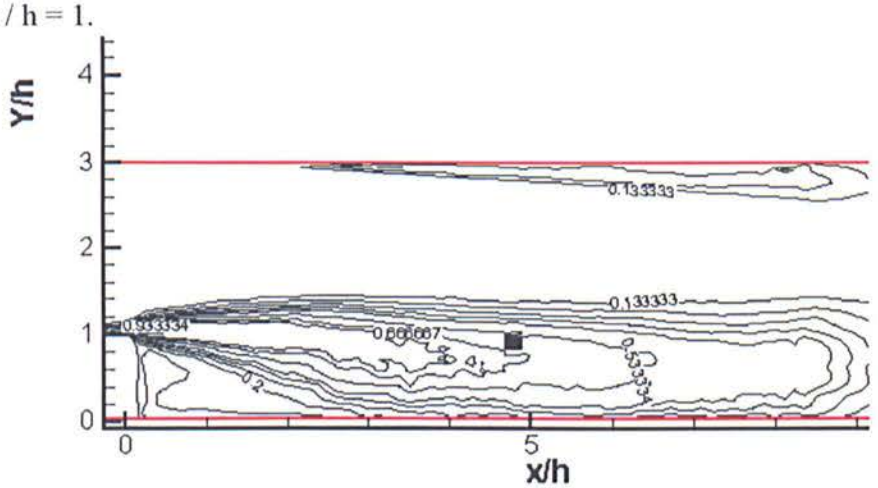

Figure 4.5. Contour lines of normalised turbulent kinetic energy.

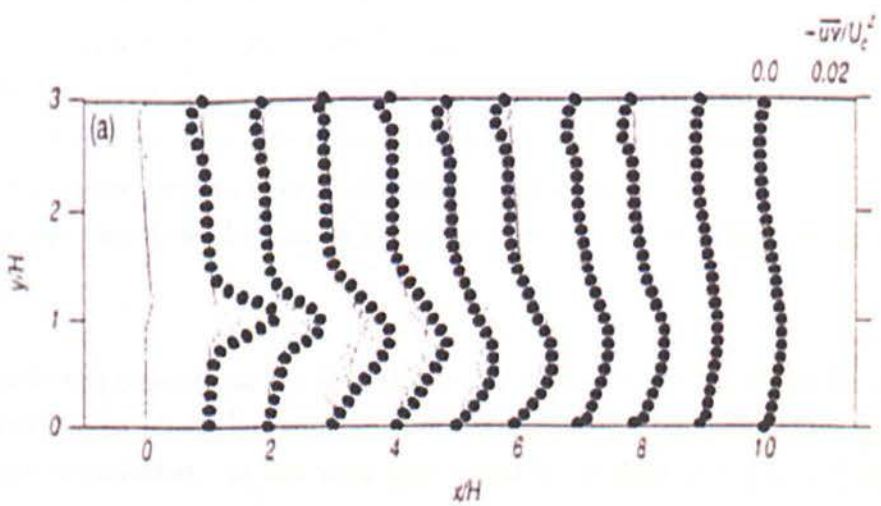

Figure 4.6. Reynolds shears stress cross-stream distribution. — (line) measurements, • (circle) Lagrangian model.

Kasagi and Matsunaga [112] found that their results were in excellent agreement with those of the DNS of Le at al.[133] even though there was a considerable difference in the inflow conditions. In the simulation carried out by Le et al., the inflow conditions were not of a full-developed turbulent channel but of a partially turbulent inflow as we used in this study.

Reynolds shear stress

The profile of the Reynolds shear stress ($\overline{uv}$) is depicted in Fig. 4.6. It is, in general, very similar to the distribution of the turbulent kinetic energy. Particularly, in the separating shear layer. The measurements exhibit a small peak at y / h = 1 that diffuses toward the channel centre and the lower wall. It reaches its maximum of 0.013 at x / h ≈ 4. The simulation predicts good agreement downstream of x / h = 4, although near the step, the simulation over predicts the shear stress. This might be associated with the over prediction of both v' at x /h = 1 and u' at x / h = 1.

Subgrid-scale turbulence model

Fig. 4.7 shows the contour profile of the mean value of $\overline{C_s^2}$. There are two main issues to address. Firstly, the mean overall Smagorinsky constant is lower than the commonly assumed value of $\overline{C_s^2}$ = 0.04; confirming that this value might produce excessive dissipation in a LES of a backward facing step. In consequence, the new SGS model dissipates less energy and, thus, more turbulence is expected. Secondly, $\overline{C_s^2}$ becomes zero near the wall without the necessity of wall function or artificial treatment.

In the mid-high channel, at the shoulder of the step (x / h = 0), it can be seen that $\overline{C_s^2}$ is very low (≈ $3.0\ 10^{-4}$), indicating that the flow in this region is laminar as it was previously commented. As the separation point is reached at x / h = 0 this value becomes larger.

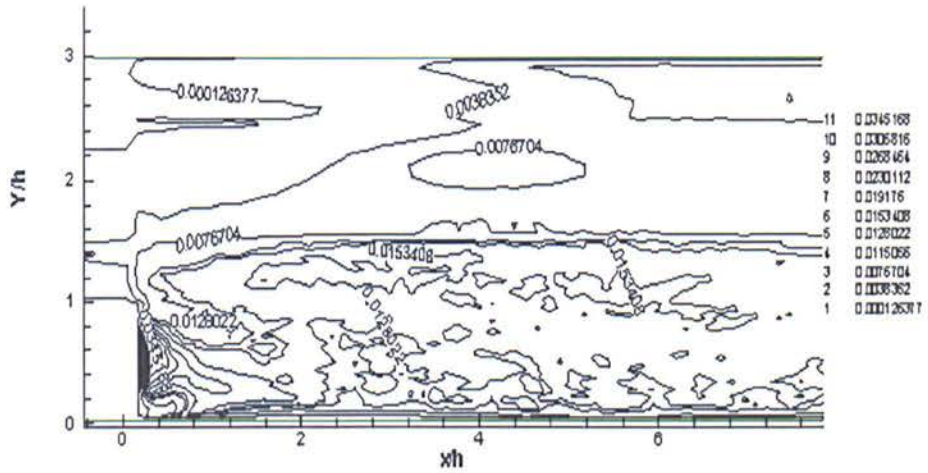

Figure 4.7. Contour profile of C_s^2.

In the zone downstream the step, two regions can be recognized; one in the upper section of the channel and another underneath it. The region above has small values of C_s and the lower area has larger values. This is in accordance with the level of turbulence in the channel.

It can be observed from Eqs. 4.12 and 4.13 that $\overline{C_s^2}$ is a transported scalar quantity and that a source term can be expected in high strained regions of the flow. Consequently, large values of $\overline{C_s^2}$ are seen close to the point where the two eddies (primary and secondary) met at the bottom wall, at the reattachment point and at the separation point. All these are regions of high stress. From each of these points, $\overline{C_s^2}$ is transported along the path lines either inside or outside the principal eddy. From this point of view $\overline{C_s^2}$ can be thought to have a similar behaviour to the dynamic one-equation sub-grid model.

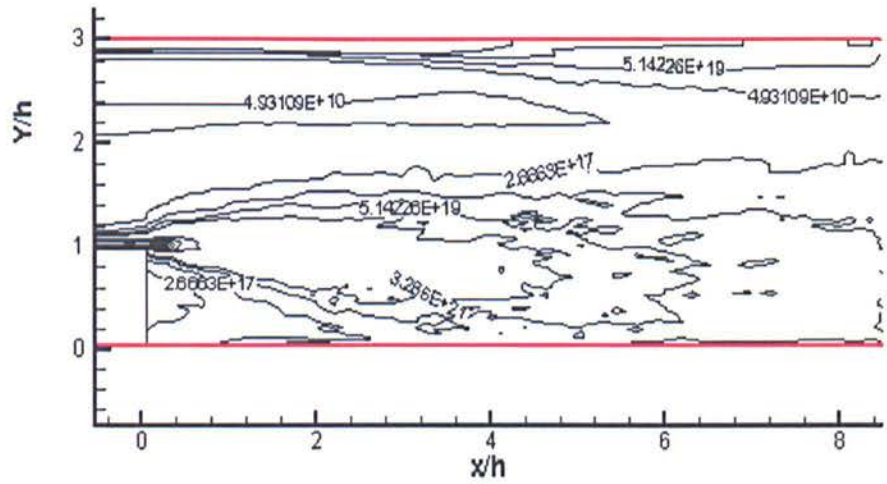

Figure 4.8. Contour profile of f_{mm}.

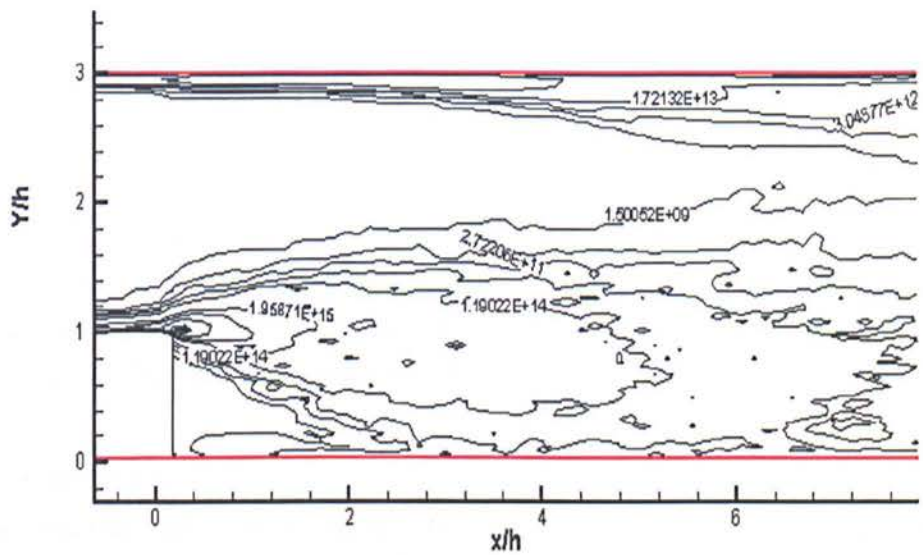

Figure 4.9. Contour profile of f_{lm}.

The $\overline{f_{MM}}$ profile is depicted in Fig. 4.8. f_{MM} depends on the fourth order of strain tensor (S_{ij}). The peak located at x / h = 0 and y / h = 1 is transported both downstream

and toward the lower wall. Close to the step bottom, from x / h > 0 to x / h < 1 there is a region of low mean strain and therefore $\overline{C_s^2}$ is small.

The $\overline{f_{LM}}$ profile is depicted in Fig. 4.9. The qualitative behaviour is similar to $\overline{f_{MM}}$, with an important exception, the boundary condition of $\overline{f_{LM}}$ was set to zero to satisfy the condition $\overline{C_s}$ = 0 at the non-slippery walls. The $\overline{f_{LM}}$ profile resembles to the Reynolds shear stress ($-\overline{u'v'}$) profile. There is a region on the step wall and for x / h = 0 to x / h < 2.5 where the $\overline{f_{LM}}$ is low.

In order to asses for the model performance, the number of 'clipping' in Eq. 4.14 has been counted. This gives an idea of how many times the viscosity has been set to zero in the simulation. Fig. 4.10 shows the percentage of 'clipping' respecting the total iterations in a plane. It is seen that in the bulk of the channel the percentage is low, about 1.6 %, but in the recirculation zone it is about 16 %. There is a zone near the bottom of the step where the percentage is very low (2%). This point coincides with the second reattachment point.

In Eq.4.16 there is a constant that Meneveau chose to be $\theta = 1.5$. This value was obtained from an isotropic turbulence case. Hence, herein two more tests are carried out in order to evaluate the effect of this constant. The cases are performed with $\theta = 0.5$ and $\theta = 3.0$ and no substantial differences have been found.

Mesh sensitivity analysis

It is important to analyse the influence of the mesh refinement on the results. For this, a systematic refinement of the mesh is carried out. Considering the initial mesh of 100 x 72 x 48 (mesh 1), it is increased to 120 x 90 x 48 (mesh 2) and 120 x 120 x 48 (mesh 3).

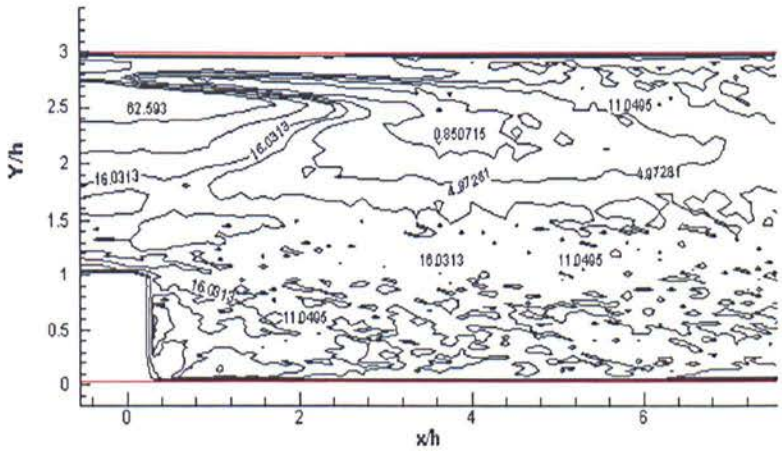

Figure 4.10. Contour profile of the percentage of 'clipping' to zero the viscosity.

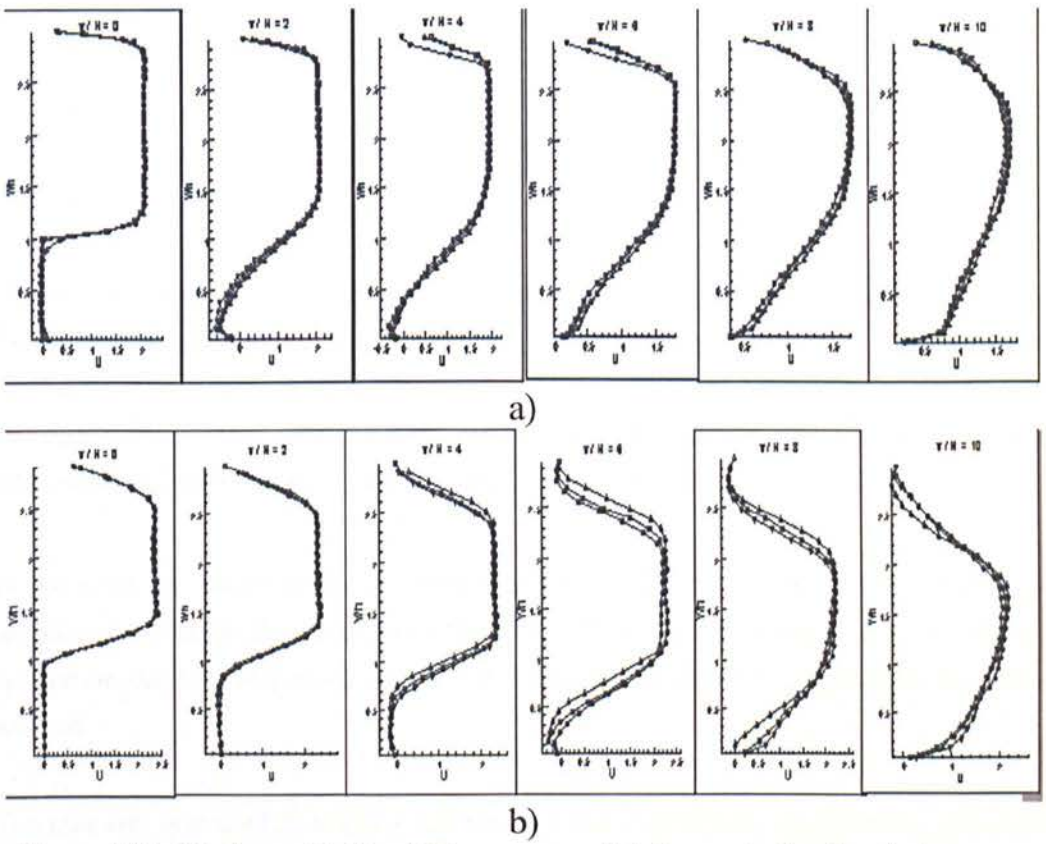

Figure 4.11. Mesh sensitivity.a) Meneveau and b) Smagorinsky. Symbols: square (mesh 1), deltas (mesh 2) and gradients (mesh 3)

Fig. 4.11 shows the velocity profiles for both turbulence models. The Lagrangian approach does not produce large variation in velocity. For the Smagorinsky model the predictions of the different meshes are more obvious, especially at x / h = 6 and x / h = 8. It is also seen that the counter flow eddy on the upper wall predicted by the Smagorinsky model does not improve with the refinement of the mesh.

It is found that the other quantities are not greatly improved using a finer mesh. It is therefore concluded that the solution is converged with mesh 1.

4.8 Simulation details and results for the turbulent plume

4.8.1 Simulation details

The dimension of the numeric domain is (1.2 x 1.2 x 2.2) m in x, y and z direction, respectively. The fluid under consideration is CO_2, with the following properties: ρ = 1.75 kg/m^3, ν = 8.5 mm^2/s.

The nozzle diameter is 9.7 mm and the inlet velocity is 1.74 m/s. The Reynolds and the Froude number at the inflow are 2000 and 7.8, respectively. The flow is directed vertically downward in still air with ambient pressure, temperature, density and kinematic viscosity of 99± 0.5 KPa, 297 ± 0.5 K, 1.16 kg/m^3 and 14.8 mm^2/s. These data are based on the experimental conditions of Dai et al. [58].

In the inlet, no perturbation is introduced as the flow is laminar at the nozzle and turbulence develops downstream in the plume. The open pressure boundary condition is used on the side and top plane. A non-slip wall condition is imposed at the bottom surface.

The numeric grid is (128 x 128 x 100) in x, y and z direction, respectively. This mesh is found to provide to be fine enough to achieve grid independent results according to preliminary tests carried out with different grid resolutions.

The self-preserving round buoyant turbulent plume conditions are considered to be reached when streamwise distances from the plume source are large in comparison with two characteristic length scales: (1) the source diameter, as a measure of conditions when the effects of the source disturbances have been lost and (2) the Morton length scale, as a measure of conditions where the buoyant features of the flow are dominant. For general buoyant jet sources, the Morton length scale is defined as follows:

$$l_M = M_0^{3/4} / B_o^{1/2} \tag{4.17}$$

For round plumes with uniform properties defined at the source, the source specific momentum flux, M_0, and the source buoyancy, B_0, are defined as follows:

$$M_0 = (\pi/4) d^2 u_0^2 \tag{4.18}$$

$$B_0 = (\pi/4) d^2 u_0 g \mid \rho_0 - \rho_\infty \mid / \rho_\infty \tag{4.19}$$

where d is the jet diameter, u_0 is inlet velocity, g is the gravity vector, ρ_0 is the flow density at the jet nozzle and ρ_∞ is the ambient density.

Substituting Eqs.4.18 and 4.19 into Eq. 4.17 yields the following expression for l_M for round plumes that have uniform properties at the source:

$$l_M = (\pi/4)^{1/4} (\rho_\infty d u_0^2 / (g \mid \rho_0 - \rho_\infty \mid d))^{1/2} \tag{4.20}$$

The radio, l_M / d, is proportional to the source Froude number, defined as follows,

$$Fr_0 = (\pi/4)^{1/4} l_M d = (\rho_\infty u_0^2 / (g \mid \rho_0 - \rho_\infty \mid d))^{1/2} \tag{4.21}$$

The measurements of Dai et al. [58] covered a region of $(x - x_0)/d \geq 87$, where the self-conserving conditions are observed, where x_0 is the origin. In this study, the plane corresponding to $(x - x_0) / d = 100$ is considered with $x_0 = 0.0$.

In order to compare the performance of the Lagrangian model, the same case is carried out using the traditional Smagorinsky sub-grid scale model with $C_s = 0.2$ and $Sc_t = 0.5$. The Schmidt turbulent number is kept constant in both set of calculations.

4.8.2 Results of the Buoyant Turbulent Plume

Mean velocity distributions

The evolution of mean and mixture fraction fluctuation from the source to the self-preserving conditions has been considered. Using Eqs.4.17-4.19 as parameters to scale the self-preserving magnitudes yields as follows:

$$\overline{u}(r/(x-x_0)) = \overline{u}(0)\exp[-k_u^2(r/(x-x_0))^2] \tag{4.22}$$

where $k_u^2 = (x-x_0)/l_u)$ and l_u is a characteristic plume radius $\overline{u}/\overline{u}_c = \exp(-1)$.

The best fit of the data obtained by Dai et al. is $\overline{u}(0) = 4.3$ and $k_u^2 = 93$, with $l_u/(x-x_0) = 0.10$.

Fig. 4.12 shows both the measured and predicted stream-wise velocity on the plane $(x\text{-}x_0) / d = 100$. The Lagrangian model predicts reasonably well the measurements of both the plume width and maximum stream-wise velocity but the Smagorinsky model over predicts the plume width.

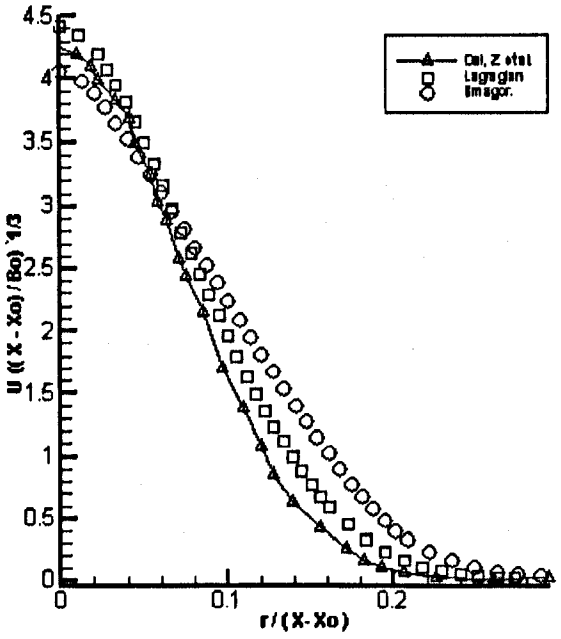

Figure 4.12. Turbulent plume mean streamwise velocity profile at $(x-x_0) / d = 100$.

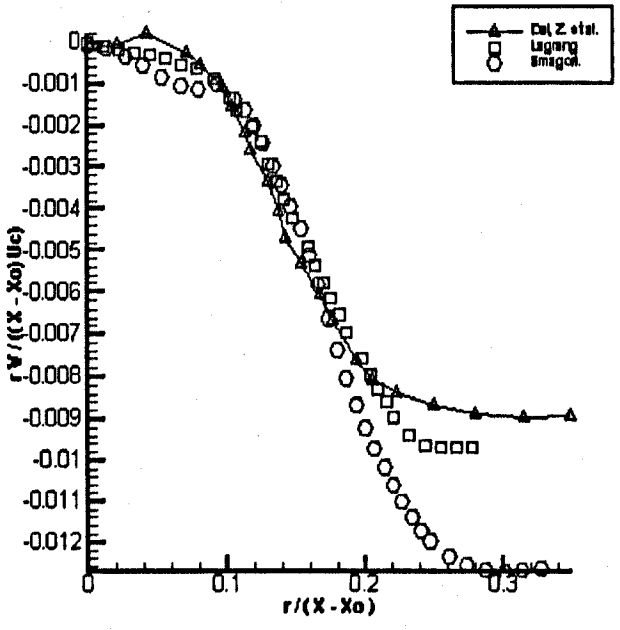

Figure 4.13. Turbulent plume mean radial velocity profile at $(x-x_0) / d = 100$.

The radial velocity profile is illustrated in Fig. 4.13. Scaling parameters have been used to provide a universal plot of the radial velocity. Even when both models predict adequately the radial velocity, the Smagorinsky model over predicts the entrainment velocity at $r / (x-x_0) = 0.2$. This is a relevant point because the over prediction of the entrainment velocity could lead to an over prediction in the plume width. This might also be the cause for the over prediction obtained with the Smagorinsky model in Fig. 4.12

Dai et al. [58] calculated the entrainment behaviour as: $-(r\bar{v})_\infty / ((x-x_0)\bar{u}_c) = 0.009$; where $\bar{v}$ is the radial velocity, $\bar{u}_c$ is the plume mean centre velocity, x is the stream-wise co-ordinate and r is the radius.

Velocity Fluctuations

Fig. 4.14 shows the stream-wise velocity fluctuation prediction. Overall, they are in good agreement with the measured data. The Lagrangian model predicts correctly the radial spread. On the other hand, the Smagorinsky model over predicts the peak at the centre axis, while the Lagrangian model does it well. The Smagorinsky model over predicts the profile width in $0.25 > r / (x - x_0) > 0.1$, as it does in the mean velocity predictions.

Dai et al. [58] observed that the centre value of $(\bar{u}'/\bar{u}_c) = 0.22$ generally is lower than values in the range of 0.25-0.32 observed in previous transitional plumes.

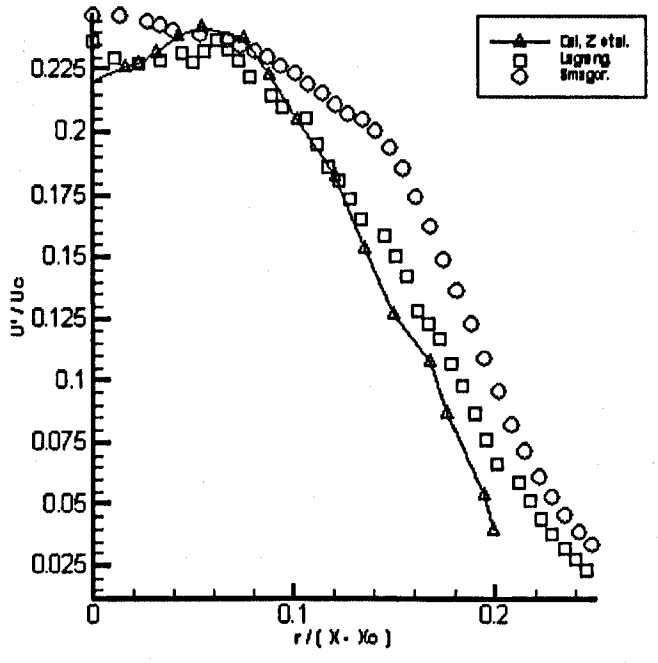

Figure 4.14. Turbulent plume mean streamwise velocity fluctuations profile at $(x-x_0)$ / d = 100.

The presence of the dip in the stream-wise velocity fluctuation measurements near the axis for the self-preserving region is also observed in non-buoyant jets. See Papanicolaou and List [181] and references cited therein. Dai et al. [58] also stated that this dip is expected as turbulence production is reduced near the axis due to symmetry. Nevertheless, this behaviour was not encountered in the mixture fraction measurements of Dai at al. [58]. They attributed it to buoyancy/turbulent iterations because such dips are observed in non-buoyant turbulent jets [14]. It is encouraging to note that the Lagrangian model captures the dip at the centre of the plume while the Smagorinsky model does not.

Sub-grid-scale turbulence model

Fig. 4.15 illustrates the contour of $\overline{C_s^2}$ at $(x - x_0) / d = 100$. It is noted that at the centre of the plume the Smagorinsky constant is approximately $\overline{C_s^2} \approx 0.1$ for turbulent plume used by Zhou [273] is obtained.

For ratios greater than $r / (x - x_0) = 0.2$ the values of $\overline{C_s^2}$ are transported by the entrainment velocity from the open boundaries to the plume centre. In this region, the velocity fluctuations are negligible and the flow remains laminar, thus, it is of no significance for neither the transport of $\overline{f_{MM}}$ nor $\overline{f_{LM}}$.

In the outermost zone of the plume, at $r / (x - x_0) = 0.25$, $\overline{C_s^2}$ is about ≈ 0.004 and increases to a value of 0.0096 as the centreline is reached, where more turbulence is expected.

The total percentage of iterations necessary to clip to zero the solution in order to avoid negative viscosity is about 12%, which is in the same order of the backward faced case. Although, some peaks of 20% around $r / (x - x_0) = 0.2$ are found. These results are of special interest regarding the performance of the Lagrangian model with respect to the complex solution of Eq. 4.12. It is interesting that for these two flows with very different characteristics, both percentages are in the same order. This indicates a certain independence of the model on the flow type.

The $\overline{f_{LM}}$ is shown in Fig. 4.16. High values of $\overline{f_{LM}}$ are observed near the plume centre. This is expected since the turbulence enhances at the centre. Relatively low values of $\overline{f_{LM}}$ and $\overline{f_{MM}}$ were predicted in contrast with the backward faced step. This is also expected as the shear stress tensor in the latter case is bigger due not only to the walls but also to the separation point.

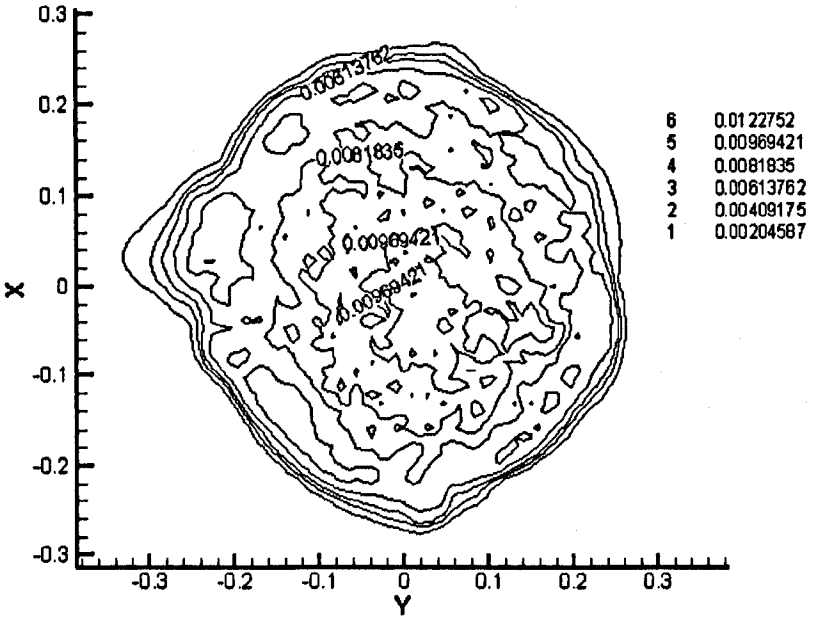

Figure 4.15. Contour profile of C_s^2.

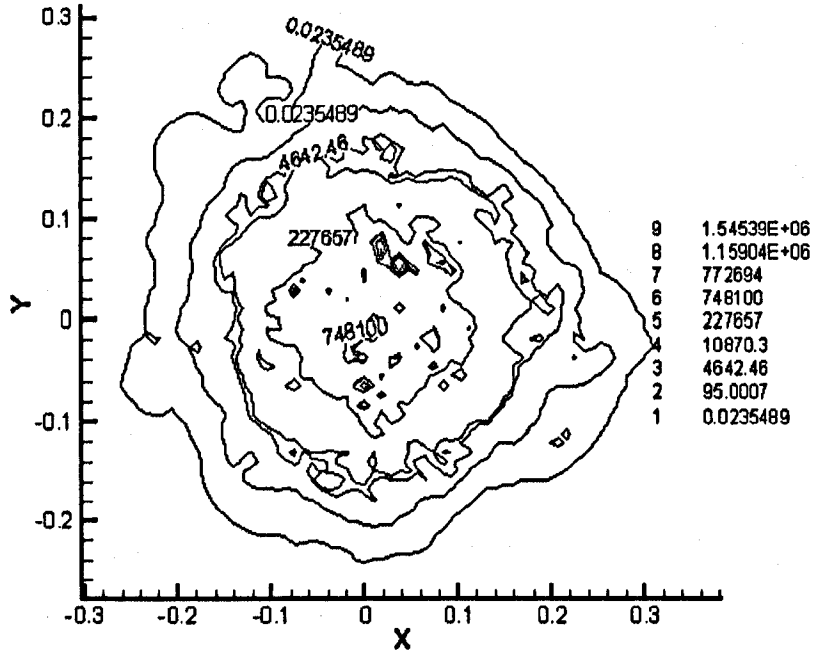

Figure 4.16. Contour profile of f_{lm}.

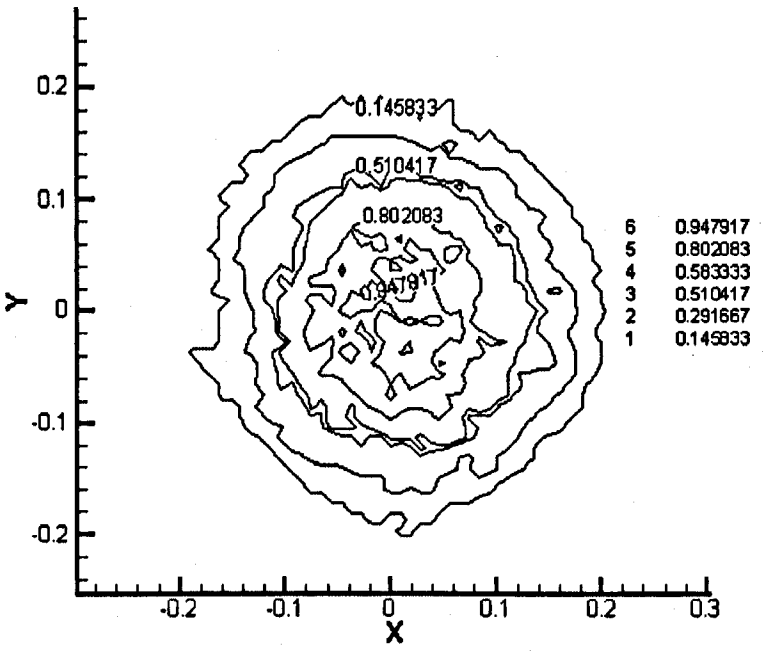

Figure 4.17. Profile of the relation SGS viscosity / molecular viscosity.

Finally, to quantify the performance of the Lagrangian SGS model, Fig. 4.17 illustrates the ratio SGS viscosity/molecular viscosity. As it was underlined above, the role of the sub-grid-scale turbulence model is not as important as in the backward face step. At the plume centre, the turbulence viscosity equals the molecular viscosity and the relation diminishes toward the outer region of the plume.

4.9 Summary and conclusions

Backward facing step

- From the study of the backward-facing step simulation, it was found that the performance of the Lagrangian model in shear walled flows was as good as the Germano et al. model [88]. But with the advantage of not being necessary to select any plane of homogenous turbulence, the new method develops correctly the profile of the Smagorinsky constant at the wall without using any wall function or similar. Moreover, it is not greatly affected by the selection of the constant θ.

- It is shown that the lagrangian model represents adequately the physical behaviour of the flow when it remains laminar. The predicted $\overline{C_s^2}$ in those regions of low turbulence is also small. Hence, it duly diminishes the turbulent dissipation in the outer region of the plume and at the step shoulder.

- Even though the model predicts well the mean velocity in the backward facing step, it fails to predict the velocity fluctuations around x / h = 1. In particular, the model tends to over predict u', v' and w' and thereafter, to over estimate the Reynolds stresses in this region. It is interesting to underline the good agreement with the measurements at x / h = 0 near the step shoulder; this illustrates the good agreement in the upstream flow conditions immediately above the step. Near x / h = 1, the simulation deteriorates and produces an over prediction of the fluctuations. This issue should be addressed in future works.

- The model predicts a maximum turbulence energy (k) near the step shoulder (x/h = 1.48 and y/h = 1) but the measurements locate it at x / h = 2 and y / h =1. The centre of the principal eddy is predicted at x / h = 2.29, while Kasagi and Matsunaga [112] measured it at x / h = 3.0. The same pattern is found for the principal and secondary reattachment point locations, where the model

under predicts both values. It is thought that these under predictions might be related to the over predictions of the fluctuations described in the previous paragraph.

- The percentage of "clipping" due to negative values of the viscosity is about 12%, which is slightly larger than the value obtained by Meneveau. If this condition remains for a long period of time it may easily destabilize the numerical scheme. Additionally, it is noted that the model predicts low values for $\overline{C_s^2}$ in the present configurations.

Buoyant plume

From the results obtained in the buoyant turbulent plume, it can be drawn that the Lagrangian model does slightly better than the classical Smagorinsky model. Specifically, the Smagorinsky model estimates wider profiles for stream-wise velocity, radial velocity and velocity fluctuations.

It is interesting to note that in the turbulent plume the Smagorinsky constant, predicted by the Lagrangian model, is very close to the best value for this type of flow $\overline{C_s^2} = 0.1$.

It should also be pointed out that the lagrangian approach requires approximately 20% or more processing time than its Smagorinsky counterpart. This time is mostly consumed in calculating the stress tensor at the 2Δ grid.

Chapter 5

Conditional Source Estimation (CSE)

In this chapter a variation of the original Laminar Flamelet Decomposition (LFD) for Conditional Source Estimation (CSE) model, developed by Bushe and Steiner [35], is introduced and used to simulate the turbulent non-premixed piloted SANDIA Flame D.

The CSE model is originally based on the Conditional Moment Closure (CMC) concept, which was introduced in chapter 3. Briefly, it calculates the conditional source term as function of conditional species and temperature. In order to obtain the conditional variables, a set of equations must be solved in the conditional space. These equations are very stiff and models are necessary for closing unclosed terms. Bushe and Steiner [35] proposed the CSE as an alternative. This method closes the conditional source term from filtered variables without solving the set of conditional equations.

5.1 Conditional Moment Closure (CMC) background

The pdf method was proposed by Pope [203] and was used extensively in many studies. The CMC, originally developed by Bilger and co-workers [17], is based on a pdf transport equation for the velocity and the reactive scalars. Within this framework, they represent a very general statistical description of turbulent reacting flows, applicable to premixed, non-premixed and partially premixed flows. The pdf has been extended to LES using filtered density function at sub-grid level [51]. The concept of sub-grid scale pdfs has been adopted in conserved scalar methods as the Laminar Flamelet Model (LFM).

Presuming the sub-grid scale pdf of the mixture fraction P(Z), the filtered species mass fractions Y_i in each computational cell can be evaluated by

$$\widetilde{Y}_i(\bar{x},t) = \int_0^1 Y_i(Z,t)\widetilde{P}(Z,Z',\bar{x},t)dZ \tag{5.1}$$

Provided the functional dependence $Y_i(Z,t)$ is known. Here, the tilde denotes density-weighted spatial filtering. For clarity, the pdf will be referred to as $\widetilde{P}(Z)$ and the conditional quantity as $Y_i(Z)$.

The pre-assumed pdf approach, $\widetilde{P}(Z)$, usually follows a Beta distribution parameterised with two moments: the filtered mixture fraction and its variance. Usually, the first moment is determined by solving the transport equation for a conserved scalar. The variance, or second moment, can be either calculated by a sub-grid model or solved through a transport equation. The validity of the assumption of the beta function distribution at sub-grid scale for the mixture fraction has been successful by validated for LES applications.

Different approaches have been used to specify the function $Y_i(Z,t)$ in Eq. 5.1. Broadly speaking, these are: the infinitely fast chemistry, the equilibrium assumption [52], the steady or unsteady Laminar Flamelet Model (LFM) [54, 55, 195, 199, 249]

and the Conditional Moment Closure (CMC) model [75, 120].

In the Laminar Flamelet Model (LFM), the turbulent diffusion flame is viewed as consisting of an ensemble of stretched laminar flamelets attached to a conserved scalar, usually the mixture fraction (Z). The flamelet equations depend on both the mixture fraction, Z, and the scalar dissipation rate, χ. In this approach, the flamelets are viewed as thin reactive-diffusive layers embedded within the turbulent flow field at the stoichiometric value. Therein, the scalar dissipation rate is responsible for the chemistry-turbulence interaction. Cook et al. have introduced LFM into LES using look-up tables for the reaction rate for different turbulence-combustion conditions [52, 55].

The steady flamelets are not capable of predicting unsteady effects like ignition and extinction. A lagrangian flamelet model was proposed for LES in different studies [194, 195, 197]. This model solves the unsteady laminar flamelet equation, which can be seen as the residence time of the flamelet in the flow field. Even tough this approach does not require any steady-state assumption for the flamelet equations, it considers that individual flamelets do not change with time in the flow.

The concept of Conditional Moment Closure (CMC) was developed simultaneously by Klimenko and Bilger [16, 124]. The essence is that, rather than considering conventional averages, one should condition the reactive scalars on the mixture fraction space. Bilger based his derivation on the observation that most fluctuations of the reactive scalars can be associated with fluctuation of the mixture fraction. This concept was originally developed for non-premixed combustion, but conditioning on the progress variable for premixed combustion has been also developed [17]. CMC has been applied to turbulent jet diffusion flames [128], turbulent lifted flames [65], predictions of NO formation in hydrogen jet [13] and non-premixed methanol bluff-body flames [119]. This approach has been successfully compared against DNS calculations in non-premixed hydrocarbon flames [233] and further development allowed to include differential diffusion [127]. On conditioning the source term with the mixture fraction, a first order approximation is considered for all known CMC

applications. Consequently, the source term can be well predicted, when calculated through the conditioned quantities.

Nevertheless, CMC needs to solve an extra dimension system, so it would be necessary to solve a four dimension equation. Moreover, in CMC equations there are unclosed terms that need to be model such as the conditional dissipation rate and the conditional velocity. Additional transport equations for each new species are necessary if complex chemistry is required. In order to account for extinction-ignition process, some researchers introduced a second order approach to the conditional source term [120].

Bushe and Steiner [34] made use of the CMC source term closure hypothesis and attempted to work out the conditional values needed for calculating the conditional source inverting Eq. 5.1. This approximation of the source term is called Conditional Source-Term Estimation (CSE). In principle, this method does not need any steady state assumption, either in Z or in the physical space.

5.2 The Conditional Source Estimator model (CSE)

The CSE methodology was firstly proposed by Bushe [34].There are many approaches to establish the function of the species mass concentrations and temperature in the mixture fraction space. Originally, CSE follows the Conditional Moment Closure (CMC) concept developed by Bilger [16]. In the CMC approach, the energy source term is considered as follow:

$$\dot{w}(Z) = F((Y_i(Z), T(Z)) \tag{5.2}$$

where F is usually the Arrenius expression, and $Y_i(Z)$ and $T(Z)$ are the conditional mass concentrations and temperature, respectively.

The advantage of this approach is that the conditional source term, $w(Z)$, becomes more stable when expressed in term of the conditional quantities. This is so even if

the first order approach is used. In CMC, a set of separated equations are solved to compute $Y_i(Z)$ and $T(Z)$.

In the Unsteady Laminar Flamelet Model (ULMF) the unsteady flamelet equations are coupled with the flow solver to obtain the conditional quantities [199]. Alternatively, the CSE approach proposes to estimate the conditional variables performing the inversion of Eq. 5.1 to obtain $Y_i(Z)$ and $T(Z)$.

Eq. 5.1 is called Fredhold equation of the first class. The inversion attempts to calculate the source function ($Y_i(Z)$ or $T(Z)$) through the 'measurements' of the unconditional variables, ($T(\bar{x})$ or $Y(\bar{x})$) and the kernel of the inversion, $\widetilde{P}(Z)$. In its simplest form the inversion is reduced to the least square method.

This method was applied with relative success to a diffusion flame D [231]. It was found feasible to approach the conditional values using an inversion of the filtered values. However, it suffers from some setbacks:

- It needs one equation for each specie to account for detailed chemistry.
- The inversion was proved to be ill-conditioned (a key issue in CSE).
- It was necessary to introduce a second conditional variable to obtain predictions of local extinction phenomena, making the model far too computationally far too expensive.

The inversion performed by simple methods was found to be very unstable and its results physically meaningless. This instability is inherent to the inversion process itself. Out of the many inversion techniques existing in the literature, some are detailed in [56, 239].

The decomposition technique was proposed in order to overcome some of these difficulties [35]. In this approach, a set of basis functions is chosen into which $Y_i(Z)$ and $T(Z)$ are projected. An obvious choice is the laminar flamelet functions. These have the advantage of being actual realisations of the flame in the flow. Thus,

$$T(Z) = \sum_{j=1}^{n} a_j \theta_{\chi_j}(Z) \tag{5.3}$$

$$Y_i(Z) = \sum_{j=1}^{n} a_j \theta^i_{\chi_j}(Z) \tag{5.4}$$

where a_j are the coefficients of the decomposition. θ_{χ_j} and $\theta^i_{\chi j}$ are the flamelets solutions of temperature and species, respectively. χ_j denotes the dissipation rate which is related to j^{th} function, n is the total number of functions considered in the basis.

One of the main difficulties that a simple inversion technique faced was the sharp gradients of the conditional quantities, resulting in either over-diffusive or highly oscillatory solutions. Certainly, using the decomposition technique reduces significantly this problem.

Therefore, Eq. 5.1, can be re-written, for temperature, as:

$$\overline{T}(x) = \int_0^1 \widetilde{P}(Z) \sum_{i=1}^{n} a_j \theta_{\chi_j}(Z) dZ \tag{5.5}$$

where the functional to be minimised takes the form:

$$\min \left\{ \|Ka - b\|^2 + \lambda \|a\|^2 \right\} \tag{5.6}$$

which has the least-squares solution of:

$$(K^T K + \lambda I)[a] = K^T [b] \tag{5.7}$$

where K is the kernel of the inversion, I is the identity matrix, λ is the regularization parameter, $[a]$ is the unknown coefficient vector and $[b]$ is the filtered unconditional variable.

Note that if $\lambda = 0$, we have an inversion in a least square sense. The coefficients of the vector $[a]$ are calculated by solving Eq 5.7.

In the decomposition method the coefficients of the vector $[a]$ might be used to perform the linear combination of each of the Y_i species in Z space. Eventually, it should be possible to perform only one inversion in order to obtain the coefficients and use them to calculate the other species and the heat release. This methodology was originally proposed by Bushe [35].

Nevertheless, the inversion process presents some issues, which are necessary to address. From the mathematical point of view, the basis chosen should be as orthogonal as possible in order to pose correctly the inversion problem and thus avoiding instabilities [239]. However, in practical terms Eq. 5.7 usually presents a difficult problem. In general, the ranks of the flamelet functions (i.e. temperature) are not large (the singular values drops to zero quickly for high frequencies) and the basis is not very orthogonal. Consequently, the inversion is negatively affected and the computation of the conditional quantities from the temperature field produces an ill-posed inversion system.

To overcome this, it was proposed to consider another scalar quantity to perform the inversion, i.e. CO_2. Through this procedure, the stability is improved but the computational cost is enhanced. Some researchers used an inversion technique called restrained method, which takes the previous time step solution as departing point for the new solution. The value of λ in the inversion of Eq. 5.7 adds enough a-priori

information to stabilize the solution. In the literature, an initial value for $\lambda =$ Tr(K)/Tr(I) is suggested [259]. In our case, this value was seen to smooth out too much the solution and was reduced by a factor of 10^{-3}.

In the present study, we follow the initial approach of Bushe [35] and we calculate the coefficients [a] using only the temperature field inversion. We believe that CSE should remain a low computational cost closure method. However, we realise that the inversion process, using the decomposition method, is not capable of clearly project the physical vector onto the 'far-from-orthogonal' flamelet temperature basis. In other words, given too many basis functions will destabilize the solution.

In the light of this, we seek for a method to reduce the number of basis functions in order to avoid the instability in the inversion process.

In order to reduce the basis, some approaches are possible. One option is to reduce the number of temperature basis functions through the application of Singular Value Decomposition (SVD), selecting those vectors whose singular values are larger than a minimum. This improves considerably the inversion convergence. Nevertheless, it has the disadvantage that the functions used for the inversion will remain unchanged throughout the flow. Another possible option, which is adopted here, is to take the dissipation rate as external parameter to select the basis functions for the inversion. As the inversion will find the best possible solution using the basis provided, there is no need to incorporate a detailed calculation of the dissipation rate and its evolution in time. We use as the central flamelet in our basis the average of χ in locations where Z is slightly on the lean side of the stoichiometric mixture ($\overline{\chi}$). Thereafter, the basis is extended to flamelets above and below the mean value. In the present case, $\Delta\chi =$ 8. Thus, the basis considered is $\theta_{\overline{\chi}\pm\Delta\chi}$.

When the coefficients of [a] are found, the average conditional $w(Z)$ is obtained for each plane and projected into the physical space using:

$$\dot{w}(\bar{x}) = \rho(\bar{x})\int_0^1 \frac{\dot{w}(Z)}{\rho(Z)}\widetilde{P}(Z)dZ \tag{5.8}$$

In order to solve the flamelets, a set of equation must be solved, the so-called unsteady flamelet equations must be solved. This system was first proposed by Peter [183]. And it reads:

$$\rho\frac{\partial Y_i}{\partial t} - \rho\frac{\chi}{2}\frac{\partial^2 Y_i}{\partial Z^2} - \dot{w}_i = 0 \tag{5.9}$$

$$\rho\frac{\partial T}{\partial t} - \rho\frac{\chi}{2}\left(\frac{\partial^2 T}{\partial Z^2} + \frac{1}{C_p}\frac{\partial C_p}{\partial Z}\frac{\partial T}{\partial Z}\right) + \frac{1}{C_p}\left(\sum_{n=1}^{N} h_n\dot{w}_n - H\right) = 0 \tag{5.10}$$

where h_i and $\dot{w}_i$ are specific enthalpy and the chemical production rate per unit volume of the species i, respectively, Z is the mixture fraction, Y_i is the species mass concentrations, C_p is the constant pressure specific heat capacity, t is the time, χ is the dissipation rate and H accounts for the enthalpy flux by mass diffusion.

In Eqs. 5.9 and 5.10, the Lewis number is assumed to be unity. These equations are solved in a co-ordinate perpendicular to the flame sheet assuming counter flow conditions [183] using the Flame Master code [193]. The adopted chemical scheme involves 28 species and 72 reactions [185]. Optically thin gases are assumed in calculating the radiation loses (CO_2 and H_2O). The steady flamelet are solved for 30 dissipation rates ranging from χ = 1.5 sec^{-1} to 220 sec^{-1}. The species boundary conditions at Z=0 and Z=1 are those of the flame D.

The dissipation rate is introduced as follows:

$$\chi = 2D_Z\nabla Z.\nabla Z \tag{5.11}$$

where D_Z is the diffusion coefficient of the mixture fraction. For the calculation of the dissipation rate we follow [93]. Many sub-grid models for the variance of the

mixture fraction can be used. The scale similarity model proposed by Cook and Riley [52] or the small-scale equilibrium assumption by Pierce [191]. The later is chosen for the present study.

5.3 SANDIA flame D configuration

The configuration used for the validation of the proposed models is a piloted methane/air jet diffusion flame. (SANDIA Flame D). The fuel is a 25/75% methane/air mixture. The fuel has been premixed with air in order to minimise the formation of polycyclic aromatic hydrocarbons and soot. The fuel nozzle has a diameter of D=7.2mm and is enclosed by a broad pilot nozzle with a diameter of Dp=18.34 mm. In the experiment, the pilot composition and temperature have been adjusted, so that the pilot stream has the same equilibrium composition as a mixture fraction of Z=0.27 at the co-pilot and Z=1 at the fuel nozzle. The stoichiometric mixture fraction is Z=0.35. The fuel bulk velocity is 49 m/s, equivalent to Reynolds number of 22400 based on the nozzle diameter. The inlet parabolic velocity profile has a maximum velocity at the centre of the fuel nozzle of Vmax = 62 m/s.

The flame has been experimentally investigated by Barlow [10, 12] who measured average and variance value for temperature and species.

5.4 Numerical scheme and implementation

The balance equations are solved by an explicit second order method in both time and space. A central difference predictor-corrector scheme is used. The equations are fully compressive and the advection term is treated in its rotation form, so this method conserves both kinetic energy and momentum. A direct Poisson solver is used for solving the mass conservation equation. The radiation losses are not considered here as this flame is not sooty. The set of basic equations can be found in chapter 4.

In the present simulation, the Smagorinsky constant is set to 0.1. $Pr_t = 0.7$ and $Sc_t = 0.5$ are used as a first approach.

Eqs. 5.9 and 5.10 are solved for 30 different values of dissipation rates. The minimum value being 1.5 sec^{-1} and the maximum 220 sec^{-1}. The species boundary conditions are $Y_{CH4} = 0.15$, $Y_{O2} = 0.2$ and T = 300 K for Z = 1 and $Y_{CH4} = 0.$, $Y_{O2} = 0.23$ and T = 300 K for Z = 0. The segmentation used in the mixture fraction space is 63 nodes, equally distributed.
The heat release, temperature and species flamelets are stored in a look-up table. The flamelet at a dissipation rate of 100 sec^{-1} is used to relate thermo-chemical variables to the mixture fraction. This value is consistent with those used in previous pdf predictions of the Sandia flames series [224].

The assumption of statistical homogeneity for the conditional variables is essential to the CSE method. If the mean conditional is not homogenous, the solution of Eq. 5.1 does not represent adequately all point of the ensemble. It is generally accepted that conditional quantities do not depend on the radius for jet flames. In other words, $Y_i(Z)$ is function only of the coordinate equidistant to the nozzle (x). Therefore, the conditional variables become $Y_i(Z,x)$. This was confirmed by experiments [10] for jet piloted flames.

Moreover, the experimental data of the piloted flame show that the conditional averages do not change very rapidly downstream from the axis of the jet. This rather slow downstream variation makes it possible to calculate the conditional averages on a coarser mesh [194, 231]. Thus, rather than using LES points located on every single plane, all the LES points on a layer of several neighbouring planes can be taken as statistical samples to establish the linear system. In the present case, the conditional variables are solved on a mesh fivefold coarser and, following Steiner [231], we use a single LES plane for each conditional cell.

As no steady-state condition for the flame is assumed, the linear system has to be inverted at every time step to obtain the conditional averages evolving in time. This can be relaxed at some point, when the flame reaches the steady state and the mean conditional variable do not change significantly in time. Thus, in our calculation the

conditional time step is $5\Delta t$. It is, however, noted that the CSE method does not require any steady-state assumption for the conditional filtered averages.

Mesh sensitivity

Two simulations are carried out using two mesh sizes. In mesh 1, the size of a cell in the near field of the flame is (1.97 x 1.97 x 2.8) mm. The physical domain is (0.16 x 0.16 x 0.6) m in X, Y and Z direction respectively and the circular nozzle is approximated using 13 cells across its diameter (D). In mesh 2, the mesh size is (1.25 x 1.25 x 2.8) mm in X, Y and Z directions, respectively in the near field. The results are shown in Fig 5.1 for Z and in Fig 5.2 for temperature. The prediction of the mixture fraction and temperature are very close to the coarse mesh. Although, there is some difference around Z/D 60 for the mixture fraction RMS which may be due to the smaller domain used in mesh 2. Therefore, mesh 1 is used in the present study.

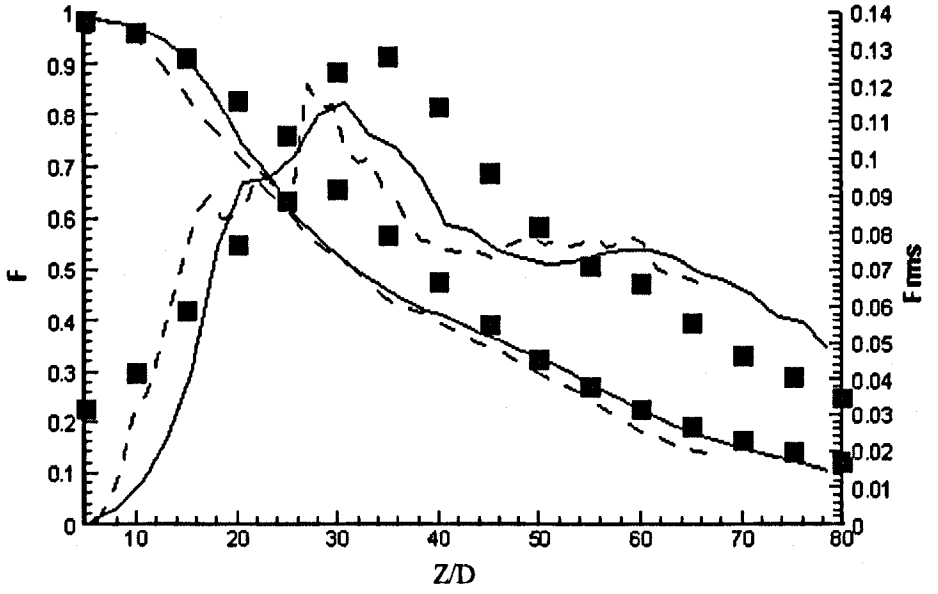

Figure 5.1. Mean and RMS central line mixture fraction. Symbols: experiment, line: simulation with coarse mesh, dashed line: simulation with fine mesh.

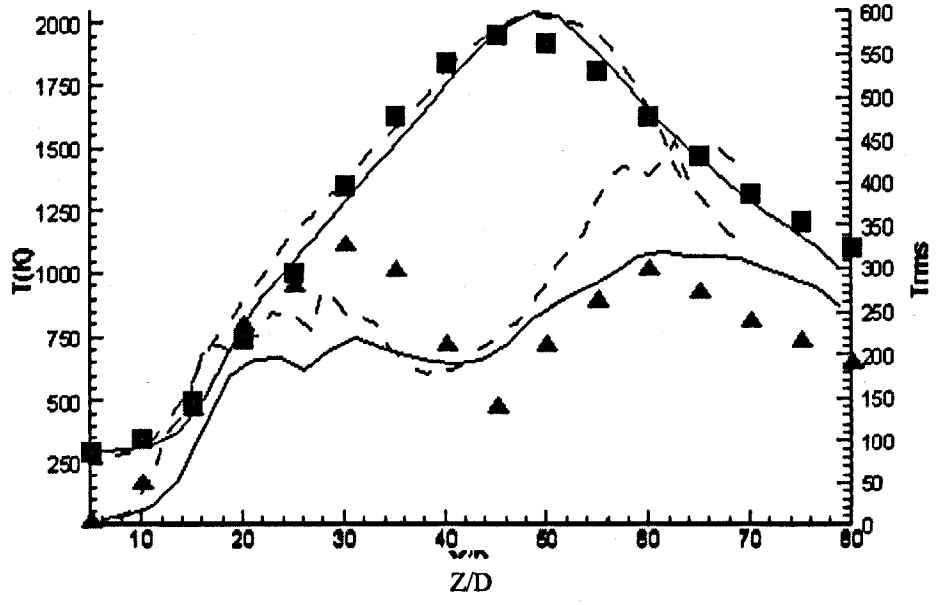

Figure 5.2. Mean and RMS central line temperature. Symbols: experiment, line : simulation with coarse mesh, dashed line: simulation with fine mesh.

5.5 Results

The mean mixture fraction along the centreline is shown in Fig. 5.1. In general terms, the mixture fraction is reasonably well predicted. Nevertheless, a region can be seen, from Z/D = 20 to Z/D = 40, where the mixture fraction is clearly under predicted. It is important to note that this diffusion flame is known to present some extinction from Z/D = 10 to 25 and, eventually, re-ignition from Z/D =25 to 50. Therefore, the under-prediction here may imply that the use of SLFM (Steady Laminar Flamelets Model) as basis functions can not capture extinction and re-ignition. As a result, the fuel and oxygen consumptions are over predicted. This behaviour can be observed in most of the average species concentrations as in CSE there is a strong relation between species and mixture fraction as indicated by Eqs.5.3 and 5.4.

Also in Fig. 5.1, the Z fluctuation is observed to follow reasonably well the measurements, despite some underprediction close to the nozzle. This may be attributed to some error in the measurements, since the RMS has to go to zero close to the nozzle. Because of the aforementioned strong link between the two, the relatively good prediction of RMS of the mixture fraction also implies good predictions in the RMS of specie concentrations

Fig. 5.2 shows the mean temperature along the centre line. It can be seen that the location of the maximum temperature is reasonably well predicted, even though the maximum value is slightly over predicted. In general, the simulation is in line with the experiments. It is somehow surprising that the temperature prediction, between Z/D = 20 and 40, is not over predicted given the under prediction of the mixture fraction mentioned above.

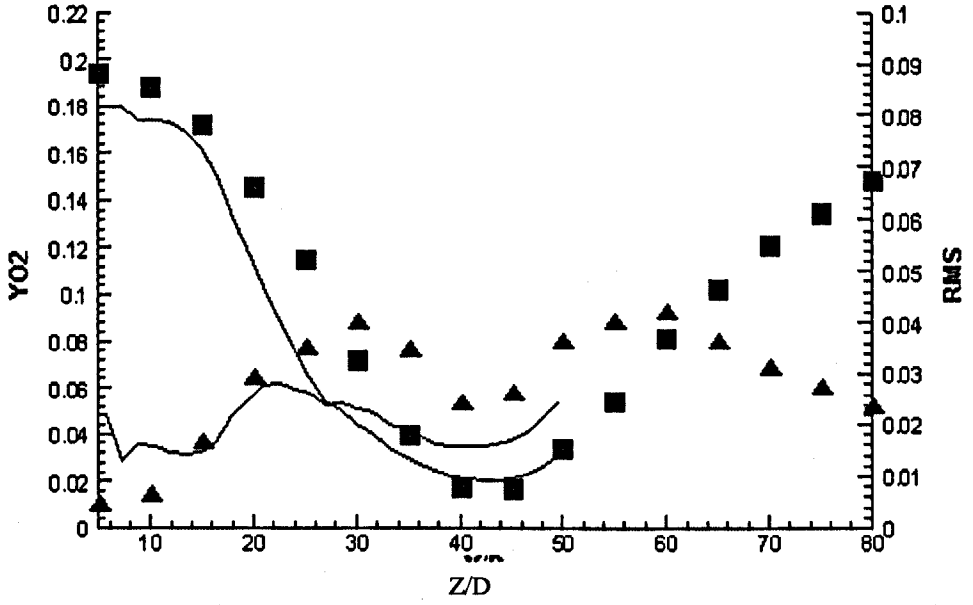
YO2
RMS
Z/D
0.22
0.2
0.18
0.16
0.14
0.12
0.1
0.08
0.06
0.04
0.02
0
0.1
0.09
0.08
0.07
0.06
0.05
0.04
0.03
0.02
0.01
0
10
20
30
40
50
60
70
80

(a)

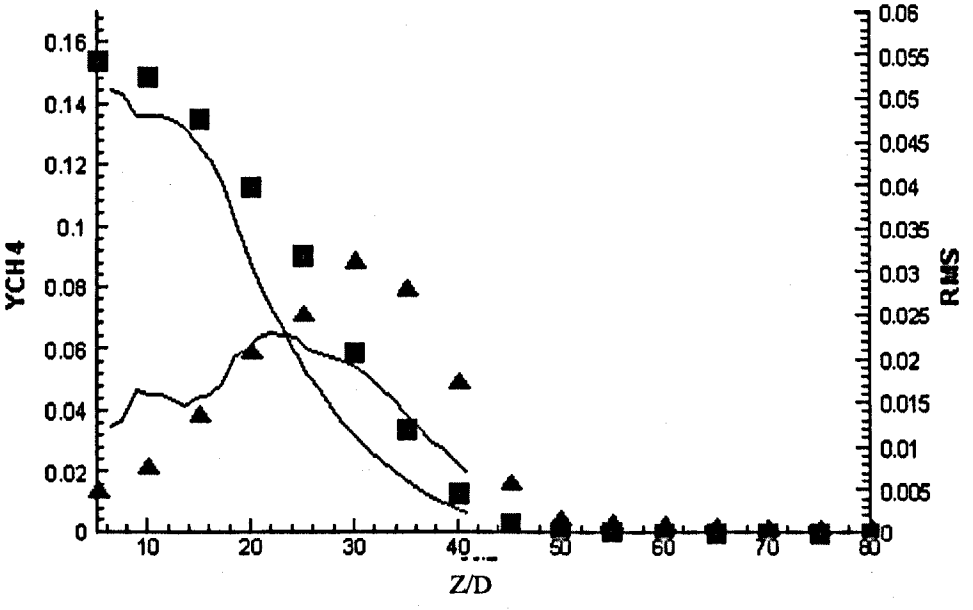
YCH4
RMS
Z/D
0.16
0.14
0.12
0.1
0.08
0.06
0.04
0.02
0
0.06
0.055
0.05
0.045
0.04
0.035
0.03
0.025
0.02
0.015
0.01
0.005
0
10
20
30
40
50
60
70
80

(b)

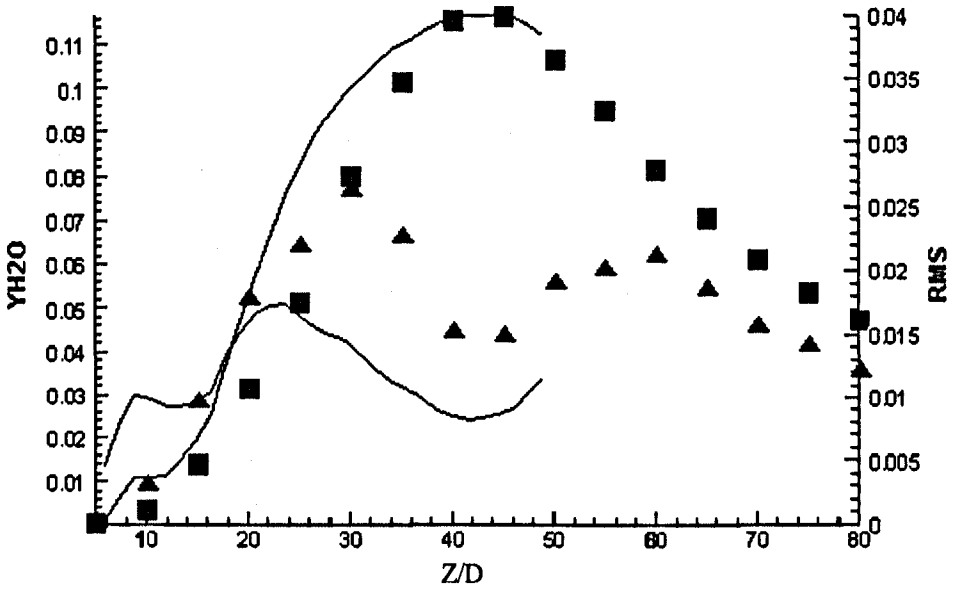
YH2O
RMS
Z/D
0.11
0.1
0.09
0.08
0.07
0.06
0.05
0.04
0.03
0.02
0.01
0.04
0.035
0.03
0.025
0.02
0.015
0.01
0.005
0
10
20
30
40
50
60
70
80

(c)

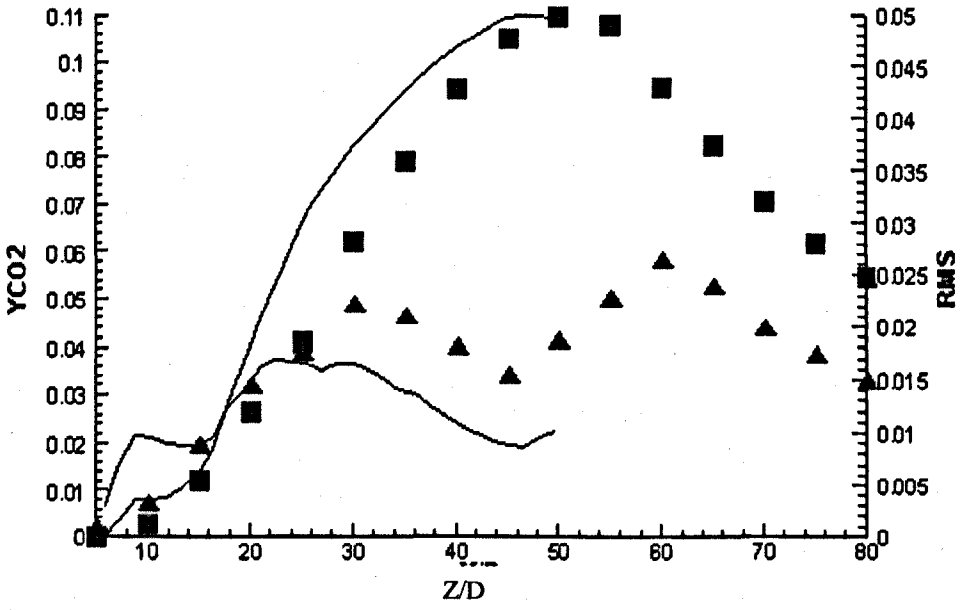
YCO2
RMS
Z/D
0.11
0.1
0.09
0.08
0.07
0.06
0.05
0.04
0.03
0.02
0.01
0
0.05
0.045
0.04
0.035
0.03
0.025
0.02
0.015
0.01
0.005
0
10
20
30
40
50
60
70
80

(d)

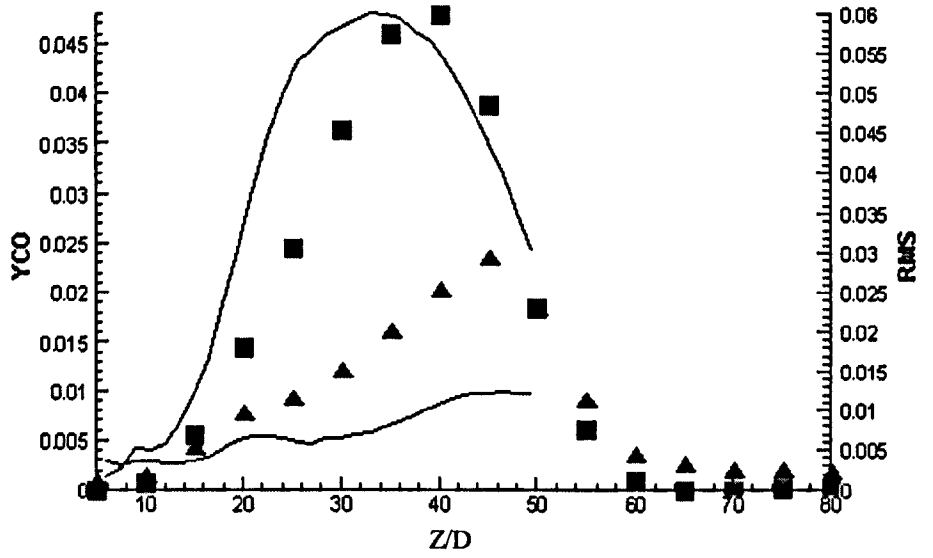

(e)

Figure 5.3. Mean and RMS central line (a) O_2, (b) CH_4, (c) H_2O, (d) CO_2 and (e) CO. Symbols: experiment, line: simulation.

Figs. 5.3a to 5.3e show the species mass concentrations of O_2, CH_4, H_2O, CO_2 and CO, respectively. Consistently, the species are either under predicted or over predicted between Z/D = 20 and 40, depending on which side of the chemical reaction they are, or, in other words, depending on whether the species are consumed or produced. As mentioned before, fuel and oxygen are consumed faster than in the experiment, and the RMS of both are under predicted within the same region. On the contrary, the products (H_2O, CO_2 and CO) are over predicted and still their RMS are under predicted. These discrepancies in the prediction of species are mainly attributed to the under prediction of the mixture fraction field in the same region (Fig. 5.1). Other factors such as the chemical mechanism, the beta-distribution assumption and uncertainties in the SGS turbulence model might contribute to the disagreement.

Unfortunately, a further study of these different factors is neither achievable nor within the scope of the present work. We limit our study to evaluate the feasibility of

CSE as a practical approach to estimate the conditional quantities. Nevertheless, it is expected that an improvement in the mixture fraction prediction will enhance the species predictions.

In Figs. 5.4a-5.4f, the radial profiles of Z, temperature, O_2, H_2O, CH_4 and CO_2 at Z/D = 15 are shown. Complementarily, the conditional values for O_2, H_2O, CH_4 and CO_2 are depicted in Figs. 5b-5e for the same plane.

Fig. 5.4a shows the mean Z and RMS predictions. On this plane, the simulated values of Z and RMS are good, except for an over prediction of the mean quantity around r/D = 1.4. In the measurements, the stoichiometric value (Z_{st} = 0.35) is located at r/D = 1.2 and in the simulation at 1.4. This disparity, between r/D>0.8 and 2.0, will roughly create either over or under predictions of the unconditioned species mass concentrations depending on the conditional dependency of the species on the mixture fraction space.

The conditional and unconditional oxygen ($Y_{O2}(Z)$ and Y_{O2}) at Z/D = 15 are shown in Figs. 5.5b and 5.4b. On this plane, the conditional value is clearly under predicted, especially close to Z_{st}. In the experiment, there is some oxygen left at the stoichiometric surface; this it is not captured by the simulation where the oxygen is completely depleted. Coincidently, we observe that in most of the radial positions the oxygen is under predicted (Fig. 5.4b) for the mean quantity and a reasonably good prediction is obtained for RMS.

Fig. 5.5c shows the conditional average $Y_{H2O}(Z)$. Here, the conditional value is slightly over predicted around Z_{st}. In Fig. 5.4c, a combined effect of discrepancy on Z and $Y_{H2O}(Z)$ produces an over prediction in the inner section of the jet r/D < 0.8, followed by an under prediction and a shift of the maximum value of Y_{H2O}. We observe that the RMS of Y_{H2O} is reasonably well predicted.

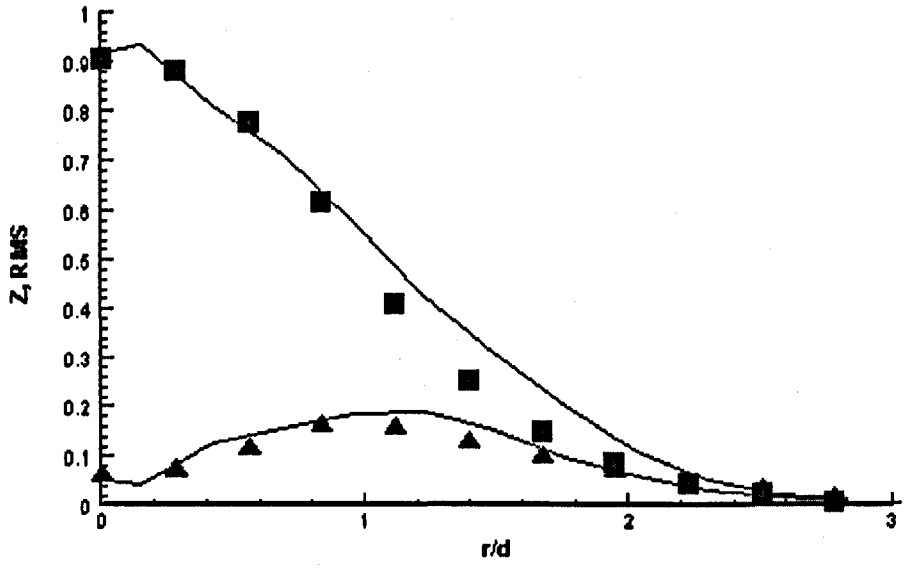

(a)

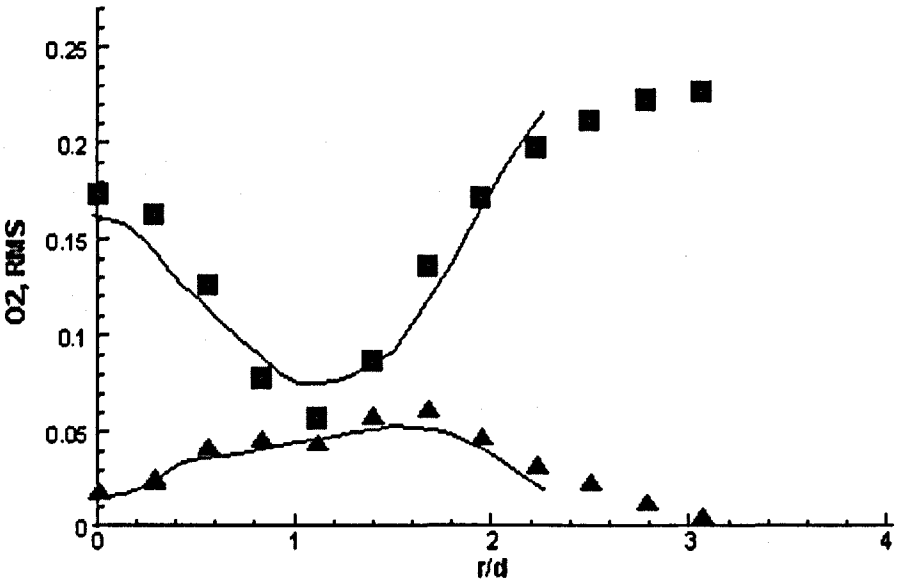

(b)

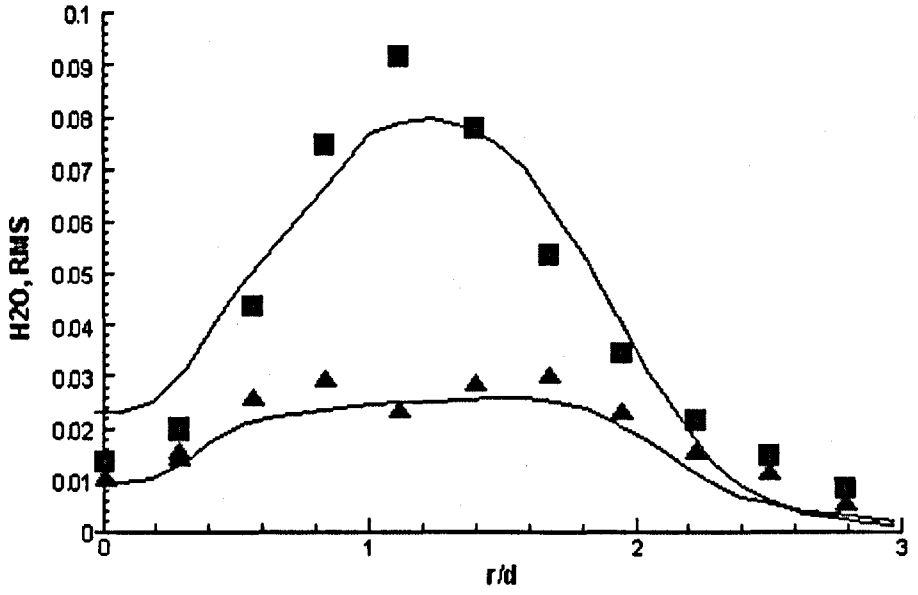
H2O, RMS
0.1
0.09
0.08
0.07
0.06
0.05
0.04
0.03
0.02
0.01
0
0
1
2
3
r/d

(c)

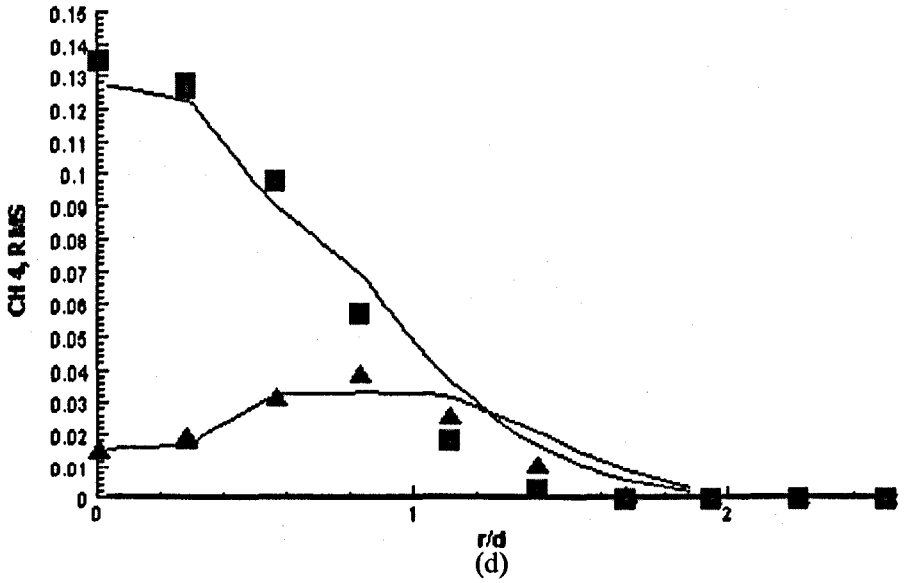
CH4, RMS
0.15
0.14
0.13
0.12
0.11
0.1
0.09
0.08
0.07
0.06
0.05
0.04
0.03
0.02
0.01
0
0
1
2
r/d

(d)

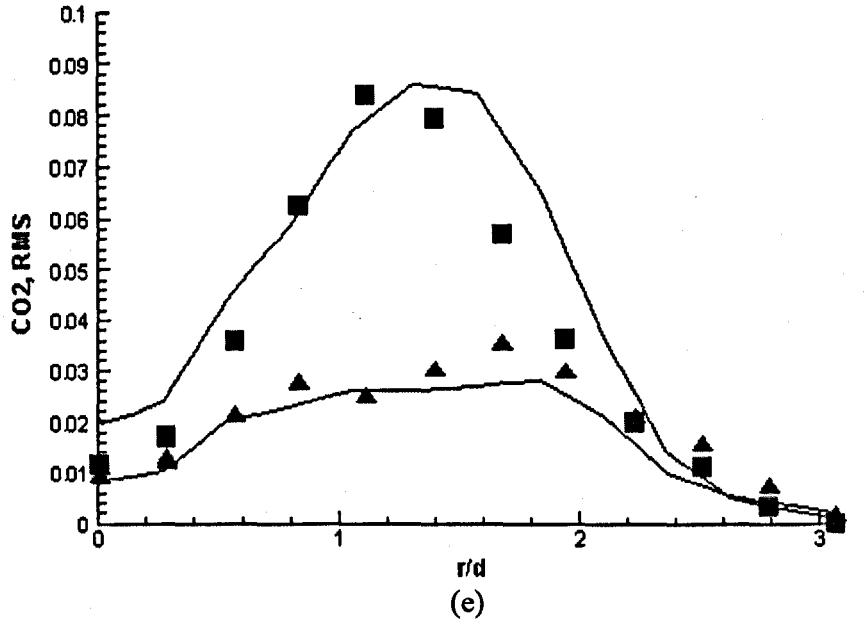

(e)

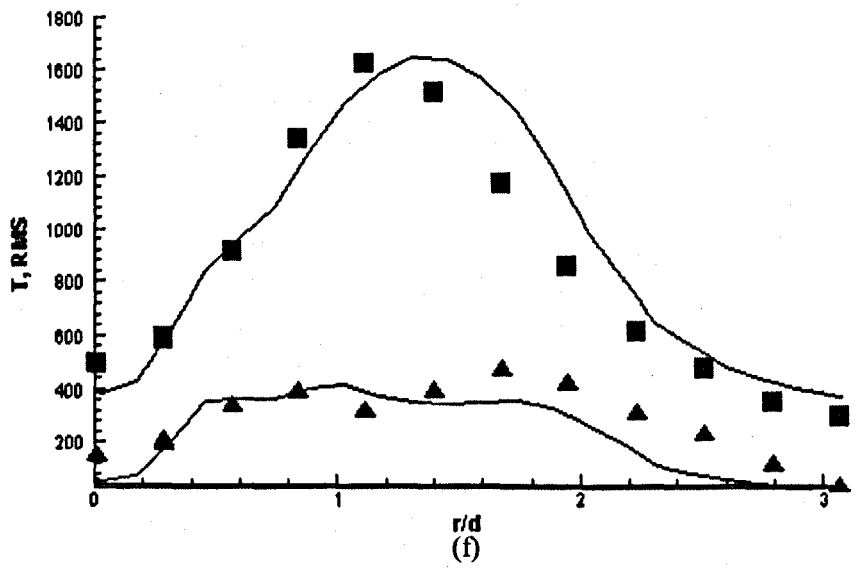

(f)

Figure 5.4. Mean and RMS radial profile at Z/D = 15 of (a) Z, (b) O_2, (c) H_2O, (d) CH_4, (e) CO_2 and (f) temperature. Symbols: experiment, line: simulation.

Figs. 5.4d and 5.5d describe the unconditional and conditional Y_{CH4}, respectively. We observe a good approximation with the experiments for the mean value and RMS.

Figs. 5.4e and 5.5e show the unconditional and conditional CO_2 mass concentrations. The conditional quantity is clearly over predicted through the mixture fraction space. Consequently, the averaged predicted variable is mostly over predicted. It shows a similar shift of the peak value as in the case of H_2O (Fig. 5.4c) and mean temperature (Fig. 5.4f).

The unconditional temperature is shown in Fig. 5.4f. The RMS is well predicted and, as it was said before, the maximum value is shifted outwardly; this later is related to the over prediction in mixture fraction shown in Fig. 5.4a. Nevertheless, the trend is correct and follows the experiments.

Finally, the conditional temperature is shown in Fig. 5.5a. This average conditional variable is calculated through the coefficients of [a] and it is not the actual inversion of the filtered values on the LES mesh. Indeed, the energy balance equation is solved by LES. It can be noted that in the three planes, Z/D = 15, 30 and 45, in Figs. 5-a, 7-a and 9-a, respectively, T(Z) is very similar. We believe that this is a direct consequence of using SLFM in the CSE approach.

Figs. 5.6 and 5.7 show the unconditional and conditional values at Z/D = 30. The radial profile of Z is shown in Fig. 5.6a. As it was seen before, the centre value is under predicted but the simulation agrees well for positions r/D > 1.2. The RMS is well predicted all along the radius.

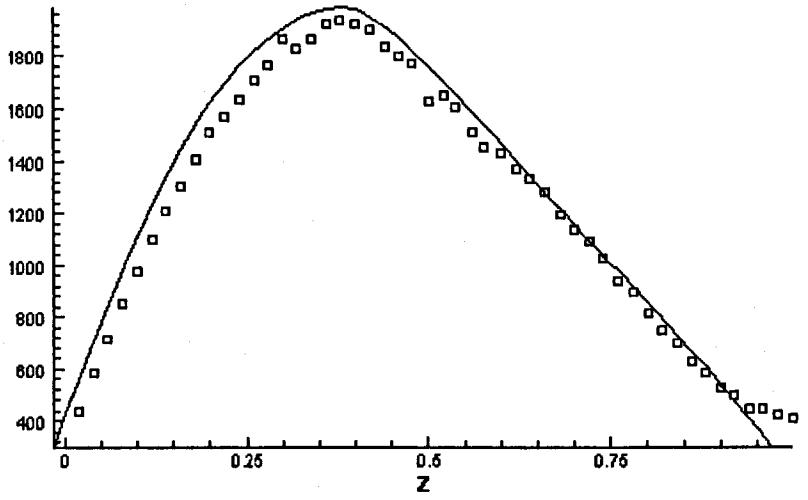
T (°C)
1800
1600
1400
1200
1000
800
600
400
0
0.25
0.5
0.75
Z

(a)

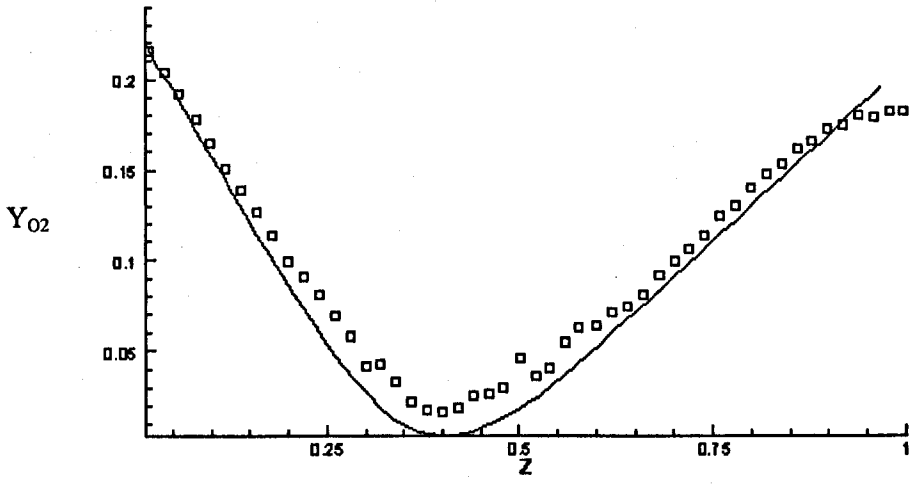
Y_{O2}
0.2
0.15
0.1
0.05
0.25
0.5
0.75
1
Z

(b)

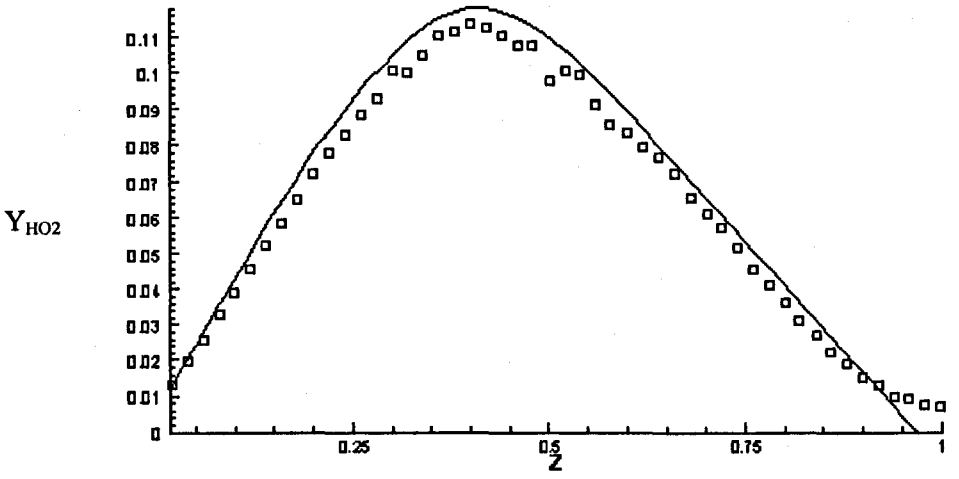
Y_{HO2}
0.11
0.1
0.09
0.08
0.07
0.06
0.05
0.04
0.03
0.02
0.01
0
0.25
0.5
0.75
1
Z

(c)

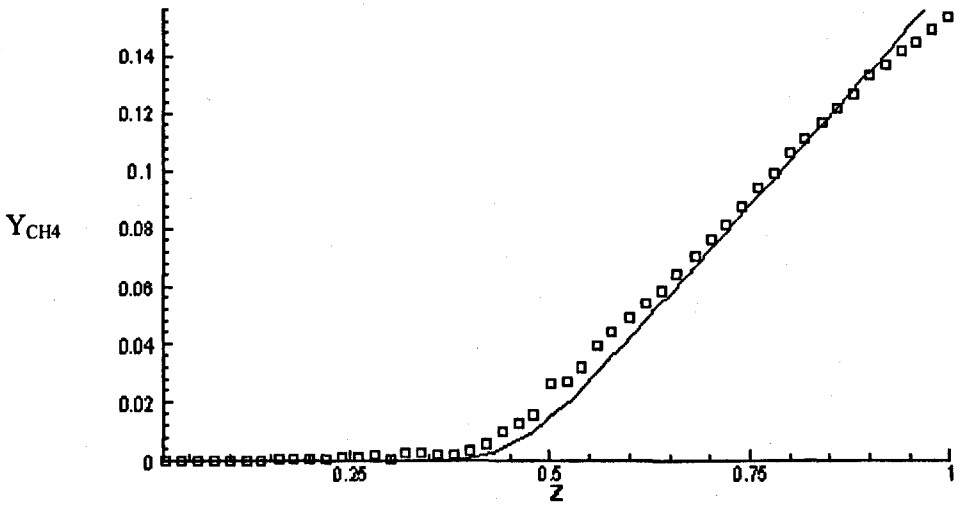
Y_{CH4}
0.14
0.12
0.1
0.08
0.06
0.04
0.02
0
0.25
0.5
0.75
1
Z

(d)

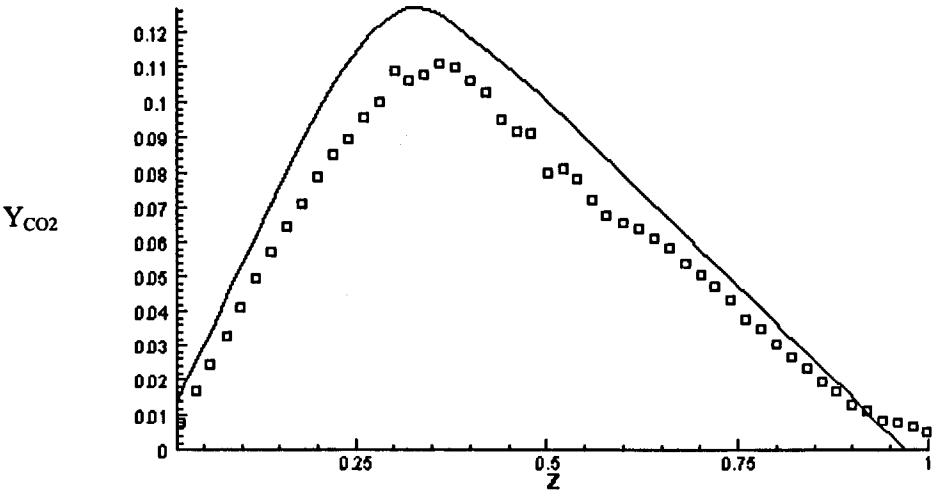

(e)

Figure 5.5. Average conditional at Z/D = 15 of (a) temperature, (b) O_2, (c) H_2O, (d) CH_4 and (e) CO_2. line: simulation, symbols: experiment.

The conditioned oxygen mass concentration in Fig. 5.7b is accurately predicted by the model and reasonable good results are obtained in Fig. 5.6b for the radial mean value. As expected, both mean and RMS predictions are under predicted at the centre. Note that, even when the Z fluctuation is well predicted, the under prediction of the Z mean in Fig. 5.6a will affect the unconditional RMS mean oxygen in Fig. 5.6b, because the unconditional oxygen fluctuations will be calculated at a shifted location on the conditional quantity. The same will be observed for all species at r/D = 0 on the plane Z/D = 30. In other words, the under prediction of Z on this plane is the main factor of discrepancy between species prediction and experiment.

In general terms, the conditional quantities are well predicted for Z/D = 30 (see Figs. 5.7b to 5.7e), except for CO_2, which is consistently over predicted through the flame. This might be related to the chemical mechanism. In line with this, the filtered species (Figs. 5.6b to 5.6e) are reasonably well predicted for r/D > 1.4.

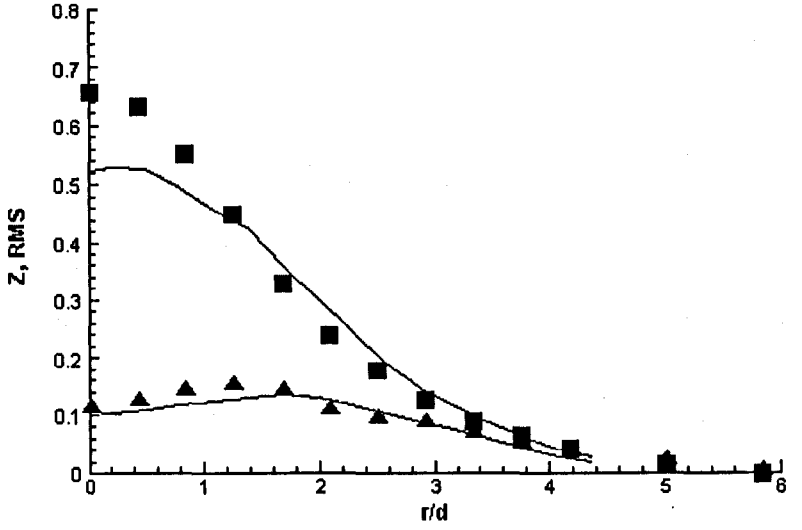
Z, RMS
r/d
0.8
0.7
0.6
0.5
0.4
0.3
0.2
0.1
0
0
1
2
3
4
5
6

(a)

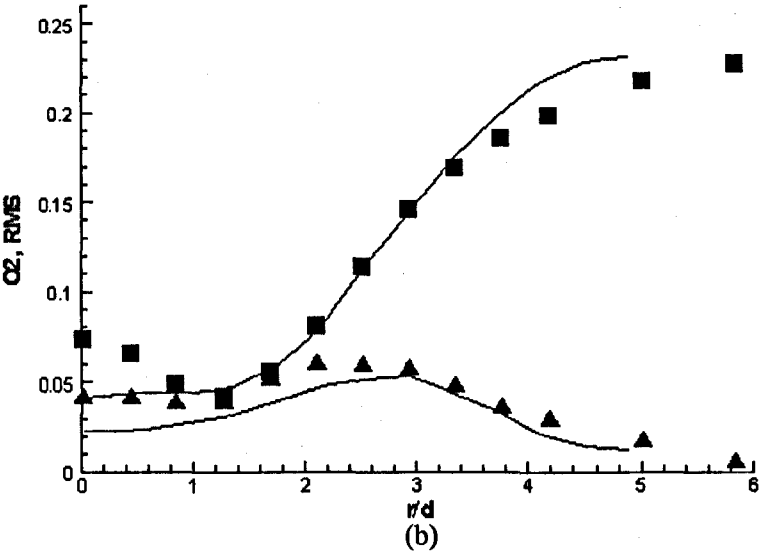
O2, RMS
r/d
0.25
0.2
0.15
0.1
0.05
0
0
1
2
3
4
5
6

(b)

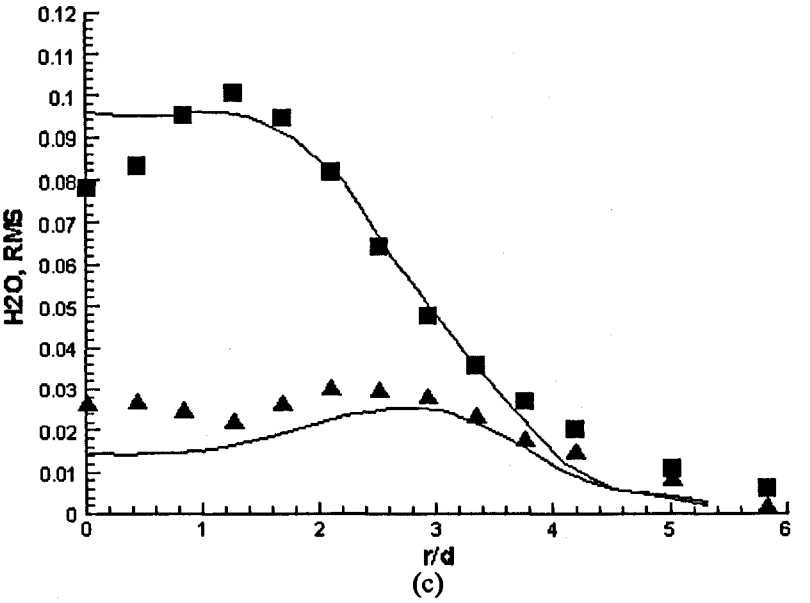
H2O, RMS
0.12
0.11
0.1
0.09
0.08
0.07
0.06
0.05
0.04
0.03
0.02
0.01
0
0
1
2
3
4
5
6
r/d

(c)

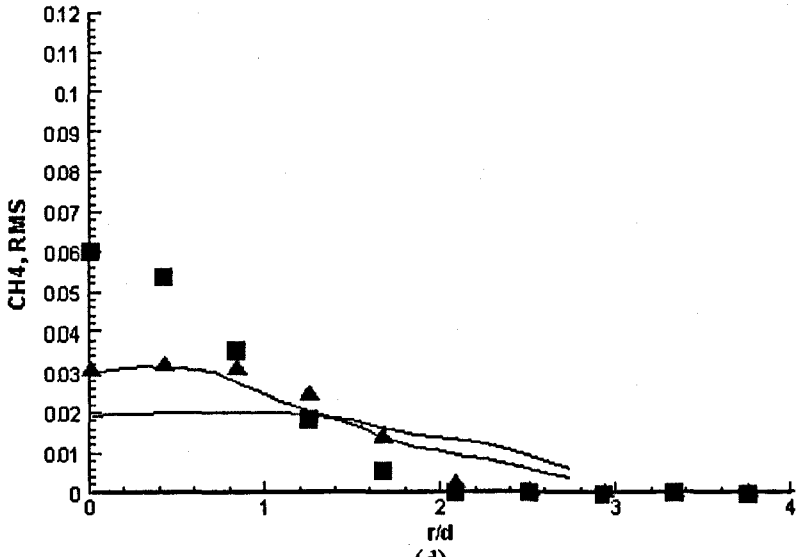
CH4, RMS
0.12
0.11
0.1
0.09
0.08
0.07
0.06
0.05
0.04
0.03
0.02
0.01
0
0
1
2
3
4
r/d

(d)

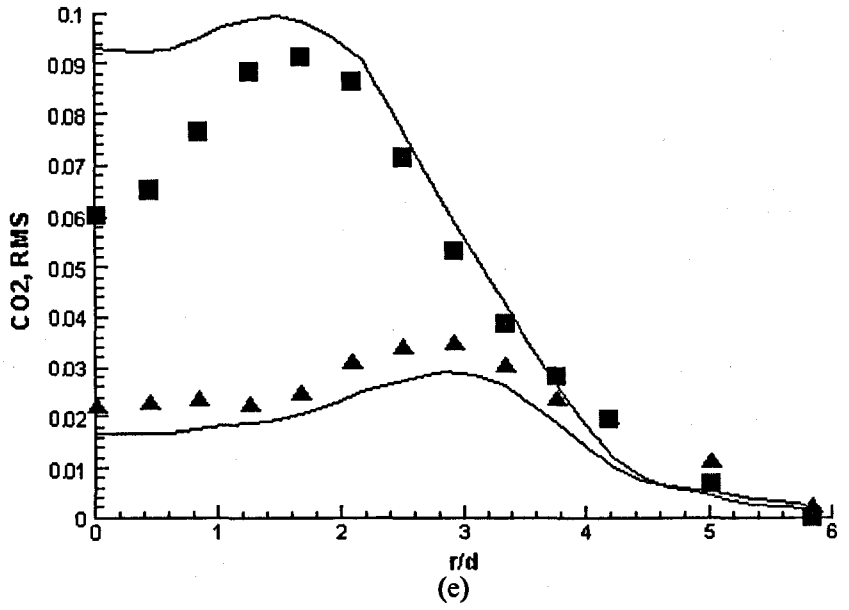

(e)

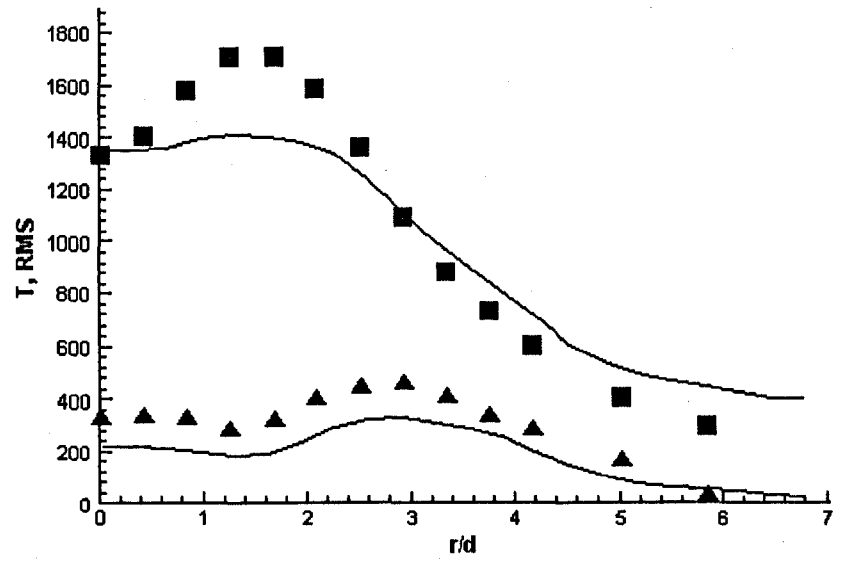

(f)

Figure 5.6. Mean and RMS radial profile at Z/D = 30 of (a) Z, (b) O_2, (c) H_2O, (d) CH_4, (e) CO_2 and (f) temperature. Symbols: experiment, line: simulation.

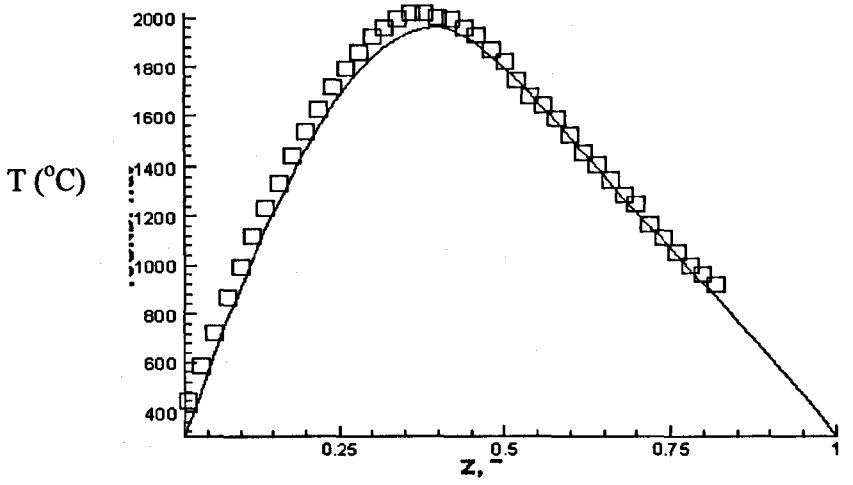
T (°C)
2000
1800
1600
1400
1200
1000
800
600
400
0.25
0.5
0.75
1
z,

(a)

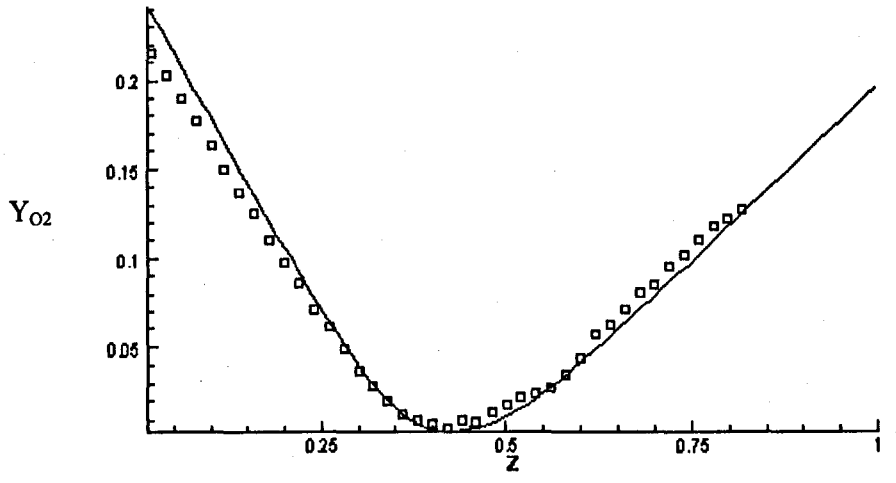
Y_{O2}
0.2
0.15
0.1
0.05
0.25
0.5
0.75
1
z

(b)

Y_{HO2}

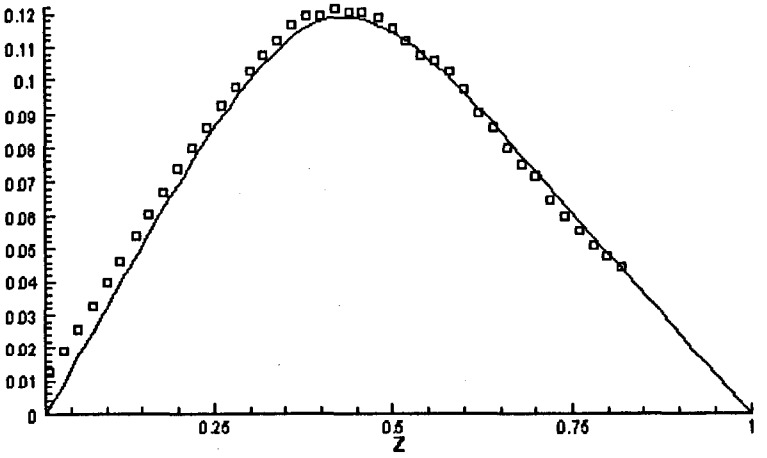
0.12
0.11
0.1
0.09
0.08
0.07
0.06
0.05
0.04
0.03
0.02
0.01
0
0.25
0.5
0.75
1
Z

(c)

Y_{CH4}

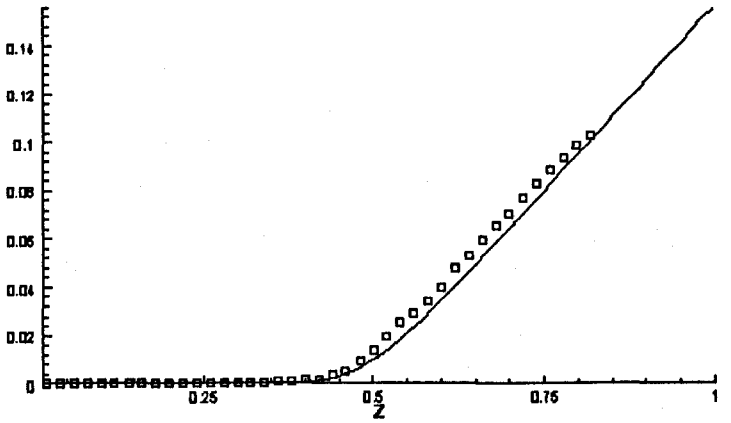
0.14
0.12
0.1
0.08
0.06
0.04
0.02
0
0.25
0.5
0.75
1
Z

(d)

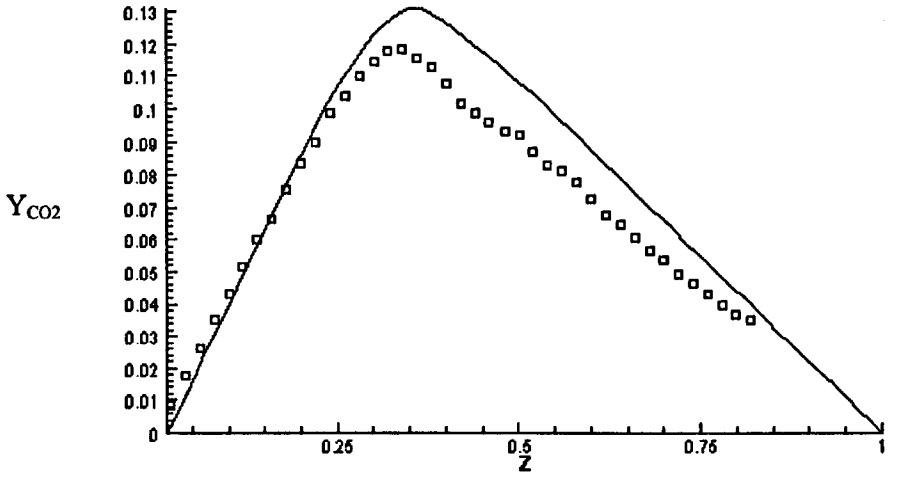

(e)

Figure 5.7. Average conditional at Z/D = 30 of (a) temperature, (b) O_2, (c) H_2O, (d) CH_4 and (e) CO_2. line: simulation, symbols: experiment.

Fig. 5.6-f shows the mean temperature profile at Z/D = 30. Even when the predicted value at the jet centre is accurate, the simulation does not capture the temperature peak at r/D = 1.4.

In the Figs. 5.8 and 5.9, the mean profiles are shown for a plane at Z/D = 45. The prediction of the mixture fraction is reasonably accurate for both the mean value and the RMS. The conditional values for H_2O, CH_4, O_2 and CO_2 are reasonably predicted too. The major discrepancy on this plane corresponds to CH_4. On Z/D =45 the RMS of CH_4 is larger than the mean value and the simulation error might have a connection with lack of statistics. As mentioned before, CO_2 is over predicted even when Z is accurate enough: this support the idea of some over prediction in the chemical mechanism.

We must highlight the good prediction obtained for the conditional values at the boundaries Z = 0 and Z = 1 throughout the flame. This is especially meaningful for

CSE because, even though each individual flamelets fulfils these boundary conditions through eqs. 5.9 and 5.10, there is no mathematical restriction in this implementation which guarantees that a linear combination of the flamelets using the coefficient vector [a] will satisfy the same boundary condition. In other words, the restriction $\sum a_i = 1$ is necessary for the boundary conditions at Z = 0 and Z = 1 to be fulfilled.

Obviously, this is automatically accomplished for flamelets whose values at Z = 0 and Z =1 are zero such as H_2O and CO_2; although, for O_2, CH_4 and temperature, whose values at the feeding streams are different from zero, this condition is necessary. Correspondingly, this restriction is forced in the early stages of the flame to assure the inversion stability. Thereafter, it is relaxed and automatically fulfilled by the inversion in the steady state of the flame.

Throughout the flame, the total number and range of flamelets involved at the different planes are: 20 (1.5 – 120) sec^{-1}, 14 (1.5 – 50) sec^{-1} and 12 (1.5 – 40) sec^{-1}, for the plane Z/D = 15, 30 and 45, respectively. Apparently, the selected flamelets do not change too much for Z/D > 15. This is somehow expected, since the dissipation rate drops as $\chi \propto Z^{-4}$ downstream of the nozzle.

Fig. 5.10 shows the average vector [a] for three planes Z/D = 15, 30 and 45. On average, on the plane Z/D = 15 there are about 17 flamelets with dissipation rate raging from 1.5 sec^{-1} to 90 sec^{-1}. On the plane Z/D = 30, the number of flamelets is 13, ranging from 1.5 sec^{-1} to 45 sec^{-1} and on plane Z/D = 45, there are 12 flamelets from 1.5 sec^{-1} to 40 sec^{-1}.

Clearly, the drop form Z/D = 15 to 30 is larger than from 30 to 45, as verified in experiments. It is also noted that the dissipation rate fluctuations are not very important from the basis point view, implying that the selected basis do not change considerably on the same plane throughout the simulation. This verifies the assumption made regarding the quasi-steady state reached by the flame in time.

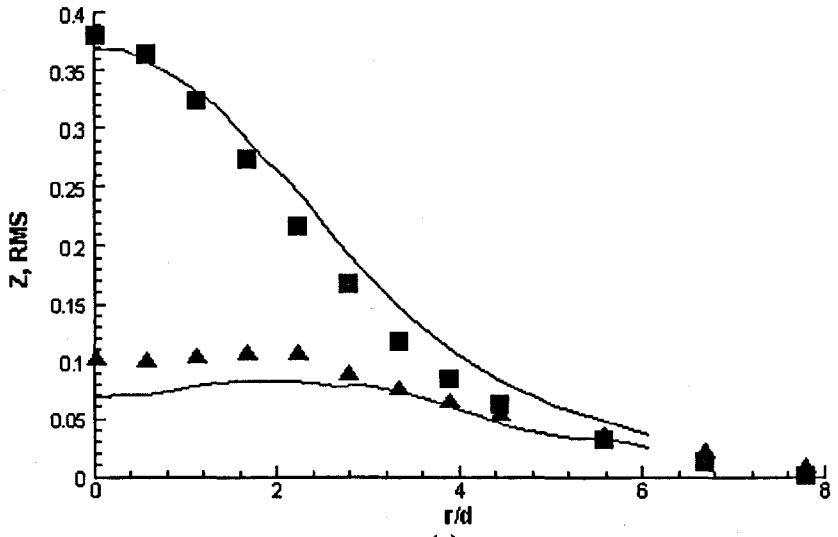
Z, RMS
r/d
0.4
0.35
0.3
0.25
0.2
0.15
0.1
0.05
0
0
2
4
6
8
(a)

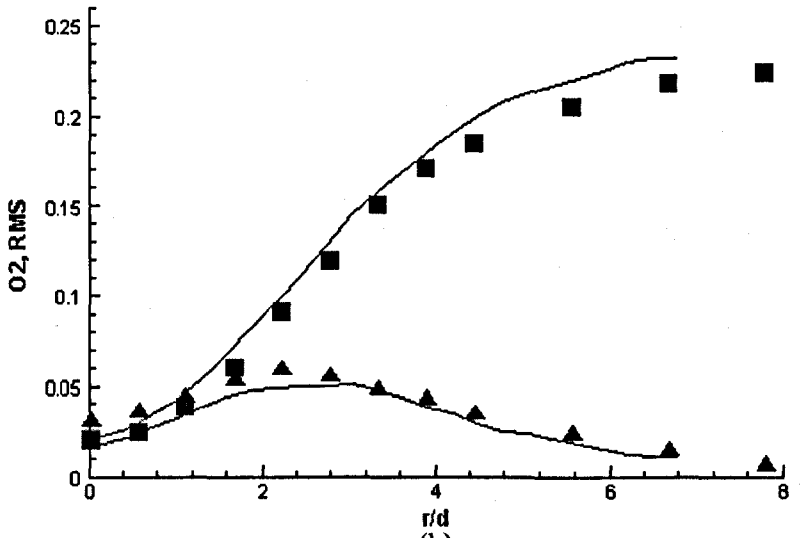
O2, RMS
r/d
0.25
0.2
0.15
0.1
0.05
0
0
2
4
6
8
(b)

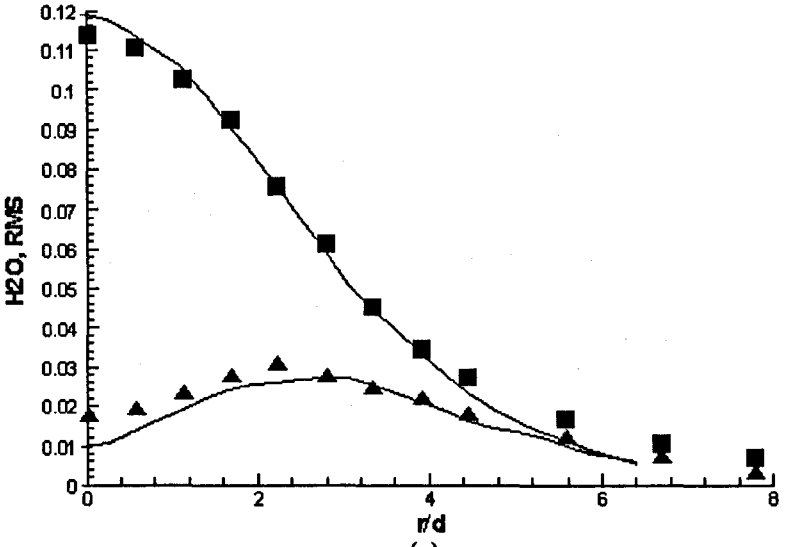
H2O, RMS
0.12
0.11
0.1
0.09
0.08
0.07
0.06
0.05
0.04
0.03
0.02
0.01
0
0
2
4
6
8
r/d

(c)

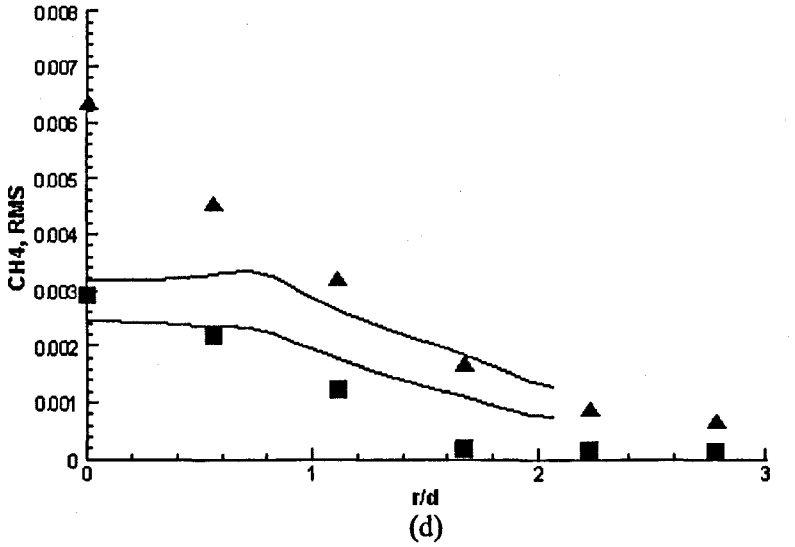
CH4, RMS
0.008
0.007
0.006
0.005
0.004
0.003
0.002
0.001
0
0
1
2
3
r/d

(d)

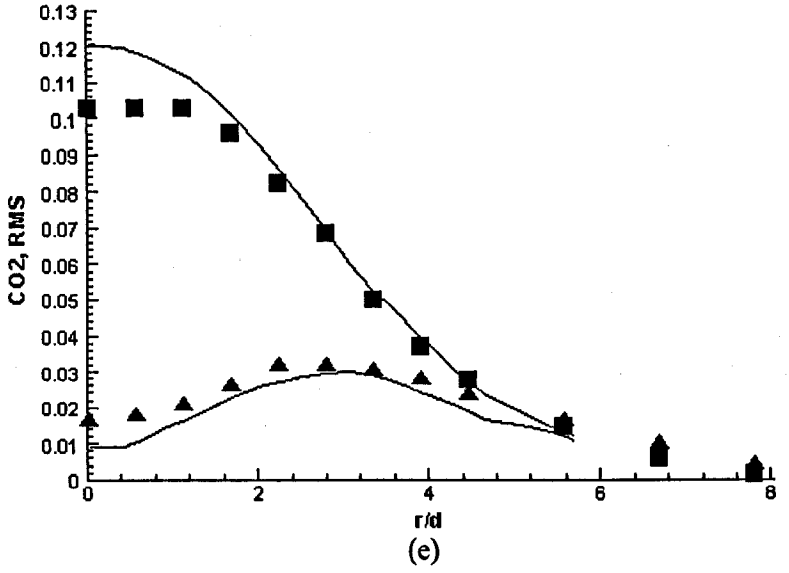

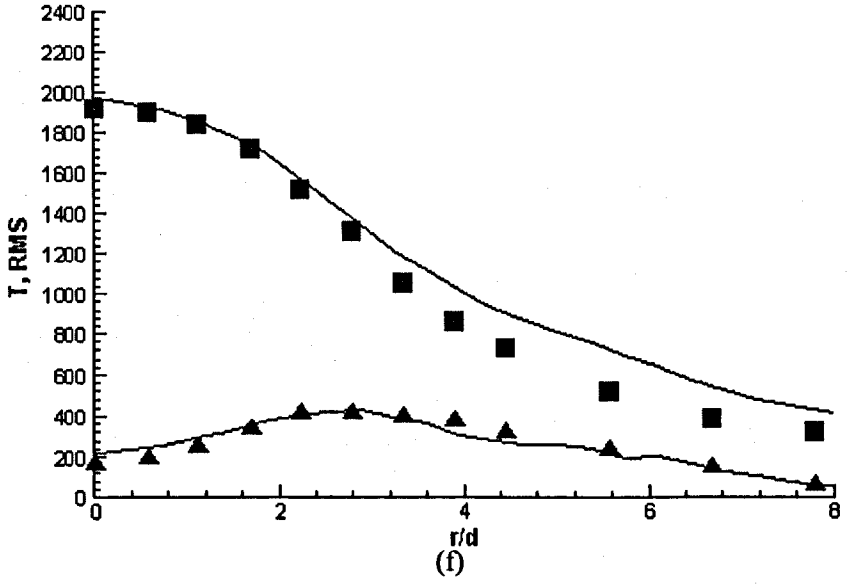

Figure 5.8. Mean and RMS radial profile at Z/D = 45 of (a) Z, (b) O_2, (c) H_2O, (d) CH_4, (e) CO_2 and (f) temperature. Symbols: experiment, line: simulation.

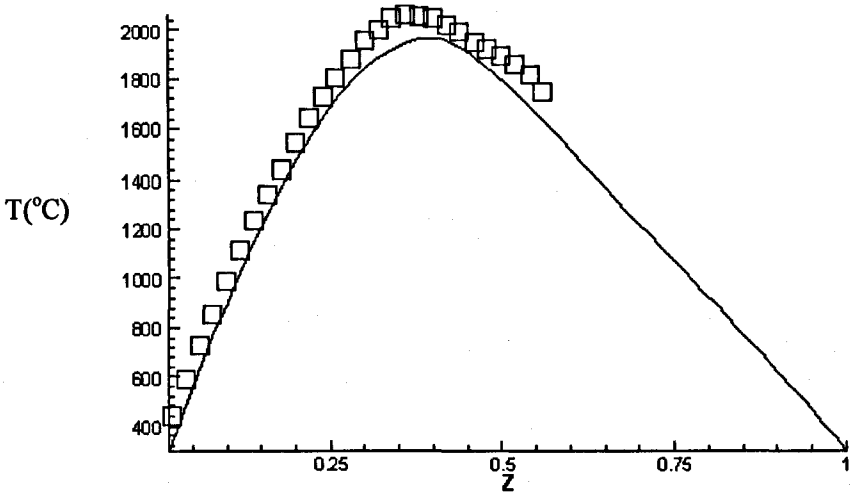
T(°C)
2000
1800
1600
1400
1200
1000
800
600
400
0.25
0.5
0.75
1
Z

(a)

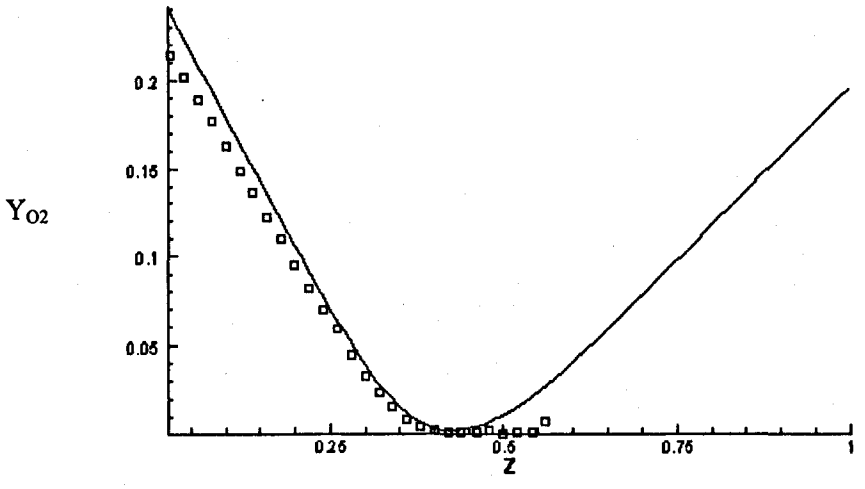
Y_{O2}
0.2
0.15
0.1
0.05
0.25
0.5
0.75
1
Z

(b)

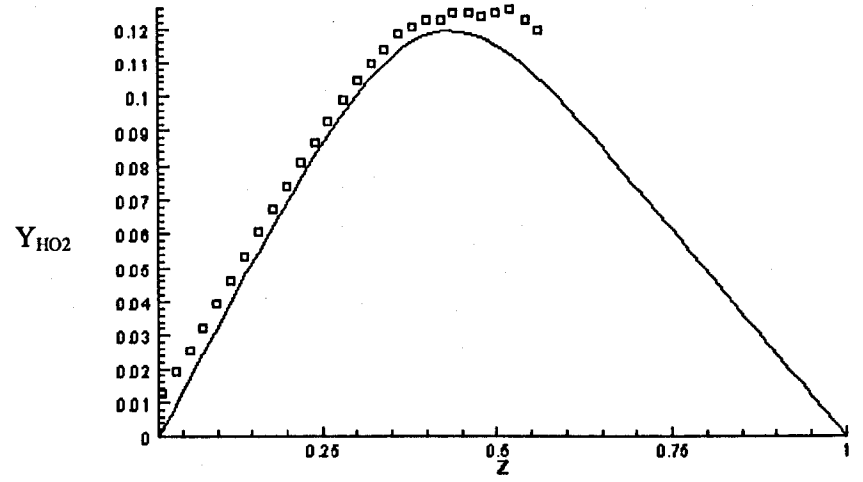
Y_{HO2}
0.12
0.11
0.1
0.09
0.08
0.07
0.06
0.05
0.04
0.03
0.02
0.01
0
0.25
0.5
0.75
1
Z

(c)

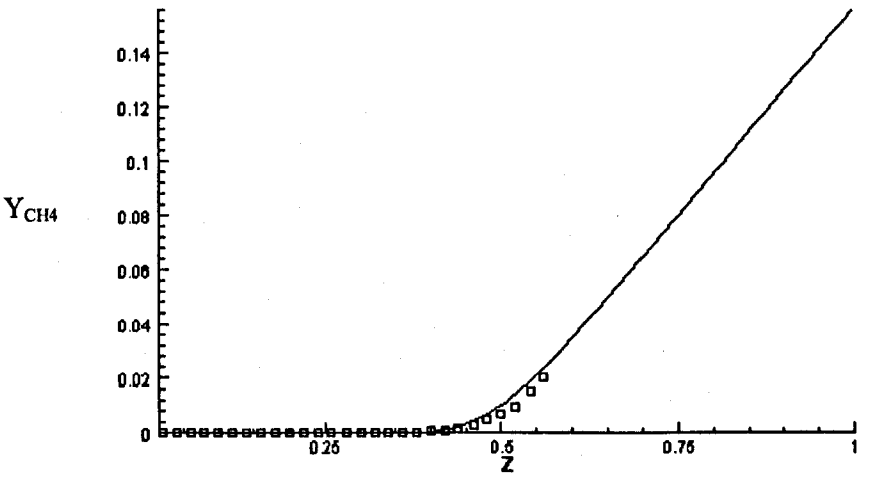
Y_{CH4}
0.14
0.12
0.1
0.08
0.06
0.04
0.02
0
0.25
0.5
0.75
1
Z

(d)

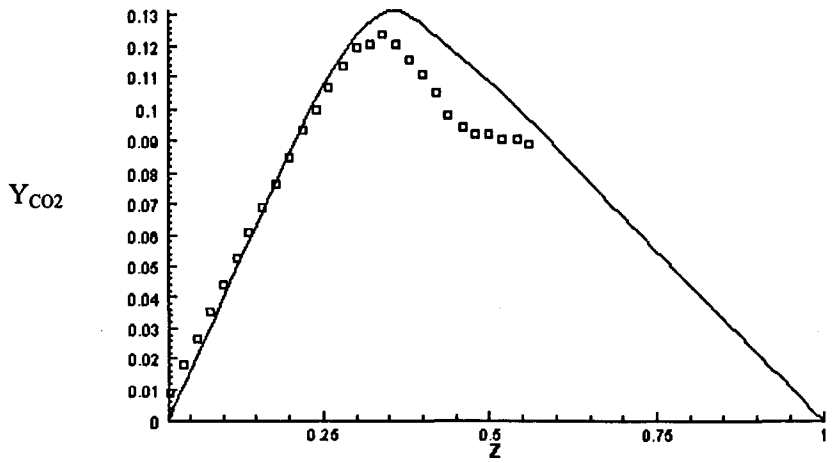

(e)

Figure 5.9. Average conditional at Z/D = 45 of (a) temperature, (b) O_2, (c) H_2O, (d) CH_4 and (e) CO_2. line: simulation, symbols: experiment.

Bushe and Steiner [34] discussed the coefficient of [a] as performing the role of the pdf of χ, being equivalent to the quantity $P(\chi)\, d\chi$. They also encountered some limitations to this interpretation, because in their work they found coefficients with negative values. We do not attempt to interpret [a] from a physical point of view, but from a mathematical one. We do not observe negative coefficients in this study, which could influence the stability of the inversion process. On the other hand, one could anticipate, following the physical interpretation, that the flamelet belonging to the mean dissipation rate at a given plane should have more weight than the rest of the coefficients. However, this does not happen as it is shown in Fig. 5.10. Thus, our understanding of their physical meaning remains unclear. More study is needed in this regard but is considered to be beyond the scope of this project.

The conditional heat release for planes Z/D = 15, 30 and 45 are shown in Fig. 5.11. This figure also shows clearly the impact that small changes in the vector [a] have on the total heat release. It is observed that the heat release decreases as the plane is

located further downstream.

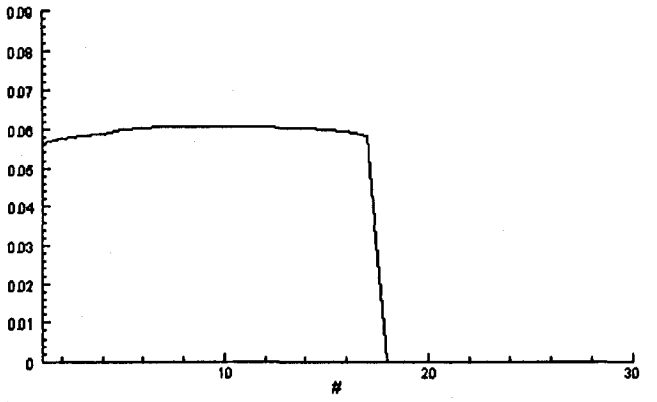

(a)

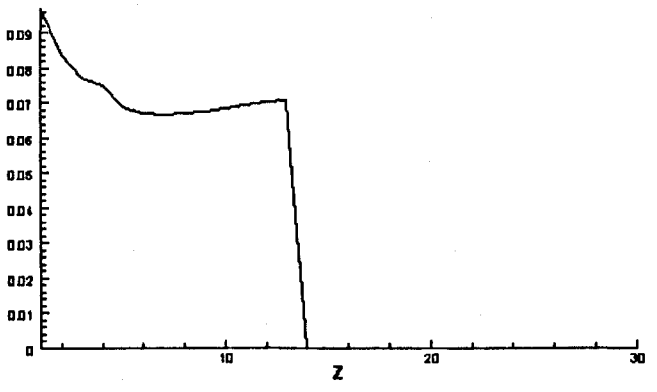

(b)

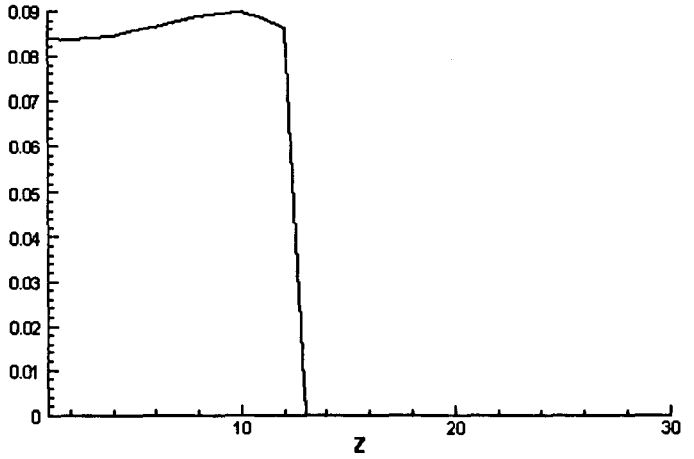

(c)

Figure 5.10. Mean coefficients of [a]: (a) at Z/D = 15, (b) at X/Z = 30 and (c) at X/Z = 45.

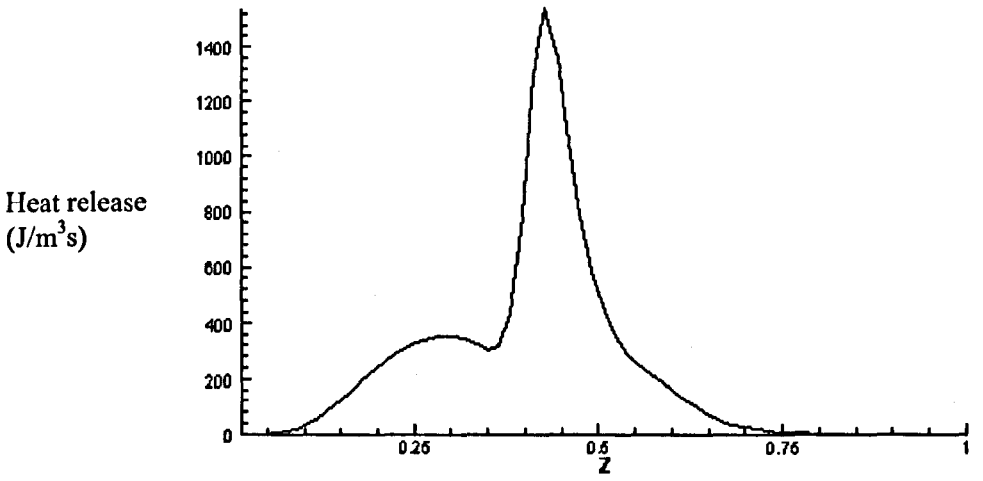

(a)

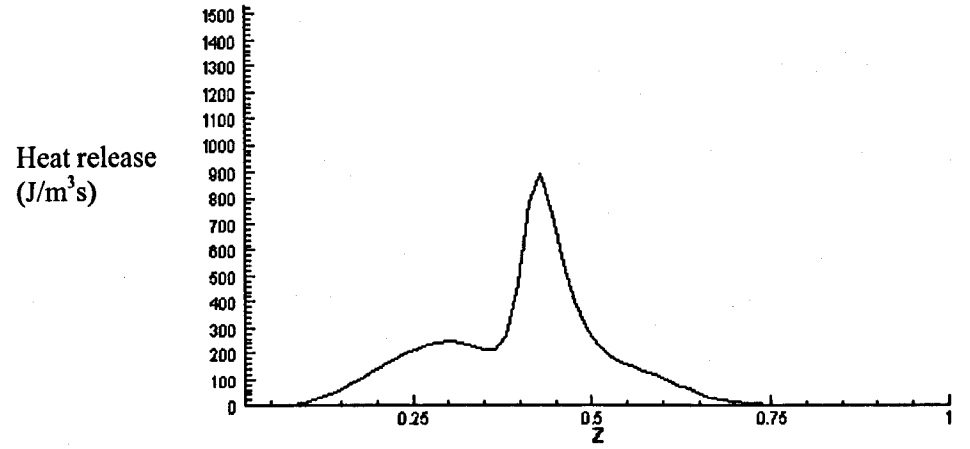

(b)

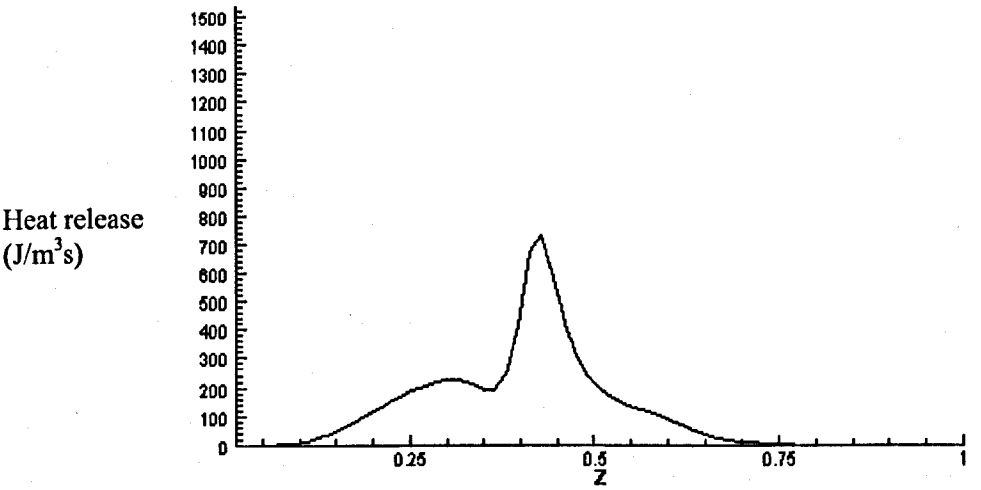

(c)

Figure 5.11. Average conditional heat release: (a) at Z/D = 15, (b) at Z/D = 30 and (c) at Z/D = 45.

5.6 Summary and conclusions

The present simulation of a turbulent reacting jet is the first test of the Laminar Flamelet Decomposition (LFD) approach in a realistic scenario. Some point can be noted:

- The model proved to be robust and very economic from the computational point of view. The present calculation of 1.6 M cells took 3 days on a 3.0 GHz processor to resolve 5 residential times. Kemp et al [113] obtained good results in 3 weeks for the flame D using steady flamelets on a mesh of approximately 2 M cells and using a 3.0 GHz processor. Pitsh (2000) obtained excellent results using the computationally expensive unsteady flamelet model with 1 M cells.

- It was found that the use of this implementation of CSE model is feasible to approximate the unconditional source term. It only necessary to solve the energy, momentum and mixture fraction balance equations and one inversion each 5 Δt on a fivefold coarser mesh to obtain the coefficient

- In the present study, an attempt was made to improve the inversion process. It was found that reducing the number of flamelets would stabilise the inversion. Consequently, the dimension of the lineal system remains small.

The success of CSE lies on the feasibility to obtain a good approximation of the conditional quantities through inversion. There are many useful concepts in the literature, which can be used to further improve the inversion. To mention but just a few: the weighted least square approach, changing the mixture fraction space distribution, introducing the temperature fluctuation into the inversion, considering the upstream cell solution as first guest for the inversion, etc. It is believed that all these possibilities are worth exploring.

On the other hand, the limitations linked with the use of steady laminar flamelets as basis functions are evident. In this study, all the flamelets were burning flamelets and no extinction events were considered. Even so, the fuel consumption was over

predicted from Z/D > 15 to Z/D < 30.

In order to cope with cases where extinction is important, one should introduce flamelets that represent such scenarios. It is not clear, to our understanding, how these flamelets could be introduced. Incorporating a time dissipation rate dependency could possibly improve the prediction in these areas. The capability to predict local extinction becomes more important when the diffusion flames is close to blow off, as in the case of flames E and F.

The present study suggests that the quality of the CSE predictions depends mainly on the validity of the following assumptions:

(1) Surfaces of homogeneity for the conditional averages must be specified in the flow field,

(2) Enough physical nodes are solved between Z = 0 and Z = 1, in order to calculate properly the inversion and

(3) Only assumptions about small gradients in conditional averages and about the pdf of mixture fraction are needed.

The first point is probably the most restrictive of all. The situation of homogeneity on conditional quantities is not very obvious for different configurations. It is not yet clear how a complete 3D conditional inversion could be done. A possible solution could be found in selecting those nodes perpendicular to flame sheet, in a similar way to the flamelets approach, then expanding perpendicular lines through the flame and selecting the corresponding temperatures at different distances from the combustion zone. This is the principal reason why CSE is not suitable for the backdrat simulation where it is not possible to choose a surface of homogeneity for the conditional averages.

Chapter 6

Sub-models for partially premixed combustion

Combustion in non-premixed systems such as jets does not always start at the location where fuel and oxidizer come into stoichiometric condition. In many occasions, the combustion zone is lifted away from the nozzle creating a stabilized partially premixed system several diameters above the nozzle. Flame stabilization of partially-premixed systems is a phenomenon which needs to be controlled in numerous industrial applications (boiler, rocket engine, turbine reactor, etc.). In many applications, the flame is usually anchored at the nozzle to avoid instabilities of the pressure field, extinction (leading to unburnt hydrocarbon emission) and blow-out for safety reasons. On the other hand, in some burner designs, lifted flames are favoured in order to protect the burner nozzle.

In the present chapter, the sub-grid models necessary to deal with turbulent partially premixed combustion are introduced. In the next chapter, a LES of a turbulent lifted flame experimentally tested by Mansour [150] is carried out among other simulations to test the models' performances.

As it was seen in chapter 3, there are mainly three approaches when dealing with propagating premixed flame fronts: 1) the G-equation, 2) the thickened flame model (TFM) and 3) the filtered progress variable approach.

In the G-equation approach, a turbulent burning velocity model, S_T, is needed; which presents several setbacks from the numeric point of view. The TFM artificially thickens the flame front by a factor α (between 5 and 30) so that the flame can be

resolved by the computational grid and conserves the flame burning velocity multiplying the material diffusivity by α. This model presents very attractive features for predicting unsteady phenomena such as re-ignition and extinction because it uses an Arrenhuis expression for the heat release. Nevertheless, TFM has not been extensively tested within the LES framework. In the present work, we chose the filtered progress variable approach. To our mind, this model presents more suitable properties both from the numerical point of view and the implementation. Moreover, it has a clear physical interpretation as it can be assigned to the temperature or species fields alike.

In the progress variable approach, C is filtered using a filter larger than the LES grid; thus, the thin premixed front is resolved on a grid larger than the actual LES grid. In filtering the C transport equation like this, two extra terms appear in the filtered equation, which need to be closed; namely the surface density function, Σ and the average mass-weighted displacement speed, $\langle \rho w \rangle_s$.

In order to test this approach, a simple hydrogen laminar 1-D premixed flame simulation is carried out in chapter 7

The Steady Laminar Flamelet Model (SLFM) already introduced in chapter 3 is chosen for coping with non-premixed combustion. It is important to note that more advanced models can be used for diffusion combustion, such as CSE or ULFM, although, it is though that SLFM is a good first approach.

As a partially-premixed combustion system is expected to have a combined combustion regime, a mechanism is required to ensemble them together to reproduce the total heat release throughout the flame, the so-called flame index.

The flame index concept developed by Domingo [67] for LES is used in this study to capture the partially premixed structure. This concept is based on the product of fuel and oxidizer gradients. When a flame is non-premixed, the two streams oppose each other having different gradient signs, while, for premixed combustion both gradients

have the same sign.

It is known that turbulence increases the flame sheet surface, producing a larger combustion rate. The surface density function is contorted by the un-resolved eddies and increases its area at sub-grid scale. This augment of the source term in the C balance equation is modelled using the so-called wrinkling factor, Ξ.

6.1 Transport equations for Z and C

Non-premixed and premixed combustion regimes are two idealized scenarios, which are often mixed but conceptually very different. It is hard to construct a model that can cope with both regimes simultaneously. The premixed front is thin and propagates through the unburnt region while the diffusion flame is mixing controlled and does not propagate by itself.

Assuming global single-step chemistry and neglecting radiative heat transfer, two basic control parameters are needed to capture partially premixed flames, i.e. the mixture fraction Z(x,t) and a reaction progress variable C(Z;x,t). Fiorina [80] used Z and C to tabulate complex chemistry in partially premixed conditions with good results for a counter flow jet at different equivalence ratios. Gicquel [91] considered detailed chemistry using FPI (flame prolongation of ILDM) and Oijen [243] used FGM (flamelet-generated manifold) for the same goal. These two techniques are based on the tabulation of a set of unstrained premixed laminar flames as functions of the equivalence ratio into a database, which is parameterized by two variables (Z and C).

The mixture fraction is a conserved scalar satisfying $Z = 0$ in the air stream and $Z = 1$ in the fuel stream. The progress variable C(Z;x,t) is a non-conserved scalar satisfying $C = 0$ in fresh gases and $C = 1$ in burnt products. Due to the existence of partial premixing ahead of the premixed flame front, the progress variable is also a function of the mixture fraction.

Assuming a one-step reaction, the equivalence ratio for the non-premixed flame can be expressed as:

$$\phi = \frac{\nu_o W_o}{\nu_f W_f} \frac{Y_{f,0}}{Y_{0,0}} \tag{6.1}$$

where ν_i (i=o, f) are the molar coefficients, W_i the molar weights and $Y_{i,0}$ the reactant mass fractions in the feeding streams. The mixture fraction can be expressed as a function of the concentration of reactants as:

$$Z = (\phi(\frac{Y_f}{Y_{f,0}}) - (\frac{Y_0}{Y_{o,0}}) + 1)/(\phi + 1) \tag{6.2}$$

Supposing the premixed front propagates in a normal direction from the fresh to the burnt gases, the progress variable C, may be defined either from the fuel or oxygen mass fraction point of view. The fuel or oxygen mass fraction will evolve from a frozen (pure mixing) state at the upstream location of the premixed front to the local equilibrium condition further downstream. One of the possible definitions of the progress variable in terms of the fuel mass fraction can be written as:

$$C(Z;x,t) = \frac{Y_{f,0}Z - Y_f(x,t)}{Y_{f,0}Z - Y^{EQ}(Z)} \tag{6.3}$$

where $Y^{EQ}(Z)$ is the complete combustion downstream of the front and $Y_{f,o}$ is the fuel mass concentration at the fuel stream. Domingo et al. [67] assumed infinitely fast reaction when the diffusive regime is reached and equilibrium chemistry was chosen.

In principle, Eq. 6.3 gives a full description of the progress variable for both premixed and non-premixed flames. Moreover, complex chemistry could be built into

C in the same fashion as it is done for the mixture fraction (Z) in non-premixed systems.

As it was stated above, both Z and C are needed throughout the flame to describe the co-existing of premixed and non-premixed combustion processes.

Assuming laminar flamelet concept, the Favre-filtered transport equation for mixture fraction may be written as [111]:

$$\frac{\partial(\overline{\rho}\widetilde{Z})}{\partial t}+\frac{\partial(\overline{\rho}\widetilde{u}_j\widetilde{Z})}{\partial x_j}=-\frac{\partial}{\partial x_j}(\overline{\rho u_j Z}-\overline{\rho}\widetilde{u}_j\widetilde{Z})+\frac{\partial}{\partial x_j}(\overline{\rho D\frac{\partial Z}{\partial x_j}}) \tag{6.4}$$

where D is the scalar diffusivity. the second term of the RHS is modelled similar to sub-grid scale (SGS) turbulence.

Different expressions have been proposed for the progress variable, C. It is related to one specie either fuel, oxidizer or other and depends on the mixture fraction space and fluxes inside the Z dimension. Departing from the fuel transport equation and Eq. 6.4, Domingo [67] derived the following equation for C:

$$\frac{\partial(\rho C)}{\partial t}+\frac{\partial(\rho u_j C)}{\partial x_j}=\frac{\partial}{\partial x_j}\left(\rho D\frac{\partial C}{\partial x_j}\right)+\dot{w}_C+\left(\frac{2}{Y_{f,0}Z-Y_f^{EQ}(Z)}\right)\left(Y_{f,0}-\frac{dY_f^{EQ}(Z)}{dZ}\right)\rho\chi_{Z,C}$$

$$-\left(\frac{C}{Y_{f,0}Z-Y_f^{EQ}(Z)}\right)\frac{d^2Y_f^{EQ}(Z)}{dZ^2}\rho\chi_Z \tag{6.5}$$

where $\dot{w}_C=-\dot{w}_f/(Y_{f,0}Z-Y_f^{EQ}(Z))$ is the source term, $\chi_Z=D|\nabla Z|^2$ is the scalar dissipation rate of the mixture fraction field and $\chi_{Z,C}=D\nabla Z\cdot\nabla C$ is the cross-scalar dissipation rate defined between the progress variable and the mixture fraction.

Eq. 6.5 is valid for both premixed and non-premixed combustion. It is the exact expression for the progress variable as a function of the mixture fraction.

Domingo et al. [69] in his DNS analysis solved Eq. 6.5 fully and considered separately each of its terms and their influence on the different combustion regimes in a gaseous weakly lifted turbulent flame. It was found that in the double regime section of the flame (diffusion and rich premixed combustion) the first and fourth terms on the right hand side (RHS) of Eq. 6.5 are relevant. In the pure premixed region the first and second terms are the most important, although the fourth term is not completely negligible. The third term of the RHS of Eq. 6.5 appears to be small throughout the flame, especially when the stoichometric value is close to the air, as it is in the methane-air system. This term is also negligible at the premixed flame front where C and Z are perpendicular. The cross scalar gradient can be aligned in the double combustion regime of the flame [69].

Following Domingo [34] and neglecting the cross dissipation rate term and the term proportional to the mixture fraction dissipation rate in Eq. 6.5, the Favre-filtered equation of the progress variable, calculated using the filter: $F(x)=\left(\frac{6}{\pi\Delta_c^2}\right)^{3/2}\exp\left[-\frac{6}{\Delta_c^2}\left(x^2+y^2+z^2\right)\right]$, is then ,:

$$\frac{\partial(\overline{\rho}\widetilde{C})}{\partial t}+\frac{\partial(\overline{\rho}\widetilde{u}_j\widetilde{C})}{\partial x_j}=-\frac{\partial}{\partial x_j}(\overline{\rho u_j C}-\overline{\rho}\widetilde{u}_j\widetilde{C})+\frac{\partial}{\partial x_j}(\overline{\rho D\frac{\partial C}{\partial x_j}})+\overline{\dot{w}}_c \qquad (6.6)$$

for a premixed front alone.

where $\overline{\dot{w}}_c$ is the source term of the progress variable and must be closed. The unresolved scalar flux, $\overline{\rho u_j C}-\overline{\rho}\widetilde{u}_j\widetilde{C}$ is non-zero for a laminar flame because of thermal expansion. For a one-dimensional steady propagating laminar flame, this term is counter-gradient. Boger et al.[19], as a first step to overcome this, combined

the laminar contribution with the modelled filtered reaction rate. In their LES of a V-shaped flame, Boger et al. found gradient scalar transport close to the flame-holder, which is progressively replaced by counter-gradient features further down stream. Their findings show that unlike RANS, despite using simple sub-grid scale models, LES is able to predict counter-gradient transport due to the dynamics of the resolved large structures.

For the flame considered here the main difference between the exact expression for C, Eq. 6.5, and the approximation used in this study, Eq. 6.6, is the term proportional to the scalar dissipation rate. Regarding this simplification some conclusions will be drawn further in the next chapter in the lifted flame simulation.

In order to close $\overline{\dot{w}_c}$ we adopt a classical flamelet viewpoint and choose to write the volumetric chemical reaction rate as the product of a laminar-like reaction rate per unit flame surface area times a flame surface density.

$$\frac{\partial}{\partial x_j}(\overline{\rho D \frac{\partial C}{\partial x_j}}) + \overline{\dot{w}_c} = (\rho_u s_l^0)\Sigma \tag{6.7}$$

where ρ_u is the unburnt gas mass density, s_l^0 the laminar flame speed and Σ the LES filtered flame surface density.

The surface density (Σ) can be expressed either in an algebraic form or in a balanced equation. In the present study, the algebraic form is used. This approach was developed by Boger et al [20]. They carried out 3-D DNS analysis of a laminar flame propagating in a homogeneous and isotropic turbulent flow field. They proposed to LES-filter the progress variable equation using a filter larger than the mesh size. The surface density function (Σ) was modelled with DNS data in their calculations. Later, Boger et al. [19] also used this approach to simulate a v-shape flame.
The proposed LES-filtered surface density reads as:

$$\Sigma = \Xi 4\sqrt{\frac{6}{\pi}}\frac{\widetilde{C}(1-\widetilde{C})}{\Delta_C} \tag{6.8}$$

where Ξ denotes the SGS flame front wrinkling factor ($\Xi = 1$ in absence of sub-grid-scale flame surface wrinkling) and Δ_C is the filter size larger than the actual LES mesh.

Finally, Eq. 6.6 for the filtered C balance equation becomes:

$$\frac{\partial(\overline{\rho}\widetilde{C})}{\partial t}+\frac{\partial(\overline{\rho}\widetilde{u}_j\widetilde{C})}{\partial x_j}=\frac{\partial}{\partial x_j}\left[\left(\overline{\rho}_u\frac{\widetilde{S}_L\Delta_C}{16\sqrt{6/\pi}}+\frac{\mu_t}{Sc_t}\right)\frac{\partial\widetilde{C}}{\partial x_j}\right]+4\overline{\rho}_u\widetilde{S}_L\Xi\eta\frac{\widetilde{C}(1-\widetilde{C})}{\Delta_C} \tag{6.9}$$

where μ_t is the turbulent viscosity, Sc_t is the turbulent Schmidt number, $\overline{\rho}_u$ is the filtered unburnt gases density, η is a model constant for the algebraic approach of Σ and $\widetilde{S}_L$ is the filtered laminar flame speed.

$\widetilde{S}_L$ is an important ingredient in the present formulation. This flame speed is defined by averaging the response of methane-oxygen flame speed $s_l^0(Z)$ over the sub-grid fluctuations of the mixture fraction:

$$\widetilde{S}_L=\int_0^1 s_l^0(Z^*)\widetilde{P}(Z^*)dZ^* \tag{6.10}$$

In the present case, a complex chemistry is used to calculate the laminar flame speed for the CH_4-Air system.

The extra diffusion term in Eq. 6.9 is added to preserve the correct flame propagation speed and thickness even in the laminar regions of the flow [18, 67].

The filter Δ_C is a LES filter that is not necessarily the one used in the transport equations. The choice of Δ_C ensures that the flame front is well-resolved. In cases where the mesh is fine enough Δ_C should be adjusted accordingly. In the present study, $\Delta_C = 5\Delta$ is chosen, the flame front is therefore resolved approximately with ten grid points. Another important aspect for choosing the correct Δ_C is the conservation of the filtered laminar flame speed $\widetilde{S}_L$ established by Eq. 6.9. In order to test it, a 1-D laminar flame front is simulated (see chapter 7). It was found that $\Delta_C = 5\Delta$ preserves the correct unstrained burning velocity.

Eq. 6.9 needs a closure for the wrinkling factor Ξ. Domingo et al.[67] assumed a constant value for a 2-D turbulent lifted flame. In the present case, a model which depends on local quantities is used, which will be explained in the following sections.

As pointed out before, Eq. 6.9 is only valid for a pure premixed front. Hence, it is unlikely to describe completely the progress variable throughout a combined combustion system, namely premixed and non-premixed. The description of the diffusion and premixed flame part would need the modelling of terms proportional to χ_Z and $\chi_{C,Z}$. Instead of developing closure models to solve Eq. 6.5, Domingo introduced the 'flame index' to distinguish between diffusion and premixed combustion so Eq. 6.9 can still be used to 'describe' only the premixed front progress.

6.2 Flame Index

A flame indicator based on the scalar product of fuel and oxidizer normal vectors was first proposed by Yamashita et al. [264]. The 'flame index' concept was also used in different studies by several authors [67, 69, 80, 264]. More recently, independent direct numerical simulations studies have endorsed the viability of this approach in multidimensional problems [168].

The cross-scalar dissipation rate $\chi_{F,O} = -D\nabla Y_F \cdot \nabla Y_O$ was found to be an indicator of the combustion regime. The quantity $\chi_{F,O}$ appears as a source term in the transport

equation for the product of species mass fractions $f = Y_F Y_O$:

$$\frac{\partial(\overline{\rho} f)}{\partial t} + \frac{\partial(\overline{\rho u}_j f)}{\partial x_j} = \frac{\partial}{\partial x_j}(\rho D \frac{\partial f}{\partial x_j}) + 2\rho\chi_{F,O} + (\dot{w}_F Y_O + \dot{w}_O Y_F) \tag{6.11}$$

In non-premixed flames stabilized by a propagating partially premixed front, $f = 0$ at the inlets. The cross-scalar dissipation rate between fuel and oxidizer may be written as,

$$\xi = -D\nabla Y_f \nabla Y_o = -D|\nabla Y_F||\nabla Y_O| N_{F,O} \tag{6.12}$$

where $N_{F,O} = n_F n_O$ is a cross-orientation factor with $n_i = -\nabla Y_i / |\nabla Y_i|$ the normal vector to an iso-reactant surface. The ξ coefficient might be interpreted as a flame index to distinguish premixed flames from diffusion flames. The variable ξ is negative for a premixed flame and positive for a diffusion flame. The absolute value of ξ increases as the supplying rate of fuel and oxygen by molecular diffusion increases. This concept has also been used to characterize the impact of partially premixed combustion during the development of holes in a diffusion flame due to extinction caused by high strain stress [77]. Domingo et al. [69] applied an improved version of the flame index concept to a turbulent lifted flame-base where it was used as weighting factor in a linear combination of the source terms of premixed and non-premixed combustion to obtain the total heat release rate. An indicator of premixing ξ_p may be constructed as follows,

$$\xi_p = \frac{1}{2}\left(\frac{N_{F,O}}{|N_{F,O}|} + 1\right) = \frac{1}{2}\left(1 - \frac{\chi_{F,O}}{|\chi_{F,O}|}\right) \tag{6.13}$$

where $\xi_P = 1$ corresponds to a fully premixed mixture and $\xi_P = 0$ to diffusion flamelets.

In the present study, we follow Domingo et al. [67] who developed a closure term for the flame index in the LES context where the fuel and oxygen gradients can fluctuate at SGS level. The filtering operation is expressed as,

$$\overline{q}(x,t) = \int_{-\infty}^{+\infty} q(x',t)G(x-x')dx' \tag{6.14}$$

where $G(x-x')$ is a normalized filter.
The orientation of the species vectors at the resolved scale is indicated by,

$$\overline{n}_F.\overline{n}_O = \left(\frac{\nabla \overline{Y}_F \nabla \overline{Y}_O}{|\nabla \overline{Y}_F||\nabla \overline{Y}_O|} \right) \tag{6.15}$$

Since the orientation of the vector at sub-grid level can fluctuate and affect the structure of the combustion at the resolved scale, the burning rate at LES grid level should give consideration to sub-grid reorientation. A mass Favre-weighted filtering is introduced. The filtered cross-scalar dissipation rate is decomposed into resolved and sub-grid parts. Following Domingo [67] :

$$\widetilde{\chi}_{F,O} = \widetilde{\chi}^r_{F,O} + \widetilde{\chi}^s_{F,O} \tag{6.16}$$

where the resolved part is expressed as $\widetilde{\chi}^r_{F,O} = -D\nabla\widetilde{Y}_F\nabla\widetilde{Y}_O$. A closure for the sub-grid part is derived, resulting in,

$$\widetilde{\chi}_{F,O} \approx \widetilde{\chi}^r_{F,O} - Y_{F,o}Y_{O,o}\left(\overline{F}_Z\widetilde{\chi}^s_C + \overline{F}_c\widetilde{\chi}^s_Z\right) \tag{6.17}$$

where $Y_{F,o}$ and $Y_{O,o}$ are the fuel and oxidizer concentration at the feeding stream, $\widetilde{\chi}^s_C = \widetilde{C}(1-\widetilde{C})/\tau_t$ and $\widetilde{\chi}^s_Z \approx \widetilde{Z}_v/\tau_t$ are sub-grid scalar dissipation rates expressed with eddy break-up type closure. $\overline{F}_Z$ and $\overline{F}_C$ are functions fully defined by the

resolved quantities. $\widetilde{Z}_v$ is the mixture fraction variance.

Using the same approximations as Domingo [67], the turbulent time scale can be expressed as $\tau_t = \Delta^2 \overline{\rho} / \mu_t$.

$\overline{F}_Z$ and $\overline{F}_C$ are functions defined following Domingo's development of the following expression for the cross-scalar dissipation rate,

$$\chi_{F,O} = -Y_{F,o} Y_{O,o} \left(F_C \chi_Z + F_Z \chi_C + F_{Z,C} \chi_{Z,C} \right) \tag{6.18}$$

where $\chi_C = D|\nabla C|^2$ is the scalar dissipation rate of the progress variable field, $F_C = -A_C B_C$, $F_Z = A_Z B_Z$ and $F_{Z,C} = A_C B_Z - B_C A_Z$, with A_C, B_C, A_Z and B_Z dependent on C, Z, and the equilibrium state as follows,

$$A_C = (1-C) - \frac{C}{Y_{O,o}} \frac{\partial Y_O^{Eq}(Z)}{\partial Z} \tag{6.19}$$

$$B_C = (1-C) - \frac{C}{Y_{F,o}} \frac{\partial Y_F^{Eq}(Z)}{\partial Z} \tag{6.20}$$

$$A_Z = (1-Z) - \frac{Y_O^{Eq}(Z)}{Y_{O,o}} \tag{6.21}$$

$$B_Z = Z - \frac{Y_F^{Eq}(Z)}{Y_{F,o}} \tag{6.22}$$

To further illustrate the implementation of the above, we take a lifted flame as an example. Three separate combustion regimes exist in a lifted flame. Firstly, the pure mixing zone where there is no combustion upstream of the flame front, secondly the

flame base where diffusion and premixed regimes co-exist and finally, downstream of the flame front where the diffusion trail prevails. Upstream of the varying, premixed front, frozen flow mixing occurs $C = 0, Y_F = Y_{F,o}Z$ and $Y_O = Y_{O,o}(1-Z)$, then $F_c = -1$ and $\chi_{F,O} = Y_{F,o}Y_{O,o}\chi_Z$. The cross-scalar dissipation rate appears as source in the transport equation of f. The reactants are mixed before reaching the base of the flame and $N_{F,O} < 0$.

At the flame base, the burning is divided between premixed and diffusion combustion. The mixture fraction changes in the flame interface and the progress variable varies in the perpendicular direction to the flame front, therefore $\nabla C \nabla Z \approx 0$ and $\chi_{Z,C} \approx 0$. It is also patent that $\nabla C >> \nabla Z$ and therefore $\chi_{F,O} \approx -Y_{F,o}Y_{O,o}F_Z\chi_C$, which is a negative source term in the transport equation of f. The cross-orientation vector $N_{F,O}$ is positive since the gradients of both reactants are oriented towards the flame front.

In the trailing diffusion flame, downstream of the flame front, C is expected to be weakly dependent on Z and assuming C(Z) ≈ 1 one can write $\chi_{F,O} \approx -Y_{F,o}Y_{O,o}F_C\chi_Z$. In this region the mixing process of the reactants is enhanced and f increases accordingly. In diffusion flames, $\chi_{F,O}$ is a source term for the transport equation of f and $N_{F,O}$ is negative.

These three regions are characteristic of a lifted flame, the flame index behavior throughout the flame can be summarized by,

$$\chi_{F,O} \approx -Y_{F,o}Y_{O,o}(F_Z\chi_C + F_C\chi_Z) \tag{6.23}$$

Domingo [67] proposed to close Eqs. 6.16 and 6.23 by:

$$\tilde{\chi}_{F,O} \approx -D\nabla\tilde{Y}_F\nabla\tilde{Y}_O - Y_{F,o}Y_{O,o}(\tilde{F}_Z\tilde{\chi}_C^S + F_C\tilde{\chi}_Z^S) \tag{6.24}$$

and a normalization of the flame index by,

$$\bar{\xi}_P \approx \frac{1}{2}\left(1 - \frac{\tilde{\chi}_{F,O}}{F_{NORM}}\right) \tag{6.25}$$

where F_{NORM} is used to normalize $\tilde{\chi}_{F,O} = \tilde{\chi}^r_{F,O} + \tilde{\chi}^s_{F,O}$. It is obtained from the following expression,

$$F_{NORM} = \left|\tilde{\chi}^r_{F,O}\right| + \left|\tilde{\chi}^s_{F,O}\right| \tag{6.26}$$

The normalization is used in such a way that $\bar{\xi}_P = 1$ means premixed combustion and $\bar{\xi}_P = 0$ refers to non-premixed combustion.

The introduction of the flame index allows premixed and non-premixed combustion models to be implemented separately, assuming that any flame can be divided into a collection of diffusion and premixed reaction zones [69]. Taking advantage of this, the complexity of each model can be improved independently, i.e. separate extinction, ignition, auto-ignition models could be implemented for premixed and non-premixed combustion.

In order to describe the composed combustion zones involving premixed and diffusion regimes, C is chosen to represent the premixed region and Z for the non-premixed. These two parameters represent two idealized turbulent flame regimes. C and Z are resolved at grid level and $\bar{\xi}_P$ is used to distinguish between them. Hence, the total heat release can be calculated as follows:

$$\tilde{Q}_T = \bar{\xi}_P \tilde{Q}_p + (1 - \bar{\xi}_P)\tilde{Q}_d \tag{6.27}$$

where $\tilde{Q}_p$ and $\tilde{Q}_d$ are calculated independently using separate premixed and diffusion combustion models.

6.3 Sub-grid scale combustion models

The distinction between the combustion regimes is undertaken in order that two simple models for each regime can co-produce the total heat release of a combined system.

6.3.1 SGS model for non-premixed combustion

For non-premixed combustion, the Laminar Flamelet approach for a counterflow configuration is used [54, 55]. In this approach a thin flame is assumed to be attached to the stoichometric iso-surface in the mixture fraction space. The main gradient is perpendicular to the stoichometric surface. The flamelets are assumed to be steady. This assumption is valid for high Damkohler numbers [183]. Fluctuations of the mixture fraction are taken into account by introducing a pre-assumed beta probability density function (pdf). Equations for the filtered mass fractions of species are expressed as:

$$\widetilde{Y}_{i,d} = \int_0^1 \overline{Y_i \middle| Z^*, \widetilde{\chi}_Z} P(\widetilde{Z}, \widetilde{Z}'', Z^*) dZ^* \tag{6.28}$$

where $\overline{Y_i \middle| Z^*, \widetilde{\chi}_Z}$ are the conditional values and $P(\widetilde{Z}, \widetilde{Z}'', Z^*)$ is the pdf distribution. The conditional values are obtained using the FlameMaster code developed by Pitsch [193]. This code solves the laminar flamelet equations for a counter-flow configuration at fixed scalar dissipation rates. The kinetic scheme used involves 28 species and 72 reactions [185]. For radiation, the gaseous mixtures are assumed to be optically thin. The heat release, temperature and mass concentrations were stored a-priori in a Look-up table.

The probability density function $P(\widetilde{Z}, \widetilde{Z}'', Z^*)$ is usually assumed to follow a Beta distribution parameterised with two moments, the filtered mixture fraction $\widetilde{Z}$ and its variance $\widetilde{Z}''$. The first moment is determined by solving the transport equation for the conserved scalar. The second moment can either be calculated using a SGS model or

solved through another transport equation. We follow the first option by using the following expression:

$$\widetilde{Z}'' = C_V \overline{\rho} \nabla \widetilde{Z} \nabla \widetilde{Z} \tag{6.29}$$

where C_V must be modelled.

Different methods have been proposed to calculate C_V. In the present study, we follow the approach of Moin [170] in which the small-scale equilibrium assumption is used and C_V is calculated dynamically.
Another important input parameter of the Look-up table is the scalar dissipation rate. Here, we follow Girimaji et al. [93] to use the following expression:

$$\widetilde{\chi}_Z = 2(D_Z + D_t) \nabla \widetilde{Z} \nabla \widetilde{Z} \tag{6.30}$$

where D_t is the turbulent diffusivity and D_Z is the scalar diffusivity.

Finally, the look up table with the mean heat release rate $\overline{\dot{w}(\widetilde{Z})}$ is stored and it is accessed by $\widetilde{Z}$, $\widetilde{Z}''$ and $\widetilde{\chi}_Z$.

6.3.2 SGS model for premixed combustion

The freely propagating one-dimensional premixed flame model is used for the premixed combustion regime.
When combustion does not start at the burner but further downstream, fuel and oxidizer mass fractions evolve across the partially premixed flamelets according to:

$$Y_{F,p} = (1-C) Y_{F,o} Z + C Y_F^{EQ}(Z) \tag{6.31}$$

$$Y_{O,p} = (1-C) Y_{O,o} (1-Z) + C Y_O^{EQ}(Z) \tag{6.32}$$

The filtered mass fraction $\widetilde{Y}_{i,p}$ may be obtained from the joint pdf of C and Z:

$$\widetilde{Y}_{i,p} = \int_Z \int_C Y_{i,p}(Z^*, C^*)\widetilde{P}(Z^*, C^*)dZ^*dC^* \tag{6.33}$$

The joint pdf is decomposed into $\widetilde{P}(Z^*, C^*) = \widetilde{P}(Z)\overline{P}(C^*|Z)$. Assuming thin and uncorrelated premixed flamelets, the pdf is expressed following BML hypothesis [31] :

$$\overline{P}_C(C^*|Z) \approx \overline{P}(C^*) = (1-\overline{C})\delta(C^*) + \overline{C}\delta(1-C^*) \tag{6.34}$$

which results in,

$$\widetilde{Y}_{F,p} = (1-\overline{C})Y_{F,o}\widetilde{Z} + \overline{C}\widetilde{Y}_F^{EQ} \tag{6.35}$$

$$\widetilde{Y}_{O,p} = (1-\overline{C})Y_{O,o}(1-\widetilde{Z}) + \overline{C}\widetilde{Y}_O^{EQ} \tag{6.36}$$

$\overline{C}$ is estimated from $\widetilde{C}$ using the BML relation extended to partially premixed combustion,

$$\overline{C} = \frac{\overline{\rho}_u \widetilde{C}}{\overline{\rho}_b + (\overline{\rho}_u - \overline{\rho}_b)\widetilde{C}} \tag{6.37}$$

where the subscripts u and b correspond to unburnt and burnt, respectively. These are calculated using the pdf of Z, which is assumed to be a beta-function,

$$\overline{\rho}_i = \int_0^1 \rho_i(Z^*)\widetilde{P}(Z^*)dZ^* \tag{6.38}$$

6.4 Flame front wrinkling factor Ξ

In Eq. 6.9, it is necessary to close the factor Ξ, namely sub-grid-scale flame front wrinkling factor, which is defined as the sub-grid scale flame surface divided by its projection in the resolved propagating direction. This can be regarded as the ratio of the sub grid turbulent flame speed ($S_{T\Delta}$) and the laminar flame speed (s_l^0). The sub-grid wrinkling factor is linked to Σ by $\Sigma = \Xi|\nabla\widetilde{C}|$, where $\widetilde{C}$ is the filtered progress variable. Domingo et al. [67] assumed a constant (Ξ=1.1) wrinkling factor, which is convenient for low turbulence.

A dynamic model for the wrinkling factor is introduced to capture the changes of the turbulent burning velocity at the flame base following Colin et al. [50]. This is based on the following expression which, relates local quantities with the wrinkling factor from spectral analysis as follows:

$$\frac{S_{T\Delta}}{s_l^0} = \Xi_\Delta\left(\frac{\Delta_e}{\delta_l^0}, \frac{u'_{\Delta_e}}{s_l^0}, \mathrm{Re}_t\right) = 1 + \alpha\frac{2\ln(2)}{3c_{ms}(\mathrm{Re}_t^{0.5}-1)}\Gamma\left(\frac{\Delta_e}{\delta_l^1}, \frac{u'_{\Delta_e}}{s_l^0}\right)\frac{u'_{\Delta_e}}{s_l^0} \tag{6.39}$$

where α is a model constant whose value 1.0 is recommended by Colin et al. [50], Δ is the LES mesh size, δ_l^0 is the laminar flame thickness, s_l^0 is the laminar flame speed, u'_{Δ_e} is the velocity fluctuation at Δ_e level, Δ_e is in the order of the flame front thickness ($\Delta_e \approx \Delta_C$ in the present case), Γ is the efficiency function, δ_l^1 is the resolved flame thickness and $\mathrm{Re}_t = u'L_t/\upsilon$ is the turbulence Reynolds number based on the velocity fluctuation and integral length scale L_t and a model coefficient C_{ms} = 0.28. The function Γ has been fitted by Colin as:

$$\Gamma\left(\frac{\Delta_e}{\delta_l^1}, \frac{u'_{\Delta_e}}{s_l^0}\right) = 0.75\exp\left[-\frac{1.2}{\left(u'_{\Delta_e}/s_l^0\right)^{0.3}}\right]\left(\frac{\Delta_e}{\delta_l^1}\right)^{2/3} \tag{6.40}$$

Note that Eqs. 6.39 and 6.40 require three inputs: $\mathrm{Re}_t, \Delta_e/\delta_l^1$ and u'_{Δ_e}/s_l^0. The laminar unstrained premixed flame thickness is normally between δ_l^0= (0.1-1.0) mm and the laminar flame velocity (s_l^0= 0.36 m/s). For Eq. 6.40 δ_l^0=0.4 mm, which corresponds, as first approximation, to the flame thickness for the unity equivalence ratio. The laminar flame speed s_l^0 and thickness δ_l^0 were calculated using the

FlameMaster by Pitsch. It is important to note that Colin's model was initially developed considering a fully premixed mixture and it has been extended here to partially premixed.

It can be noted that the wrinkling factor is affected by both the grid size and the local turbulence intensity. As expected, as the mesh size is increased the unresolved or sub-grid-scale flame surface becomes larger and consequently it has to be incorporated into the resolved-grid level by the wrinkling factor model. Similarly, the stronger the sub-grid turbulence the larger is Ξ.

Charlette et al. [42, 43] developed a model which does not need the turbulent Reynolds number as input. The general performance of both models were found to be similar for isotropic turbulence if α is adjusted accordingly. In the present study, Collin's method is chosen using $\alpha \approx 1.0$, which was the value in Charlette's work for $Re_t \approx 100$.

Colin et al. [50] established some constrains in selecting Δ_e and stated that Δ_e may be different from the actual LES mesh size and in fact corresponds to the filter size required to extract sub-grid scale information needed to estimate the efficiency function developed in the same study inside of a Thickened Flame Front approach. They recommended that Δ_e should be of the same order as the flame front thickness. This recommendation is followed in the present study.

Another important element in the calculation of the flame wrinkling factor is the estimation of u'_{Δ_e}. In the absence of turbulence, Colin et al. [50] suggested the use of other methods rather than the sub-grid turbulent viscosity provided by SGS turbulence models to obtain u'_{Δ_e} as the strain is dominated by thermal expansion in such situations. The local evaluation of the sub-grid fluctuation u'_{Δ_e} is thus considered using the Laplacian of the resolved vorticity field,

$$u'_{\Delta_e} = c_2 \Delta \left| \nabla \times \left(\nabla^2 (\tilde{u}) \right) \right| \tag{6.41}$$

6.5 Summary

A brief summary of sub-models for partially premixed combustion was given in this chapter. In this study, it is assumed that premixed and non-premixed combustion regimes can be modelled independently. Thus, the progress variable balance equation represents the advancement of a premixed flame front and the mixture fraction balance equation represents the mixing process which is fundamental for non-premixed combustion.

The filtered of the progress variable in a LES grid is chosen as flame front tracking technique. To our mind, this approach presents more suitable properties both from the numerical point of view and the implementation. Moreover, due to its relatively smooth gradient at the flame front, this approach lacks the cups present in the G-equation and has a clear physical interpretation as it can be assigned to the temperature or specie field alike.

In this chapter, the complete C balance equation (Eq. 6.5) was introduced, which contains unclosed terms such as cross-dissipation rates and second derivatives of the fuel conditional. As a first approximation these terms are not considered in this study. Finally, Eq. 6.6 is the simplified LES filtered balance equation for C. In order to close the source term of the C balance equation some approaches such as sub-grid density function, laminar burning velocity and sub-grid wrinkling factor were introduced. It is important to note that none of the sub-models presented here use empirical constants. In other words, the parameters are not set for a specific situation. The parameters are mostly obtained using filtered DNS data and are, in principle, general as far as the flow characteristics at sub-grid level in the LES simulation are relatively close to the DNS.

A flame indicator based on the scalar product of fuel and oxidizer normal vectors was introduced in order to couple premixed and non-premixed combustion. The flame index model developed by Domingo et al. [67] for LES was implemented in the FDS code. This model is capable of distinguishing both regimes from filtered quantities of

specie mass fractions and introduces the effects of their respective sub-grid fluctuations.

Chapter 7

LES of Premixed and partially-premixed systems

In this chapter, different premixed and partially-premixed flame structures are simulated within the LES framework using the sub-models introduced in chapter 6.

In order to test the different sub-grid models, three reacting flow configurations are chosen. Firstly, a 1-D laminar planar premixed front; secondly, a laminar triple flame and finally, a turbulent lifted flame. These flow configurations are selected as they pose challenges for the individual sub-models.

In the progress variable approach, C is filtered using a filter larger than the LES grid; thus, the thin premixed front can be resolved on an enlarged LES grid. In order to test this approach, a 1-D premixed hydrogen laminar flame is simulated.

The triple flame is chosen in order to analyze the behaviour of the flame index concept. In this specific configuration, there are three branches, the rich and lean premixed fronts and the diffusion trail. The triple point is located at the intersection of these three branches.

Finally, a turbulent lifted flame is simulated. Turbulence enhances the burning velocity due to flame sheet contortions at sub-grid level. This is considered in a form of a wrinkling factor sub-model, which is included into the calculation of the sub-grid density function. This wrinkling factor is unity when there is no turbulence and greater than one when turbulence is present. The turbulent lifted flame is chosen in order to test the wrinkling factor model along with all the other sub-models.

7.1 1-D laminar planar premixed front

In order to test the filtering approach for the progress variable approach, a 1-D laminar hydrogen premixed front is simulated using Eq. 6.9..

The initial mixing is composed of oxygen and hydrogen in such a proportion to obtain $\phi = 1$. At P = 1 atm, the laminar burning velocity s_l^0 is 2.14 ms^{-1} and $\rho_u/\rho_b = 6.89$. In this case Eq. 6.9 is used with $s_l^0 = 2.14$ m/s as laminar speed, Ξ = 1 for laminar flow and $\Delta_C = 5\Delta$ the progress variable filter.

The hydrogen heat of combustion $\Delta H = 14.29$ Kw/Kg is used and it is assumed that the hydrogen is completely depleted downstream the flame front. The domain consists of a 40 m long tunnel with square section of (5x1) m in Y and Z, respectively. The mesh is (300 x 7 x 7) in X, Y and Z directions, respectively. The progress variable is initiated at X = 0 with C = 1 and is left to propagate through the fresh gases. Between 1 and 2 sec after ignition the flame is stabilized at $s_l^0 = 2.14$ m/s.

Fig. 7.1 shows the profiles of the progress variable (C), heat release rate ($\dot{w}$), oxygen (O_2), hydrogen (H_2) and temperature (T) through the laminar premixed front.

It is observed that Eq. 6.9 predicts accurately the burning velocity and the predicted density ratio $\rho_u/\rho_b = 6.66$, is very close to the experimental value of $\rho_u/\rho_b = 6.82$. The flame front is solved using about $2\Delta_C \approx 10$ points as it was mentioned above.

In Fig. 7.1, it is also noted that the progress variable C reaches unity from the fresh to the burnt gases and when the $\nabla C \neq 0$ the source term is non-zero. It can be observed, as well, the depletion of both fuel and oxygen mass concentrations.

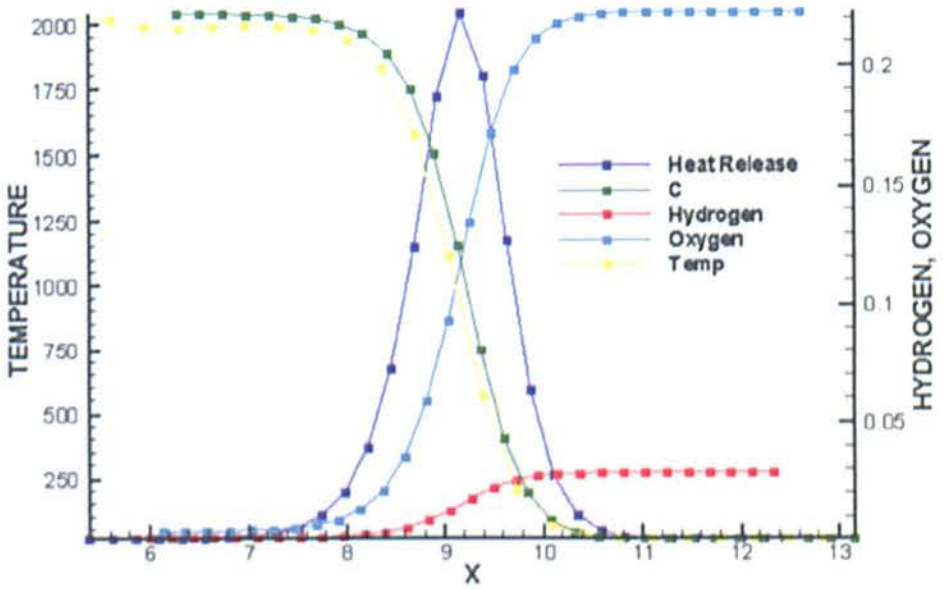

Figure 7.1. Profile for 1-D hydrogen laminar premixed flame front.

7.2 Triple Flame

A tribrachial (or triple) flame can form in a mass diffusive mixing layer with a flammable concentration. The triple flame consists of a lean premixed flame, a rich premixed flame and a diffusion flame. The junction of the three reaction branches is called triple point. This structure was first reported by Philips [189], who experimented on flame propagation in a horizontal methane-air stratified mixing layer. Philips showed that the propagation velocity of the triple flame is much larger than the laminar burning velocity of a stoichometric mixture.

There are many works dedicated to analyze both experimentally and numerically triple flames [66, 99, 117, 118, 121, 122], especially with regard to the dependency of the propagation velocity on the gradient of the fuel mass fraction.

Dold [66] developed analytically a low heat-release model and showed that the triple-flame propagation speed depends on the transverse mixture fraction gradient. Kim et

al. [118] measured the lift off heights of triple flames at different strain rates; they found a critical value for which the lift off height reached a minimum. Guo et al. [99] carried out a very interesting direct numerical simulation of a triple flame with detailed chemistry. They established that the displacement velocity at the premixed front of the triple flame is mainly controlled by flame stretching. While in the rich and lean branches, the diffusion of radical from the non-premixed regime to the premixed branches modifies the reaction in the later and increases the burning velocity of the premixed branches. This later effect is enhanced when the fuel gradient is increased as the premixed branches are closer to the diffusion flame.

Guo et al. [99] attributed the difference between the planar burning velocity in homogeneous mixing and the displacement velocity of the triple flame mainly to the interaction of the branches and especially in regions far from the stoichometric mixture.

The triple flame configuration is an attractive flame structure for many reasons. Firstly, it is laminar by definition, which is an advantage in the sense that avoids uncertainties from the sub-grid scale turbulence model. Secondly, it presents a complex partially premixed structure, composed by rich and lean branches and a diffusion trail, this characteristic is very suitable to test the flame index concept delineated above and, finally, it is generally easy to set up and the running times are usually short.

In the present section, the triple flame studied by Kioni et al. [121] is simulated. Fig. 7.2 shows the inlet conditions for fuel and oxygen concentrations. The inlet velocity is a planar profile of 0.8 m/sec. The computational domain is (6 x 6 x 15) cm in x, y and z directions, respectively and a grid of (40 x 40 x 100) in x, y and z.

The simulation includes the flame index approach detailed in section 6.3 and the combustion models specified in section 6.2 for premixed and non-premixed regimes. The balance equations for C and Z as noted in section 6.1 are solved by the LES code. The flame front is originally initiated at a given location downstream the inlet and

thereafter it is left to evolve by itself until it is stabilized at the lift off height.

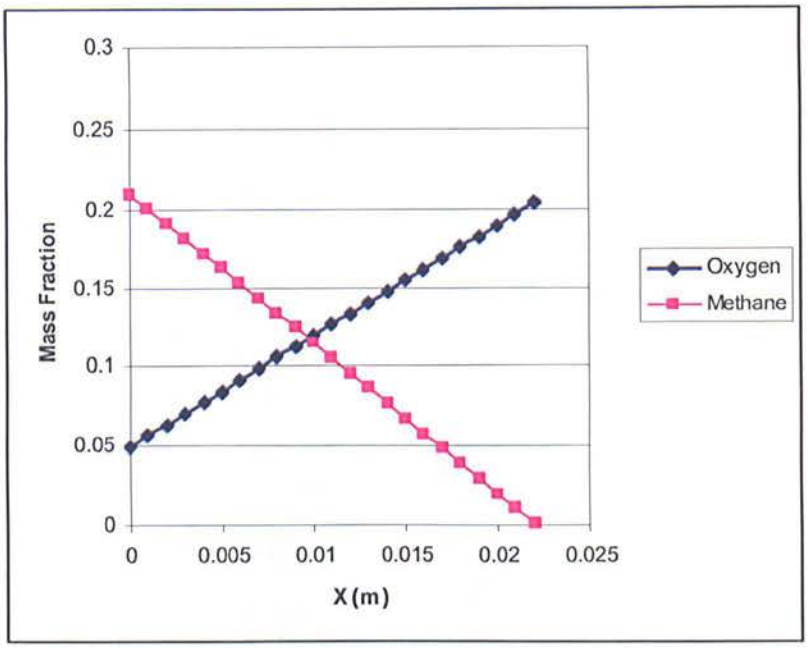

Figure 7.2. Inlet conditions for the triple flame.

The main goal is to study the performance of the flame index in a complex laminar flame structure. Here, the comparison with the experiment will be limited to the lift-off height, velocities, maximum temperature and structure of the triple flame.

Kioni et al. [121] measured a lifted-off of approximately 0.02 m from the nozzle exit. Fig. 7.3 shows the progress variable. It is observed that the flame is stable at 0.017 m, slightly over predicting the displacement velocity.

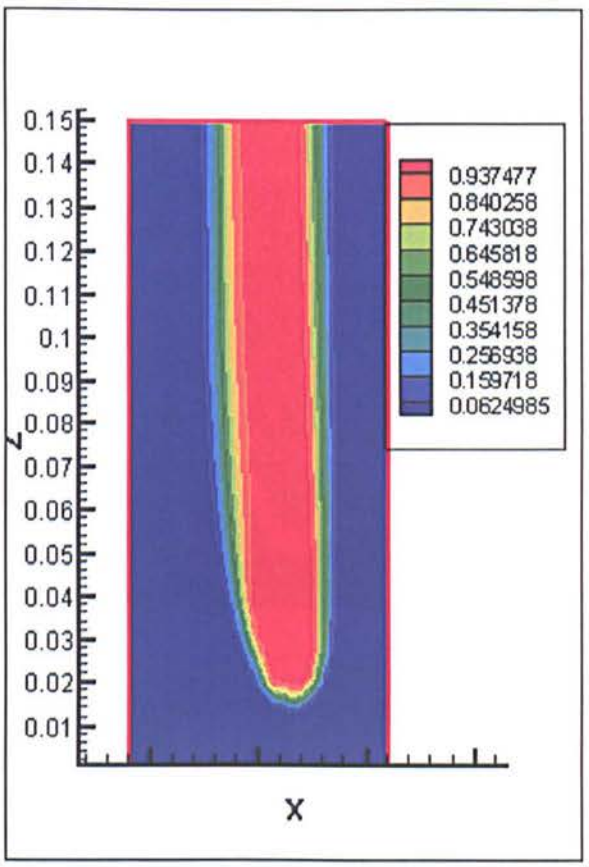

Figure 7.3. Progress variable C of the triple flame.

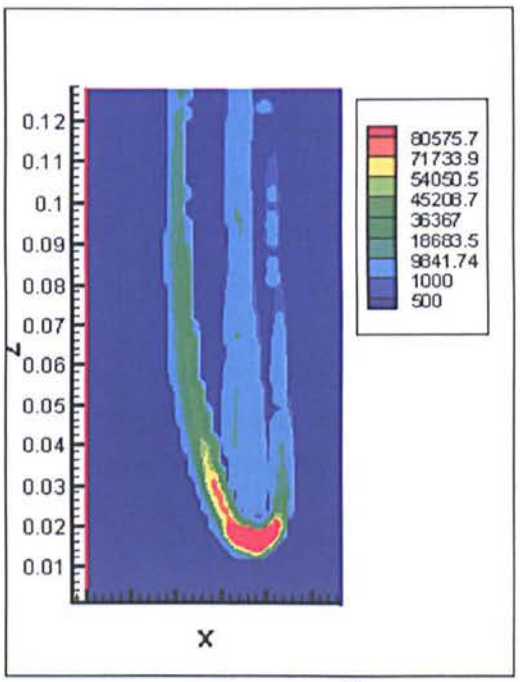

Figure 7.4. Total heat release rate $\widetilde{Q}_T$ for the triple flame.

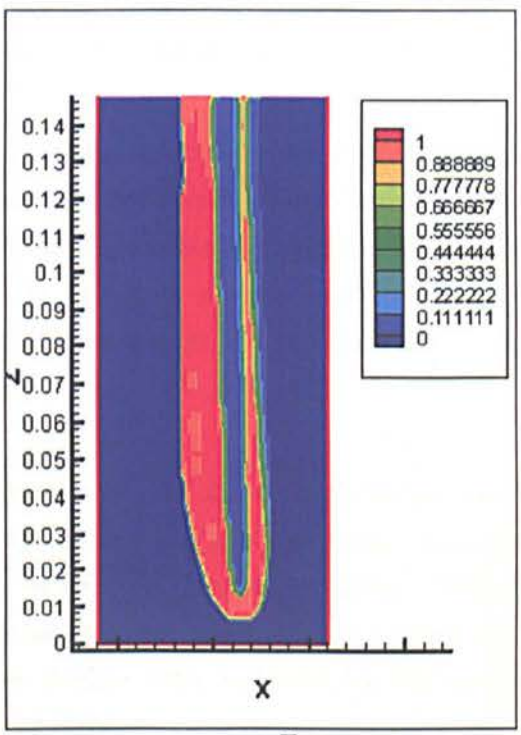

Figure 7.5. Flame index $\overline{\xi}_P$ for the triple flame.

Figs. 7.4 and 7.5 show the total heat release rate and the flame index, respectively. The rich, lean and diffusion branches can be seen in Fig. 7.4. On the fuel side, the rich premixed branch is longer than the lean one. This is also observed in the experiment. This may be due to the low stoichometric value of the methane-air system.

As it is seen in Fig. 7.6, the fuel mass concentration on the lean side is very low. On the contrary, Fig, 7.7 shows bigger oxygen mass concentration on the rich side. Coming back to Fig. 7.4, it can be observed that the diffusion trail merged with the two premixed branches as in the experiments.

Fig. 7.5 depicts the flame index along the triple flame. A unit value of the flame index means premixed combustion and zero implies diffusion regime. At the centre of the flame, a region of non-premixed combustion can be observed, while at both sides of it the premixed branches are predicted. The flame index is only calculated where there is a minimum of heat release from either premixed or non-premixed combustion.

The fuel and mass concentrations are shown in Figs. 7.6 and 7.7, respectively. As it was mentioned above, the fuel and oxygen are almost completely depleted downstream the flame front. This is also observed in the experiments. It can be noted that the gradients of the fuel and oxygen concentration along the flame in the premixed region are of the same sign. On the contrary, along the diffusion regime they have opposite signs.

Fig. 7.8 displays the temperature field for the triple flame. The maximum temperature is around 2000 K. In the experiment, the maximum temperature is not given but a numerical calculation predicts a maximum about 1992 K. In line with the measurements, the maximum temperature is placed along the diffusion flame. This might be attributed to further heat released by the non-premixed combustion downstream the premixed front.

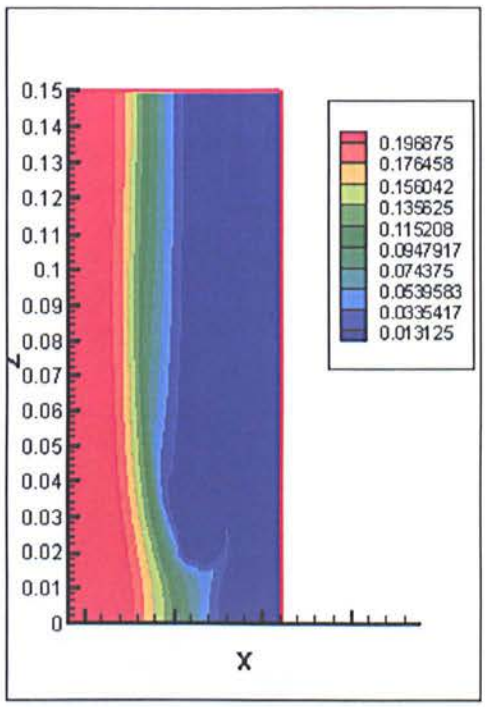

Figure 7.6. Fuel mass concentration for the triple flame.

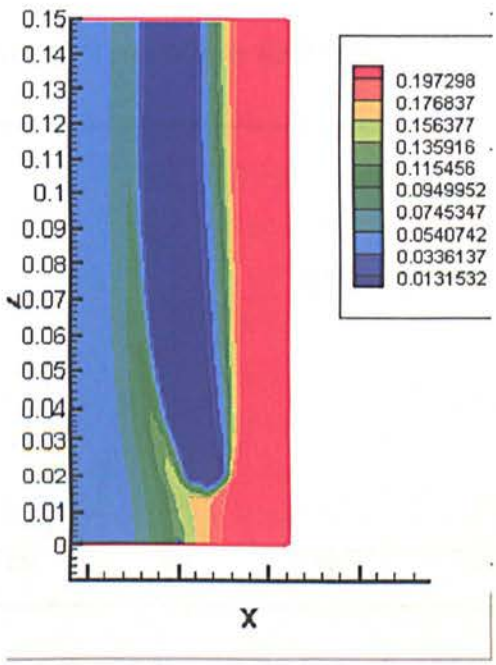

Figure 7.7. Oxygen mass concentration for the triple flame.

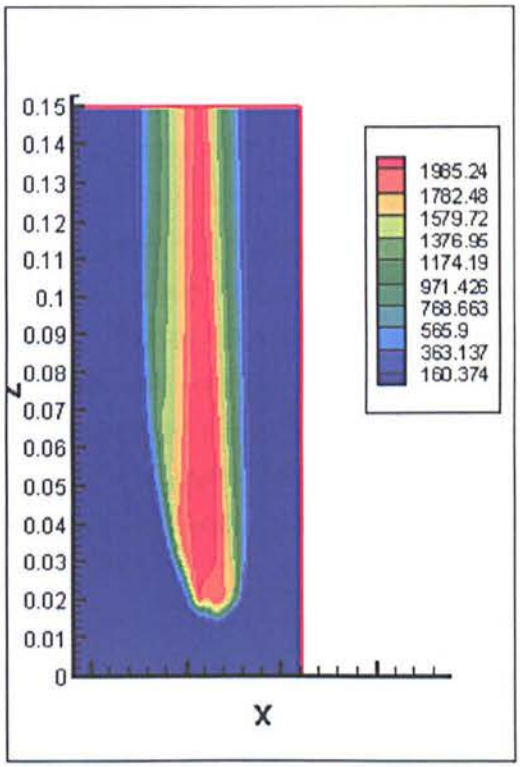

Figure 7.8. Temperature field for the triple flame.

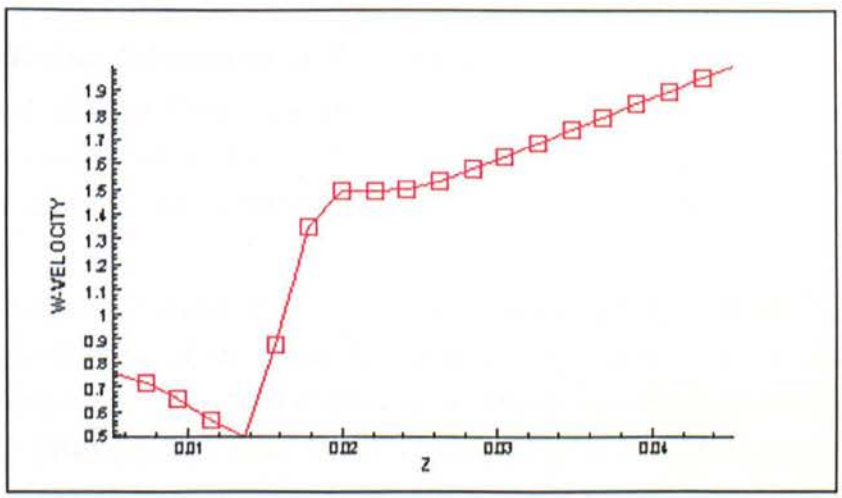

Figure 7.9. Axial velocity through the flame front for the triple flame.

Finally, Fig. 7.9 shows the axial velocity through the triple point. As it is observed in many studies [117, 118, 121], the flow velocity immediately upstream the flame front is close to the laminar burning velocity for the stoichometric mixture, in this case 0.4 m/sec for methane-air. This process is similarly present in the turbulent lifted flame in the following section and might be in part responsible for the flame stabilization in a flow whose velocity is far larger than the premixed counterpart. This might explain why, in this case, without considering any sub-grid scale wrinkling ($\Xi=1$), the model is able to predict the displacement velocity for the triple flame. Furthermore, this means that LES is resolving the large eddies which affect the flame front and modify the displacement velocity of the triple flame. Nevertheless, we do not want to speculate excessively on this issue and we believe further study is needed in this regard.

If the flame front is under a strong turbulence, the wrinkling of the surface density Σ may be affected by small eddies in such a way that the total surface per unity of volume is increased and the overall burning speed is enhanced. Therefore, a wrinkling factor model, Ξ, must be included in the model.

7.3 Turbulent partially premixed lifted flame

Stabilization of lifted flames has been addressed by different research groups based on two approaches: the first is related to the flamelet quenching in diffusion flames [220, 240] and the second is related to premixed flame propagation [27, 222, 236].

The stabilization of lifted flames on jets is controlled by specific combustion properties at the base of the flame, the interaction of mixture fraction gradient and local turbulence upstream of the reaction zone plays an important role in this process. In laminar lifted jets the base flame develops into a tribrachial or triple flame structure composed by a rich branch, lean branch and a trailing diffusion flame across the mixture fraction gradient [25, 122]. The three branches meet at a point called triple point. These flame structures have been measured as laminar triple flames [121,

122, 136] and investigated theoretically [24, 45, 66] and by Direct Numerical Simulations (DNS) [74, 200] techniques.

In turbulent jets, the interaction between turbulence and combustion becomes more evident and the triple flame structure is contorted. The premixed branches are deflected and sometimes can overlap the diffusion flame, making their identification very difficult [40, 150, 174, 248].

In the context of laminar and turbulent lifted jet flames, many experimental studies are available [49, 134, 137, 150, 151, 251]. Due to the restriction of low Reynolds numbers in DNS calculations, only laminar lifted flames and weakly turbulent lifted-flames have been numerically solved using DNS [25, 69, 200]. Relatively few investigations have been carried out using Large Eddy Simulation (LES) [67].

Most of the above-mentioned to studies used the triple flame propagation front concept to represent the lifted flame at its base. The basic structure is described using a triple point anchored at the base of the flame with the lean and rich premixed branches and the trailing diffusion flame departing downstream from it. Previous investigations found that the speed of the triple-flame is controlled by two parameters: the curvature of the partially premixed front, determined by the dissipation rate at the leading edge, and the heat release from the combustion. Increasing the dissipation rate reduces the flame speed [45]. The heat release causes the deflection of the flow upstream of the flame front and has the effect of making the triple flame propagate faster than fully laminar premixed front [25]. It was found that even when the heat release modifies the mixture fraction gradient and the flame speed, the flow velocity at the flame base still remains in the same order of magnitude as premixed laminar flames.

The development of advanced laser-based techniques has resulted in the exploration of stabilization mechanisms of turbulent lifted flames [150, 174]. Mansour [150] and Muñiz [174] reported a detailed account of flame structure at the turbulent base and its interaction with the turbulent eddies. Mansour [150] measured lift-off heights,

blow out and reattachment Reynolds numbers as well as the triple point at the flame front. His measurements revealed the inner structure of the double-reaction-zone in highly stabilized turbulent partially premixed flames. These double flames were numerically simulated using DNS by Domingo et al. [69] for a weakly turbulent-lifted flames with a central jet width of 1 mm. Further measurements on the lift off heights have also been reported by Schefer [222] and Chung [49]. Measurements on blow out and reattachment velocities were conducted by Lee [135, 136].

7.3.1 Experiment considered

The experimental set up of Mansour [150] for lifted turbulent jet flames is considered here. The burner consists of a vertical tube of 4 mm inner diameter and 6 mm outer diameter surrounded by an 8 mm diameter (d) tube. The two tubes are concentric, but at different levels. The inner tube exit is below the outer tube exit, by a distance of 205 mm. The air flows through the inner tube, while the fuel flows through the outer tube. The burner is located in a wind tunnel that provided laminar co-flowing air at 0.2 m/s. Table 7.1 shows the values of mean axial velocity (U), equivalence ration (ϕ) and mixture fraction (Z) at the nozzle exit.

Table 7.1. Parameters of the turbulent lifted flame PF1.

Flame	U(m/s)	ϕ	Z	Re	Lift-off height(H/d)
PF1	4.74	4.52	0.208	2446	6 ~ 6.75

Using advanced laser techniques, Mansour [150] extracted instantaneous shots of stoichometric mixture fraction, rich reaction zone and non-premixed reaction zone contours at the stabilization height and some diameters downstream. Three sets of experiments with different jet Reynolds numbers were tested, but only the first set PF1 was simulated in the present study. As this set has the lowest Reynolds number, the contortion of the structure at the flame front was less than the other two cases, which had stronger turbulence, and therefore its inner structure is easier to identify. It is known that, as the flame recedes downstream caused by larger flow velocity, the

flame fluctuation becomes larger [188, 232].

7.3.2 Simulation details

Apart from the inflow conditions for the fuel and air jets, the other boundaries are treated as shear-free (open). The simulations are initiated from an iso-thermal flow field with a numerical spark located at Z/d = 8.7 for a few milliseconds. This time is enough to allow the progress variable to develop either up or downstream through the field, depending on the flow conditions. The numeric spark consists of an arbitrary value of C. In this case C = 1.0 is used, but, in principle, another value could be used, without affecting the evolution of C.

The viscous stress tensor $\tau_{ij} = -(\mu_t + \mu_l)\overline{S}_{ij}$ is closed following Smagorinsky [227] and the viscosity term is modelled as $\mu_t = \overline{\rho}(C_S\Delta)^2|\overline{S}|$ where C_s is the Smagoringsky constant which needs to be chosen. Zhou et al. [273] used a value of 0.1 in his study of a turbulent forced plume with Reynolds number of 1273. They obtained good agreement with the experimental data. We have used the Lagrangian dynamic sub-grid-scale model of Meneveau [166] to simulate a similar plume configuration of Reynolds number 1135 and found that the Smagorinsky constant predicted by the Lagrangian model is 0.11. In the present study, the jet Reynolds number is 2440 and C_s is set to 0.1 on the basis of these previous studies. Higher C_s values were also tested but found to produce laminar-like results. The Prandtl and Schmidt numbers are set to 0.7 and 0.6, respectively

7.3.3 Grid sensitivity study

To test the grid sensitivity of the flame index approach, the computation is performed using three grids which have cell sizes at the leading edge of the flame of Δ_1 = 1.5 mm, Δ_2 = 1.0 mm and Δ_3 = 0.8 mm. As stated earlier, considering that δ_l^0 = 0.4 mm is used in Eq. 6.40, the ratios Δ/δ_l^0 for the three meshes are therefore 3.74, 2.5 and 2, respectively. This degree of fine resolution means that Ξ is kept low for all the three meshes. In fact, the dynamically calculated wrinkling factors for the three meshes

using Eq. 6.39 are between 1.1 and 1.3. As expected, the lowest value corresponds to mesh 3 and the biggest to mesh 1. Hence, the sensitivity of the wrinkling factor model to the grid size is not important to the overall prediction. This was verified for mesh 3 where α in Eq. 6.39 was changed from 0.9 to 1.1, the predicted wrinkling factors were seen to be unaffected.

In order to decide the lift-off height, we draw from the DNS calculations of Boger et al. [20], who found that the flame surface density Σ peaks at $\widetilde{C} = 0.6$, and use this value to locate the flame front. Mansour [150] measured the lift-off height (L), normalized by the nozzle diameter (d), to be within the range of H/d = 6-6.75. The simulations of all three meshes predict about the same lift-off height of H/d = 6.3, which is right at the centre of Mansour's measured range. As may be seen from the predicted contours of the mean progress variable in Fig. 6.10, the 'leading edge' (here this term refers to the most upstream point of the flame base) in all the three predictions is located at about z/d = 6.25. However, it is also observed that the profile of $\widetilde{C}$ downstream of the flame front is not exactly the same for meshes 1 and 2. In mesh 1, $\widetilde{C}$ is wider than in meshes 2 and 3. This might be caused by larger fluctuations of the stabilization point (the point of maximum premixed heat release, Q_D^{MAX}) observed in mesh 1. It is also seen that the predictions of meshes 2 and 3 are almost identical. The predictions of mesh 2 are therefore used in the following analysis.

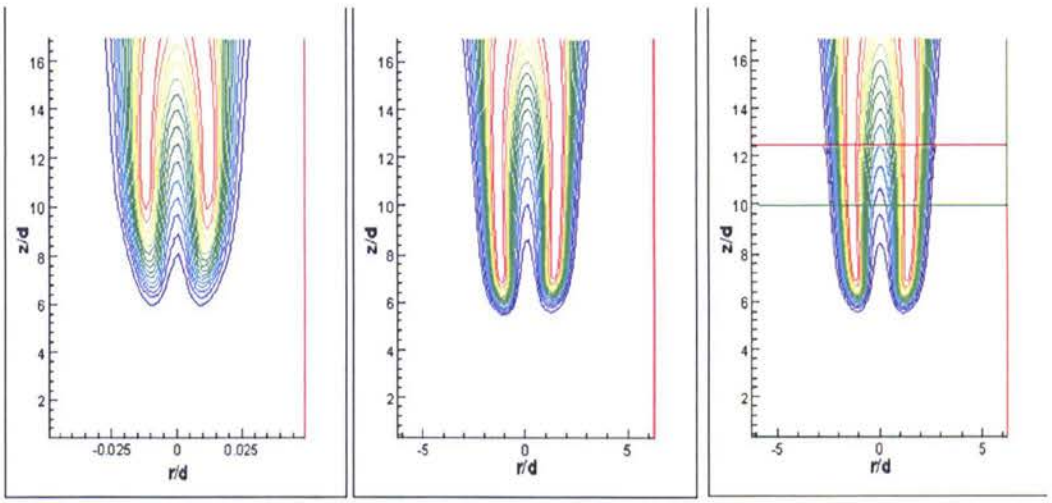

Figure 7.10. Mean progress variable for mesh 1, 2 and 3, respectively.

7.3.4 Mean structures

The mean mixture fraction contour is illustrated in Fig. 7.11. The expansion of the gases due to the heat released by the combustion can be seen downstream of the flame front. This affects the mixture fraction distribution and causes the relatively high gradient at the flame base to be gradually reduced. Simultaneously, the gas expansion modifies the scalar dissipation rate at the flame front which, in time, can influence the flame speed through the curvature of the partially premixed front [25]. Boulange et al. [25] studied the effect of heat release in diffusion lifted flames on round jets and found that heat release at the flame base affects the mixture fraction downstream the flame front, decreasing its gradient in the trailing diffusion flame and, as a result, the mixture fraction gradient there becomes even milder than the isothermal jet flow.

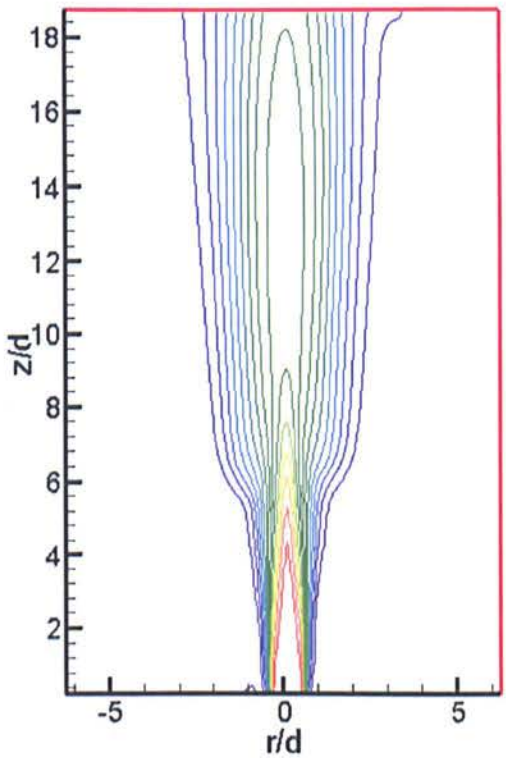

Figure 7.11. Mean mixture fraction contour.

Fig. 7.12 shows the radial profile of the mean mixture fraction at different planes immediately downstream from the jet exit up to the stabilization plane. The predictions agree well with the experiment. By drawing a line at constant stoichometric mixture fraction, Mansour found that the length of the line enclosed by the mixture fraction profile at the stabilization height is very close to the flame base width (D_B), defined as the distance between the two most upstream points of the flame on the central plane. The model has predicted this with very good accuracy and therefore reinforced the experimental finding that the flame stabilizes in the vicinity of stoichometric mixture fraction. These results support the theory that the flame is stabilized close to position where the local flame speed is approximately same as the flow velocity. This is also found to be the case in the experiment carried out by Su et al. [232].

The present model uses the progress variable (C) to detect the position and evolution of the flame front. In LES, this transport equation needs to be closed by models and is therefore subject to approximation. As pointed out previously, in partially premixed systems the complete transport equation for C should be used to capture the correct evolution of C. Considering that Eq. 6.5 is solved here instead of Eq. 6.9, it is interesting to study to which extent this approximation is valid.

Fig. 7.13 shows the mean reaction progress variable (C), which is overlapped by black solid lines of the iso-mixture fraction at Z_{st} = 0.054. In line with Mansour's observation, the stoichiometric mixture fraction and C contours are slightly directed toward the inside of the flame centreline. A core of low C is formed between the two branches of the flame front. The rich premixed branches are located in this region, closing further downstream in a sort of arc (see also discussion concerning Fig. 7.15). The iso Z_{st} can be seen progressing almost through the centre of the burnt gases zone and the diffusion burning region. Similar structure was also found in Domingo's DNS study [69].

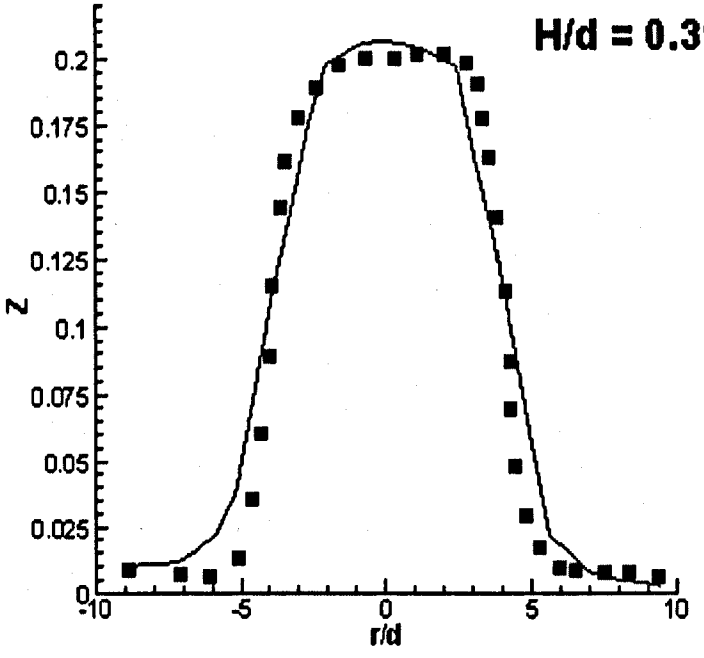

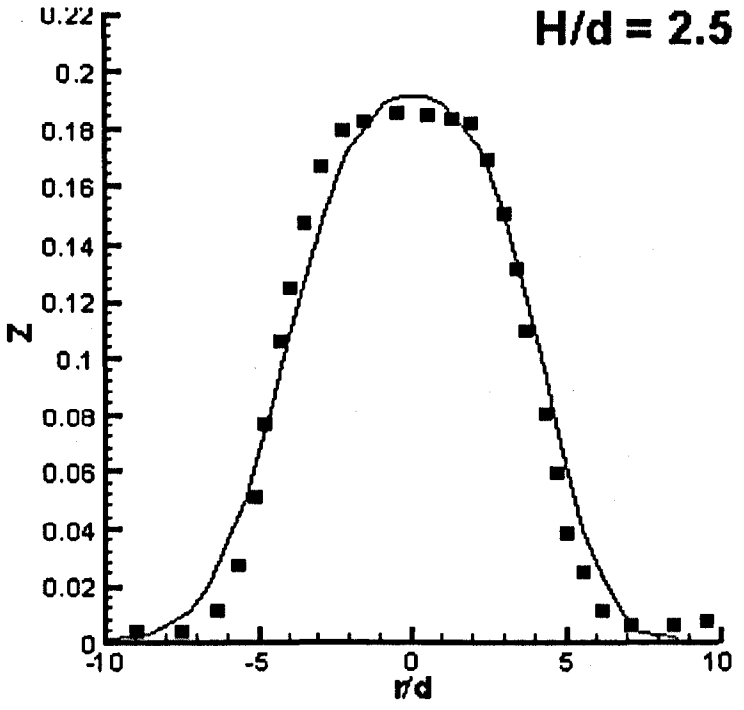
H/d = 2.5
Z
r/d
0.22
0.2
0.18
0.16
0.14
0.12
0.1
0.08
0.06
0.04
0.02
0
-10
-5
0
5
10

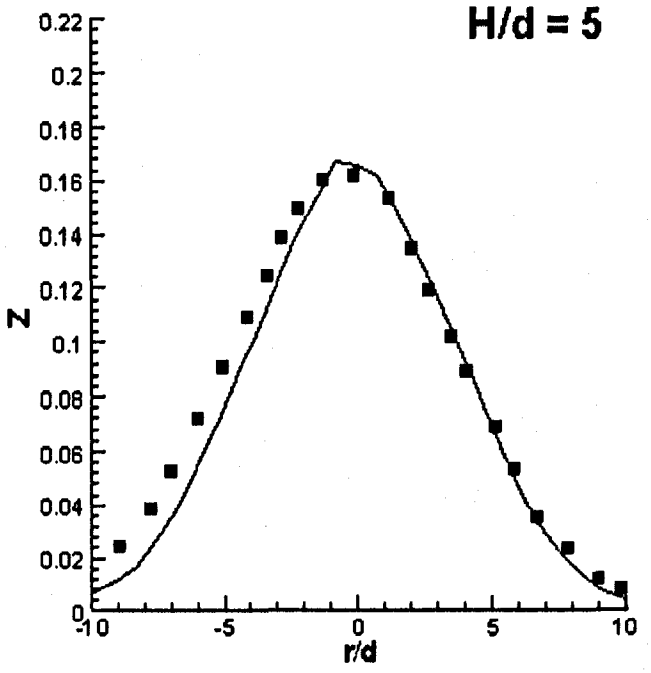
H/d = 5
Z
r/d
0.22
0.2
0.18
0.16
0.14
0.12
0.1
0.08
0.06
0.04
0.02
0
-10
-5
0
5
10

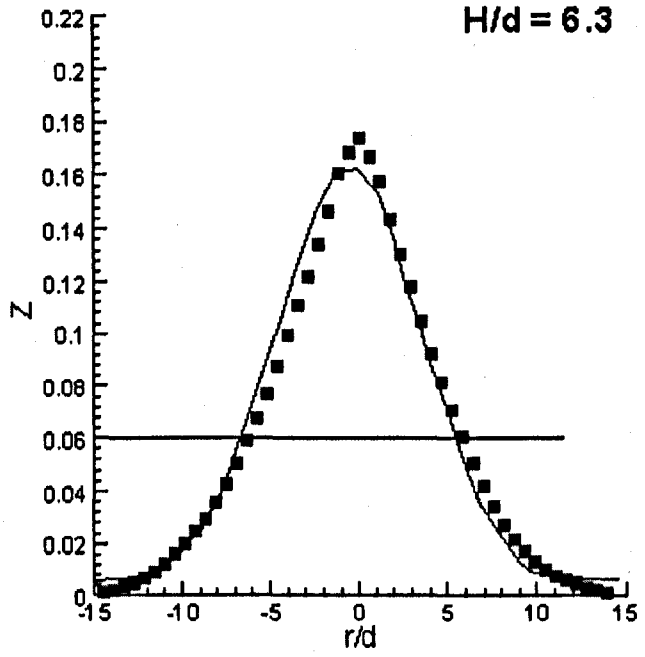

Figure 7.12. Mean mixture fraction profiles at different downstream locations. Symbols: experiment, line: simulation.

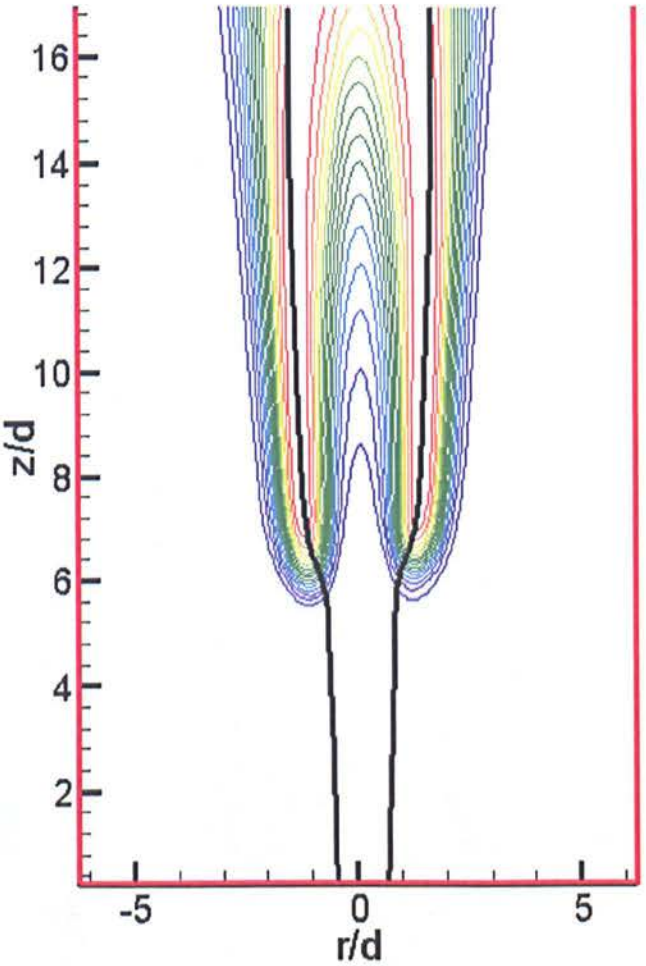

Figure 7.13. Mean stoichiometric mixture fraction value (black solid line) and progress variable (contour).

The iso-C and iso-Z lines are almost perpendicular at the flame base, implying small values of the cross-scalar dissipation rate (third RHS term in Eq. 6.5) at the premixed front. Further downstream, the iso-lines become parallel and hence, the cross-scalar dissipation rate is expected to be of finite value and it can be important in the balance equation. However, in the DNS carried out by Domingo [69], where the complete transport equation for C (Eq. 6.5) was solved for a similar lifted flame with double flame structure, the contribution of the cross-scalar dissipation rate for low

stoichiometric values, such as in the present case ($Z_{st} \approx 0.054$), was found to be negligible. The fourth RHS term, which is proportional to the mixture fraction dissipation rate, was found to be important in the diffusion burning zone and not totally negligible at the premixed front. Domingo also found that this term became negative in the diffusion region, and hence it balanced the diffusion of C (first term of RHS in Eq. 6.5). This might cause some discrepancy in the present simulations, and it indicates the need for an improved balance equation for C, in which the extra terms could be closed. Nevertheless, the current predictions have captured the flame structure well.

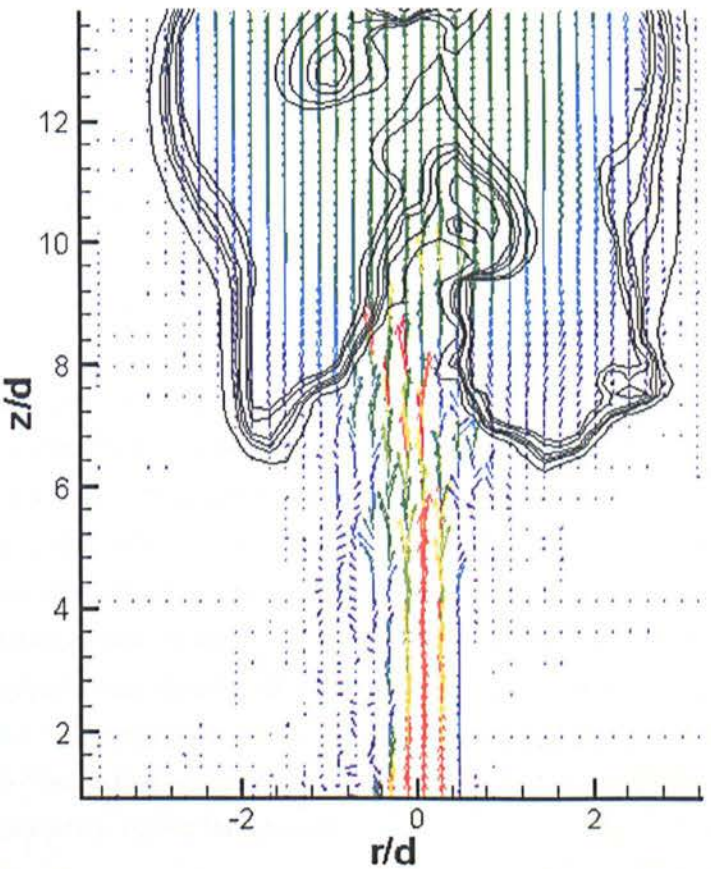

Figure 7.14. Instantaneous velocity vectors and progress variable.

7.3.5 Instantaneous structures

Fig. 7.14 illustrates the instantaneous profile of the progress variable $\widetilde{C}$ at 0.6, where the peak of flame surface density was found to be located [20]. This is plotted on top of the instantaneous velocity vectors. The meandering at the jet centreline, which was observed experimentally by Muñiz [174], is also noted here.

In line with the measurements, a low velocity zone exists in the flame front, about 1.25 r/d from the centre. The divergence of the flow, redirecting the flow outwardly, is also evident there. Immediately upstream of the flame front the velocity is in the order of the premixed laminar flame speed. Further up the flow is accelerated through the flame front by thermal expansion. Su et al. [232] found that the flow field, several diameters upstream the leading front, is not modified by the flame. They further identified that the species concentrations and velocities there are close to an iso-thermal jet. On the other hand, closer to the flame base, the flow is affected by the expansion of the combustion products and the velocity is considerably reduced.

The flame fronts are located at each tip in the scalar field of the progress variable, typically this corresponds with the most upstream point of the flame. The turbulent characteristic of the flame is evident. Violent contortions of C can be seen in the central core of the flame, between the two branches where the flow velocities are large. The evolution of the flame front in time presents displacements both upstream and downstream, depending on local conditions of the flow upstream from the flame front. Radial movements of the leading front are found to exist. The amplitude of the vertical oscillations, which mainly depend on the turbulence at the flame base, is found to be around one nozzle diameter (d) for the present case. Mansour [150] commented that the amplitude of the displacement is proportional to the Reynolds number. It is believed that eddies from the jet centre interact with the flame front and produce the contortion of the flame front.

7.3.6 Flame index ($\overline{\xi}_P$)

The experimental work of Mansour [150] revealed the inner structure of the double-reaction-zone, which consists of a rich reaction zone, trailing diffusion zone and a possible lean reaction zone. The rich zone was found to lean toward the flame centreline, followed by the diffusion reaction zone and the lean reaction zone at the outside. The three reaction zones meet at one point, which is usually called the triple point.

Fig. 7.15 shows the instantaneous profile for the flame index ($\overline{\xi}_P$), the progress variable (C), the diffusion heat release (iso-Q_D), the premixed combustion (iso-Q_P) and the stoichiometric line (Z_{st}) at the flame base. As stated, the flame index is used in the present study to identify different combustion regimes. In Fig. 7.15, $\overline{\xi}_P$ =1 (red in the shaded contour) indicating premixed and $\overline{\xi}_P$=0 (blue) indicating diffusion are clearly identifiable. The instantaneous $\overline{\xi}_P$ profile shows that the rich reaction zone is more wrinkled than the diffusion reaction zone as it is directly subjected to the turbulence field at the reactants side, while the diffusion zone is subjected to less turbulence behind the rich zone. This is also observed in the experiments (Fig. 8 in [150]).

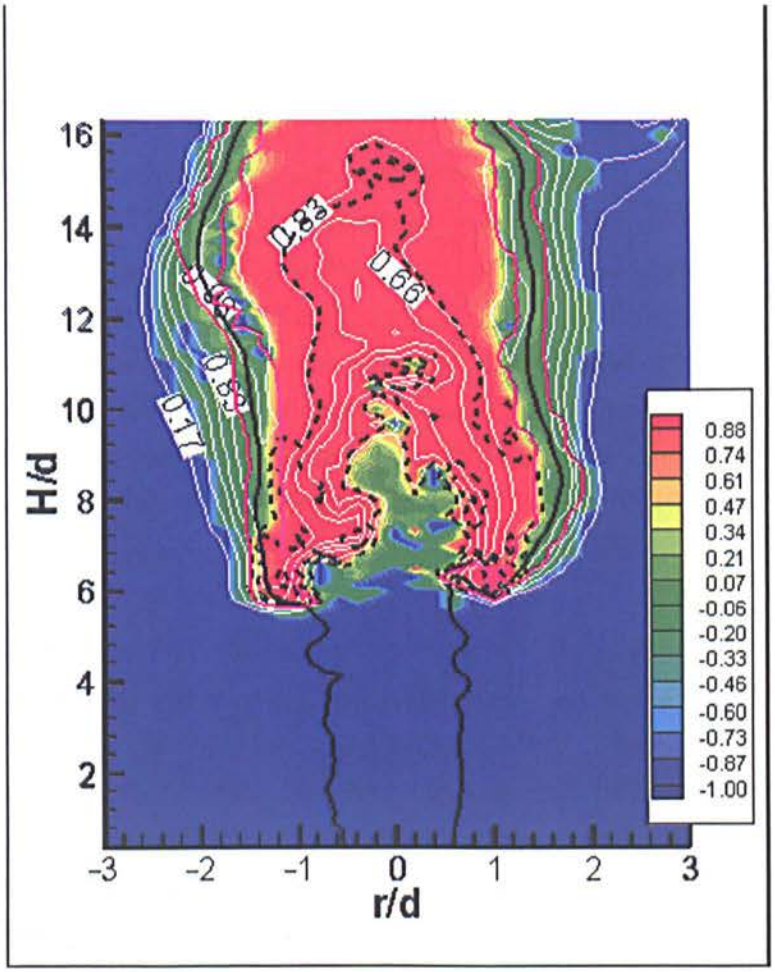

Figure 7.15. Instantaneous flame index, ξ, (contour), iso-stoichiometric mixture fraction, Z, (solid black line), iso-diffusion heat release, Q_D (pink line), progress variable, C, iso-contour (white line) and premixed iso-heat release, Q_P (dash black lines).

In the same graph, the iso-Q_P (dashed black line) is overlapped. It is observed that a rich premixed branch closes the two rich branches in a form of arc further downstream at the core of the lifted flame. In the central core of the jet, C (white line) is driven downstream, because the central jet velocity is too high for this rich mixture to sustain combustion. The front recedes until equilibrium is reached, when the flow

axial velocity is in the same order of the laminar burning velocity. This part of the flame was not studied by Mansour, but the 2D DNS and experimental work of Plessing et al. [200] for a lifted laminar flame revealed a similar structure of the rich branch. Several nozzle diameters downstream, the rich premixed branch is consumed and only the diffusion flame is left. This finding was also made in [25, 200] where Q_D became gradually larger than Q_P, as the position moved downstream into the pure diffusion section. This was echoed by Domingo et al. [69] in their DNS of a weakly turbulent-lifted flame base where the rich flame was found to be consumed and, eventually, only the diffusion trail remains. However, as Mansour's measurements only covered a domain of 5 mm from the flame base and no data is available for a direct comparison on this. In fact, few experimental studies of lifted flames provided information for this region.

Fig. 7.15 also shows iso-Z_{st} (black line) from the nozzle to the leading edge of the flame and right through the iso-Q_D (light pink lines). The iso-Q_D lines lay right to or set off from the triple point and envelopes the iso Z_{st} line. It is worthy to note that the diffusion flame is not consuming pure fuel, but a mixture of fuel and burnt products from the attached rich premixed flame. Therefore, the exact choice of the boundary conditions for the flamelets is a difficult task. More detailed discussion of this can be found in Ferreira [79].

In the same figure, it can be observed that $\bar{\xi}_P$ is almost 0 along the iso-Q_D, indicating diffusion combustion. At the flame front, the trailing diffusion branch and the rich branch merge at one point, which is the possible triple point. However, the lean reaction zone is not shown in the present simulation. In the experimental work of Mansour [150], the lean premixed branch was not clearly captured either, implying that the triple flame structure is, to some extent, contorted by the turbulence from the incoming jet. The predicted stoichiometric line is found to pass through the triple point.

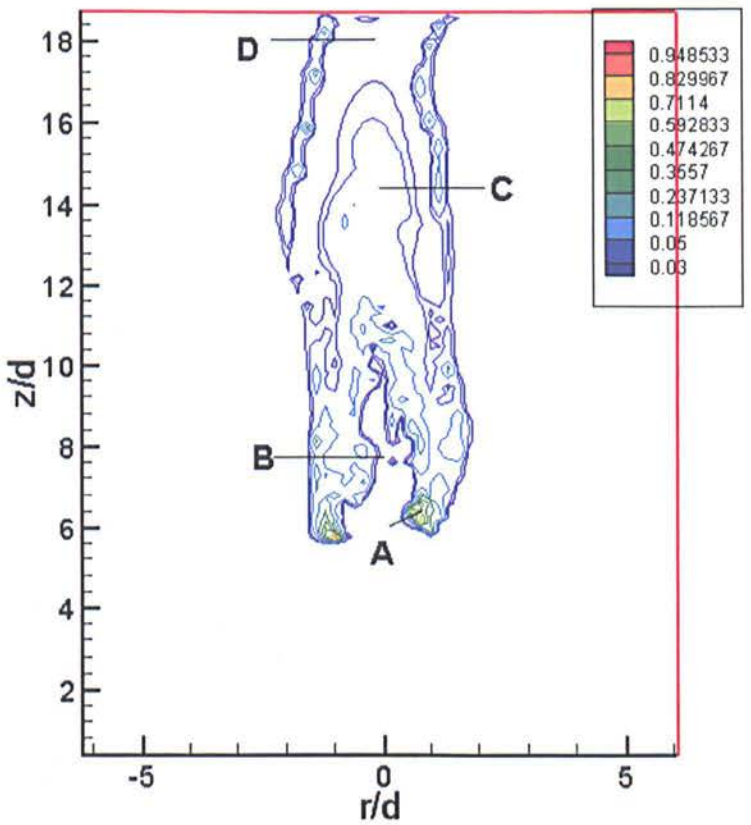

Figure 7.16. Instantaneous total heat release normalized with Q_T^{MAX}.

Fig. 7.16 shows the total heat release (Q_T) normalized by Q_{Tmax} and the three characteristic regions of the partially premixed flame, i.e. the flame front (A), the double flame structure (B and C) and the trailing diffusion branch (D).

Instantaneous values of $\overline{\xi}_P$, fuel and oxygen mass concentrations, diffusion flame heat release (Q_D) and premixed flame heat release (Q_P) are plotted in Fig. 7.17. Fig. 7.17a plots a linear section across the flame front as shown by line A in Fig 7.16. It can be seen that most of the heat release is due to premixed combustion. The progress variable (C) evolves from zero (pure mixing) to one (burnt) and, at the same time, the flame index changes form 0 to 1, indicating premixed regime. Similar results were

obtained by Domingo et al. [67] in his 2D LES study. As expected, the base is found to have the highest heat release rate and the predicted Q_T there consists of 90% Q_P and 10% Q_D. This is consistent with the previous findings of Boulanger et al. [25] and Domingo et al. [69].

Fig. 7.17 (b1) and 7.17(c1) show the predictions for the instantaneous values of $\overline{\xi}_P$, diffusion flame heat release (Q_D), premixed flame heat release (Q_P), and the total heat release, which correspond to lines B and C. Line B is closer to the flame base than line C. The double flame structure is evident in Fig. 7.17b. The maximum Q_D is located at r/d = -1.34, at this point $\overline{\xi}_P$ = 0.21, indicating mainly diffusion with some premixed combustion. Closer to the jet centre -1 < r/d < 0, the regime is purely premixed, as indicated by $\overline{\xi}_P$ = 1.0, hence $Q_T = Q_P$.

Fig. 7.17 (b2) and (c2) plot the fuel and oxidizer profiles at the same locations. It can be seen that the oxygen and fuel are well mixed in the core region, yielding a premixed front. Immediately from the core, their concentrations gradually deplete in the radial direction, as a result of combustion. Towards the outside section of the jet, unburnt fuel diffuses through the premixed zone and is in contact with fresh air, leading to a diffusion flame [69].

Fig. 7.17 (c1) and (c2) show the profiles along line C which is further downstream. At this position the two branches are more distant from each other and $\overline{\xi}_P$ = 0 at r/d = 1.18, where the peak of Q_D is located. At the centre of the jet, there is a premixed regime. The existence of the double reaction zones is evident from the fuel and oxygen mass concentrations. At r/d = 0.8 the product of oxygen and fuel gradients becomes negative and the flame index starts to decrease. This indicates the beginning of a composite section, where premixed and non-premixed regimes coexists until r/d = 1.17, when it becomes purely diffusion region.

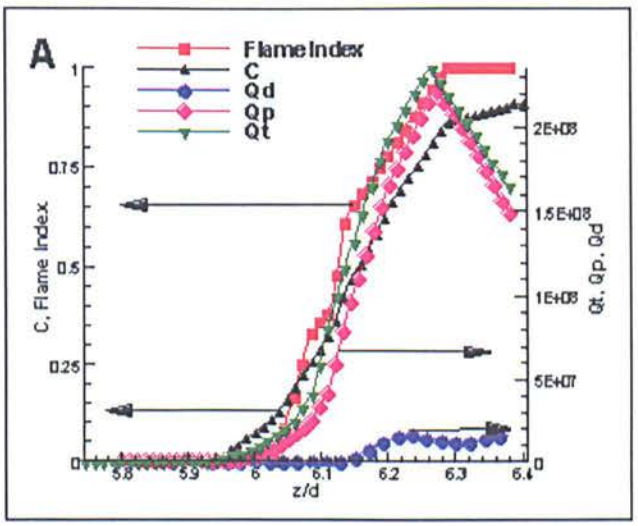
A
Flame Index
C
Qd
Qp
Qt
C, Flame Index
Qt, Qp, Qd
z/d

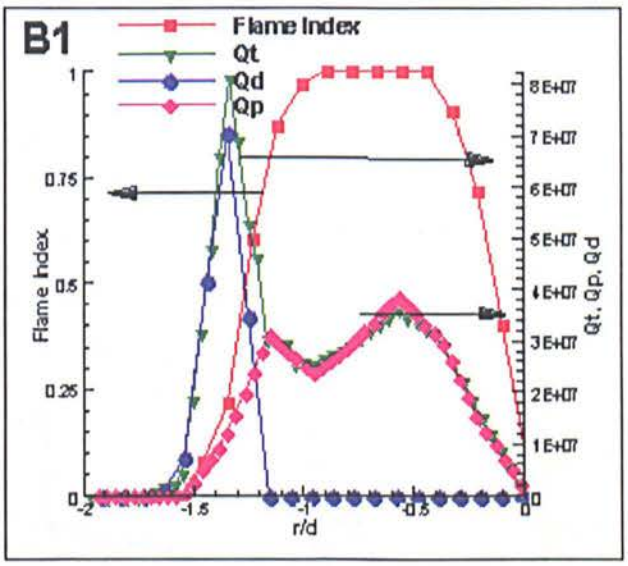
B1
Flame Index
Qt
Qd
Qp
Flame Index
Qt, Qp, Qd
r/d

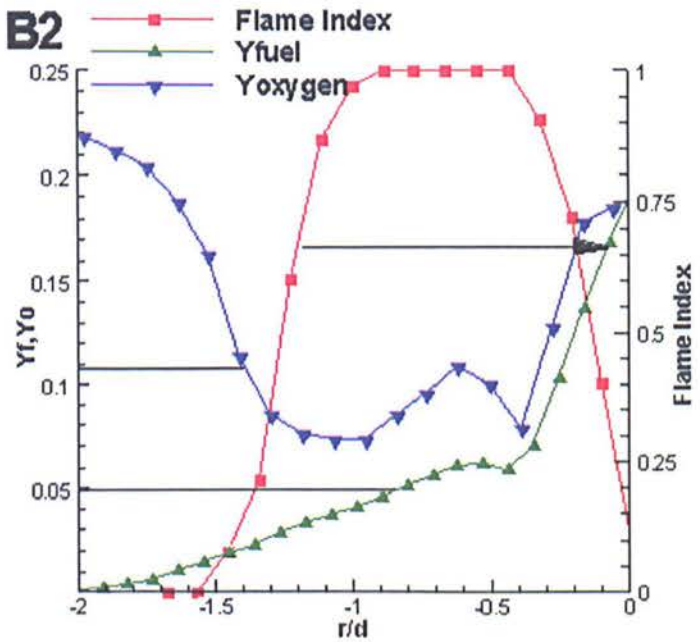
B2
Flame Index
Yfuel
Yoxygen
Yf,Yo
Flame Index
r/d
0.25
0.2
0.15
0.1
0.05
1
0.75
0.5
0.25
0
-2
-1.5
-1
-0.5
0

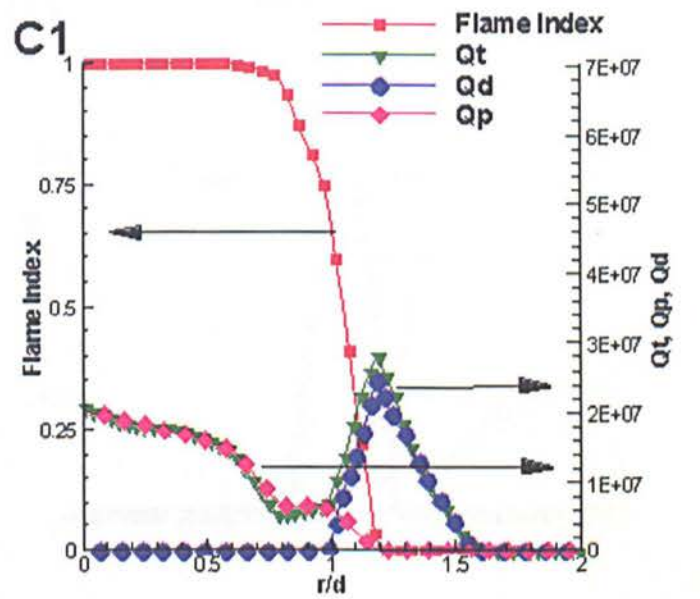
C1
Flame Index
Qt
Qd
Qp
Flame Index
Qt, Qp, Qd
r/d
1
0.75
0.5
0.25
0
7E+07
6E+07
5E+07
4E+07
3E+07
2E+07
1E+07
0
0.5
1
1.5
2

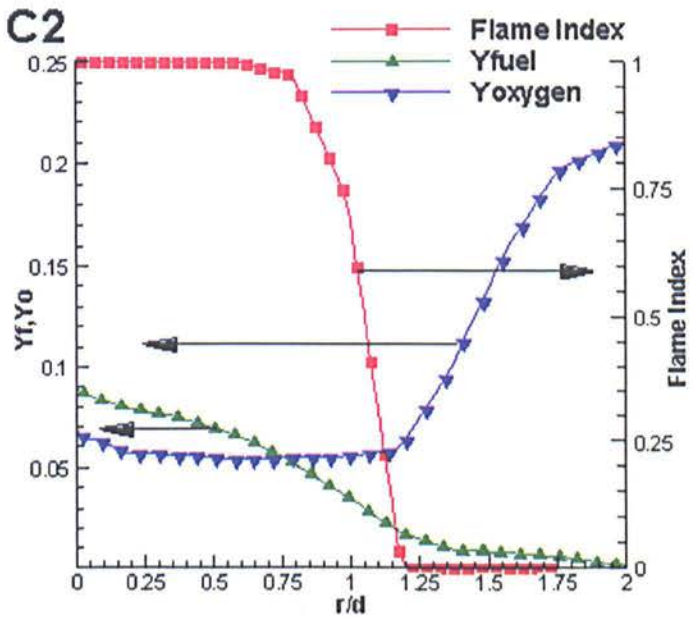
C2
Flame Index
Yfuel
Yoxygen
Yf,Yo
Flame Index
r/d
0.25
0.2
0.15
0.1
0.05
1
0.75
0.5
0.25
0
0
0.25
0.5
0.75
1
1.25
1.5
1.75
2

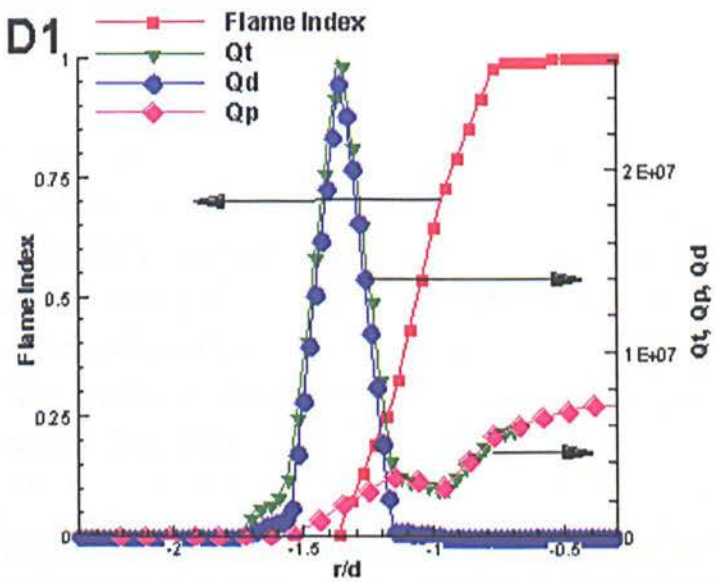
D1
Flame Index
Qt
Qd
Qp
Flame Index
Qt, Qp, Qd
r/d
1
0.75
0.5
0.25
0
2 E+07
1 E+07
0
-2
-1.5
-1
-0.5

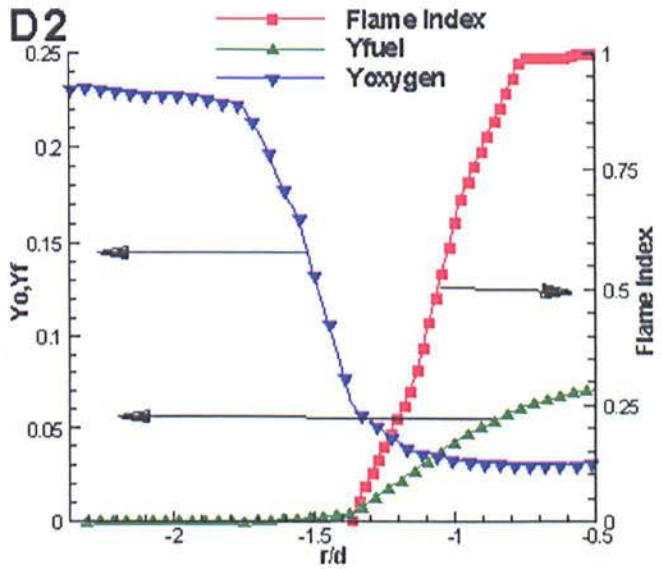

Figure. 7.17. Instantaneous profiles of flame index (ξ), premixed (Q_P), and non-premixed (Q_D), heat release, oxygen (Y_O), and fuel, (Y_F), concentrations at locations A, B, C and D in the flame of Fig. 7.16.

From the above, it is evident that the double flame structure (rich premixed-diffusion), which was previously observed experimentally [150, 232] and in DNS simulations [49, 200] is captured by the flame index approach. The rich premixed flame parallel to the diffusion flame can be seen in most of the upper part of the flame, apart from the immediate vicinity of the flame front, where the flames are contorted due to interaction with the large eddies shed by the jet. In this lower region, the premixed and diffusion flames become overlapped and in most places undistinguishable [174, 248, 251].

Finally, Figs. 7.17(d1) and (d2) show the profiles along line D. In this zone, the premixed regime has been consumed upstream and the flame is predominantly non-premixed. Although there still exists a premixed core of fuel and oxygen at the jet centre, which produces a small premixed region, the remaining premixed flame is expected to diminish completely further downstream.

7.3.7 Dynamics of flame base oscillations

The stabilization of a partially premixed turbulent flame front has been extensively studied experimentally [151, 174, 222] . Muñiz [174] measured liftoff height and velocity field for turbulent, lifted methane and ethylene flames, and obtained two criteria for stabilization. Firstly, the mixture fraction must be within the flammability limits and, secondly, the oncoming velocity must be less than three times the laminar flame speed ($3\,s_l^0$). Recent work of the same group [232] has reinforced this finding. Separate experimental investigations of Schefer [222] found that the flame front is located in the low velocity mixing regions, which are within the flammability limits. He observed that velocities immediately upstream of the stabilization point are typically less than 0.4 m/s. In other words, they are close to the planar premixed laminar burning velocity. In a recent paper, Joedicke et al. [108] stated that at the stabilization region the turbulent flame speed is equal to the local flow velocity perpendicular to the flame front. They added that the flame stabilizes at the position where the triple point anchors the flame, showing a definite triple flame structure in the stabilization region at relatively low velocity, $\sim s_l^0$. All these findings point to a general agreement about the velocities immediately upstream of the flame front.

On the contrary, there are many different views regarding the flame stabilization mechanism. Most of these are, however, consistent with theories based on partially premixed combustion. Following the same rationale, we plot the instantaneous iso-profiles of the velocity at the laminar burning velocity (s_l^0) (green line), the stoichometric mixture fraction (Z_{st}) (blue line) and the maximum premixed heat release for an instant (Q_P^{MAX}) (brown contours) in Figs. 7.18 (a-i). Figs. 7.18 (a-f) show a time sequence of downstream displacement of the right flame front. In an isothermal jet, the iso lines would run parallel and their respective locations would be determined by the inlet conditions of the jet. When combustion begins, the thermal expansion distorts the velocity field pushing the iso-velocity line towards the outer region of the jet, while the iso- Z_{st} stays in the region closer to the jet centre. The flame front is created where the two lines meet. At this point, the iso-Z_{st} line remains closer to the jet core and the iso-velocity line is deflected to the outer section of the jet due to thermal expansion. This basic turbulent flame structure is largely

maintained throughout the time evolution of the flame. Although there are small jumps down and upstream of the flame front (< 0.4d), there is no substantial change in the liftoff height. Such characteristics was also identified by Upatnieks et al. [240], who attributed these changes in lift-off height to velocity fluctuations induced by the large eddies. In the present prediction, the flame stabilization point is found to remain at a *quasi* stable height.

Su et al. [232] have recently studied a turbulent lifted flame of similar characteristics. They concluded that the leading edge point of the flame does not overlap, but correlates with the stabilization point. The later lies more towards the jet centre. Su et al. [232] also found high-temperature regions (leading point) outside and upstream of the reaction zones (stabilization point). In line with this, the present study suggests that the stabilization point is in the region with the maximum premixed heat release (Q_P^{MAX}), and it is most likely located closer to the jet axis, rather than to an upstream location of the flame. We believe that this point is more suitable for analyzing the stabilization mechanism than the leading point, since it drives the flame front upstream through the turbulent flow, creating a low velocity and low turbulence region ahead.

To follow this reasoning, we identified instantaneous moments when the flame front advances upstream around 0.7d. The upstream displacement is not regular, but it contains a series of small 'jumps', characteristic of the predicted flame profile. Eddies are shed from the jet exit towards the flame base. These eddies provoke re-circulating regions at the flame front, which, if strong enough, can distort the structure and expose the iso-Z_{st} line into a low velocity zone. This can be seen in Fig. 7.18a, where the iso-Z_{st} (blue line) is located in the lower velocity region in comparison to the iso-velocity line, enabling the flame front to evolve upstream through a flammable low normal-speed region (Fig. 7.18b). When the flame front is carried upstream, the stoichometric line moves towards the centre, therefore the stabilization point is diverted to the central axis of the jet, as shown in Fig. 7.18c. The stabilization point is exposed to high velocities coming from the jet centre, as shown in Figs. 7.18e and 7.18g. It is observed that, when the stabilization point is located in the very inner

section of the jet, Q_P^{MAX} tends to be stretched downstream with its normal vector pointing to the inner jet, leading to the characteristic radial-inwardly shaped flame tip. This stretching effect might be attributed to the interaction between the turbulent eddies and the reaction zone. Typically at this stage, the stabilization point is located both closer to the nozzle central axis and in a more downstream position than the leading point (Figs. 7.18c, e and g). When the stabilization point is exposed to high velocity, the front can either evolve radially outwards (Fig. 7.18d), or downstream and radially outwards to a lower velocity region. At this stage, a new *quasi*-equilibrium is established and the flame jumps are usually reduced up to 0.4d, oscillating between the flammable region and the high velocity flow in the inner central jet. This typical flame structure is shown in Figs. 7.18h and i. In general, the iso- Z_{st} line is located in the higher velocity region, i.e. on the left of the iso-velocity line at s_l^0. The initial position of the flame base is not immediately/periodically recovered, as suggested by Su et al. [232] , who proposed an explanation of flame stabilization in terms of the large-scale the jet mixing. Following Yoda et al. [269], Su stated that a pair of counter rotating helices, which appear axisymmetric, and helical modes in different planar sections through the jet axis, are responsible for the periodical oscillations of the flame base.

This behaviour of the flame front seems to follow the stabilization concept called "edge flame", where the flame creates its own local low-velocity, low turbulence-level region due to streamline divergence caused by heat release.

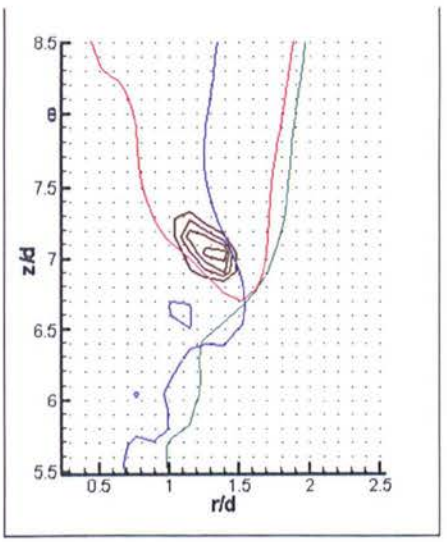
8.5
8
7.5
7
6.5
6
5.5
z/d
0.5
1
1.5
2
2.5
r/d

(a)

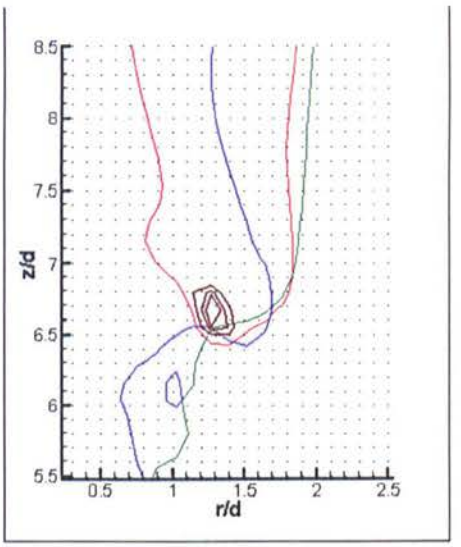
8.5
8
7.5
7
6.5
6
5.5
z/d
0.5
1
1.5
2
2.5
r/d

(b)

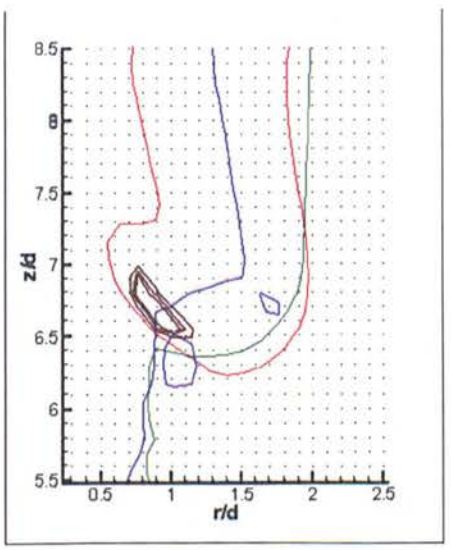
8.5
8
7.5
7
6.5
6
5.5
z/d
0.5
1
1.5
2
2.5
r/d

(c)

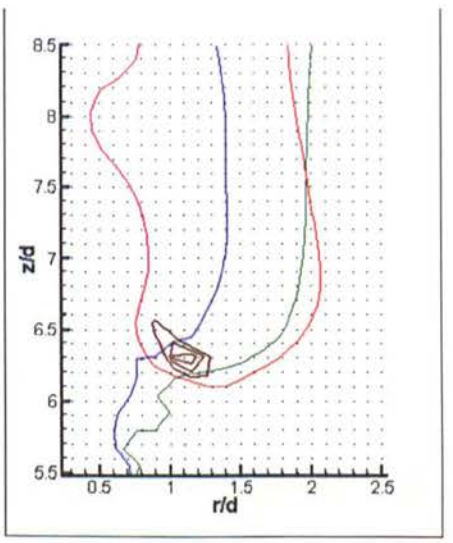
8.5
8
7.5
7
6.5
6
5.5
z/d
0.5
1
1.5
2
2.5
r/d

(d)

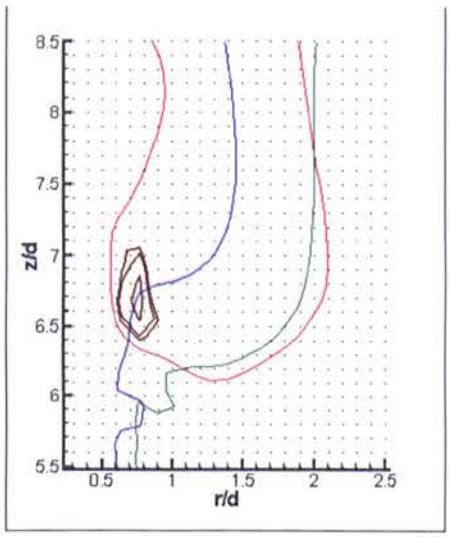
8.5
8
7.5
7
6.5
6
5.5
z/d
0.5
1
1.5
2
2.5
r/d

(e)

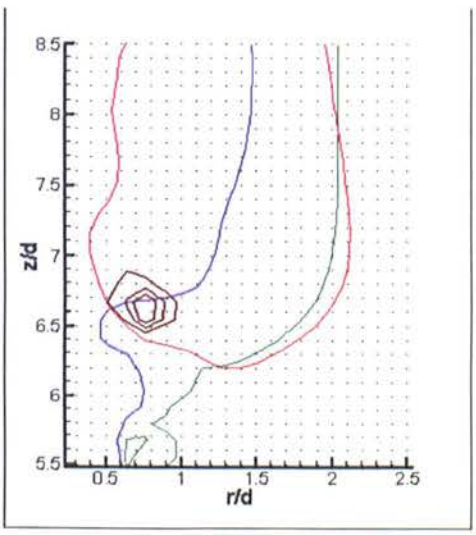
8.5
8
7.5
7
6.5
6
5.5
z/d
0.5
1
1.5
2
2.5
r/d

(f)

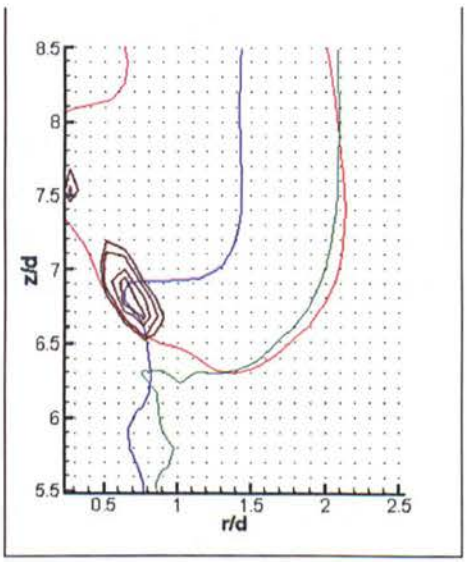
8.5
8
7.5
7
6.5
6
5.5
z/d
0.5
1
1.5
2
2.5
r/d

(g)

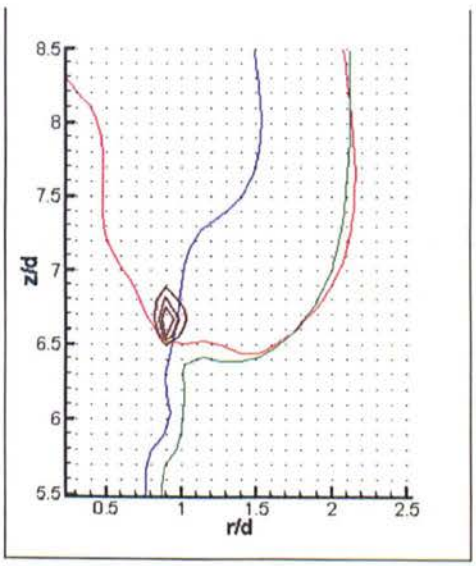
8.5
8
7.5
7
6.5
6
5.5
z/d
0.5
1
1.5
2
2.5
r/d

(h)

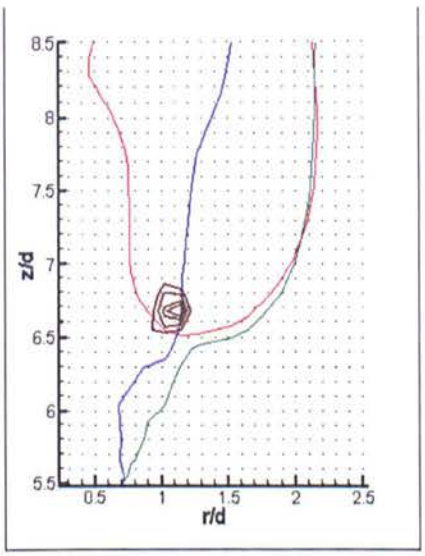

(i)

Figure 7.18. Instantaneous evolution of the flame leading point and the stabilization point. Red line: C=0.6, blue line: stoichiometric mixture fraction value and green line: iso-profiles of the velocity at the laminar burning velocity (s_l^0), and brown contours: maximum premixed heat release, Qp^{MAX}. The time interval is Δ_t = 3 msec

7.4 Summary and conclusions

The following conclusions may be drawn from the present LES simulations:

- The models have predicted reasonably well the mean structures of the lifted flame, triple flame and planar propagating front. In particular, the predictions of lift-off height, mixture fraction profiles and flame structure are all in good agreement with the data.

- The predicted structure of the lifted flame base was in line with previous experimental findings and some limited DNS analysis. At the stabilization point, most of the total heat release was found to be due to premixed combustion and the predicted inner structure of the flame front, especially at the rich core, was found to be in good accordance with the measurements of Mansour [150]. The model has also captured the double flames (rich premixed and diffusion flames) meeting at the so-called 'triple point', and propagating almost in parallel further up from the base.

- The results for the lifted flame have led us to propose a definition for the stabilization point as the location with the maximum premixed heat release (Q_P^{MAX}). This definition is in line with the observation of Su et al. [232] , who found that this point is located closer to the jet centre than the leading edge of the flame front. Although there are small jumps down and upstream of the flame front (< 0.4d), there is no substantial change in the predicted lift-off height and the flame stabilization point is found to remain at a *quasi* stable height. Such characteristics was also identified by Upatnieks et al. [240], who attributed these changes in lift-off height to velocity fluctuations induced by the large eddies.

- The stabilization was found to be due to equilibrium of local conditions at the flame front. The large fluctuations of the flame front, approximately one diameter in amplitude, are thought to be induced by its interaction with the large eddies in the jet. The front of the flame is exposed to low-velocity-

flammable region and, consequently, it propagates upstream until the combustion can not be sustained due to high velocity and lean fuel concentration below the flammability limit. At this point, the flame shifts inward in search of the stoichiometric mixture and, subsequently, small 'jumps' (< 0.4d) downstream and upstream are observed in the new position. This pattern was also noted in the experimental work of Upatnieks et al. [240]. The periodic cycles of flame displacement proposed by Su et al. [232] are not found here, neither was it identified in the experimental work of Upatnieks et al. [240].

The lifted flame simulation has also provided insight for the downstream region which was not covered in the experimental measurements. It reveals structure patterns such as size (length and width) of the rich premixed branch at the jet centre, and width of the burnt gases and scalar fields several diameters downstream from the flame base.

However, the present work also has some limitations. First of all, it should be pointed that the flame index approach adopted here will not be able to capture the physics in the transition zone, where, even through the oxygen and fuel gradient have the same direction, the combustion is diffusion controlled [80]. This would broaden the diffusion region further and narrow the premixed flame. Secondly, in order to eliminate any uncertainty associated with the modelling of the wrinkling factor at sub-grid level this was kept low by using relatively small grid size at the flame base. More work is desirable to investigate the sensitivity of the model to wrinkling factor. Particularly, it would be useful to test the performance of different flame wrinkling factor models. Its coupling with the surface density function, when the mesh size is in the order of the unstrained flame thickness and in situations with stronger turbulence is equally important. Similarly, further studies are also needed to address issues regarding the filter size (Δ_C) and the error this might introduce by using different filter sizes for the basic equations in the LES approach.

Chapter 8

LES of the Backdraft Phenomenon

In the present chapter, the sub-grid scale model for partially premixed combustion introduced in chapter 6 is applied to simulate the backdraft phenomenon. A fast deflagration or backdraft is produced when into a hot, fuel-rich compartment an inflow of fresh air is suddenly allowed through an opening. It is essentially a violent combustion process involving both premixed and non-premixed regimes. Due to the lack of detailed experimental measurements, the results are largely analyzed qualitatively.

The predictions have provided valuable insight into the backdraft phenomenon suggesting that the development of backdraft can be divided into five phases, i.e. initial condition, free "spherical propagation, "plane" front propagation, stretching of the flame front through the opening and fireball outside the container.

8.1 Backdraft background

A backdraft can develop from fires of either ordinary combustibles or ignitable liquids that after burning for a period of time in an enclosure become oxygen starved but yet continue to generate a fuel-rich environment. In the case of poor ventilation, the fire does not normally die out but becomes ventilation-controlled [242] and its behaviour dependents on the geometry of the opening. In the case that an opening allows fresh air to come in, a fast deflagration known as backdraft can happen. Ignition can be triggered once the flammable mixture comes into contact with an ignition source along its path.

Following ignition, the temperature will increase creating an expansion of the hot gases raising the pressure at the back of the enclosure. This will produce an outgoing flow through the door containing hot gases in the upper part of the opening and cold gases in the lower part. The flame soon develops and it will propagate through the unburnt region towards the opening. This process of deflagration is called backdraft. It is essentially a violent combustion process involving both premixed and non-premixed regimes.

The critical condition for the occurrence of backdraft is, therefore, of considerable importance in fire safety. As such, this phenomenon has been the subject of several experimental investigations. Fleischmann [81] conducted backdraft experiments in a half scale domestic room and supplemented these with small scale salt-water tests. Similar experiments have also been conducted by other groups [33, 81, 94, 95, 161, 253-256].

Yang et al. [266] attempted to use CFD approach to simulate the experiments of Weng [253, 254], but the combustion model used was not really suitable for such a system where premixed and non-premixed combustion regimes might co-exist.

In a closely related area, the mitigation of backdraft have been studied by Weng and Fan [254] and Gottuk et al. [95]. They found that water mist is an effective mitigating

tactic and it suppresses backdraft primarily by means of reducing the unburnt fuel mass fraction rather than by thermal cooling.

Both non-premixed or premixed flames have been the subjects of extensive theoretical and experimental investigations resulting in numerical models of varying complexity. A thorough review of these models can be found in Veynante and Vervisch [247]. Nevertheless, hazardous phenomena like ghosting flames and backdraft are neither perfectly non-premixed nor premixed. They can indeed be classified as partially premixed combustion. For example, studies of lifted flames (see previous chapter) have revealed the existence of lean and rich premixed regimes at the bottom of the flame called triple flame followed by a diffusion flame downstream [25, 121, 122, 136, 150, 174]. The coupling of non-premixed and premixed combustion models is essential for better understanding of such mixed combustion processes [67, 68]

In the present chapter two separate simulations are carried out. Firstly, the experimental set up of Gojkovic [94] is used and secondly the configuration of Weng and Fan [254]. Unfortunately, for the first experiment, little quantitative data is available for the actual fast deflagration process. Most of the data is either of qualitative value or measurements of temperature, pressure and species mass concentrations at few unclassified positions rendering them difficult for comparison with numerical predictions. As such, our analysis, for the Gojkovic's experiment will mainly focus on the characteristics and development, mainly qualitative, of the backdraft. On the other hand, the experiment carried out by Weng and Fan is more extensively studied. In their experiment, mean mass concentrations, layer temperatures and pressures before and during the deflagration are available for different opening geometries. Moreover, Weng and Fan introduced water vapour to the vitiated environment in order to investigate the mitigating effects of water mist.

8.2 Gojkovic's experiment

In this section, the experimental set up of Gojkovic [94] is considered. The test compartment is built from a standard shipping container, measuring 5.5m (L) × 2.2m (W) × 2.2m (H). The opening covers the total width of the side and has a third of the total side height. A 1 m electric wire located vertically at half height of the back wall of the enclosure is used as ignition source. The wire is heated up in order to produce the ignition due to high temperature. Initially, fuel is pumped into the container and after a given period of time the hatch is opened to let the gravity current to set in.

8.2.1 Simulation details

Gojkovic [94] measured temperature, gas concentration and pressure at different positions inside the container. Most of the data presented was either before the actual deflagration occurred or qualitative. This limited the amount of quantitative comparison with the experimental data.

In the numerical simulation a domain of 10m (L) × 4m (W) × 4m (H) with three uniform meshes (mesh 1, mesh 2 and mesh 3) with a cell size of (0.1 x 0.05 x 0.05) m, (0.04 x 0.04 x 0.04) m and (0.03 x 0.03 x 0.03) m; respectively.

Inside the enclosure, the initial velocity was set to 0 m/sec and the initial temperature to 90.0 ^{0}C. The initial mass concentrations inside the container before the establishment of the gravity current is considered as Y_{CH4}= 0.5, Y_{AIR}= 0.25 and Y_P= 0.25. These are approximations from the experiment since the data for the initial condition are very scarce.

Outside the enclosure still air and temperature at 5° C is assumed. Non-slip and adiabatic conditions are imposed at the walls. On the external domain surfaces a free shear condition (open) is used.

In the present simulation, the Smagoringsky constant value is 0.15., $q_r = 0$ is assumed during the process of deflagration and $\mathrm{Pr}_t = 0.7$ and $Sc_t = 0.6$

The value of Δ_C will depend on with which resolution the flame front will be solved. In cases where the mesh is fine enough Δ_C should be adjusted accordingly, i.e. $\Delta_C = 5\Delta$ will resolve the flame front with ten grid points. In the present calculation $\Delta_C = 3\Delta$ is considered due to the extension of the domain, the ratio $\Delta / \delta_l^0 \approx 200$.

For the wrinkling factor model, Eq. 6.39, $\alpha = 4.5$ in order to counterbalance the relatively coarse mesh and Δ_e is considered, as first approach, equal to Δ. The sub-grid velocity fluctuation u'_{Δ} .is obtained using the sub-grid turbulent viscosity provided by SGS. [67].

8.2.2 Results

Ignition time

Only very scattered data of the ignition time against methane concentration is available in the experimental report. This is mainly due to the lack of accuracy of the initial fuel concentration measurements before the hatch of the container is open. However, the author is aware that FDS has previously undergone validations for gravity currents predictions against salt water experiments in the context of the backdraft phenomena [163]. Therefore, we rely on the accuracy of the simulation for the gravity current phase.

The predicted time elapsed from the hatch opening until the ignition was about 18s for the three meshes. In the experiments, the ignition delay times were measured for a range of initial fuel concentrations. While it is impossible to make an exact comparison with the available experimental data, the predicted ignition time was in line with the measured values.

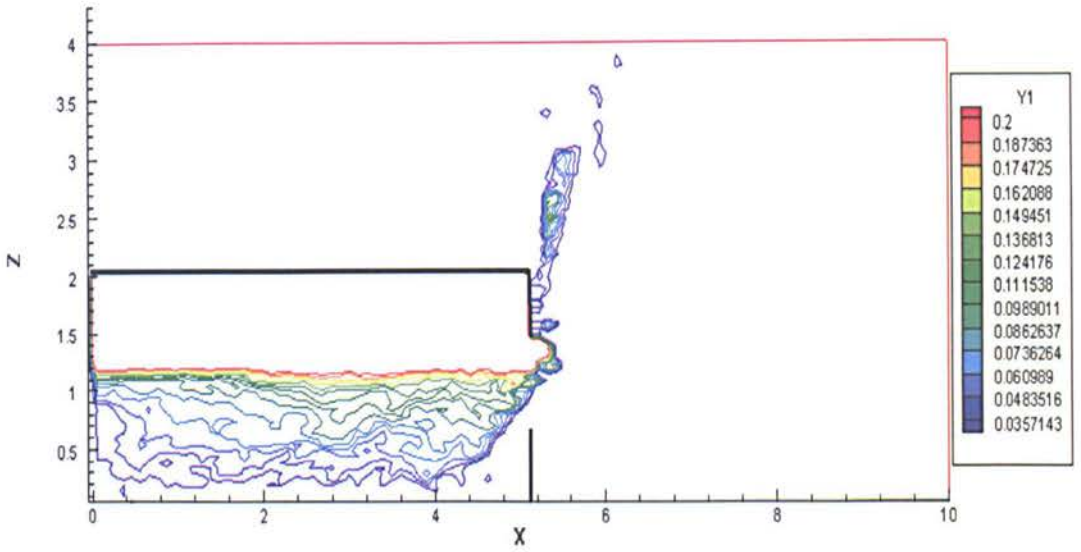

Figure 8.1. Mixture fraction for the initial conditions at ignition.

The five phases in the development of a backdraft

Detailed analysis of the results have led us to divide the development of a backdraft into five phases beginning with the onset of the ignition and finishing with the fireball outside the compartment. The five phases include: 1) Initial condition at ignition, 2) Free "Spherical" propagation, 3) "Plane" front propagation, 4) Stretching of the flame front through the opening and 5) Fireball outside the container.

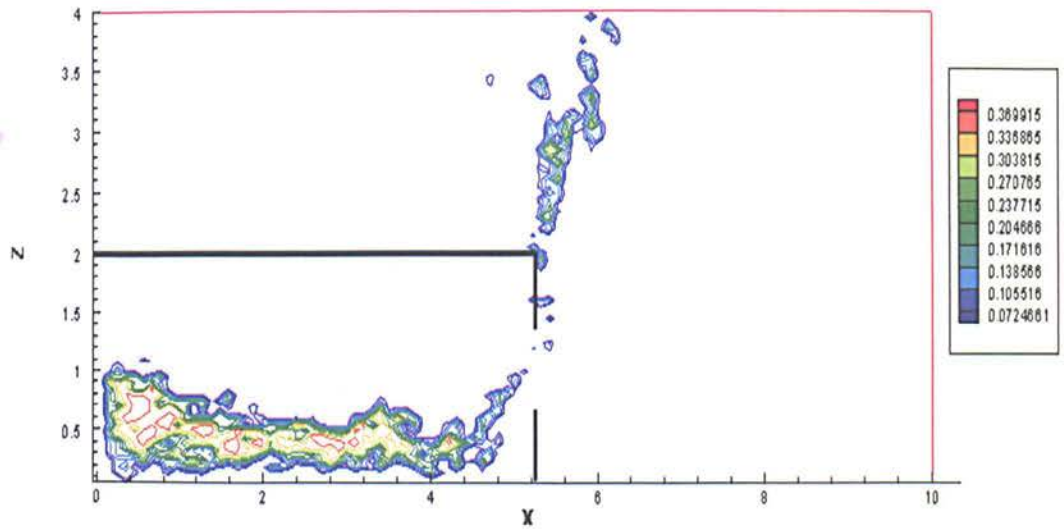

(a). Initial conditions at ignition.

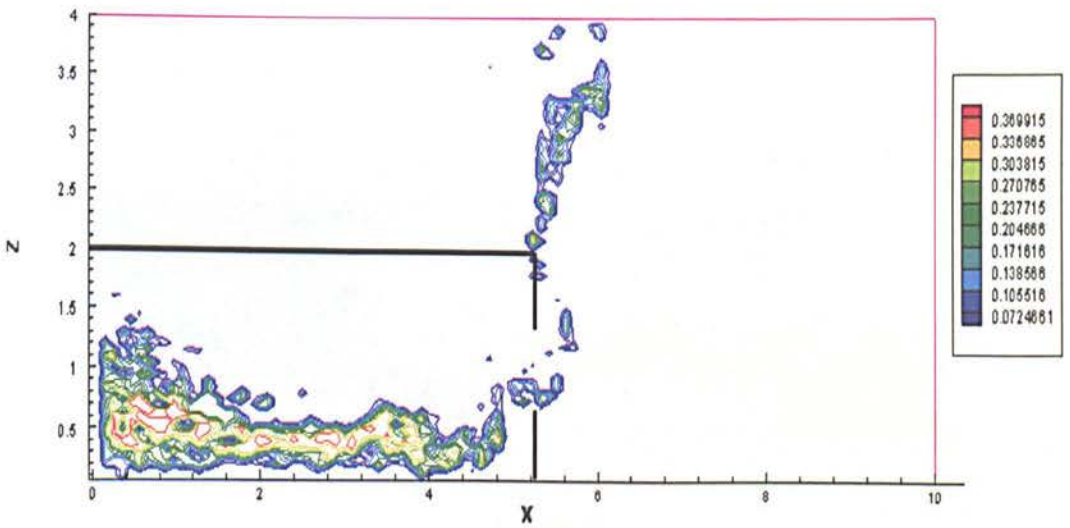

(b) Phase 1.

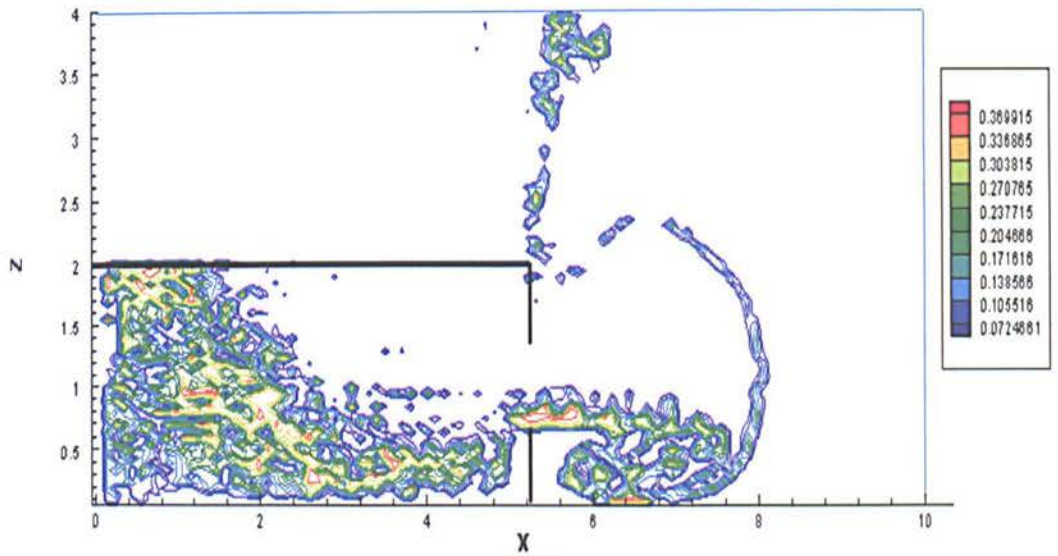

(c) Phase 2.

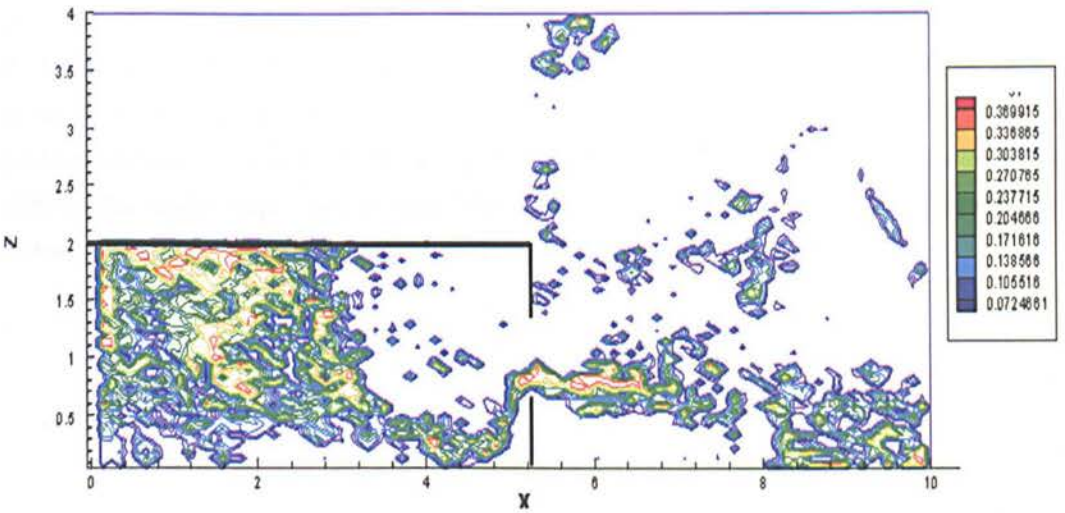

(d) Phase 3.

Figure 8.2. Laminar flame propagation velocity.

Initial Condition at ignition

We call 'initial condition at ignition' the state when the gravity current reaches the ignition source position just before the ignition occurrs. At this instance, the progress variable throughout the container is zero. The stoichiometric flammable mixture (Z_{st} = 0.054) is spread along a surface at approximately 0.5 m from the floor and it reaches half height of the back wall as shown in Fig. 8.1.

The initial pattern of this surface is of key importance for the front spreading during the backdraft because it will determine the main 'path' of the flame towards the opening through the term $\widetilde{S}_L$ in Eq. 6.10. As shown in Fig.. 8.2(a), $\widetilde{S}_L$ is the laminar burning speed (0.38 m /s) at the stoichiometric value.

The initial condition suggests that the premixed flame front would propagate downwards following the maximum laminar burning speed.

Figs. 8.3 (a) and 8.4 (a) show the initial oxygen and methane concentrations. In the upper layer of Fig. 8.3(a) the oxygen concentration is close to the initial value of 2% in mass, while the oxygen concentration is around 20% in mass is roughly found in the bottom layer. It can be seen in Fig. 8.4(a) that the methane concentration is about 50% in the upper layer and around 4% at the ignition source location. The later is within the flammability limit (2.8-8.0%) for methane-oxygen system.

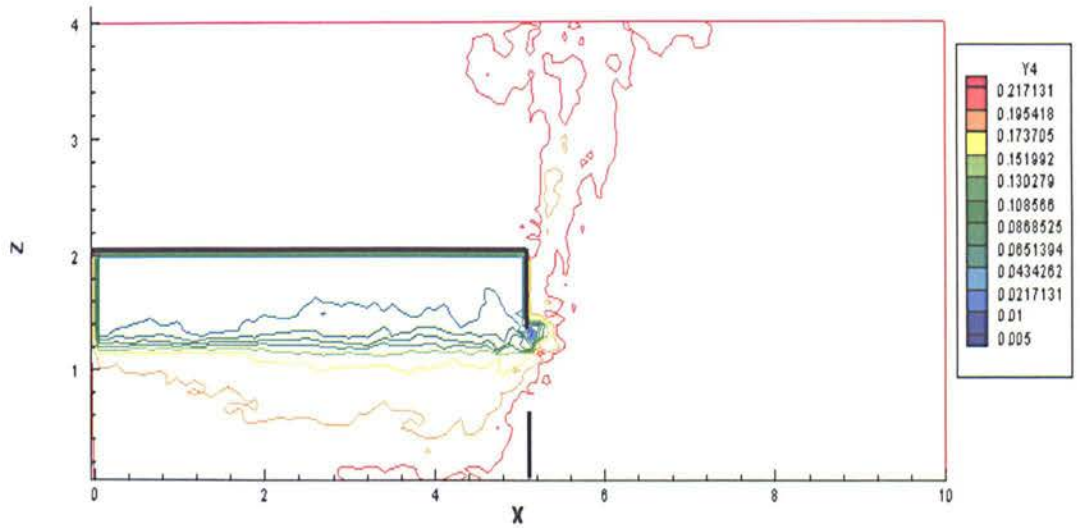

(a) Initial conditions.

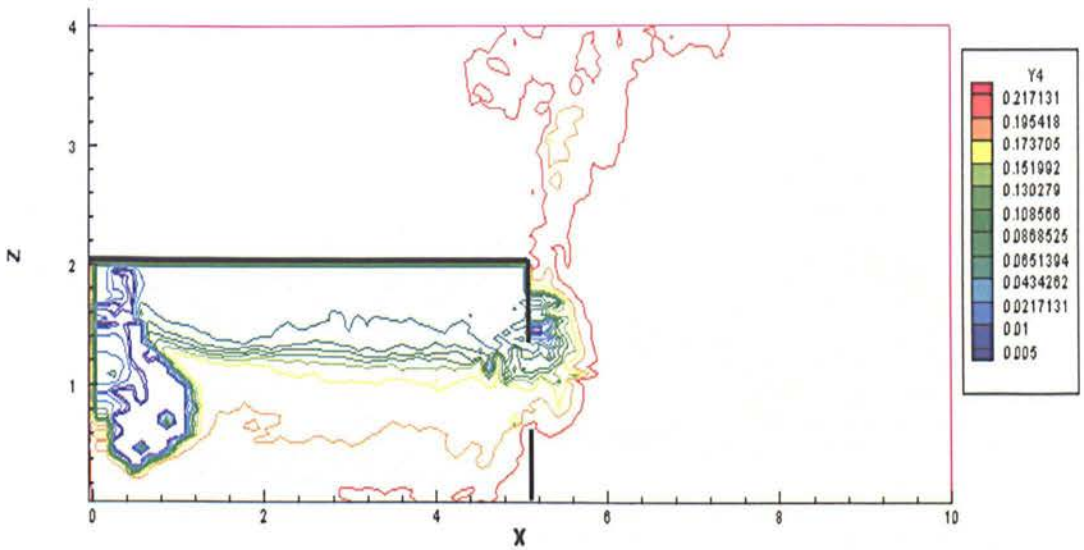

(b) Phase 1.

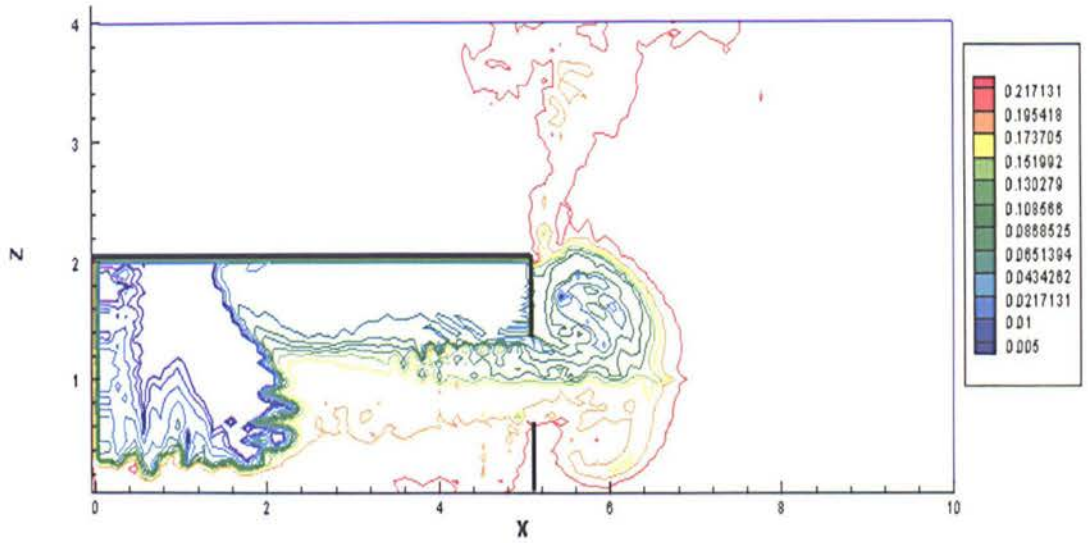

(c) Phase 2.

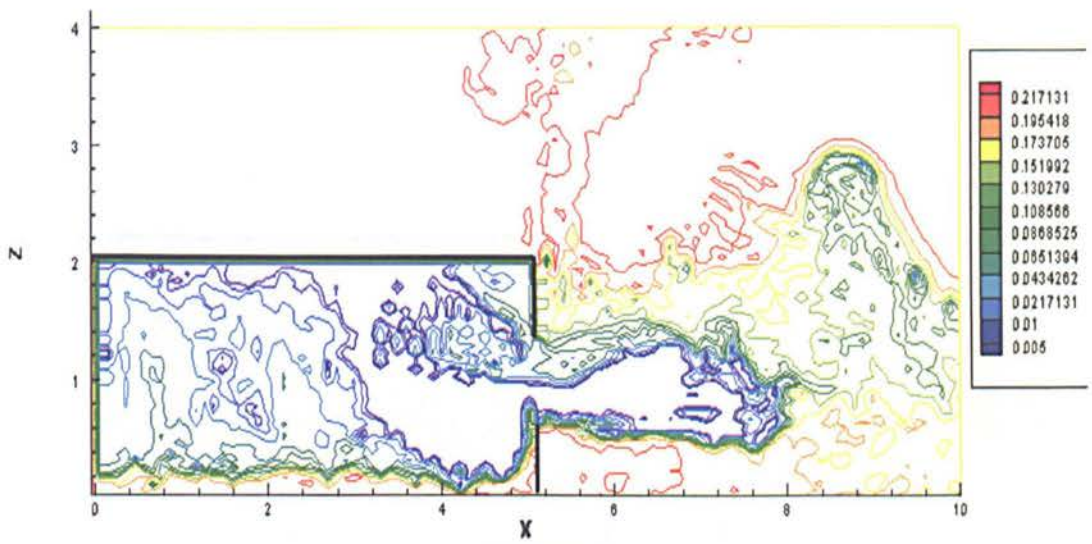

(d) Phase 3

Figure 8.3. Oxygen mass concentration.

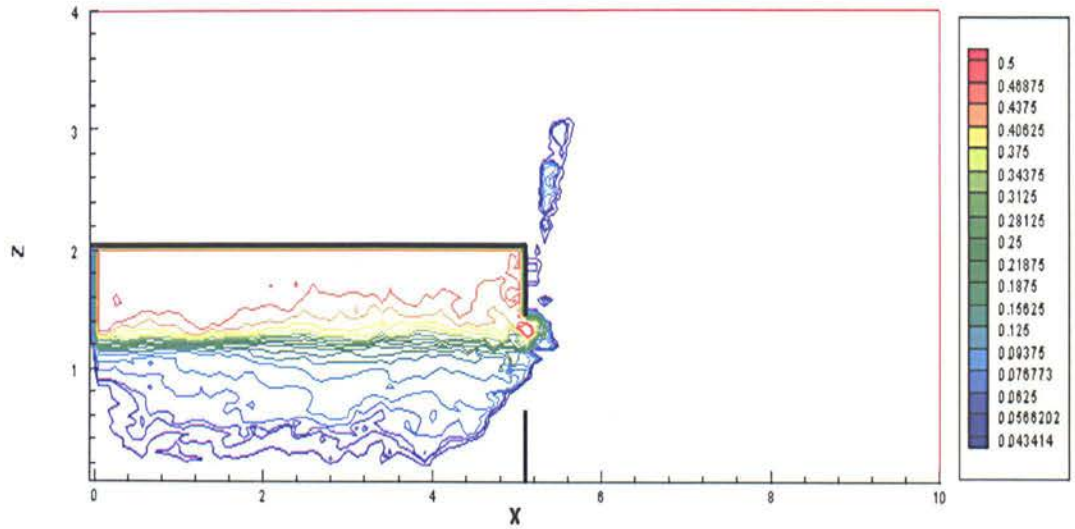

(a). Initial conditions at ignition.

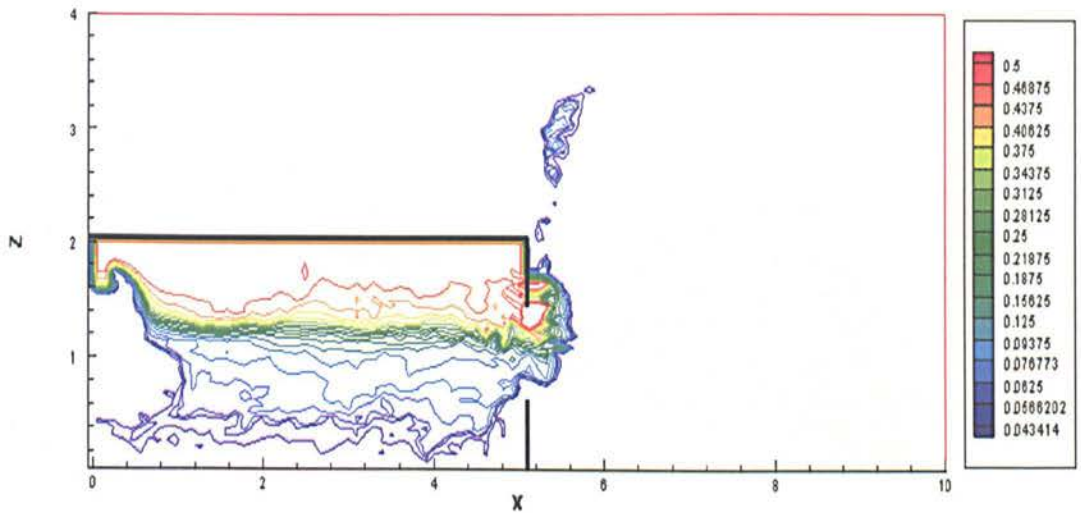

(b). Phase 1.

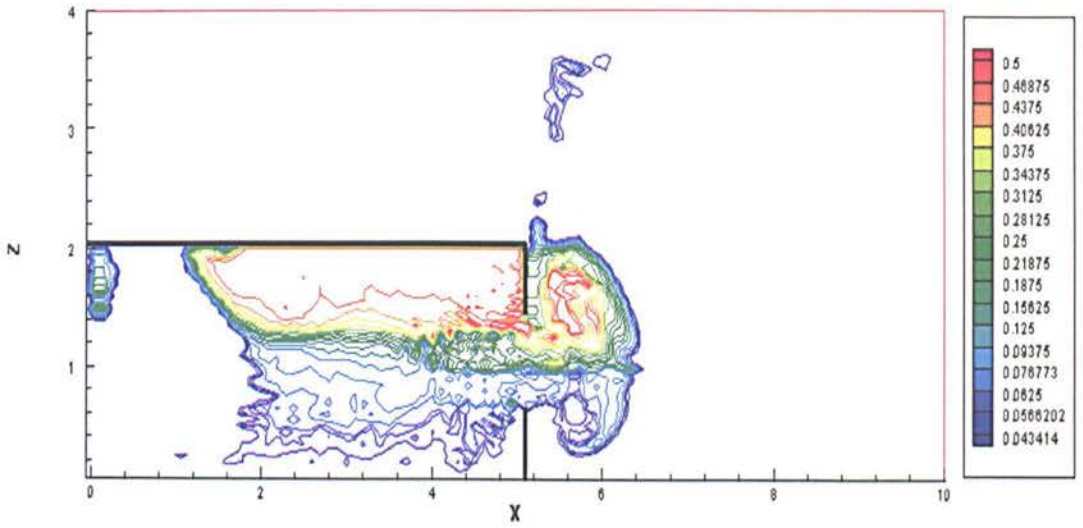

(c). Phase 2.

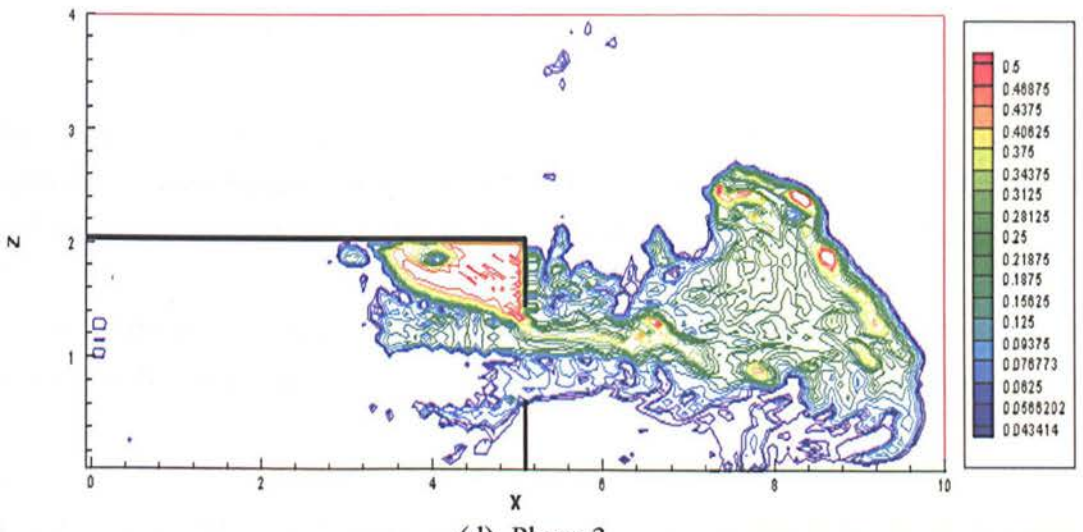

(d). Phase 3.

Figure 8.4. Methane mass concentration.

Free "Spherical" Propagation

When the stoichiometric mixture reaches the ignition source, a numerical spark is inserted in the calculation. $\widetilde{C}$ = 1.0 and a turbulence fulfilling $u_{\Delta}^{'}/s_{l}^{0}$= 1 are set to reproduce the combustion initial conditions at half height along the back wall of the container. These initial conditions are maintained for 3 msec after ignition

The phase of free "Spherical" propagation begins shortly after the ignition until the progress variable ($\widetilde{C}$) develops into a slopped plane front travelling towards the opening. This phase is characterized by the spherical shape evolution of the flame centred around the ignition point and spreads radially towards the walls of the container.

The driving forces which spread the reaction progress variable ($\widetilde{C}$) are:

a.) The thermal convection of the gases.
b.) The progress variable source term.

The thermal convection drives $\widetilde{C}$ upwards, while the progress variable source term spreads C downwards along the stoichometric line. Fig. 8.2 (b) shows the stoichiometric mixture close to the floor with the maximum laminar burning speed.

Fig. 8.7 (a) illustrates this clearly, the reaction progress variable source term ($\widetilde{Q}_{C}$) forms a front advancing towards the floor and is zero right at the top of the spreading region.

Fig. 8.9 (a) depicts $\widetilde{C}$ spreading uniformly around the ignition point driven upwards by the thermal convection and downwards by its source term . In Fig. 8.9, it is also visible the same front facing downwards as in Fig. 8.7.

In this phase, a premixed front is established travelling downwards, this can be verified by the flame index ($\widetilde{\xi}$) profile given in Fig. 8.8 (a). Fig. 8.8 shows a

premixed semicircular front ($\overline{\xi} \approx 1$) at the flame border expanding radially. Ahead the flame and closer to the opening a diffusion flame configuration ($\overline{\xi} \approx 0$) can be seen, this corresponded to $\nabla Y_F \nabla Y_O = -1$, indicating non-premixed combustion. However, the mixture does not ignite because of the low temperature.

An important feature of the backdraft process is that the flame spreads through a mixture, which is being constantly modified by the upstream flame front. From this point of view there exists a significant difference between a backdraft and a lifted jet flame, where the near field (the flow closest to the nozzle) is unaffected by the premixed flame front. This raises particular issues that are of concern only to the backdraft phenomena.

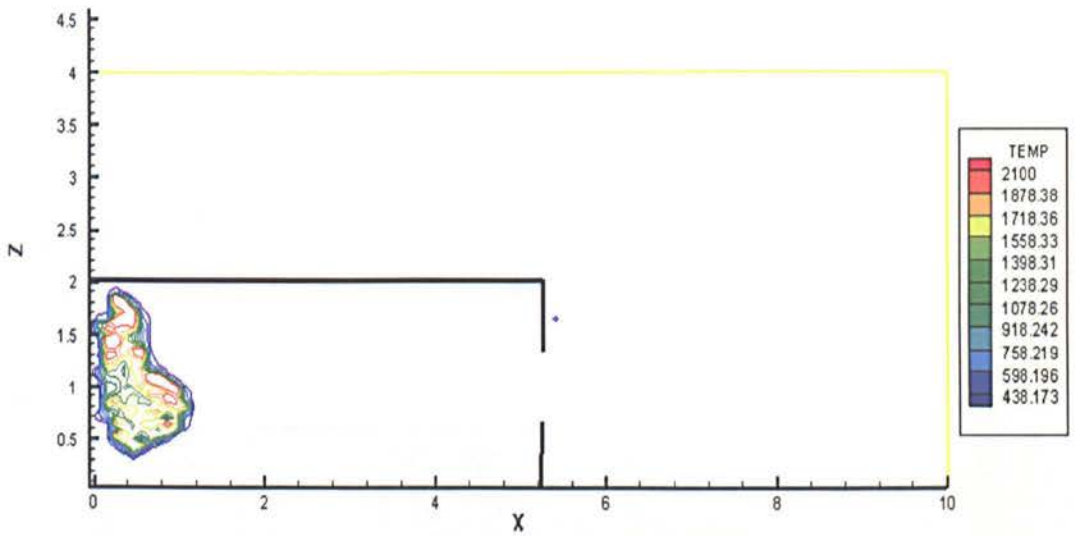

(a). Phase 1.

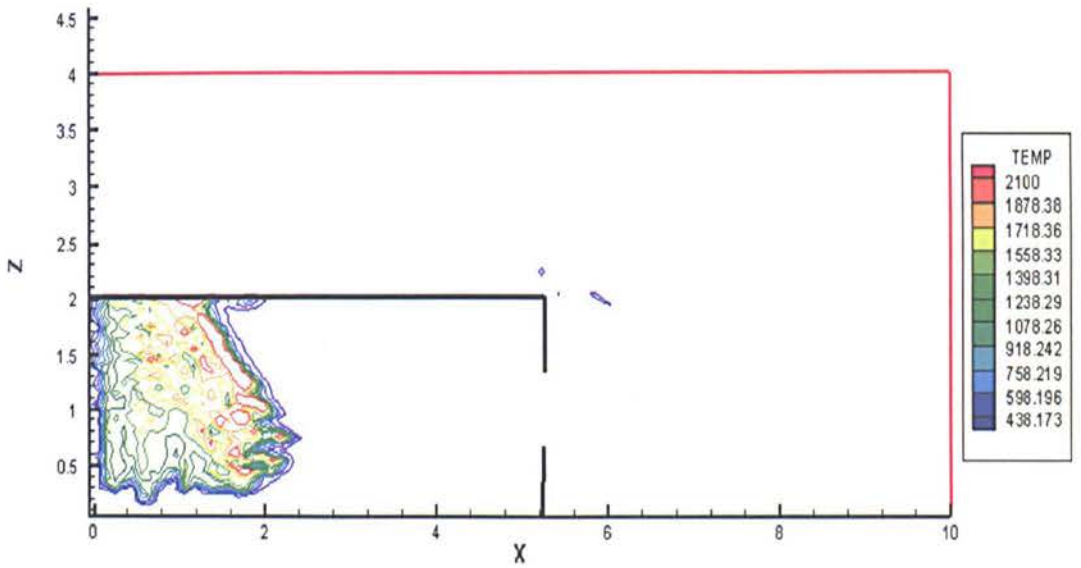

(b). Phase 2.

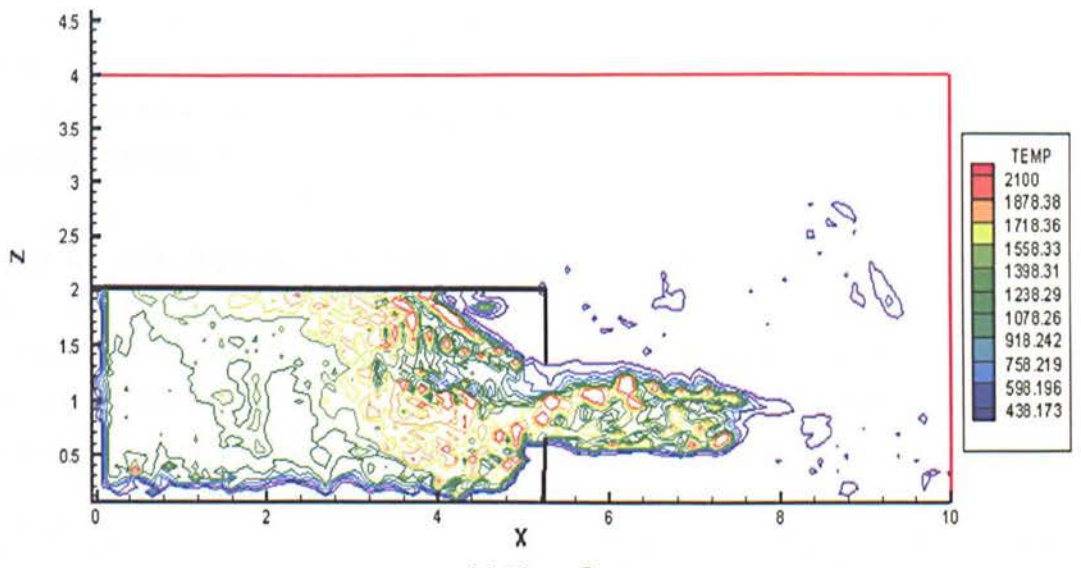

(c) Phase 3.

Figure 8.5. Temperature profile.

Following ignition, the thermal expansion of gases increases the pressure at the back of the enclosure. This produces a force, which drives the fuel, oxygen and products towards the opening and out of the container as seen in Figs. 8.4(b) and 8.3 (b). In the upper layer the gases are pushed in the direction of the opening by buoyancy force, and in the bottom layer, where the combustion is taking place, they are consumed. It can be observed in Fig. 8.3 (b) that the turbulence developed in the upper layer close to the wall modifies the stoichometric surface producing spots with maximum flame speed as shown in Fig. 8.2 (b). The locations of these spots match the maximums in the $\widetilde{Q}_C$ profile plotted in Fig. 8.7 (a).

Fig. 8.5 (a) shows the temperature profile. It is seen that the buoyancy force drives $\widetilde{C}$ upwards. As shown in Fig. 8.9 (a), $\widetilde{C}$ propagates faster upwards than laterally towards the opening in the first stage of the deflagration. In time, $\widetilde{C}$ reaches the top and starts spreading towards the opening.

The flame wrinkling factor (Ξ) can be seen in Fig. 8.6 (a). The turbulence at the flame front is larger than at the upper layer. At the premixed flame front, Ξ is about 1.3 and increased to 1.6 at the upper layer because of the more intense thermal instabilities there.

After the free propagation, $\widetilde{C}$ continues to evolve in both directions, i.e. upwards to the top and laterally towards the opening at the maximum burning speed $\widetilde{S}_L$. Then, $\widetilde{C}$ turns towards the exit and a premixed front travels parallel to the floor at the bottom of the enclosure. In this way, a 'plane' front is formed encompassing the whole cross section of the container.

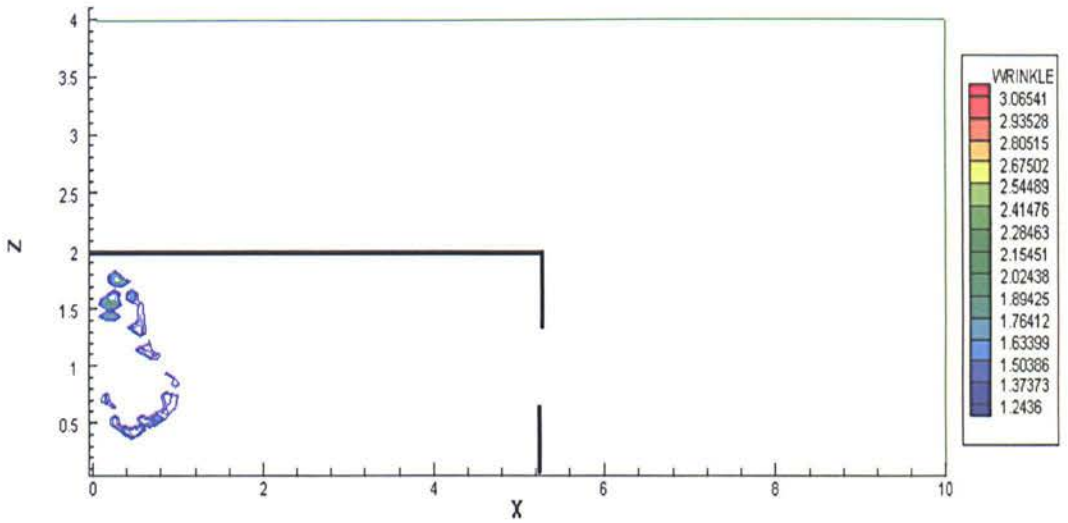

(a). Phase 1.

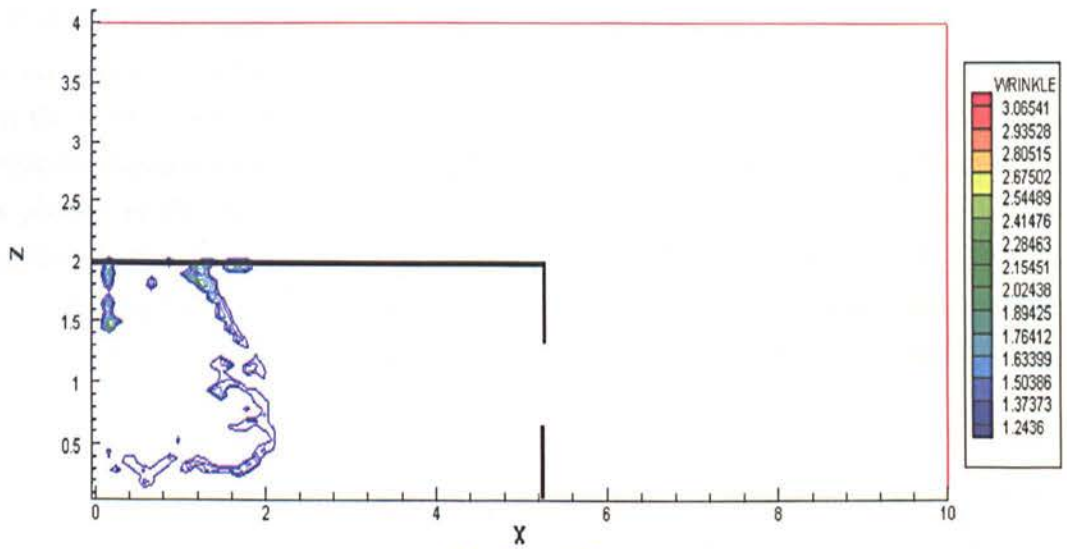

(b). Phase 2.

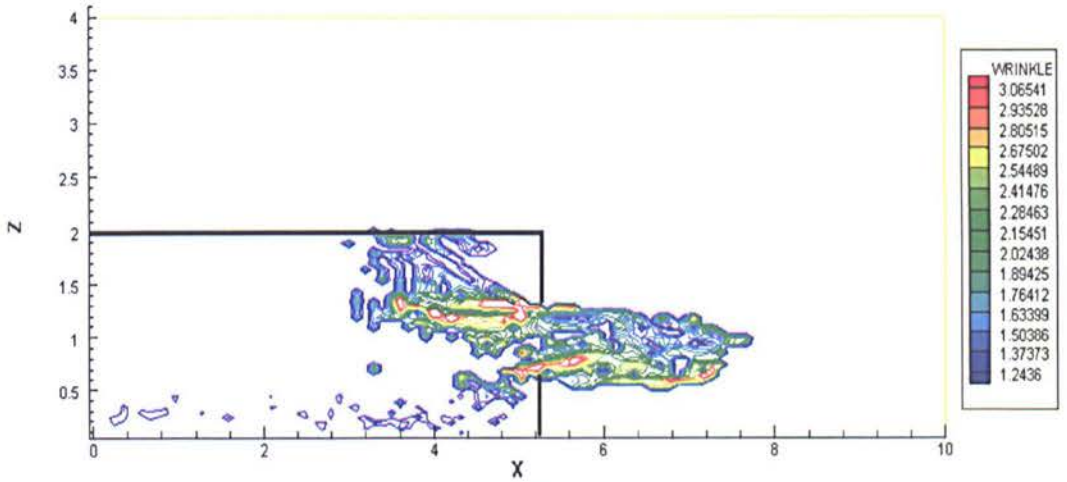

(c). Phase 3.

Figure 8.6. Wrinkling factor profile.

"Plane" Front Propagation.

In this phase, a sloped "planar" front is formed as shown in Figs. 8.9 (b) and 8.10 (b). At the bottom layer, the premixed front is 0.5m ahead of that at the top layer. This structure remains unchanged through the 3rd phase of the backdraft. The flame index is plotted in Fig. 8.8 (b), it is observed that the premixed front is located at the bottom. In Fig. 8.7 (b) it can be noticed that the flame is travelling close to the floor, i.e. following the stoichiometric mixture surface. In Fig. 8.2 (c), as the mixture in the upper layer is not within the flammability limit, both $\overline{S}_L$ and $\overline{Q}_C$ are shown to be zero.

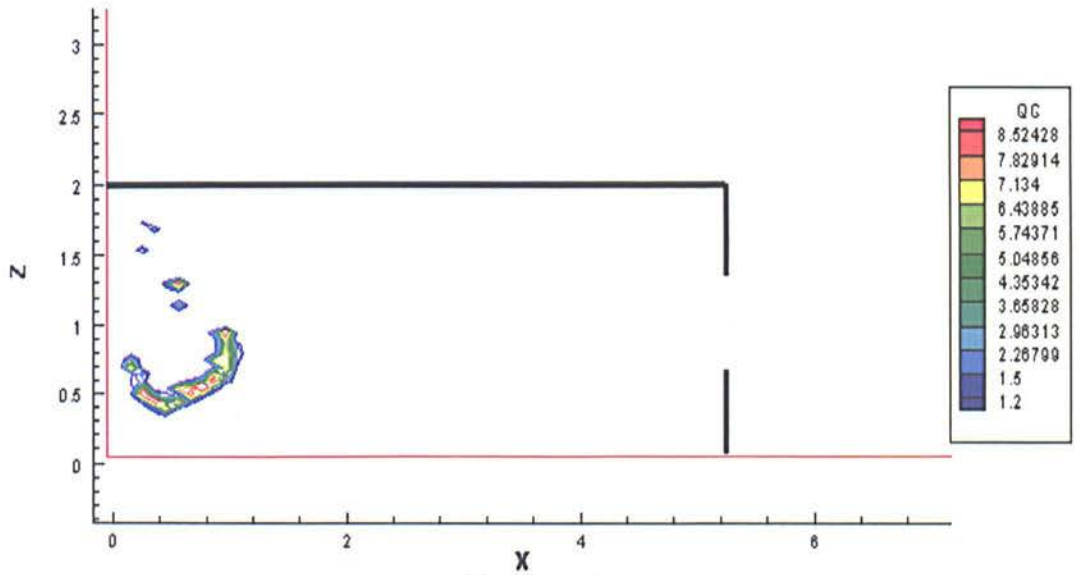

(a). Phase 1.

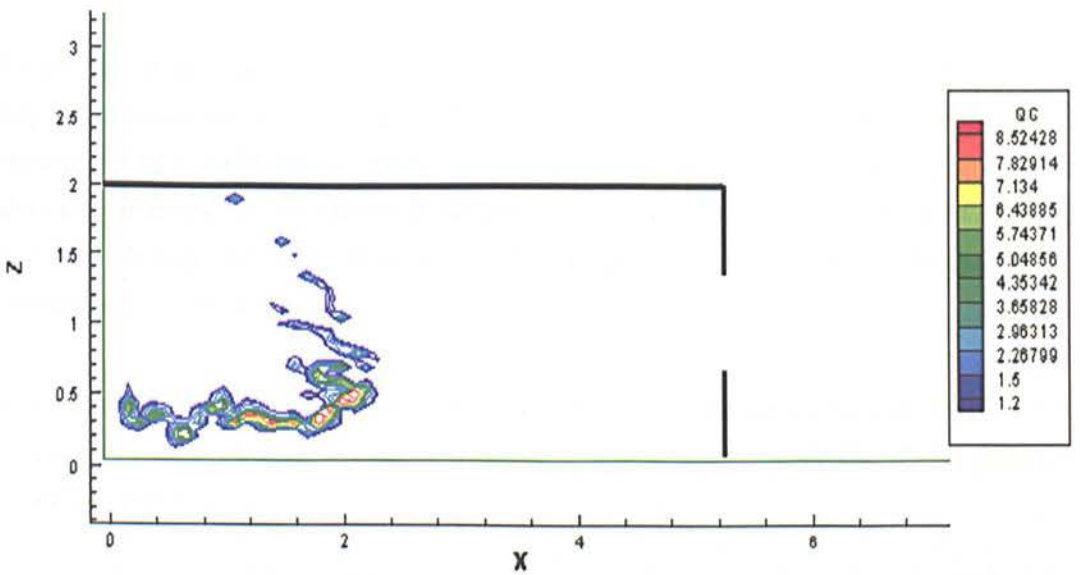

(b). Phase 2.

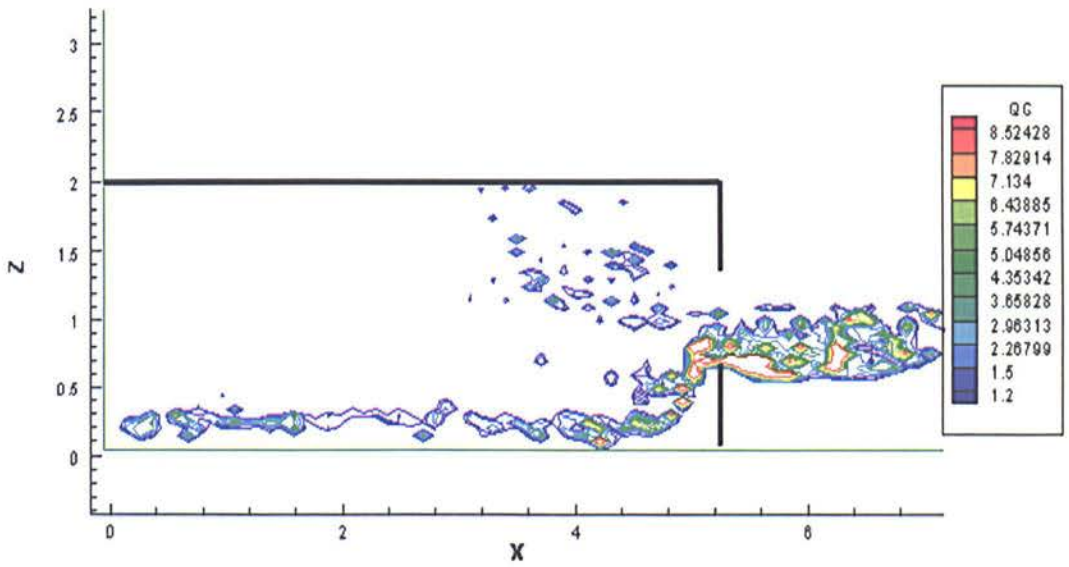

(c) Phase 3

Figure 8.7. Reaction progress variable source term (Qc).

At the tip of the flame front some turbulence develops increasing the flame speed, this is reflected by an increase of the wrinkling factor up to about (Ξ = 1.5). As shown in Fig. 8.6 (b). At the lower section of the container, some mixing process can also be observed at the flame front due to the turbulence in that section as it is depicted in Fig. 8.9 (b). This fluctuation increases as the flame approaches the opening of the enclosure.

The heat release by the combustion drives the hot gases upwards and thus, in the upper layer, a high temperature region is found to travel with the flame front as shown in Fig. 8.5 (b)

At the same time, some methane and oxygen are being pushed out of the enclosure as shown in Figs. 8.3 (c) and 8.4 (c). The oxygen concentration in the lower half of the opening is 20% and in the upper about 8%. The methane concentration pushed out from the top part of the opening top was 43% and 6% from the lower part.

Behind the flame front, the oxygen and fuel are practically depleted except for the layer very close to the bottom of the container, which is left unburnt because the mixture is outside the flammability limit.

Throughout the deflagration process, the stoichiometric mixture at the opening remained very close to the lower border. The velocity of gases flowing out of the container at the opening is around 20 m/s and the average propagation velocity of the flame is around 5 m/s.

The flame front propagates through the container towards the opening. As it is closer to the exit, the turbulence intensifies further and the flame speeds up. The lower part of the flame accelerates more rapidly than the upper section and therefore the "plane" shape is lost and is transformed into a more pronounced spike. The upper front recedes in relation with the rest of the flow because of the wall ahead of it. The flame gains momentum because of the reduction of the flame front total area. With this new structure, the flame is expelled through the opening coming into the 4th phase.

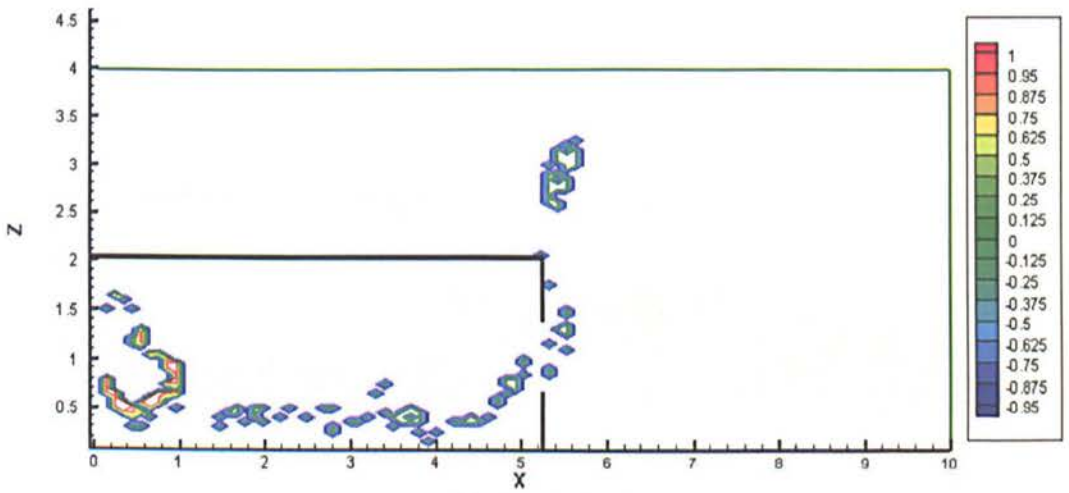

(a). Phase 1.

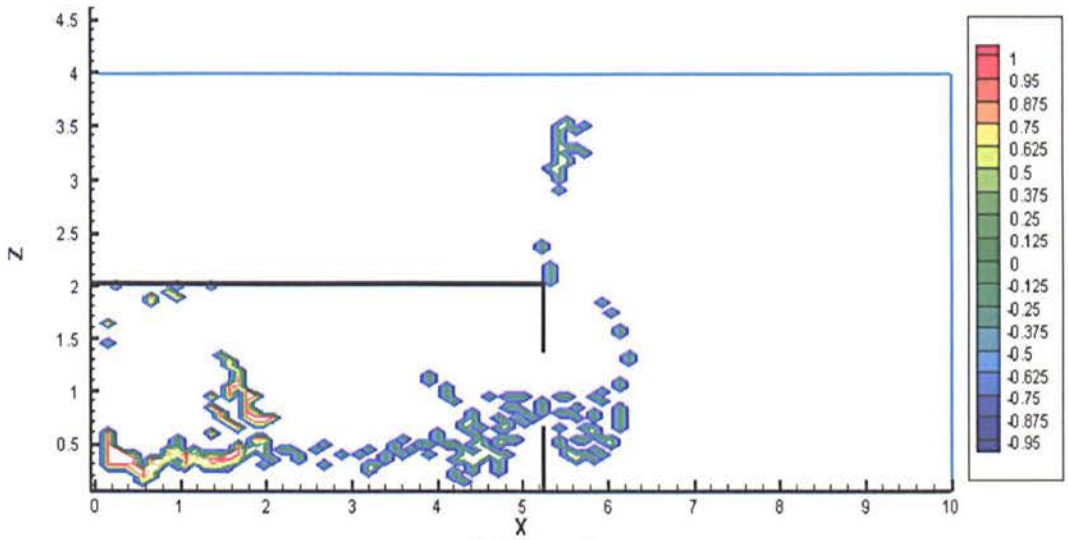

(b) Phase 2.

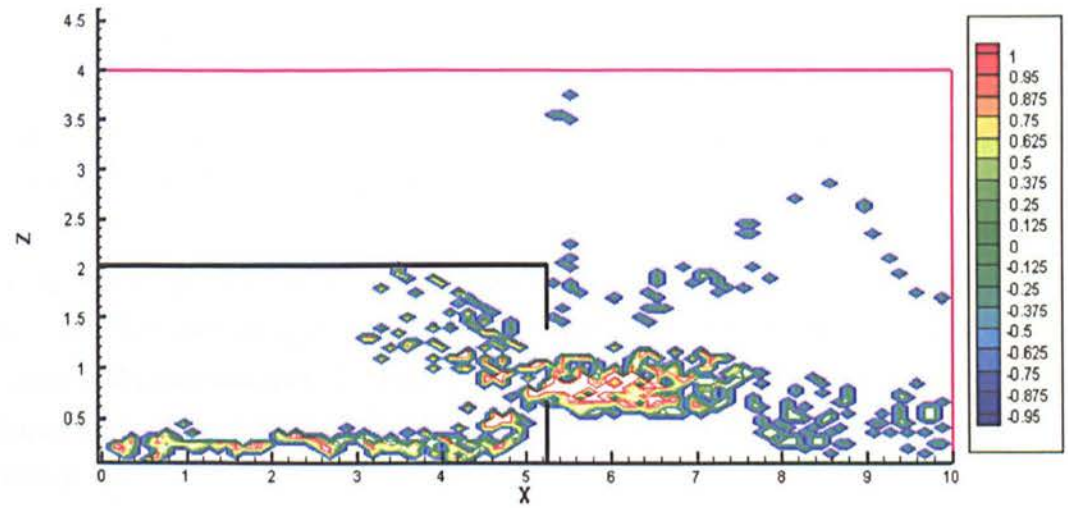

(c). Phase 3.

Figure 7.8. Flame index.

Stretching of the Flame Front through the Opening

During this phase, the flame is thrown out of the enclosure through the opening at high speed. In Fig. 8.9 (c) the long tip of $\widetilde{C}$ passing through the exit can be seen, while the upper front remains aback. Fig. 8.2 (d) shows clearly the stoichiometric path along the bottom line and through the lower section of the exit.

The flame front is accelerated due to the high turbulence developed previously along the stretching process. In this phase, the flame wrinkling factor is of vital importance in predicting the flame speed. Values of up to 3.0 are found as shown in Fig. 8.6 (c). It is shown in Fig. 8.7 (c) that the progress variable source term $\widetilde{Q}_C$ is enhanced threefold. The combustion process continues outside the container as it is seen in the experiment.

Fig. 8.8 (c) shows the flame is about 3 m out of the enclosure and its structure is practically totally premixed. The flame is driven out by both the deflagration pressure and the source term, $\widetilde{Q}_C$. It is not easy to discern which of these two has more importance. While the flame front is approaching the exit its velocity increases to reach a maximum speed of 13 m/s and the mixture speeds up to 40 m/s outside the container.

In this phase, the pressure within the container also pushes the remaining unburnt fuel out. The hot fuel is ignited after mixing with the fresh air outside the container creating the characteristic fireball. In Fig. 8.4 (d), the methane concentration in the upper layer of the exiting gases is about 25 % of CH4, while in the lower section it is almost zero.

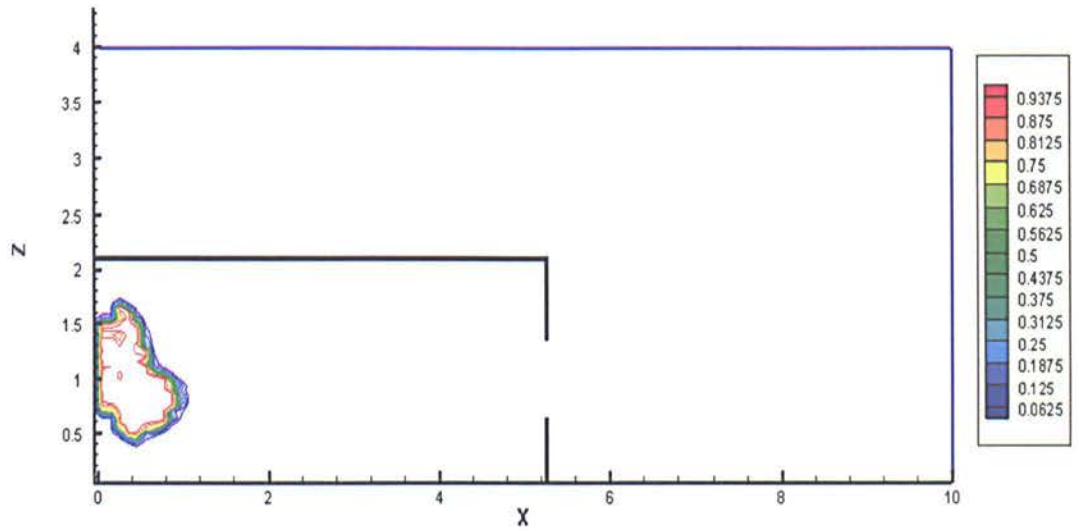

(a). Phase 1.

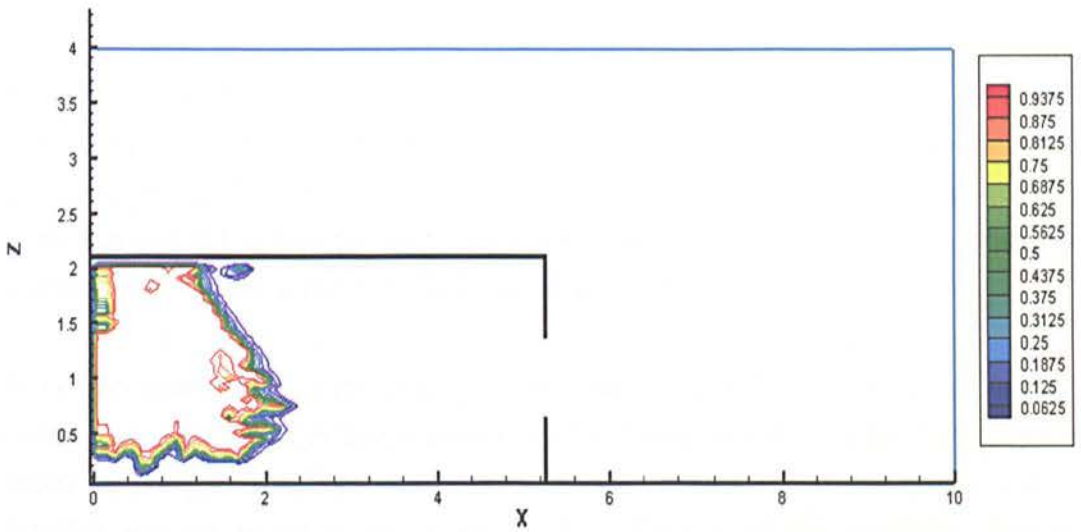

(b). Phase 2.

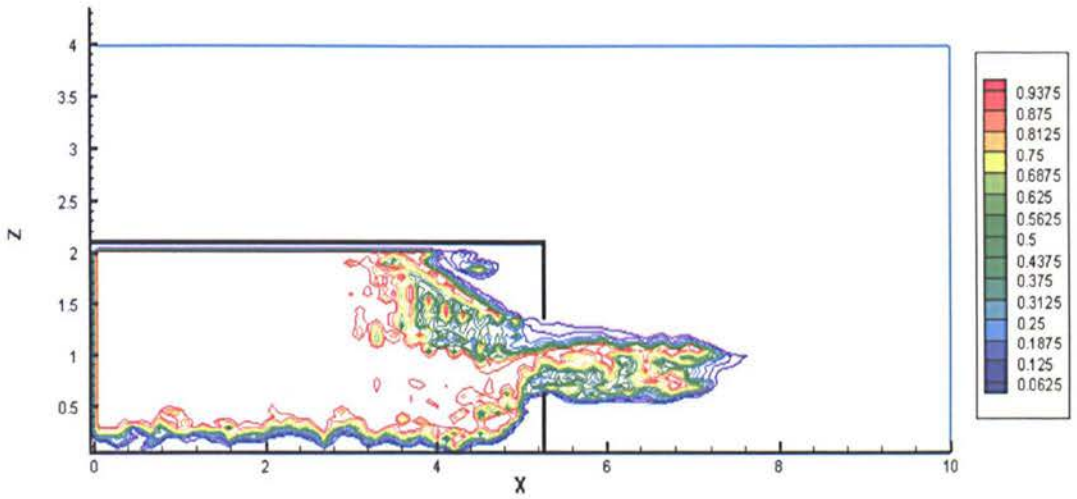

(c). Phase 3.

Figure 8.9. Reaction progress variable.

Fireball outside the container

The mixture began to lose momentum after the flame is expulsed out of the container, as shown in Fig. 8.10 (d) and the characteristic fire ball is formed. The jet velocity decreases and the buoyancy force becomes more important, driving the hot gases upwards and creating large areas of high temperature.

It is not clear which percentage of the unburnt fuel expulsed out is actually combusted. This is a relevant parameter since it determines the energy of the fireball, which is a real hazard for people. In order to investigate this phenomena a more detailed analysis needs to be carried on the 5th phase of the backdraft. This is, however, beyond the scope of the present study.

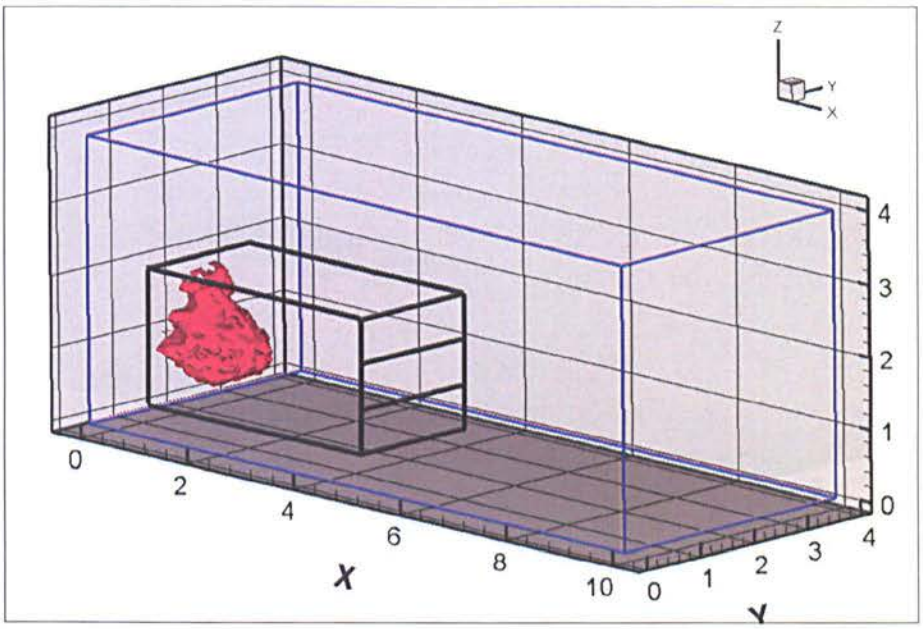

(a). Phase 1.

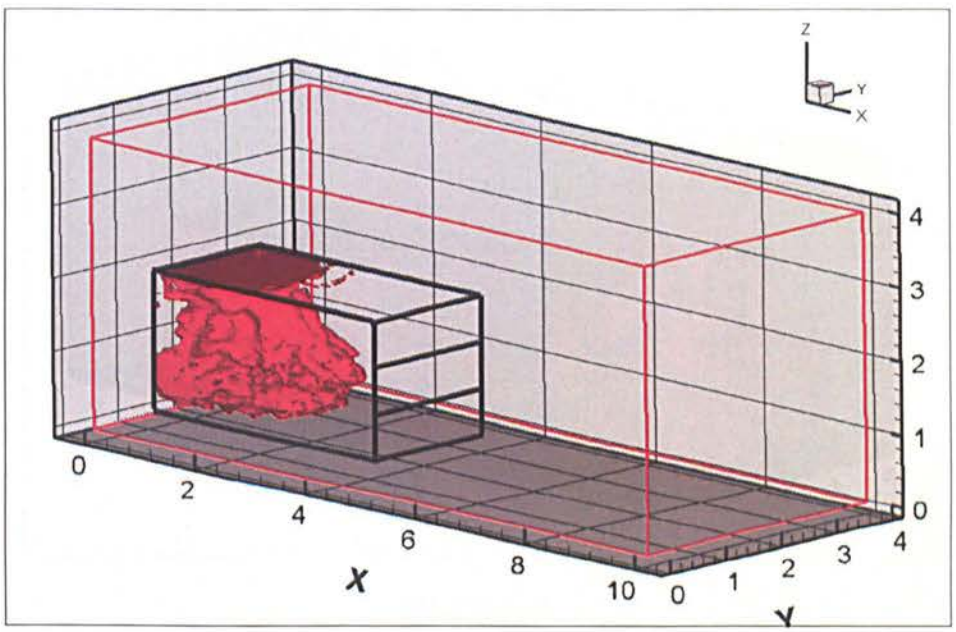

(b). Phase 2.

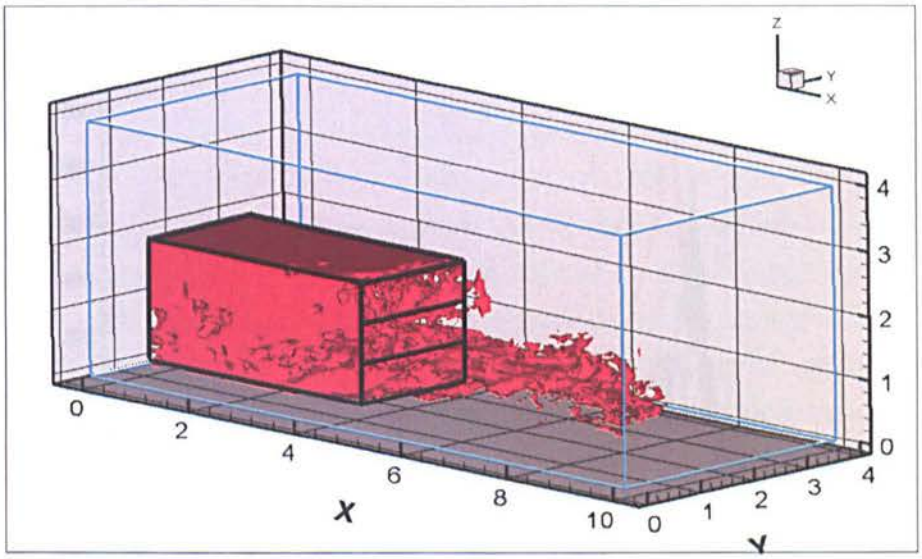

(c). Phase 3.

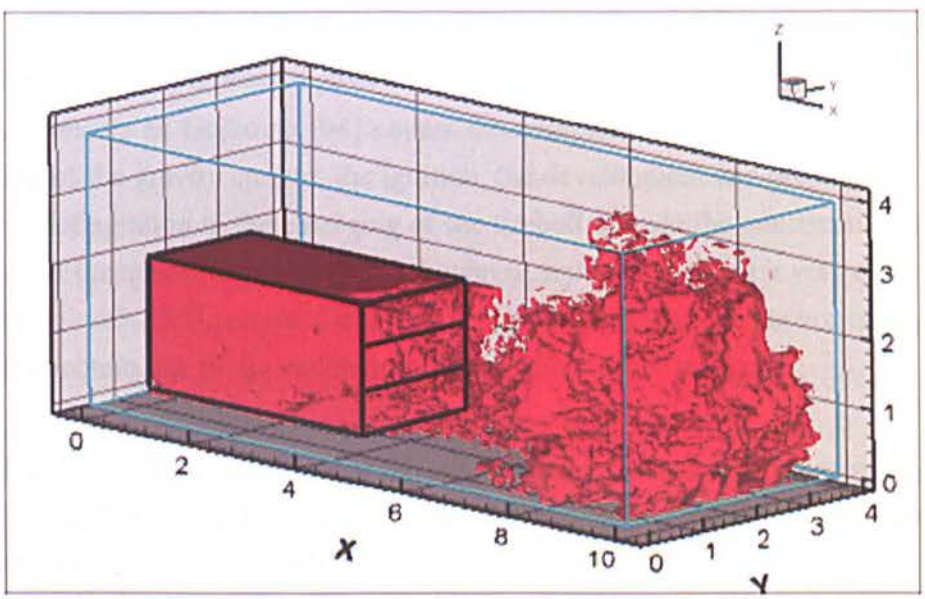

(d). Phase 4.

Figure 8.10. Iso-contour of the reaction progress variable.

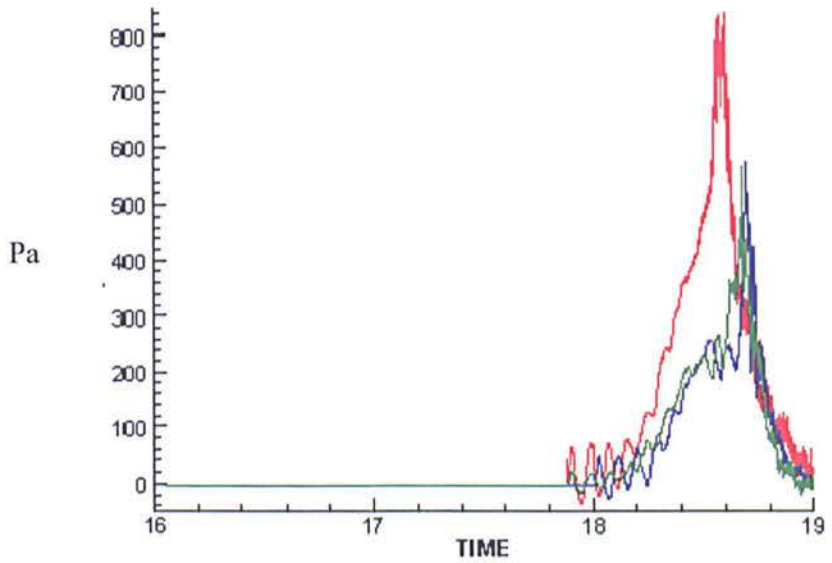

Figure 8.11. Pressure history for mesh 1 (red), mesh 2(blue) and mesh 3(green).

Comparison with experimental observations

The experiments of Gojkovic [94] covers the complete backdraft process, from the beginning of the gravity current, the ignition, the development and propagation of the turbulent deflagration to the emerging of the fireball outside the container. The exact locations of the measuring points were, however, not clear making it very difficult for comparison with CFD results. Detailed experimental measurements are indeed very difficult to obtain due to the violence and suddenness of the process.

Overall, the qualitative behaviour of the species mass concentrations, temperature and flame propagation in the experiments were captured in the numerical simulation from a phenomenological point of view.

As only a small number of pressure measurements were made in the experiments, it is not possible to compare the detailed pressure history. However, the time-dependant pressure history for the three meshes is depicted in Fig. 8.11. It can be observed that

the pressure evolution is almost identical for mesh 2 and mesh 3, meaning that the solution has reached a grid convergence. The predicted time elapsed between the maximum over- and under- pressure caused by the expansion of hot gases was found to be around 0.7 seconds (herein considered between the time when the pressure begins to raise until the pressure is close to 0 again), reasonably close to the experiment (0.5 seconds). This time is representative of the travelling speed of the flame. This good agreement indicates that the present model can capture the overall behaviour of the backdraft phenomena and predicts the propagation of the turbulent deflagration with reasonable accuracy. Nevertheless, it can be said that the model over predicts the measured pressure. The maximum pressure measured was 225 Pa and the simulation predicts 600 Pa. This may be attributed to the fact that the present model does not take into account the dilution presents in the fuel mixture. The dilution would reduce significantly the laminar burning velocity of the mixture. In the next subsection, the dilution is considered in the laminar burning velocity correlation and the same model is applied to a deflagration in a small container.

It is important to note that in Gojkovic's experiment there are not information regarding the dilution in the fuel inside the container. For this reason, we were not able to consider it into the laminar burning velocity correlation.

8.3 Weng and Fan's experiment

The reduced scale tests carried out by Weng and Fan [254] are simulated in this section. In their experiment, Weng and Fan used a compartment whose dimensions are (1.2 × 0.6 × 0.6) m and was fitted with a variety of opening geometries. A methane burner of (0.15 x 0.15) m square (99.8% pure) was placed against the wall opposite the end opening.

A downward–directed pressure nozzle was positioned 0.3 m from the end opening wall, 0.078m from the ceiling and 0.3m from the side wall with the observation window. The nozzle was operated with a cone angle of 60° and a volume mean diameter of 38 μm.

The flame was ignited at 0 s. As the compartment was sealed, the flame dies out due to oxygen starvation. The burner was left on for a predetermined period of time. Optionally, during this time, a known amount of water mist was injected into the compartment and allowed to vaporize and mix with the gases. At the time of the hatch opening, the fuel mass flow was cut off and the hatch was opened to allow fresh air to come into the vitiated environment. In this later process, the electrically heated metal wire was turned on to trigger the ignition. Following, a fast deflagration travelling towards the opening occurred when the mixture inside the container was within the flammability limits.

8.3.1 Simulation details

In the numerical simulation a domain of 2.5 m (L) × 1.2m (W) × 1.2m (H) with non uniformed mesh elements is used. Inside the container the cell is about 1 cm in size and outside is about 2 cm.

The initial conditions are 0 m/s, ambient temperature of air on both inside and outside of the container. Non-slip and appropriated thermal conditions taken from the experiment are imposed at the walls. On the external domain surfaces a free shear condition (open) is used.

We perform simulations for three types of end geometries. Each set up has different combination of fuel flow rate, burner time, injection time and water mist mass.

In the present simulation, the variable $s_l^0(Z^*)$ in Eq. 6.10 is replaced by $s_l^0(Z^*,\widetilde{Y}_d)$, where $\widetilde{Y}_d$ is the total fuel dilution due to products and water vapour. The dilution is initiated as the addition of water vapour and products when the hatch is opened. Then, a transport equation is solved for the dilution along the gravity current and deflagration process. The averaged value, $\widetilde{Y}_d$, is then used as input parameter into the laminar burning velocity correlation. As expected, the laminar burning velocity is considerably reduced by the presence of dilution. Broadly speaking, the dilution

expected in the container is considerably large and consequently the mixture is close to the lower flammable limit (LFL). The correlation used considers nitrogen as diluents and it is valid between $0.6 < \phi < 1.4$ and $0 <$ % diluents in fuel $< 43\%$. As higher than 43% diluents in fuel mass concentration are expected, a linear extrapolation outside this range is used.

Considering the relatively fine grid used in this simulation $\Delta_C = 3\Delta$ in Eq. 6.8 is used. This will preserve the correct laminar burning velocity and will solve the flame front in approximately 6 grid points.

8.3.2 Results

The entire process encompasses very different types of mixing and combustion processes. Following a short well ventilated fire in the initial stage of the experiment, the fire is extinguished due to the lack of oxygen. Later, only mixing occurs as the burner is still on and there is no combustion. Afterwards, the door is opened and gravity current is established travelling towards the back wall. Fresh air comes into contact with hot products, unburnt fuel and oxygen. Eventually, when the mixture reaches the flammable limits close to the ignition source a deflagration towards the opening is produced.

For clarity, the subsequent discussion is organized into the following four stages:

1) Initial fire
2) Fuel mass injection and mixing
3) Gravity Current
4) Ignition and deflagration

1) Initial fire

In this stage the original mixture fraction combustion model in FDS was used. A stable diffusion flame is established on the burner for 20 s. The oxygen mass fraction decreases quickly from its initial value of 0.23 to 0.15, where it is assumed to be below the flammable limits.

In this phase, FDS overpredicts the oxygen consumption in the first few seconds and consequently the predicted extinction time is considerably shorter in the simulation (60 s) than in the experiment (around 150 s).

2) Fuel mass injection and mixing

After the fire is extinguished, only mixing of fresh fuel injected through the burner and hot products occur. This phase lasts up to the time when the hatch is opened.

In order to account correctly for this mixing process, a pure mixing relation, without combustion, is considered where Z = 0 represents $\widetilde{Y}_O$ = 0.15 and $\widetilde{Y}_F$ = 0 and Z = 1 represents $\widetilde{Y}_O$ = 0.0 and $\widetilde{Y}_F$ = 1.

In the simulation, the mixing process is started when there is no combustion in the upper layer and the oxygen mass concentration is considered to be 0.15 uniformly distributed. This is a simple approach of a complex physical process. Nevertheless, this assumption predicts reasonable oxygen and fuel mass concentrations at the time when the hatch is opened.

3) Gravity Current

When the hatch is opened, a current of fresh air at ambient temperature is established travelling to the back wall of the compartment. Weng and Fan [254] measured average quantities just before the gravity set in. Table 8.1 presents the temperature, fuel and oxygen mass concentrations in the upper layer. It can be noted that the oxygen and fuel concentrations are reasonable predicted in all the configurations

The gravity current proved of vital importance in determining the time to reach the ignition source and establishing the structure of the backdraft development. Depending on the opening geometry and the initial conditions, prior to the hatch opening, the gravity current determines the degree of mixing between unburnt methane and fresh air.

Considering the same geometry, higher fuel concentration in the container will require more fresh air in order that the mixture reaches the flammable limits. Therefore, the time delay from hatch opening until ignition will increase with the increase of fuel concentration.

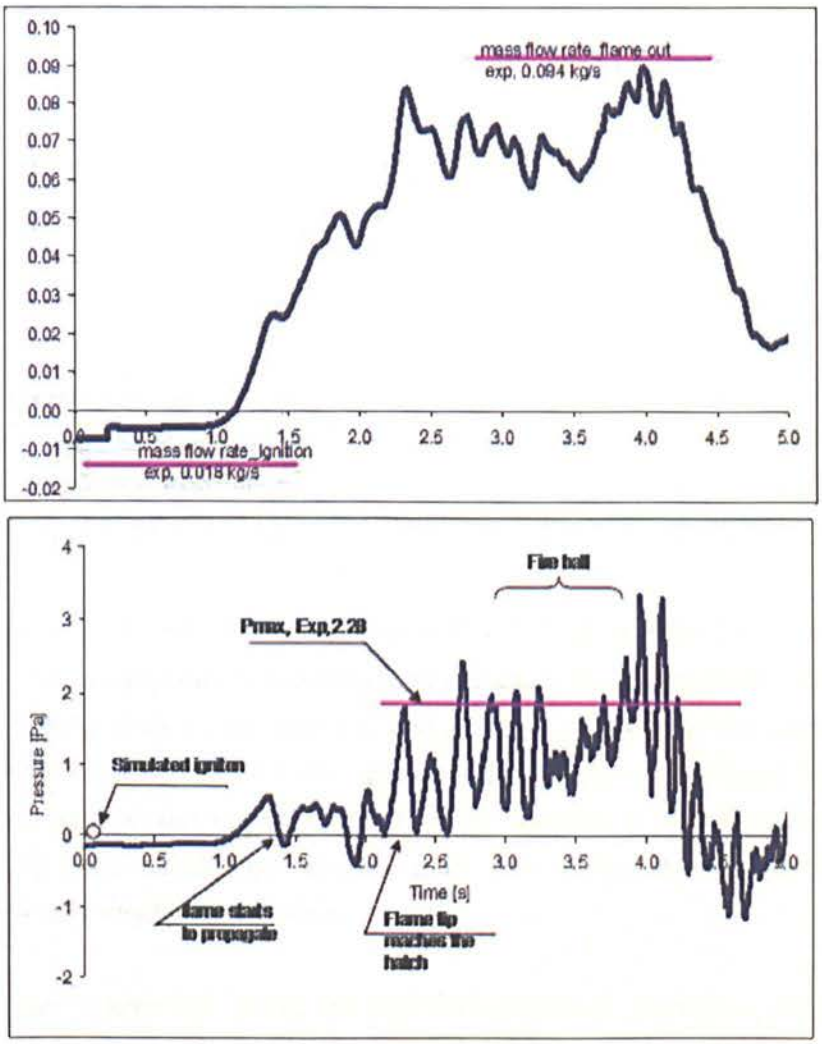

3

Figure 8.12. Pressure and integrated mass flow history from the ignition time for the door opening. Blue line: simulation, violet line: experiment value

There is no experimental data for the ignition time in Weng and Fan's study, although the predicted ignition times are presented in Table 8.1. The ignition time is influenced by many factors such as the geometrical disposition of the wire above the burner, measurement errors, under prediction of the temperature prior to the gravity current, thermal inertia of the wire, etc. Although the gravity current is not the main point in this study, it is pointed out that FDS has been previously successfully tested on this point.

4) Ignition and deflagration

In order to ignite the mixture in the numerical model, methane and oxygen concentrations are checked in a small cylinder volume at the back of the enclosure at each time step. When the flammability range is reached, a numerical spark in the form of $\widetilde{C} = 1.0$ is introduced and is kept on throughout the backdraft.

When the flammable limit is reached at the ignition point, the stoichiometric surface is located close to the floor. Therefore, the flame propagation is expected to exit the container close to the floor. Because of the highly diluted fuel, the initial deflagration velocity is low. The buoyant forces drive the products upwards and towards the exit.

Typical results for a vertical door opening without water mist are shown in Fig. 8.12. The figure shows the pressure and the integrated mass flow through the door histories from the ignition time to the expulsion of the fire ball outside the container. The negative value of mass flow at t = 0 represents the time integrated mass flow into the compartment due to the gravity current. After ignition, a sharp positive slope is shown in Fig. 8.12, which represents the mass flow exiting through the door due to the over pressure inside the container.

It is important to note that Weng and Fan measured total mass flow and pressure at

the time when the flame leaves the container.

In the same Fig.8.12, it can be noted that the predictions of inflow and outflow rates are reasonably predicted . This is a relevant result of the simulation implying a good overall prediction in pressure, flame speed and temperature for the gravity current and deflagration processes.

In the same figure, the pressure history from the ignition time is shown. In this case, more fluctuation is observed, although at the time when the tip of the flame reaches the door, the predicted pressure is in good agreement with the experiment.

Table 8.1 summarizes the results for three different opening geometries with and without water mist.

Table 8.1 Experimental and predicted results for three openings for the scale compartment.

Type of the opening geometry	Run	Water mist		Species concentration		Compartment temperature (K) and layer height (m)			Ignit. time (s)	Maxim pressure (Pa)	Opening total mass flow (kg)		Fire ball
		Time(s)	Mass (g)	Y_{O2}	Y_{HC}	T_U	T_l	h_L		P_{max}	$m^{t=ti}$	$m^{t=to}$	
Downside slot opening	Exp	-		12.7	10.42	388	348	0.25	-	1.71	0.011	0.164	yes
	Sim			12.3	9.10	425	314	0.2	9.75	2.13	0.013	0.04	yes
	Exp	20-30	40.4	14.16	8.79	386	354	0.22	-	0.80	0.015	0.013	no
	Sim					400	305	0.19		1	0.018	-	no
Door Opening	Exp	-		**11.6**	**9.31**	**375**	**337**	**0.28**	-	**2.28**	**0.018**	**0.094**	**yes**
	Sim			**12.5**	**8.29**	**415**	**306**	**0.18**	**6.07**	**2.30**	**0.017**	**0.093**	**yes**
	Exp	**30-40**	**34**	**14.2**	**9.11**	**371**	**327**	**0.25**	-	**2.02**	**0.010**	**0.092**	**yes**
	Sim			**12.58**	**8.08**	**423**	**311**	**0.19**	**6.05**	**1.7**	**0.014**	**0.103**	**yes**
Window Opening	Exp	-		12.5	9.33	372	332	0.28	-	27.18	0.025	0.165	no
	Sim			12.5	8.29	415	306	0.18	18.84	31.89	0.02	0.153	no

For the cases with water mist, the water mist injection time and total amount of mass are provided. The upper layer oxygen and fuel mass concentrations are given at the time when the hatch is opened. Similarly, the upper and lower layer temperatures and layer height are shown. The predicted ignition time is also shown, but unfortunately there is no any experimental data on this quantity. The maximum pressure is considered at floor level when the tip of the flame passes the opening. Equally for the integrated mass flow through the opening: $m^{t=ti}$ is the total mass through the door during the gravity current and $m^{t=to}$ is the total amount of mass through the opening until the flame passes the opening. The "fire ball" column indicates whether or not there was a fire ball coming out of the container.

It can be seen that, the predictions of oxygen and fuel mass concentrations are in good agreement with the experimental data. These predictions are important for an accurate prediction of the deflagration given that the fuel and oxygen distribution in

the container will determine the location of the stoichiometric plane.

The upper and lower layer temperatures, as well as the lower layer height are also reasonably well predicted. The temperature plays an important role in the gravity current development. The temperature in the container will modify the gravity current flow to the ignition point and hence the deflagration.

Also shown in table 8.1 are the maximum pressures at the time when the flame tip passes through the door. It can be seen that the pressures are very low. Nevertheless, the model is able to capture the trend for each case. As expected, in the window's case, the pressure is considerably higher due to the small opening area. This is also captured by the model.
The total mass flow through the opening is shown in the same table. A direct link exists between the pressure over prediction and the mass flux over prediction. In the downside slot opening without water mist, the maximum pressure is over estimated and so is the total mass flow. For the door case, the prediction of pressure is good and so is the total mass flow.

Finally, the last column in Table 8.1 shows whether there was a fire ball expelled out of the container. Here the predictions are in qualitative agreement with the experiments in all cases.

8.4 Summary and conclusions

Numerical investigation on the Gojkovic's backdraft experiment suggests that the backdraft process can be divided into five phases, i.e. 1) the initial condition, (2) the free spreading of the combustion in a 'sphere' shape centred at the ignition point, (3) a slopped 'planar' front travelling towards the exit, (4) the stretching and acceleration of the plane and (5) the burst of the fireball outside the compartment.
Throughout the process, some points can be made:

- The inner structure of the deflagration front was found to be mainly a premixed flame advancing along the stoichometric mixture 'line' close to the floor and towards the opening of the compartment.

- Not all of the unburnt fuel expulsed out of the compartment was burnt. For instance, the unburnt fuel driven out during the early stages of the deflagration was beyond the reach of the flame front and therefore it never ignited.

- Qualitatively, the predictions were in agreement with the experimental data of Gojkovic [94]. As the majority of the measurements were made up to the occurrence of the backdraft and the locations of the measuring points were not exactly known, it is very difficult to perform a detailed quantitative comparison. However, the predicted and experimental time elapsed between the maximum over- and the under- pressures caused by the expansion of the hot combusted gases were in close agreement; indicating that the present model is capable of predicting the propagation speed of the turbulent deflagration with reasonable accuracy.

- A source of uncertainty is the wrinkling factor model. This model takes into account the wrinkling of the flame front at sub-grid level. It is very difficult to quantify this variable as no measurements were carried out. In this study, in order to account for the relatively coarse mesh the default model constant has been increased accordingly. This was done based on the grid Reynolds number.

In the simulations of Weng and Fan's experiment, the fuel dilution caused by burnt gas and water mist is considered.

- As expected the maximum pressure decreases substantially and compares well with the experiment. Due to the smaller scale of the container a finer mesh was used (up to 1 cm) and a better approximation was obtained. This is seen in the overall good prediction obtained for a range of relatively complex

deflagrations with different opening geometries and water mist injection times and amounts.

- The simulation considered the entire process from the initial fire development, extinction, fuel injection, water mist injection, gravity current and deflagration. The process is acceptably reproduced by the model.

Two extra backdraft simulations using Gojkovic's experiment and two finer meshes were carried out using the Lagrangian SGS turbulence model. This approach proved to consistently under predict the classical Smagoringsky range of 0.11-0.22. Consequently, the numerical scheme is greatly unstable and suffers of convergence problems. As such, no meaningful results were obtained. Further investigation would be desirable to asses the suitability and advantages of the Lagrangian SGS model for reacting flows.

Chapter 9

Conclusions

Enclosure fires are extremely complex phenomena, which bring together many fields of expertise such as radiation, soot production, fire growth, ventilation and combustion. In this thesis, the main stress is on combustion models and primarily in coupling premixed and non-premixed regimes. Other important processes such as radiation, soot production, etc., were not considered in order to isolate the problem.

Probably due to the necessity of obtaining results for industrial design, fire safety, etc. the application of numerical modelling to fires has preceded its concise and mathematically sounded derivation. Particularly, combustion models whose first derivations were carried out in the RANS context are largely phenomenological and adjustable empirical constants are necessary.

Since the onset of the computational fluid dynamics applied to reactive flows, the principal concern was and still is the prediction of the burning rate. In the long process of modelling development, the researchers have been trying to minimize those adjustable constants which, initially, were empirically set up.

As a result, the trend of the new models is not to consider any *a priory* constant, so that, ideally, they should perform under any circumstances. Nevertheless, the state of the art in combustion modelling, and generally in CFD, has not yet achieved a complete development, and it is far from the maturity reached by the finite element in stress analysis or energy calculations in solids. Models such as pdf, EBU, etc have been included in commercial packages for quite some time, but effective use of most of them require a previous knowledge of the simulated process.

In the particular case of enclosure fires, researchers have previously used the available combustion models originally developed for open fires, even when their suitability for these cases was dubious. Despite of this, relatively good results were obtained in some cases, although, for specific scenarios, such as backdraft, new sub-models needs to be developed/implemented in order to capture the underlying physics.

A complex flame structure is expected in a backdraft or turbulent deflagration. Contrarily to the classical pure diffusion combustion, in a turbulent deflagration premixed and diffusion combustions might both be present in the form of partial premixed combustion.

Sub-models for dealing with partially-premixed combustion systems were introduced into the FDS code. The "flame index" was used in order to combine premixed and non-premixed combustion. This concept makes use of the gradient signs of oxygen and fuel mass concentrations in both regimes to distinguish between premixed and diffusion. Domingo developed this concept for LES considering the fluctuations of the species gradients at sub-grid level.

An extra balance equation for the progress variable C was also implemented into the FDS code in order to track the flame front. This approach uses a LES filter larger than the grid size in order to capture the thin premixed front. In this case, the progress variable was associated with the fuel mass concentration.

Three different LES were carried out in order to test the sub-models for partially premixed combustion:

- An unstrained planar 1-D hydrogen flame was simulated to test the premixed front tracking model. Good results were obtained for the laminar burning velocity, density, temperature and species concentration ratios at both sizes of the flame front. For this case the progress variable filter was fivefold larger than the actual LES grid size.

- A laminar triple flame was simulated using the progress variable approach for the flame front detection and the steady laminar flamelets for non-premixed combustion. The triple flame was chosen because it is relatively simple to set up, because the computational time is relatively short and finally because, being laminar, there are no uncertainties about the turbulent fluxes and the wrinkling of the flame sheet at sub-grid level. Moreover, the triple flame offers a clear complex structure with two premixed branches and a diffusion trail, which meet at the triple point.

- A partially premixed turbulent lifted flame was simulated. In this case, it was necessary to introduce into the model the augment of burning velocity, induced by the wrinkling of the flame front at sub grid level. Good agreements were found in the lift-off height prediction, in the flame structure and in the mixture fraction profiles. A stabilization mechanism was discussed, based on the concepts, previously exposed, that the flame base faces a high velocity flow and a flammable mixture upstream; thereafter, the flame tries to find its way upstream between low-speed flammable sectors of the flow. It was found that in this process the stabilization point, which is here identified as the maximum premixed heat release, plays an important role, driving the flame base upstream of the flow.

In all of these, it was observed that the flame index captures the regimes acceptably and the lift off is reasonably well predicted. The triple point is well defined and the three branches further downstream can be discerned by the flame index. For the triple flame case, it is well known that increasing the fuel gradient increases the lift-off height as well, with the exception of for a small range. The response of the model to fuel gradient might be a topic for further studies.

Two real scenarios for backdraft were simulated:

- The experiment of Gojkovic was first considered [94] and Wen and Fan's backdraft experiment second.. The sub-models used for the backdraft simulations are the same utilized in the previous simulations.

Unfortunately, for the Gojkovic's experiment, the measurements in existence are neither extensive nor accurate and hence, the comparison against the numerical simulation was largely done on qualitative grounds.

A numerical spark was ignited at the back wall of the container when the flammable limit was reached, after fresh air was allowed to get into the room through an opening. Immediately afterwards, the flame front heads towards the opening, following the flammable mixture close to floor. Some points can be highlighted:

- The ignition time (the time from the opening of the hatch to when the ignition occurs) was well predicted by the FDS, even when there is a large scatter in the measurements.
- The flame structure in the backdraft was found to be mainly premixed, as it is indicated by the flame index.
- Not all the unburnt fuel in the container is consumed by the deflagration.

Regarding the latter point, during the first stages after ignition, the raise of pressure at the back wall expulses product and fuel through the opening and, eventually, this fuel is not reached by the flame front and it does not burn. Consequently, the power of the backdraft is not directly linked to the total amount of unburnt fuel inside the container. Experiments have showed otherwise, but this can be attributed to the less diluted mixture inside the container. As products and fuel mix, the dilution of the mixture is enhanced and therefore, the burning velocity decreases.

Oppositely, if more fuel is injected, the laminar burning velocity will increase and with it the total power of the deflagration. In order to deal with this, and to account for the dilution, a dilution parameter was introduced in the laminar burning velocity correlation to simulate Weng and Fan's experiment.

Weng and Fan carried out a set of backdraft experiments in a scale compartment with and without water mist for different openings geometries and measured integrated

mass flow through the openings, pressure, upper layer temperature and mass concentrations. Due to the smaller scale of the experiment it was possible to use a finer mesh in the LES simulation and grid independency was achieved.

In this simulation, the following points were clear:

- The dilution present in the fuel before the deflagration was considered, diminishing substantially the overall flame propagation velocity.
- The performance of the model proved to be satisfactory and achieved reasonable agreement with the measurements.
- The model could capture with acceptable accuracy the maximum pressure and integrated mass flow through the openings for each geometry and even predict the occurrence of backdraft for each case.

SGS turbulence model

During the earlier stages of the study, some effort was devoted to improving the SGS turbulence models and to implement a CMC type SGS combustion model into the code. Unfortunately, both models were later found to be unsuitable for the backdraft simulation. The first one suffered numerical instabilities caused by the under prediction of the Smagorinsky constant when applied to the backdraft case. The second one was deemed inappropriate due to its requirement of an homogeneous plane of conditional values. Nevertheless, some reasonably good results have been obtained with both models during the validation using simple geometrical configurations, namely a buoyant plume, a backward facing step and the Sandia-D non-premixed turbulent flame.

- A lagrangian SGS model was implemented into the FDS code. This model overcomes the drawbacks of previous models regarding the homogeneous plane of turbulence and the selection of a constant value, namely the Smagorinsky constant. In the Maneveour's approach, the model works without such restrictions and the Smagorinsky constant is dynamically

calculated. Good results were obtained for classical benchmarking flow configurations such as the buoyant turbulent plume and the backward facing step. Nevertheless, it was observed that the SGS turbulence viscosity became negative in a larger proportion than originally stated by Maneveour, and issues of numerical instability are then more likely to occur.

Additionally, the computational cost is increased by 25% or more compared with the classical Smagorinsky mode.

Non-premixed turbulent model

A variation of the traditional conditional source estimation (CSE) approach was developed. This approach is based on the CMC concept; however, CSE does not need to solve the computational demanding conditional equations but, alternatively, approximates the conditional source term by an inversion process.

- This shortcoming predicted relatively good results for the turbulent diffusion flame (SANDIA flame D). Even though the present implementation is not capable of predicting extinction/re-ignition events, it was observed that it is very economic from computational point of view. Additional improvements, such as unsteady laminar flamelets, might be incorporated into the model for improving the inversion process.

- On the other hand, CSE needs a homogeneous plane of conditional values to perform the inversion, which is not always an obvious choice and sometimes can condition the model to be used.. A possible alternative to relax this restriction might be to select an ensemble of points normal to the flame surface (where the conditional quantities are constant) but this would require a very fine mesh at the stoichiometric mixture.

Further work could be similarly invested on testing different inversion techniques; which are abundant in the literature. This could lead to great improvement in the inversion and, consequently, to the approximation of the conditional quantities.

References

[1] Abdel-Gayed, R. and Bradley, D., Lewis number effects on turbulent burning velocity. Twenty Symposium (International) on Combustion. The Combustion Institute., 1984 (1984) p.

[2] Abdel-Gayed, R. and Bradley, D., Combustion regimes and the straining of turbulent premixed flames. Combust. and Flame, 1989. **76** (1989) p. 213-218.

[3] Adams, E., Johnston, J. and Eaton, J., Experiments on the Structure of Turbulent Reattaching Flow. 1984, Thermosciences Division, Dept. of Mech Eng., Stanford University.

[4] Akselvoll, K. and Moin, P., Large Eddy Simulation of Turbulent Confined Coannular Jets and Turbulent Flow Over a Backward Facing Step. 1995, Department of Mechanical Engineering, Stanford University.

[5] Angelberger, C., et al. Large eddy simulation of combustion instabilities in turbulent premixed flames. in *Proceedings of the Summer Program*. 1998. Center for Turbulence Research.

[6] Armaly, B., et al., Experimental and Theoretical Investigation of Backwrad-Facing Step. J. Fluid Mech., 1983. **127** (1983) p. 473-496.

[7] Babrauskas, V., Reneke, P. and Peacock, R., Defining flashover for fire hazard calculations: Part II. Fire safety journal, 2003. **38** (2003) p. 613-622.

[8] Bailly, P., Contribution á l'étude de l'interaction turbulence-combustion dans les flammes turbulentes de prémélange á l'aide de modéles du second ordre. PhD thesis. 1996, Université de Poitiers.

[9] Bailly, P., et al., Experimental and numerical study of a premixed flame stabilized by a rectangular section cylinder. Twenty-sixth Symposium (International) on Combustion. The Combustion Institute., 1996 (1996) p. 923-930.

[10] Barlow, R., Piloted mehtane/air jet flames: Transport effects and aspects of scalar structure. Combust. and Flame, 2005. **143** (2005) p. 433.

[11] Barlow, R., et al., Effect of Damkoler number on superequilibrium OH concentration in turbulent nonpremixed jet flames. Combust. and Flame, 1990. **82**(3-4) (1990) p. 235-251.

[12] Barlow, R. and Frank, J., Effect of turbulence on species mass fractions in methane/jet flames. Proc. Combust. Inst., 1998. **27**(1087) (1998) p.

[13] Barlow, R., et al., Nitric oxide formation in dilute hydrogen jet flames: isolation of the effects of radiation and turbulence-chemistry submodels. Combust. and Flame, 1999. **117** (1999) p. 4-31.

[14] Becker, H., Hottel, H. and Williams, G., The Nozzle-Fluid Concentration Field of the Round, Turbulent, Free jet. J. Fluid Mech., 1967. **30** (1967) p. 285-303.

[15] Bilger, R. The structure of turbulent nonpremixed flames. in *Twenty-second symposium (international) on combustion. The combustion institute.* 1988.

[16] Bilger, R., Conditional moment closure for turbulent reacting flow. Phys. Fluids, 1993. **5**(2) (1993) p. 327-334.

[17] Bilger, R. and Klimenko, A., Conditional moment closure for turbulent combustion. Progress in Energy and Combustion Science, 1999. **25** (1999) p. 595-687.

[18] Boger, M., Modélisation de sous-maille pour la simulation aux grandes échelles de la combustion turbulente prémélangée. 2000, Ecolde Centrale: Paris (France).

[19] Boger, M. and Veynante, D. Large Eddy Simulation of a Turbulent Premixed V-Shape Flame. in *Proceeding of the Eighth European Turbulence Conference.* 2000: CIMNE, Barcelona 2000.

[20] Boger, M., et al. Direct Numerical Simulation Analysis of Flame Surface Density Concept for Large Eddy Simulation of Turbulent Premixed Combustion. in *Twenty-Seventh Symposium (International) on Combustion.* 1998: The Combustion Institute.

[21] Borghi, R., On the structure and morphology of turbulent premixed flames. Rec. Adv. Aerosp. Sci., 1985 (1985) p. 117-138.

[22] Borghi, R., Turbulent combustion modelling. Prog. Energy Combust., 1988. **14** (1988) p. 245-292.

[23] Borghi, R. and Destriau, M., Combustion and Flames, chemical and physical principles, ed. TECHNIP. 1998.

[24] Boulanger, J. and Vervisch, L., Diffusion Edge-Falme: Approximation of the Flame Tip Damköhler Number. Combust. and Flame, 2002. **130** (2002) p. 1-14.

[25] Boulanger, J., et al., Effects of heat release in laminar diffusion flames lifted on round jets. Combust. and Flame, 2003. **134** (2003) p. 355-368.

[26] Bourlioux, A., Moser, V. and Klein, R. Large eddy simulation of turbulent premixed flames using a capturing/tracking hybrid approach. in *Sixth International Conference on Numerical Combustion.* 1996. New Orleans, Louisiana.

[27] Bradley, D., Gaskell, P. and Gu, X., Application of a Reynolds Stress, Stretched Flamelet, Mathematical Model to Computations of Turbulent Burning Velocities and Comparison with Experiments. Combust. and Flame, 1994. **96** (1994) p. 221-248.

[28] Bray, K., Turbulent flows with premixed reactants in turbulent reacting flows. Topics in applied physics, ed. P.A.L.a.F.A. Williams. Vol. 44. 1980, New York: Springer Verlag. 115.

[29] Bray, K., The challenge of turbulent combustion. Twenty-Sixth Symposium (International) on Combustion. The Combustion Institute, Pittsburgh, 1996 (1996) p.

[30] Bray, K., Champion, M. and Libby, P., The interaction between turbulence and chemistry in premixed turbulent flames, in *Turbulent Reacting Flows, volume 40 of Lecture Notes in Engineering*, R.a.M. Borghi, S., Editor. 1989, Springer. p. 541-563.

[31] Bray, K. and Libby, P., Recent developments in the bml model of premixed turbulent combustion, in *Turbulent Reacting Flows*, P. Libby and F. Williams, Editors. 1994: London:Academic. p. 116-51.

[32] Bray, K. and Peters, N., Laminar flamelets in turbulent flames, in *Turbulent Reacting Flows*, P.a.W. Libby, F., Editor. 1994, Academic Press: London. p. 63-113.

[33] Bukowski, R., Modeling a Backdraft: The Fire at 62 Watts Street. NFPA, 1995. **89**(6) (1995) p. 85-89.

[34] Bushe, W. and Steiner, H., Conditional moment closure for large eddy simulation of nonpremixed turbulent reaction flows. Phys. Fluids, 1999. **11**(7) (1999) p. 1896-1906.

[35] Bushe, W. and Steiner, H., Laminar flamelet decomposition for conditional source-term estimation. Phys. Fluids, 2003. **15**(6) (2003) p.

[36] Butler, T. and O'Rourke, P., A numerical method for two-dimensional unsteady reacting flows. Sixteenth Symposium (International) on Combustion. The Combustion Institute., 1977 (1977) p. 1503-1515.

[37] Calhoon, W. and Menon, S. Subgrid modeling for large eddy simulation. in *AIAA 34th Aerospace Science Meeting*. 1996. Reno, Nevada: AIAA paper.

[38] Candel, S. and Poinsot, T., Flame stretch and the balance equation for the flame area. Combust. Sci. Tech., 1990. **70** (1990) p. 1-15.

[39] Cant, R., Pope, S. and Bray, K., Modelling of flamelet surface to volume ratio in turbulent premixed combustion. Twenty-third Symposium (International) on Combustion. The Combustion Institute. Pittsburgh, 1990 (1990) p. 809-815.

[40] Cessou, A., Maurey, C. and Stepowski, D., Parametric and statistical investigation of the behavior of a lifted flame over a turbulent free-jet structure. Combust. and Flame, 2004. **137** (2004) p. 458-477.

[41] Chang, C., Dahm, W. and Trygvason, G., Lagrangian model simulations of molecular mixing, incluiding finite rate chemical reactions, in temporally developing shear layer. Phys. Fluids, 1991. **3**(5) (1991) p. 1300-1311.

[42] Charlette, F., Meneveau, C. and Veynante, D., A power-law flame wrinkling model for LES of premixed turbulent combustion. Part I: Non-dynamic formulation and initial tests. Combust. and Flame, 2002. **131** (2002) p. 159-180.

[43] Charlette, F., Meneveau, C. and Veynante, D., A Power-Law Flame Wrinkling Module for LES of Premixed Turbulent Combustion. Part II:Dynamic Formulation. Combust. and Flame, 2002. **131** (2002) p. 181-197.

[44] Chen, C. and Rodi, W., Vertical Turbulent buoyant Jets: A Review of Experimental Data. 1980, Pergamon Press, Oxford: Oxford. p. 16.

[45] Chen, Y. and Bilger, R., Stabilization Mechanisms of Lifted Laminar Flames in Axisymmetric Jet Flows. Combust. and Flame, 2000. **123** (2000) p. 23-45.

[46] Cheng, W. and Diringer, J., Numerical modelling of si engine combustion with a flame sheet model, in *International Congress and Exposition*, e. S.P. 910268, Editor. 1991: Detroit.

[47] Choi, C. and Huh, K., Development of a coherent flamelet model for a spark ignited turbulent premixed flame in a closed vessel. Combust. and Flame, 1998. **114**((3/4)) (1998) p. 336-348.

[48] Chow, W. and Zou, G., Correlation equations on fire-induced air flow rates through doorway derived by large eddy simulation. Building and Enviroment, 2005. **40** (2005) p. 897-906.

[49] Chung, S.H. and Lee, B.J., On the Characteristics of Laminar Lifted Flames in a Nonpremixed Jet. Combust. and Flame, 1991. **80** (1991) p. 62-72.

[50] Colin, O., et al., A Thickened flame Model for Large Eddy Simulations of Turbulent Premixed Combustion. Phys. Fluids, 2000. **12**(7) (2000) p.

[51] Colucci, P., et al., Filtered density function for large eddy simulation of turbulent reacting flows. Phys. Fluids, 1998. **10**(499) (1998) p.

[52] Cook, A. and Riley, J., A subgrid model for equilibrium chemistry in turbulent flows. Phys. Fluids, 1994. **6**(2868) (1994) p.

[53] Cook, A. and Riley, J., Direct numerical simulation of a turbulent reactive plume on a parallel computer. J. Comp. Phys., 1996. **129**(2) (1996) p. 263-283.

[54] Cook, A. and Riley, J., Subgrid scale modeling for turbulent reacting flows. Combust. and Flame, 1998. **112** (1998) p. 593-606.

[55] Cook, A., Riley, J. and Kosály, G., A laminar flamelet approach to subgrid-scale chemistry in turbulent flows. Combust. and Flame, 1997. **109** (1997) p. 332-341.

[56] Craig, I. and Brown, J., Inverse problems in astronomy. A guide to inversion strategies for remotely sensed data. 1986: Adam Hilger Ltd.

[57] Cuenot, B. and Poinsot, T., Effects of curvature and unsteaddiness in diffusion flames, implications for turbulent diffusion combustion. Twenty-Fifth

Symposium (International) on Combustion. The Combustion Institute, Pittsburgh, 1994 (1994) p.

[58] Dai, Z., Tseng, L. and G., F., Velocity Statistics of Round, Fully Developed, Buoyant Turbulent Plumes. J. of Heat Transfer, 1995. **117** (1995) p. 138-145.

[59] Dally, B., Flectcher, D. and Masri, A., Flow and mixing fields of turbulent bluff-body jets and flames. Combust. Theory Modelling, 1998. **2** (1998) p. 193-219.

[60] de Bruyn Kops, S., et al., Investigation of modeling for non-premixed turbulent combustion. Flow, Turbulence and Combustion, 1998. **60** (1998) p. 105-122.

[61] Deardorff, J., On the Magnitude of the Subgrid-Scale Eddy Coefficient. J. Comp. Phys., 1971. **7**(120-133) (1971) p.

[62] Delhaye, B., Simulation and modeling of reactive shear layers. Theoretical and Computational Fluid Dynamics, 1994. **6** (1994) p. 67-87.

[63] Delichatsios, M., et al., Mass pyrolysis rates and excess pyrolysate in fully developed enclosure fires. Fire safety journal, 2004. **39** (2004) p. 1-21.

[64] DesJardin, P. and Frankel, S., Large eddy simulation of a nonpremixed reacting jet: Application and assesment of subgrid-scale models. Phys. Fluids, 1998. **10** (1998) p. 2298-2314.

[65] Devaud, C. and Bray, K., Assessment of the applicability of conditional moment closure to a lifted turbulent flame: first order model. Combust. and Flame, 2003. **132** (2003) p. 102-114.

[66] Dold, J.W., Flame Propagation in a Nonuniform Mixture: Analysis of a Slowly Varying Triple Flame. Combust. and Flame, 1989. **76** (1989) p. 71-88.

[67] Domingo, P., Vervisch, L. and Bray, K., Partially Premixed Flamelets in LES of Non-Premixed Turbulent Combustion. Combust. Theory Modelling, 2002. **6** (2002) p. 529-551.

[68] Domingo, P., et al., DNS of a premixed turbulent V flame and LES of a ducted flame using a FSD-PDF subgrig scale closure with FPI-tabulated chemistry. Combust. and Flame, 2005. **143** (2005) p. 566-586.

[69] Domingo, P., Vervisch, L. and Réveillon, J., DNS Analysis of Partially Combustion in Spray and Gaseous Turbulent Flame-Bases Stabilized in Hot Air. Combust. and Flame, 2005. **140**(3) (2005) p. 172-195.

[70] Dopazo, C., Non-isothermal turbulent reactive flows: stochastic approaches. PhD thesis. 1973, Univeristy of New York: Stony Brook.

[71] Duclos, J. and Veynante, D., A comparison of flamelet models for premixed turbulent combustion. Combust. and Flame, 1993. **95**((1/2)) (1993) p. 101-108.

[72] Durst, F. and Pereira, J., Time-Dependent Laminar Backward-Facing Step Flow in a Two-Dimensional Duct. Trans. ASME J. Fluids Engng., 1988. **110** (1988) p. 289-296.

[73] Durst, F. and Tropea, C. Turbulent, Backward-Facing Step Flows in Two-Dimensional Ducts and Channels. in *Proc. Third Intl. Symp. on Turbulent Shear Flows*. 1981: University of California. Davis.

[74] Echekki, T. and Chen, J.H., Structure and Propagation of Methanol-Air Triple Flames. Combust. and Flame, 1998. **114** (1998) p. 231-245.

[75] Fairweather, M. and Woolley, R., First-order conditional moment closure modeling of turbulent, nonpremixed methane flames. Combust. and Flame, 2004. **138**(3) (2004) p.

[76] Favier, V. and Vervisch, L., Effects of unsteadiness in edge-flames and liftoff in non-premixed turbulent combustion. Twenty-Seventh Symposium (International) on Combustion. The Combustion Institute., 1998 (1998) p. 1239-1245.

[77] Favier, V. and Vervisch, L., Edge Flame and Partially Combustion in Diffusion Flame Quenching. Combust. and Flame, 2001. **125** (2001) p. 788-803.

[78] Favier, V. and Vervisch, L., Edge flame and partially premixed combustion in diffusion flame quenching. Combust. and Flame, 2001. **125** (2001) p. 788-803.

[79] Ferreira, J., Flamelet modelling of stabilization in turbulent non-premixed combustion. PhD thesis. 1996, Swiss Federal Institute of Technology (ETH) Zurich.

[80] Fiorina, B., et al., Approximating the Chemical Structure of Partially Premixed and Diffusion counterflow Flames using FPI Flamelet Tabulation. Combust. and Flame, 2005. **140**(3) (2005) p. 147-160.

[81] Fleischmann, C., Pagni, P. and Williamson, B., Exploratory Backdraft Experiments. 1993, University of California in Berkeley: California.

[82] Fox, R., Computational methods for turbulent reacting flows in the chemical process industry. Revue de L'Institut Francais du Pétrole, 1996. **51**(2) (1996) p.

[83] Friedrich, R. and Arnal, M., Analysing Turbulent Backward-Facing Step Flow with the Lowpass-Filtered Navier-Stokes Equations. J. Wind. Eng. Indust. Aerod., 1990. **35** (1990) p. 101-128.

[84] Fureby, C., A fractal flame-wrinkling large eddy simulation model for premixed turbulent combustion. Proceedings of the Combustion Institute, 2005. **30** (2005) p. 593-601.

[85] Fureby, C. and Löfström, C., Large eddy simulation of bluff body stabilized flames. Twenty fifth Symposium (International) on Combustion. The Combustion Institute., 1994 (1994) p. 1257-1264.

[86] Fureby, C. and Möller, S., Large eddy simulation of reacting flows applied to bluff body stabilized flames. AIAA, 1995. **33**(12) (1995) p. 2339.

[87] Gao, P., et al., Large eddy simulation for studying tunnel smoke ventilation. Tunnelling and Underground Space Technology, 2004. **19** (2004) p. 577-586.

[88] Germano, M., et al., A Dynamic Subgrid-Scale Eddy Viscosity Model. Phys. Fluids, 1991. **3**(7) (1991) p. 1760-1765.

[89] Geyer, D., et al., Turbulent opposed-jet flames: A critical bemchmark experiment for combustion LES. Combust. and Flame, 2005. **143** (2005) p. 524-548.

[90] Giacomazzi, E., Battaglia, V. and Bruno, C., The coupling of turbulence and chamistry in a premixed bluff-body flame as studied by LES. Combust. and Flame, 2004. **138** (2004) p. 320-335.

[91] Gicquel, O., Darabiha, N. and Thévenin, J., Laminar premixed hydrogen/air counterflow flame simulations using flame prolongation if ILDM with differential diffusion. Proc. Combust. Inst., 2000. **28** (2000) p. 1901-1908.

[92] Girimaji, S., On the modeling of scalar diffusion in isotropic turbulence. Phys. Fluids, 1992. **4** (1992) p. 2529-2537.

[93] Girimaji, S. and Zhou, Y., Analysis and modeling of subgrid scalar mixing using numerical data. Phys. Fluids, 1996. **8**(5) (1996) p.

[94] Gojkovic, D., Initial Backdraft Experiments. 2001, Lund University: Sweden.

[95] Gottuk, D., et al., The Development and Mitigation of Backdraft: A Real-Scale shipboard study. Fire safety journal, 1999. **33** (1999) p. 261-282.

[96] Gouldin, F., Combustion intensity and burning rate integral of premixed flames. Twenty-sixth Symposium (International) on Combustion. The Combustion Institute., 1996 (1996) p. 382-388.

[97] Graham, T., Makhviladze, G. and Roberts, J., The effects of the thermal inertia of the walls upon flashover development. Fire safety journal, 1999. **32** (1999) p. 35-60.

[98] Grinstein, F. and Fureby, C., LES studies of the flow in a swirl gas combustor. Proceedings of the Combustion Institute, 2005. **30** (2005) p. 1791-1798.

[99] Guo, H., Liu, F. and Smallwood, G., A numerical study of laminar methane/air triple flames in two-dimensional mixing layers. International Journal of Thermal Science, 2006. **45** (2006) p. 586-594.

[100] Hawkes, R. and Cant, R., Implications of a Flame Surface Density Approach to Large Eddy Simulation of Premixed Turbulent Combustion. Combust. and Flame, 2001. **126** (2001) p. 1617-1629.

[101] Haworth, D., et al., The importance of time-dependent flame structures in stretched laminar flamelet models for turbulent jet diffusion flames. Twenty-second Symposium (International) on Combustion. The Combustion Institute. Pittsburgh, 1988 (1988) p. 589-597.

[102] Hulek, T. and Lindstedt, R., Joint scalar-velocity pdf modelling of finite rate chemistry in a scalar mixing layer. Combust. Sci. Tech., 1998. **136** (1998) p. 303-331.

[103] Hwang, C. and Edwards, J., The critical ventilation in tunnel fires- a computer simulation. Fire safety journal, 2005. **40** (2005) p. 213-244.

[104] Ihme, M., Cha, C. and Pitsch, H., Prediction of local extinction and re-ignition effects in non-premixed turbulent combustion using a flamelet/progress

variable approach. Proceedings of the Combustion Institute, 2005. **30** (2005) p. 793-800.

[105] Im, H., Lund, T. and Ferziger, J., Large eddy simulation of turbulent front propagation with dynamic subgrid models. Phys. Fluids, 1997. 9(12) (1997) p.

[106] Isomoto, K. and Honami, S., The Effect of Inlet Turbulence Intensity on the Reattachment Process Over a Backward-Facing Step. Trans. ASME J. Fluids Engng, 1989. **111** (1989) p. 87-92.

[107] Itoh, N. and Kasagi, N., Turbulence Measurements in a Separated and Reattaching Flow Over a Backward-Facing step with the Three-Dimensional Particle Tracking Velocimeter. J. Flow Visualization Soc. Jpn., 1989. **34** (1989) p. 245-248.

[108] Joedicke, A., Peters, N. and Mansour, M., The stabilization mechanism and structure of turbulent hydrocarbon lifted flames. Proc. Combust. Inst., 2005. **30** (2005) p. 901-909.

[109] Kaiktsis, L., Karniadakis, G. and Orszag, S., Onset of Three-Dimensionality, Equilibria, and Early Transition in Flow Over a Backward-Facing Step. J. Fluid Mech., 1991. **231** (1991) p. 501-528.

[110] Kalmthout, E. and Veynante, D., Direct numerical simulation analysis of flame surface density models for non premixed turbulent combustion. Phys. Fluids A, 1998. **10**(9) (1998) p. 2347-2368.

[111] Kang, M., et al. The use of a laminar flamelet approach in the large eddy simulation of flame structure at the base of a pool fire. in *Interfalme 2001.* 2001. Edinburgh, UK.

[112] Kasagi, N. and Matsunaga, A., Three-Dimensional Particle-Tracking Velocimetry Measurement of Turbulence Statistics and Energy Budget in a Backward-Facing Step Flow. Int. J. Heat and Fluid Flow, 1995. **16**(6) (1995) p.

[113] Kempf, A., Flemming, F. and Janicka, J., Investigation of lenght scale, scalar dissipation, and flame oritation in a piloted diffussion flame by LES. Proc. Combust. Inst., 2005. **30** (2005) p. 557-565.

[114] Kerstein, A., Linear-Eddy modeling of turbulent tranport: Part II. Application to shear layer mixing. Combust. and Flame, 1989. **75**(3-4) (1989) p. 397-413.

[115] Kerstein, A., Linear-eddy modelling of turbulent transport. Part 3: Mixing and differential molecular diffusion in rpund jets. J. Fluid Mech., 1990. **216** (1990) p. 411-435.

[116] Kerstein, A., Linear-eddy modelling of turbulent transport. Part 6: Microstructure of diffusive scalar mixing fields. J. Fluid Mech., 1991. **231** (1991) p. 361-394.

[117] Kim, N., et al., The propagation of tribrachial flames in a confined channel. In press. Combust. and Flame, 2006. **146** (2006) p. 168-179.

[118] Kim, N., et al., Lift-off characteristics of triple flame with concentration gradient. Proc. Combust. Inst., 2005. **30** (2005) p. 367-374.

[119] Kim, S. and Huh, K., Application of the elliptic conditional moment closure model to a two-dimensional nonpremixed methanol bluff-body flame. Combust. and Flame, 2000. **120** (2000) p. 75-90.

[120] Kim, S. and Huh, K., Second-order conditional moment closure modeling of turbulent piloted Jet diffusion flames. Combust. and Flame, 2004. **138**(336) (2004) p.

[121] Kioni, P., et al., Experimental and Numerical Studies of a Triple Flame. Combust. and Flame, 1999. **116** (1999) p. 192-206.

[122] Kioni, P., et al., Flame Spread in Laminar Mxing Layers: The Triple Flame. Combust. and Flame, 1993. **95** (1993) p. 276-290.

[123] Klimenko, A., Fluid Dynamics. 1990 (1990) p. 25-327.

[124] Klimenko, A., Multicomponent diffusion of various scalars in turbulent flows. Fluid Dyn., 1990. **25** (1990) p. 327-334.

[125] Klimenko, A. and Bilger, R., Conditional moment closure for turbulent combustion. Prog. Energy Combust., 1999. **25**(6) (1999) p. 595-687.

[126] Klopovic, S. and Turan, F., Flames venting externally during full-scale flashover fires: two sample ventilation cases. Fire safety journal, 1998. **31** (1998) p. 117-142.

[127] Kronenburg, A. and Bilger, R., Modelling differential diffusion in nonpremixed reacting turbulent flow: application to turbulent jet flames. Combust. Sci. Tech., 2001. **166** (2001) p. 175-194.

[128] Kronenburg, A., Bilger, R. and Kent, J., Computation of conditional average scalar dissipation in turbulent jet diffusion flames. Flow, Turbulence and Combustion, 2000. **64** (2000) p. 145-159.

[129] Kuehn, D., Some Effects of Adverse Pressure Gradient on the Incompressible Reattaching Flow Over a Rearward-Facing Step. AIAA, 1980. **18** (1980) p. 343-344.

[130] Lahjaily, H., et al., Introduction of dilution in the BML model: application to a stagnating turbulent flame. Combust. Sci. Tech., 1998. **135** (1998) p. 153-173.

[131] Lattimer, B., et al., Modeling fire growth in a combustible corner. Fire safety journal, 2003. **38** (2003) p. 771-796.

[132] Le, H., Moin, P. and Kim, J. Direct Numeric Simulation of Turbulent Flow Over a Backward-Facing Step. in *Proc. Ninth Symp. on Turbulent Shear Flows*. 1993. Kyoto University.

[133] Le, H., Moin, P. and Kim, J., Direct Numerical Simulation of Turbulent Flow Over a Backward-Facing Step. J. Fluid Mech., 1997. **330** (1997) p. 349-374.

[134] Lee, B.J. and Chung, S.H., Stabilization of Lifted Tribrachial Flames in a Laminar Nonpremixed Jet. Combust. and Flame, 1997. **109** (1997) p. 163-172.

[135] Lee, J. and Chung, S.H., Characteristic of Reattachment and Blowout of Laminar Lifted Flames in Partially Premixed Propane Jets. Combust. and Flame, 2001. **127** (2001) p. 2194-2204.

[136] Lee, J., et al., Propagation Speed of Tribrachial (triple) Flame of Propane in Laminar Jets Under Normal and Micro Gravity Conditions. Combust. and Flame, 2003. **134** (2003) p. 411-420.

[137] Lee, J., et al., Lifted flames in laminar jets of propnae in coflow air. Combust. and Flame, 2003. **135** (2003) p. 449-462.

[138] Lee, S. and Ryou, H., A numerical study on smoke movement in longitudinal ventilation tunnel fires for different aspect ratio. Building and Enviroment, 2006. **41** (2006) p. 719-725.

[139] Lee, Y., Nonpremixed reacting flows near extinction. PhD thesis. 1994, Cornell University.

[140] Lennon, T. and Moore, D., The natural fire safety concept-full-scale tests at Cardington. Fire safety journal, 2003. **38** (2003) p. 623-643.

[141] Libby, P. and Williams, F., Turbulent combustion: Fundamental aspects and a review, in *Turbulent Reacting Flows*, P.a.W. Libby, F., Editor. 1994, Academic Press: London. p. 2-61.

[142] Lilly, D., On the Numerical Simulation of Buoyant Convection, in *Tellus*. 1962. p. 148-172.

[143] Liñan, L., The asymptotic structure of counterflow diffusion flams for large activation energies. Acta Astronautica, 1974. **1007**(1) (1974) p.

[144] Lundgren, T., Distribution function in the statistical theory of turbulence. Phys. Fluids, 1967. **10** (1967) p. 969-975.

[145] Luo, M. and Beck, V., A study of non-flashover and flashover fires in a full-scale multi-room building. Fire safety journal, 1996. **26** (1996) p. 191-219.

[146] Luo, M., He, Y. and Beck, V., Applications of field model and two-zone model to flashover fires in a full-scale muti-room single level building. Fire safety journal, 1997. **29** (1997) p. 1-25.

[147] Ma, T. and Quintere, J., Numerical simulation of axi-symmetric fire plumes: accuracy and limitations. Fire safety journal, 2003. **38** (2003) p. 467-492.

[148] Magnussen, B. and Hjertager, B., On the mathematical modeling of turbulent combustion with special emphasis on soot formation and combustion. Sisteenth Symposium (International) on Combustion. The Combustion Institute. Pitsburgh, 1976 (1976) p. 719-729.

[149] Mahalingam, S., Chen, J. and Vervisch, L., Finite-rate chemistry and transiennt effects in direct numerical simulations of turbulent nonpremixed flames. Combust. and Flame, 1995. **102** (1995) p. 285-297.

[150] Mansour, M.S., Stability characteristics of lifted turbulent partially premixed jet flames. Combust. and Flame, 2003. **133** (2003) p. 263-274.

[151] Mansour, M.S., The flow field structure at the base of lifted turbulent partially premixed jet flames. Experimental Thermal and Fluid Science, 2004. **28** (2004) p. 771-779.

[152] Mantel, T. and Borghi, R., A new model of premixed wrinkled flame propagation based on a scalar dissipation equation. Combust. and Flame, 1994. **96**(4) (1994) p. 443.

[153] Marble, F. and Broadwell, J., The coherent flame model on non-premixed turbulent combustion. 1977, Pudue University.

[154] Mare, F., Jones, W. and Menzies, K., Large eddy simulation of a model gas turbine combustion. Combust. and Flame, 2004. **137** (2004) p. 278-294.

[155] Masri, A., Pope, S. and Dally, B., Probebility density function computations of a strongly swirling nonpremixed flame stabilized on a new burner. Proc. Combust. Inst., 2000. **28** (2000) p. 123-131.

[156] Mathey, F. and Chollet, J., Subgrid-scale model of scalar mixing for large eddy simulation of turbulent flows, in *Direct and Large Eddy Simulation II*, J. Chollet, Voke, P. and Kleiser, L., Editor. 1997, Kluwer Academic Publisher. p. 103-114.

[157] Mauss, F., Keller, D. and Peters, N., A lagrangian simulation of flamelet extinction and re-ignition in turbulent jet diffusion flames. Twenty-Third Symposium (International) on Combustion. The Combustion Institute. Pitsburgh, 1990 (1990) p. 693-698.

[158] Mc Millan, O., Ferziger, J. and Rogallo, R., Tests of New Subgrid-Scale Models in Strained Turbulence. AIAA, 1980(80) (1980) p. 1339.

[159] McGrattan, K., Fire Dynamics Simulator - Technical Reference Guide. 2002, NIST.

[160] McGrattan, K., Baum, H. and Rehm, R., Numerical simulation of smoke plumes from large oil fires. Atmospheric Enviroment, 1996. **30**(24) (1996) p. 4125-4136.

[161] McGrattan, K. and Fleischmann, C., Numerical and Experimental Gravity Currents Related to Backdraft. Fire safety journal, 1999. **33** (1999) p. 21-34.

[162] McGrattan, K. and Forney, G., Fire Dynamics Simulator (Version 4). Technical Reference Guide. 2004, National Institute of Standars and Technology.

[163] McGrattan, K., Rehm, R. and Baum, H., Fire-Driven Flows in Enclosures. Computational Physics, 1994. **110**(2) (1994) p. 285-291.

[164] McMurthy, P., Menon, S. and Kerstein, A. A subgrid mixing model for nonpremixed turbulent combustion. in *AIAA 30th Aerospace Science Meeting.* 1992. Reno, Nevada.

[165] Mell, W., et al., Direct numerical simulation investigation of the conditional moment closure model for nonpremixed turbulent reacting flows. Combust. Sci. Tech., 1991. **91** (1991) p. 179-186.

[166] Meneveau, C., Lund, T. and Cabot, W., A Lagrangian dynamic subgrid-scale model of turbulence. J. Fluid Mech., 1996. **319** (1996) p. 353-385.

[167] Menon, S., et al., Prediction of NOx production in a turbulent hydrogen-air jet flame. J. Prop. Power, 1994. **10** (1994) p. 161-168.

[168] Mizobuchi, Y., et al., A numerical analysis of the structure of a turbulent hydrogen jet lifted flame. Combust. Inst., 2002. **29** (2002) p. 2009-2015.

[169] Moin, P. and Kim, J., Numerical Investigation of Turbulent Channel Flow. J. Fluid Mech., 1982. **118** (1982) p. 341-377.

[170] Moin, P. and Pierce, C., A Dynamic Model for Subgrid-Scale Variance and Dissipation Rate of a Conserved Scalar. Phys. Fluids, 1998. **10**(12) (1998) p.

[171] Moin, P., Reynolds, W. and Ferziger, F., Large Eddy Simulation of Incompressible Turbulent Channel Flow. 1978, Stanford University, Dept. of Mechanical Engineering.

[172] Molkov, V., Makarov, D. and Puttock, J., The nature and large eddy simulation of coherent deflagrations in a vented enclosure-atmosphere system. Journal of Loss prevention in the process industries, 2006. **19** (2006) p. 121-129.

[173] Moss, J. and Bray, K., A unified statistical model of the premixed turbulent flame. Acta Astronautica, 1977. **4** (1977) p. 291-319.

[174] Muñiz, L. and Mungal, G., Instanteneous Flame-Stabilization Velocities in Lifted-Jet Diffusion Flames. Combust. and Flame, 1997. **111** (1997) p. 16-31.

[175] Mustata, R., et al., A probability density finction eulerian monte carlo field method for large eddy simulation: Application to a turbulent piloted methane/air diffusion flame (Sandia D). Combust. and Flame, 2006. **145** (2006) p. 88-104.

[176] Neto, A., et al., A Numerical Investigation of Coherent Vortices in Turbulence Behind a Backward Facing Step. J. Fluid Mech., 1993. **256** (1993) p. 1-25.

[177] Neumann, J. and Richtmyer, R., A Method for the Caculation of Hydrodynamics Shocks. J. Appl. Phys., 1950. **21** (1950) p. 232-237.

[178] Newman, J. and Xin, Y., Characterization of room environments in growing enclosure fires. Fire safety journal, 2004. **39** (2004) p. 239-253.

[179] Nielsen, C. and Fleischmann, C., An anlysis of pre-flashover fire experiment with field modelling comparison. (University of Canterbury, NZ), 2000 (2000) p.

[180] Ötügen, M., Expansion Ratio Effects on the Separated Shear Layer and Reattachment Downstream of a Backward-Facing Step. Exps. Fluids, 1991. **10** (1991) p. 273-280.

[181] Papanicolaoun, P. and List, E., Statistical and Spectral Properties of Tracer Concentration in Round Buoyant Jets. Int. J. Heat Mass Trans., 1987. **30** (1987) p. 2059-2071.

[182] Peacock, R., et al., Defining flashover for fire hazard calculations. Fire safety journal, 1999. **32** (1999) p. 331-345.

[183] Peters, N., Laminar Diffusion Flamelet Models in Non-Premixed Turbulent Combustion. Prog. Energy Combust., 1984. **10** (1984) p. 319-339.

[184] Peters, N., Laminar flamelet concepts in turbulent combustion. Twenty-First Symposium (International) on Combustion., 1986 (1986) p. 1231-1250.

[185] Peters, N., ed. Reduced Kinetic Mechanisms for Applications in Combustion Systems. Chapter 4. 1993, Springer.

[186] Peters, N., The turbulent burning velocity for large-scale and small-scale turbulent. J. Fluid Mech., 1999. **384** (1999) p. 107-132.

[187] Peters, N., Turbulent Combustion. 2000.

[188] Peters, N. and Williams, F., Liftoff Characteristics of Turbulent Jet Diffusion Flames. AIAA, 1983. **21**(3) (1983) p.

[189] Phillips, H., Flame in a buoyant methane layer. Combust. Inst., 1965. **10** (1965) p. 1277-1283.

[190] Piana, J., et al., Direct numerical simulation analysis of the g-equation in premixed combustion, in *Direct and Large Eddy Simulation II*, P.V.a.L.K. J. Chollet, Editor. 1997, Kluwer Academic Publishers. p. 321-330.

[191] Pierce, C. and Moin, P., A dynamic model for subgrid-scale variance and dissipation rate of a conserved scalar. Phys. Fluids, 1998. **10**(12) (1998) p.

[192] Pierce, C. and Moin, P., Progress-variable approach for large-eddy simulation of non-premixed turbulent combustion. J. Fluid Mech, 2004. **504** (2004) p. 73-97.

[193] Pitsch, H., FlameMaster. 1996.

[194] Pitsch, H., Extended flamelet model for LES of non-premixed combustion. Center for Turbulent Research, 2000 (2000) p.

[195] Pitsch, H., Unsteady Flamelet Modeling of Differential Diffusion in Turbulent Jet Diffusion Flames. Combust. and Flame, 2000. **123** (2000) p. 358-374.

[196] Pitsch, H., A consistent level set formulation for large-eddy simulation of premixed turbulent combustion. Combust. and Flame, 2005. **143** (2005) p. 587-598.

[197] Pitsch, H., Chen, M. and Peters, N., Unsteady flamelet modeling of turbulent hydrogen/air diffusion flames. Proc. Combust. Inst., 1998. **27**(1057) (1998) p.

[198] Pitsch, H. and Fedotov, S., Investigation of scalar dissipation rate fluctuations in non-premixed turbulent combustion using a stochastic approach. Combust. Theory Modelling, 2001. **5**(1) (2001) p. 41-57.

[199] Pitsch, H. and Steiner, H., Large-eddy simulation of a turbulent piloted methane/air diffusion flame (Sandia flame D). Phys. Fluids, 2000. **12**(10) (2000) p.

[200] Plessing, T., Terhoeven, P. and Peters, N., An Experimental and Numerical Study of a Laminar Triple Flame. Combust. and Flame, 1998. **115** (1998) p. 335-353.

[201] Pope, N. and Bailey, C., Quantitative comparison of FDS and parametric fire curves with post-flashover compartment fire test data. Fire safety journal, 2006. **41** (2006) p. 99-110.

[202] Pope, S., A Monte Carlo method for pdf equations of turbulence reactive flow. Combust. Sci. Tech., 1981. **25** (1981) p. 159-174.

[203] Pope, S., Pdf methods for turbulent reactive flows. Prog. Energy Combust., 1985. **11**(119) (1985) p.

[204] Pope, S., The evolution of surfaces in turbulence. Int. J. Eng. Sci., 1988. **26**(5) (1988) p. 445-469.

[205] Pope, S., Computations of turbulent combustion: Progress and chalenges. In proceedings of the 23th Symposium (International) on Combustion (The Combustion Institute, Pittsburgh), 1990 (1990) p.

[206] Pope, S., Turbulent Flows. 2000: Cambrige University Press.

[207] Ra, S. and Chang, P., Effects of the Pressure Gradient on Reattaching Flow Downstream of Rearward-Facing Step. J. Aircraft, 1990. **27** (1990) p. 93-95.

[208] Raman, V. and Pitsch, H., Large-eddy simulation of a bluff-body-stabilized non-premixed flame using a recursive filter-refinement procedure. Combust. and Flame, 2005. **142** (2005) p. 329-347.

[209] Raman, V., Pitsch, H. and Fox, R., Hybrid large-eddy simulation/Lagrangian filtered-density-function approach for simulating turbulent combustion. Combust. and Flame, 2005. **143** (2005) p. 56-78.

[210] Ravet, F. and Vervisch, L., Modeling non-premixed turbulent combustion in aeronautical engines using pdf-generator. In 36st Aerospace Science Meeting and Exhibit AIAA paper 98-1027, 1998 (1998) p.

[211] Ravikanth, V. and Pletcher, R., Large Eddy Simulation of the Turbulent Flow Past a Backward-Facing Step ith Heat Transfer and Property Variations. Int. J. Heat and Fluid Flow, 2002. **23** (2002) p. 601-614.

[212] Réveillon, J., Simulation dynamique des grandes structures appliquée aux flammes turbulentes non-prémélangées. PhD thesis. 1996, Université de Rouen.

[213] Réveillon, J. and Vervisch, L., Response of the dynamic LES mode to heat release induced effects. Phys. Fluids A, 1996. **8**(8) (1996) p. 2248-2250.

[214] Réveillon, J. and Vervisch, L., Dynamic subgrid pdf modeling for non premixed turbulent combustion, in *Direct and Large Eddy Simulation II*, J.V. Chollet, P. and Kleiser, L., Editor. 1997, Kluwer Academic Publishers. p. 311-320.

[215] Rogg, B., The cambridge universal laminar flamelet computer code, in *Reduced Kinetic Mechanisms for Applications in Combustion Systems, Appendix C*, N.a.R. Peters, B., Editor. 1993, Springer Verlag: Berlin-Heidelberg.

[216] Rouse, H., Yih, C. and Humphreys, H., Gravitational Convection From a Boundary Source. Tellus, 1952. **4** (1952) p. 201-210.

[217] Ryder, N., Schemel, C. and Jankiewicz, S., Near and far field contamination modeling in a large scale enclosure: Fire dynamics Simulator comparison with measured observations. Journal of Hazardous Materials, 2006. **130** (2006) p. 182-186.

[218] Ryder, N., et al., Consequence modeling using the fire dynamics simulator. Journal of Hazardous Materials, 2004. **115** (2004) p. 149-154.

[219] Sadiki, A., et al., Unsteady methods (URANS and LES) for sumulation of combustion systems. International Journal of Thermal Science, 2006. **45** (2006) p. 760-773.

[220] Sanders, J.P.H. and Lamers, A.P.G.G., Modeling and Calculation of Turbulent Lifted Diffusion. Combust. and Flame, 1994. **96** (1994) p. 22-33.

[221] Sankaran, V. and Menon, S., Subgrid combustion modeling of 3-D premixed flames in the thin-reaction-zone regime. Proceedings of the Combustion Institute, 2005. **30** (2005) p. 575-582.

[222] Schefer, R. and Goix, P., Machanism of Flame Stabilization in Turbulent Lifted-Jet Flames. Combust. and Flame, 1998. **112** (1998) p. 559-574.

[223] Selle, L., et al., Compressible large eddy simulation of turbulent combustion in complex geometry on unstructured meshes. Combust. and Flame, 2004. **137** (2004) p. 489-505.

[224] Sheikhi, M., et al., Large eddy simulation of a turbulent nonpremixed piloted methane jet flame (Sandia Flame D). Proc. Combust. Inst., 2005. **30** (2005) p. 549-556.

[225] Sinai, Y., Comments on the role of leakages in field modelling of under-ventilated compartment fires. Fire safety journal, 1999. **33** (1999) p. 11-20.

[226] Sinha, S., Gupta, A. and Oberai, M., Laminar Separating Flow Over Backsteps and Cavities Part I: Backsteps. AIAA, 1981. **19** (1981) p. 1527-1530.

[227] Smagorinsky, J., General Circulation Experiments with the Primitive Equations, Part I. The Basic Experiments. Mon Weather Rev, 1963. **91** (1963) p. 99-152.

[228] Smiljanovski, V., Moder, V. and Klein, R., A capturing-track hybrid scheme for deflagration discontinuities. Combust. Theory Modelling, 1997. **1**(2) (1997) p. 183-215.

[229] Spalding, D., Mixing and chemical reaction in steady confined turbulent flames. Thirdteen Symposium (International) on Combustion. The Combustion Institute. Pitsburgh, 1971 (1971) p. 649-657.

[230] Steckler, K. and Mitler, H., Wall fires and the approach to flashover in an enclosure. Safety Science, 1995(1) (1995) p. 71-78.

[231] Steiner, H. and Bushe, W., Large eddy simulation of a turbulent reacting jet with Conditional Source-term Estimation. Phys. Fluids, 2001. **13** (2001) p.

[232] Su, L., Sun, O. and Mungal, G., Experimental investigation of stabilization mechanism in turbulent, lifted jet diffusion flames. Combust. and Flame, 2006. **144** (2006) p. 494-512.

[233] Swaminathan, N. and Bilger, R., Assessment of Combustion Submodels for Turbulent Nonpremixed Hydrocarbon Flames. Combust. and Flame, 1999. **116** (1999) p. 519-545.

[234] Tennekes, H. and Lumley, J., A first course in turbulence, ed. M.I.T. Press. 1972, Cambridge.

[235] Thibaut, D. and Candel, S., Numerical study of unsteady turbulent premixed combustion: application to flashback simulation. Combust. and Flame, 1998. **113** (1998) p. 53-65.

[236] Tieszen, S., Stamps, D. and O'Hern, T., A heuristic model of turbulent mixing applied to blowout of turbulent jet diffusion flames. Combust. and Flame, 1996. **106** (1996) p. 442-466.

[237] Trouvé, A. and Poinsot, T., The evolution equation for the flame surface density. J. Fluid Mech., 1994. **278** (1994) p. 1-31.

[238] Tsai, K. and Fox, R., The bmc/giem model for micromixing in non-premixed turbulent reacting flows. Ind. Eng. Chme. Res, 1998. **6** (1998) p.

[239] Twomey, S., Introduction to the mathematics of inversion in remote sensing and indirect measurements. Developments in geomathematics. Vol. 3. 1977, Amsterdam: Elsevier scientific publishing company.

[240] Upatnieks, A., et al., Liftoff of turbulent flames--assessment of edge flame and other concepts using cinema-PIV. Combust. and Flame, 2004. **138** (2004) p. 259-272.

[241] Urbin, G. and Metais, O., Large-Eddy Simulation of Three-Dimensional Spatially-Developing Jets, in *Direct and Large-Eddy Simulation*, K.L. Voke P.R., Chollet J.P. (Eds.), Editor. 1997. p. 35-46.

[242] Utiskul, Y., Quintiere, J. and Naruse, T. Wall-vent compartment fire behavior under limited ventilation. in *Interflame 2004*. 2004. Edinburgh, Scotland.

[243] Van Oijen, J., LAmmers, L. and De Goey, L., Modeling of complex burner systems by using flamelet-generated manifolds. Combust. and Flame, 2001. **127**(3) (2001) p. 2124-2134.

[244] Vervisch, L., Using numerics to help to understanding of nonpremixed turbulent flames. Topical review, twenty-eight Int. Symposium on combustion, 2000 (2000) p.

[245] Vervisch, L., et al., Surface density function in premixed turbulent combustion modeling, similarities between probability density function and flame surface approach. Phys. Fluids A, 1995. 7(10) (1995) p. 2496-2503.

[246] Veynante, D. and Poinsot, T., Large eddy simulation of combustion inestabilities in turbulent premixed burners. In Annual Research Briefs. Center for Turbulence Research., 1997 (1997) p.

[247] Veynante, D. and Vervisch, L., Turbulent Combustion Modeling. Progress in Energy and Combustion Science, 2002. **28** (2002) p. 193-266.

[248] Veynante, D., et al. Triple flame structure and disfusion flame stabilization. in *Proceedings of the Summer Program*. 1994. Stanfor/Ames Center of Turbulence Research.

[249] Wang, H. and Chen, Y., Steady flamelet modelling of a turbulent non-premixed flame considering scalar dissipation rate fluctuations. Fluid Dyn., 2005. **37**(133) (2005) p.

[250] Wang, H., Countin, M. and Most, J., Large eddy simulation of buoyancy-driven fire propagation behind a pyrolysis zone along a vertical wall. Fire safety journal, 2002. **37** (2002) p. 259-285.

[251] Watson, K.A., et al., Observations on the Leading Edge in Lifted Flame Stabilization. Combust. and Flame, 1999. **199** (1999) p. 199-202.

[252] Wen, J., Huang, L. and Roberts, J., The effect of microscopic and global radiative heat exchange on the field predictions of compartment fires. Fire safety journal, 2001. **36** (2001) p. 205-223.

[253] Weng, W. and Fan, W., Critical Condition of Backdraft in Compartment Fires: A reduced Scale Experimental Study. Journal of Loss Prevention in the process industries, 2003. **16** (2003) p. 19-26.

[254] Weng, W. and Fan, W., Mitigation of Backdraft with Water Mist: A Reduced-Scale Experimental Study. Process Safety Progress, 2003. **22**(3) (2003) p.

[255] Weng, W. and Fan, W., Nonlinear analysis of the Backdraft Phenomenon in Room Fires. Fire safety journal, 2004. **39** (2004) p. 447-464.

[256] Weng, W., et al., A model of Backdraft Phenomenon in Building Fires. Progress in Natural Science, 2002. **12**(2) (2002) p.

[257] Williams, F., Combustion Theory, ed. e. Addison-Wesley. 1985.

[258] Williams, F., Turbulent combustion, in *The mathematics of combustion*, J.Buckmaster, Editor. 1985, SIAM. p. 116-151.

[259] Williams, H. and Brian, P., Numerical Recipies in C, ed. C.U. Press. 1992.

[260] Xin, Y., et al., Fire dynamics simulation of a turbulent buoyant flame using a mixture-fraction-based combustion model. Combust. and Flame, 2005. **141** (2005) p. 329-335.

[261] Xue, H., Ho, J. and Cheng, Y., Comparison of different combustion models in enclosure fire simulation. Fire safety journal, 2001. **36** (2001) p. 37-54.

[262] Yakhot, A., et al., Renormalization Group Formulation of Large-Eddy Simulation. J. Sci. Computing, 1989. **4** (1989) p. 139-158.

[263] Yakhot, V. and Orszag, S., Renormalization Group Analysis of Turbulence I Basic theory. J. Sci. Computing, 1986. **1** (1986) p. 3-51.

[264] Yamashita, H., Shimada, M. and Takeno, T. A Numerical Study on Flame Stability at the Transition Point of Jet Diffusion Flames. in *Twenty-Sixth Symposium (International) on Combustion.* 1996: The Combustion Institute.

[265] Yan, Z. and Holmstedt, G., CFD and experimental studies of room fire growth on wall lining materials. Fire safety journal, 1997. **27** (1997) p. 201-238.

[266] Yang, R., et al., Subgrid Scale Laminar Flamelet Model for Partially Premixed Combustion and its Application to Backdraft simulation. Fire safety journal, 2004 (2004) p.

[267] Yeoh, G., et al., On modelling combustion, radiation and soot processes in compartment fires. Building and Enviroment, 2003. **38** (2003) p. 771-785.

[268] Yeoh, G., et al., On numerical comparison of enclosure fire in a multi-compartment building. Fire safety journal, 2003. **38** (2003) p. 85-94.

[269] Yoda, M., Hesselink, L. and Mungal, M., Instantaneous 3-dimensional concentration measurements in the self-similar region of a round high schmidt-number jet. J. Fluid Mech, 1994. **279** (1994) p. 313-350.

[270] Yuan, L., Street, R. and Ferziger, J., Large-Eddy Simulation of a Round Jet in Crossflow. J. Fluid Mech., 1999. **379** (1999) p. 71-104.

[271] Zhang, W., et al., Turbulence statistics in a fire room model by large eddy simulation. Fire safety journal, 2002. **37** (2002) p. 721-752.

[272] Zhang, Y., Rogg, B. and Bray, K., 2-d simulation of turbulent autoignition with transient laminar flamelet source term closure. Combust. Sci. Tech., 1995. **105** (1995) p. 211-227.

[273] Zhou, X., Luo, K. and Williams, J., Large-Eddy Simulation of a Turbulent Forced Plume. Eur. J. Mech. B - Fluids, 2001. **20** (2001) p. 233-254.